AD_____

Award Number: DAMD17-02-1-0238

TITLE: Endometase in Androgen-Repressed Human Prostate Cancer

PRINCIPAL INVESTIGATOR: Qing-Xiang A. Sang, Ph.D.

CONTRACTING ORGANIZATION: Florida State University
Tallahassee, Florida 32306-4166

REPORT DATE: March 2005

TYPE OF REPORT: Annual

PREPARED FOR: U.S. Army Medical Research and Materiel Command
Fort Detrick, Maryland 21702-5012

DISTRIBUTION STATEMENT: Approved for Public Release;
Distribution Unlimited

REPORT DOCUMENTATION PAGE

Form Approved
OMB No. 074-0188

1. AGENCY USE ONLY (Leave blank)	2. REPORT DATE	3. REPORT TYPE AND DATES COVERED
	March 2005	Annual (25 Feb 2004 - 25 Feb 2005)

4. TITLE AND SUBTITLE
Endometase in Androgen-Repressed Human Prostate Cancer

5. FUNDING NUMBERS
DAMD17-02-1-0238

6. AUTHOR(S)
Qing-Xiang A. Sang, Ph.D.

7. PERFORMING ORGANIZATION NAME(S) AND ADDRESS(ES)
Florida State University
Tallahassee, Florida 32306-4166

E-Mail: sang@chem.fsu.edu

8. PERFORMING ORGANIZATION REPORT NUMBER

9. SPONSORING / MONITORING AGENCY NAME(S) AND ADDRESS(ES)
U.S. Army Medical Research and Materiel Command
Fort Detrick, Maryland 21702-5012

10. SPONSORING / MONITORING AGENCY REPORT NUMBER

11. SUPPLEMENTARY NOTES

12a. DISTRIBUTION / AVAILABILITY STATEMENT
Approved for Public Release; Distribution Unlimited

12b. DISTRIBUTION CODE

13. ABSTRACT (Maximum 200 Words)

Prostate cancer invasion and metastasis is the leading cause of patient death. We reported the discovery, cloning, and characterization of human matrix metalloproteinase-26 (MMP-26), **endometase**. We have been testing three specific hypotheses: 1) The expression levels of MMP-26 is correlated with the metastatic potentials and the degrees of malignancy of human prostate cells; 2)MMP-26 has unique structure and enzymatic function; 3) MMP-26 enhances prostate cancer invasion by digesting extracellular matrix proteins and inactivating serine proteinase inhibitors, and specific inhibitors of MMP-26 block prostate cancer invasion. We report that levels of MMP-26 protein in human prostate carcinomas and high-grade prostate intraepithelial neoplasia from multiple patients were significantly higher than those in prostatitis, benign prostate hyperplasia, and normal prostate glandular tissues. Prostate cancer cells transfected with MMP-26 cDNA are more invasive and with an inactive mutant are less invasive than the parental cell lines. MMP-26 promoted prostate cancer invasion via activation of pro-gelatinase B/MMP-9. The endometase active site has an intermediate S1' pocket using synthetic MMP inhibitors. Some new synthetic MMP inhibitors are stable in cell culture media and can block the invasion of prostate cancer cells. Papers published by Sang lab are attached.

14. SUBJECT TERMS
Matrix metalloproteinase-26, endometase, advanced human prostate cancer, novel proteinases, cell biology, and biochemistry

15. NUMBER OF PAGES
124

16. PRICE CODE

17. SECURITY CLASSIFICATION OF REPORT	18. SECURITY CLASSIFICATION OF THIS PAGE	19. SECURITY CLASSIFICATION OF ABSTRACT	20. LIMITATION OF ABSTRACT
Unclassified	Unclassified	Unclassified	Unlimited

Table of Contents

Cover..... 1

SF 298..... 2

Table of Contents..... 3

Introduction..... 4

Body..... 5-9

Key Research Accomplishments..... 10-12

Reportable Outcomes..... 13-15

Conclusions..... 16

References..... 17

Appendices..... 18-
(Some unpublished preliminary data and eleven published papers/reprints are attached in the appendices)

Endometase in Androgen-Repressed Human Prostate Cancer

Introduction

Our long term goal is to understand the biochemical and cellular functions of matrix metalloproteinases (MMPs, matrixins) so that we may reveal the molecular steps and pathways of cancer angiogenesis (new blood formation to provide nutrients, oxygen, and passages for cancer cell growth and spread) and metastasis (the spread of cancer). We discovered a novel matrix metalloproteinase (MMP-26, endometase) recently. Endometase is a special biological catalyst that specifically digests some of the connective tissue barrier proteins and may facilitate tumor growth, invasion, and new blood vessel formation. *Endometase* was found to be specifically associated with the androgen-repressed human prostate cancer *(ARCaP)* cells. It was *not* expressed by normal human prostate tissues and early stage prostate cancer cells. ARCaP cells were isolated from a human patient who died of metastasis of prostate cancer. Most importantly, endometase gene was turned on in human prostate cancer tissues from patients. This project has investigated a role of endometase in advanced human prostate cancer and provided knowledge for new strategies to detect and attack prostate cancer. To understand the functions of endometase, we have identified some of its physiological and pathological substrates and developed potent proteinase inhibitors targeting this protein. We have tested the *hypothesis* that this unique endometase is partially responsible for promoting cancer cell growth and invasion because of its activity as "a molecular power drill" that breaks down connective tissue barriers. Together with our collaborators and lab members, we have been developing and testing new MMP inhibitors and identify potent and selective compounds to target endometase. The inhibitors are useful tools for the investigations of the endometase active site structure and functions, and more importantly, the prostate cancer invasion and angiogenesis. We have revealed that the active site of endometase has an intermediate S1' pocket using enzyme inhibition kinetic studies, protein sequence analyses, and homology modeling. Some of these inhibitors have been tested for their stability in cell culture media and ability in invasion through extracellular matrix proteins using modified Boyden invasion chamber model. We have also examined the endometase expression pattern in human prostate and breast cancer tissues and clinical specimens and studied its pathological role in human prostate and breast cancers. Interestingly, high grade prostate intraepithelial neoplasia (HGPIN) has the highest expression levels of MMP-26, indicating that MMP-26 may play a significant role in the conversion of non-invasive tumor to invasive cancer. This project may identify a novel marker for prostate cancer detection and a new target for prostate cancer treatment.

Body

Statement of Work

Endometase in Androgen-Repressed Human Prostate Cancer

Task 1. **To examine the endometase (matrix metalloproteinase-26, MMP-26) expression pattern in normal and malignant prostate cell lines and to correlate the endometase protein expression levels with the known malignancy and metastatic potentials of the cells (Months 1-8):**

a. Culture normal and malignant prostate cells.
b. Measure the endometase expression levels by enzyme-linked immunosorbent assay (ELISA) and immunoblot using enhanced chemiluminescence (ECL). There are four specific endometase antibodies (Abs) available at the P.I.'s lab; three Abs are against the catalytic domain, one Ab is against the pro-domain.

This task has been accomplished. For more details please see Fig. 2 and Fig. 3 of the following published paper: Y.-G. Zhao, A. Xiao, R.G. Newcomer, H.I. Park, T. Kang, L.W.K. Chung, M.G. Swanson, H. E. Zhau, J. Kurhanewicz, and **Q.-X. Sang*** (2003) Activation of Pro-Gelatinase B by Endometase/Matrilysin-2 Promotes Invasion of Human Prostate Cancer Cells. *J. Biol. Chem.* **278**, 15056-15064. Please see attached reprint.

Task 2. **To over-express endometase in endometase-negative human prostate cells and characterize endometase positive cells (Months 5-25):**

a. Prepare endometase over-expression vectors.
b. Transfect pCIMMP-26 into normal human prostate cells, an androgen-dependent prostate cancer cell line LNCaP, and an androgen-independent prostate cancer cell line DU-145.
c. Identify endometase positive cells by immunological methods (ELISA and immunoblot).
d. Characterize endometase positive cells *in vitro* (colony formation on soft agar).

This task is almost completed. For more details please see Fig. 5 and Fig. 6 of the following paper published: Y.-G. Zhao, A. Xiao, R.G. Newcomer, H.I. Park, T. Kang, L.W.K. Chung, M.G. Swanson, H. E. Zhau, J. Kurhanewicz, and **Q.-X. Sang*** (2003) Activation of Pro-Gelatinase B by Endometase/Matrilysin-2 Promotes Invasion of Human Prostate Cancer Cells. *J. Biol. Chem.* **278**, 15056-15064. Please also see attached reprint and the following preliminary results (Fig. 1 and Fig. 2).

Task 3. **Analyze structure-function relationships of the endometase active site using synthetic matrix metalloproteinase (MMP) inhibitors and identify specific and potent endometase inhibitors for the cell invasion assays (Months 10-30):**

a. Optimize the synthetic fluorogenic peptide substrate cleavage assays using a Perkin-Elmer LS-50B luminescence spectrometer.
b. Measure the IC_{50} (inhibitor concentration at 50% enzyme activity) values and inhibition constants (k_I values) of new synthetic MMP inhibitors with endometase listed in *Table 1* and *Figure 2* of the proposal. Determine the inhibition kinetics and mechanisms.

This task has been accomplished. Please see attached reprints for more details:

H.I. Park, B.E. Turk, F.E. Gerkema, L.C. Cantley, and **Q.-X. Sang*** (2002) Peptide substrate specificities and protein cleavage sites of human endometase/matrilysin-2/matrix metalloproteinase-26. *J. Biol. Chem.* **277,** 35168-35175.

H.I. Park, Y. Jin, D.R. Hurst, C.A. Monroe, S. Lee, M.A. Schwartz, and **Q.-X. Sang*** (2003) The intermediate S1' pocket of the endometase/matrilysin-2 active site revealed by enzyme inhibition kinetic studies, protein sequence analyses, and homology modeling. *J. Biol. Chem.*, 278:51646-51653.

Task 4. **Identify new substrates of endometase, compare the degrees of invasiveness of the human prostate cells selected from *Task 1* and *Task 2*, and test the efficacies of MMP inhibitors selected from *Task 3* in the prostate cell invasion (Months 20-36):**

a. Test intracelluar proteins, extracellular matrix proteins, and cell surface proteins of ARCaP and other cells to identify new endometase substrates, hence, understand its putative functions.

This task is almost completed. Please see the following published paper Figs. 6-8 and tables I and II for more details. H.I. Park, B.E. Turk, F.E. Gerkema, L.C. Cantley, and **Q.-X. Sang*** (2002) Peptide substrate specificities and protein cleavage sites of human endometase/matrilysin-2/matrix metalloproteinase-26. *J. Biol. Chem.* **277,** 35168-35175.

b. Test and compare the degrees of invasiveness of human normal, malignant, and endometase over-expression prostate cells, respectively, using modifed Boyden Chambers coated with extracellular matrix proteins or cell surface proteins.
c. Test and compare the efficacies of selective MMP inhibitors from *Task 3* in prostate cell invasion. Identify specific inhibitors that may lead to future cancer therapeutics.

This task is in excellent progress. For more details please see Figs. 4-8 of the following paper published. Y.-G. Zhao, A. Xiao, R.G. Newcomer, H.I. Park, T. Kang, L.W.K. Chung, M.G. Swanson, H. E. Zhau, J. Kurhanewicz, and **Q.-X. Sang*** (2003) Activation of Pro-Gelatinase B by Endometase/Matrilysin-2 Promotes Invasion of Human Prostate Cancer Cells. *J. Biol. Chem.* **278**, 15056-15064. Please see attached reprint and the following preliminary results (Fig. 1 and Fig. 2), as well as Appendix 1, **"Effects of Novel Matrix Metalloproteinase Inhibitors on Human Prostate Cancer Cell Invasion".**

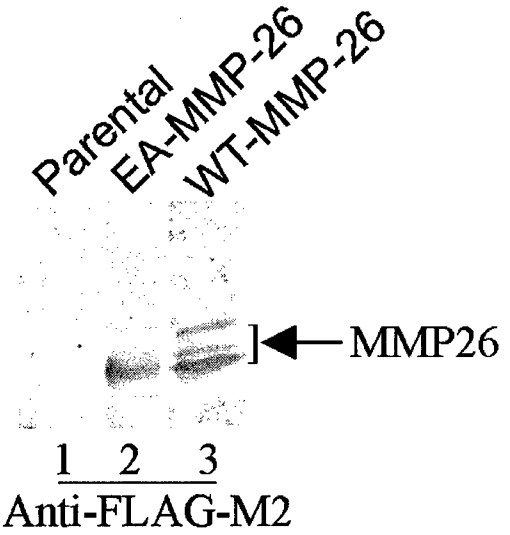

Fig. 1. Detection of MMP-26 in androgen-dependent LNCaP cells stably expressing MMP-26 wild type or an inactive form. LNCaP cells, a human prostate cancer cell line, were stably transfected with MMP-26 wild type (WT-MMP-26), or an inactive form (EA-MMP-26), both of which were tagged with FLAG tags at their C-termini. Cells were routinely cultured in DMEM supplemented with 10% fetal bovine serum and 400 μg/L of G418. For experiments, they were seeded into 24-well-plates until they reached 100% confluence. Cells were lysed with RIPA buffer, and cell lysates were analyzed by Western blotting using anti-FLAG-M2 antibody.

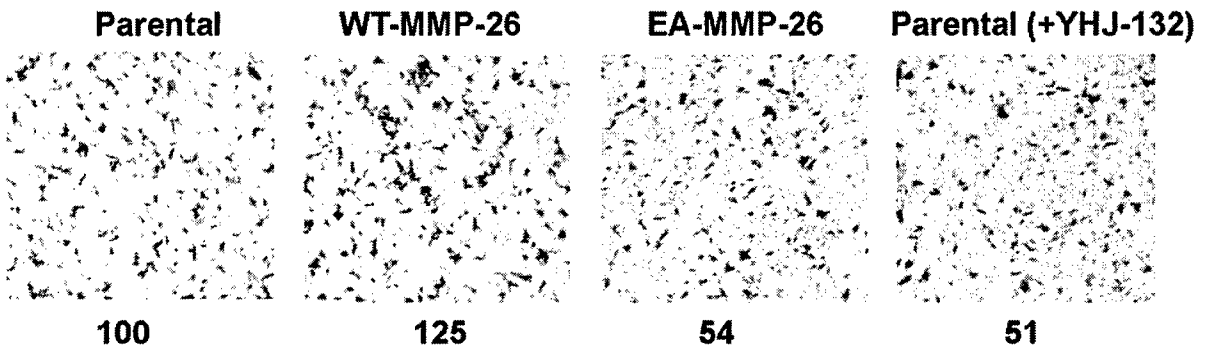

Fig. 2. MMP-26 plays a vital role in the invasion of androgen-dependent LNCaP cells. Parental LNCaP cells or its derivatives stably over-expressing MMP-26 wild type (WT-MMP-26) or inactive form (EA-MMP-26) were subjected to invasion assays utilizing a modified Boyden chamber coated with type IV collagen (25 μg/well). Following 48 hours incubation in serum-free medium alone or containing **10 μM YHJ-132, an MMP inhibitor synthesized by our group**, the inner chambers were fixed and the invading cells were photographed. Quantification of the invading cells was performed by integrated morphometry analysis (IMA); untreated parental LNCaP cells (Parental) were controls as 100% invasive. The WT-MMP-26 cells showed a 25% increase in invading cells, while the EA-MMP-26 or parental cells treated with YHJ-132 showed decreased invasion, at 54% and 51% of the parental cells, respectively.

Task 5. **Alternative approaches: Test and compare the rates of cell proliferation and apoptosis of the human prostate cells selected from *Task 1* and *Task 2* (Months 26-36):**

a. Test and compare the rates of cell proliferation of human normal, malignant, and endometase over-expression prostate cells, respectively, cultured on extracellular matrix proteins. Cell proliferation rates will be determined by assaying for 5-bromo-2'-deoxyuridine (BrdU) incorporation using the colorimetric ELISA assay kit from Boehringer Mannheim Co.

b. Test and compare the rates of cell apoptosis of human normal, malignant, and endometase over-expression prostate cells, respectively, cultured on extracellular matrix proteins. A quantitative Cell Death Detection ELISA^{PLUS} colorimetric assay kit (also from Boehringer Mannheim Co.) will be used. This assay is useful for the quantitation of apoptosis without cell labeling; it differentiates apoptosis from necrosis.

This task is in excellent progress.

Blockage of ARCaP cell invasion by MMP-26 antibodies is not due to the effects of the antibodies on cell attachment to extracellular matrix, cell proliferation, cytotoxicity, and apoptosis. Further investigation shows that the functional blocking antibodies do not affect ARCaP cell attachment to the substrates, do not inhibit ARCaP cell proliferation (**Fig. 3**), have no cytotoxicity, and do not promote the cell apoptosis, demonstrating that the diminished invasiveness of ARCaP cells is due to the functional neutralizing activity of the antibodies against MMP-26 and is not due to reduced cell numbers and is not due to reduced cell attachment to the extracellular matrix substrates.

Cells attachment experiments. 2.25×10^5 ARCap/LNCap/DU145/ PC-3 cells in serum free DMEM media containing different concentrations of one of the pre-immune-IgGs or anti-MMP-26 IgGs were cultured in fibronectin, and matrigel coated 24-well plates. The growing cells were stopped at 3 hours, 6 hours, 12 hours, 24 hours, 48 hours, and 60 hours by rinsing with PBS and fixing in 4% PFA/PBS solution. Then the cells were stained with 0.1% Crystal Violet (Sigma, USA) solution. The attached cells number was counted under in 10 high power fields (400x) of each of the duplicate samples under a microscope.

Results: The ARCaP cells number attached on the FN and Matrigel coated 24-well plate had no significant difference among the untreated wells, pre-immune IgGs treated wells and the anti-MMP-26 antibodies treated the wells ($p>0.05$) at the time points of 3 hours, 6 hours, 12 hours, 24 hours, 48 hours, and 60 hours (data not shown). These results indicate that the inhibition of ARCaP cell invasion by anti-MMP-26 antibodies is not due to the effect on the cells attachment to extracellular matrix components.

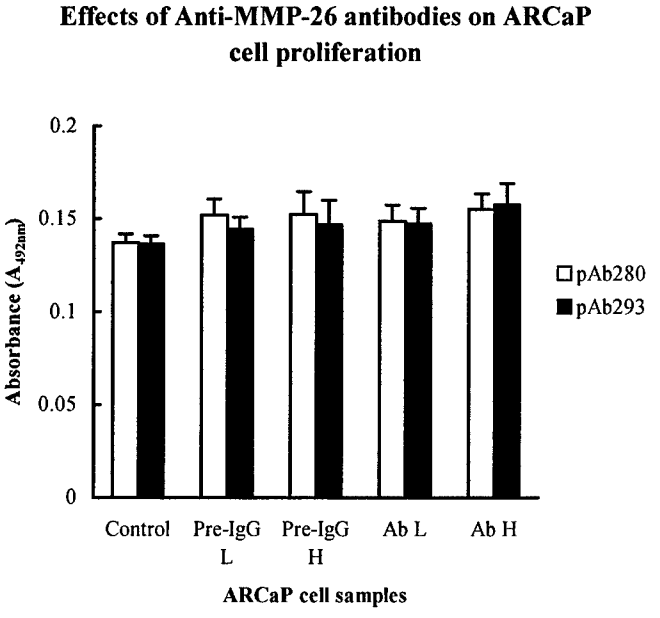

Fig. 3. The anti-MMP-26 polyclonal Abs have no effect on the proliferation of ARCaP cells. The ARCaP cells proliferation was determined using the BrdU Labeling Cell Proliferation ELISA (Roche Molecular Biochemicals, Indianapolis, IN) according to the manufacturer's instructions. **Pre-IgG L**, preimmune IgG low concentration (10μg/ml); **Pre-IgG H,** preimmune IgG high concentration (50μg/ml); **Ab L**, antibody low concentration (10μg/ml); and **Ab H,** antibody high concentration (50μg/ml).

Cells proliferation assays. ARCaP cell proliferation was determined using the Cell Proliferation ELISA from Roche Molecular Biochemicals (Indianapolis, IN) following the manufacturer's instructions. In brief, the ARCap cells were plated in a fibronectin, and matrigel pre-coated 96-well tissue culture plate (Falcon, Becton Dickinson Labware, Lincoln Park, New Jersey) at a density of 1 x 10^4 cells/well in DMEM medium containing 10% FBS for 24 hours. Then the cells were cultured in serum free DMEM medium in the presence of pre-immune IgG of 98R3, pre-immune IgG of 98R12, pAb280 and pAb293 (10μg/ml, 50μg/ml, respectively) in duplicate wells for another 24 hours. After adding BrdU (100μM) labeling solution for 12 hours in 37° C, 5%CO_2, the cells were fixed by adding FixDenat solution for 30mins at room temperature. Followed by adding anti-BrdU POD and incubated for 90 min at room temperature. Finally, added substrate and incubate for 30 mins and the values of absorbance were read at 492 nm using an Automatic Microplate Reader (Titertek Multiskan MC-340, Flow Laboratories, Virginia). Standard deviations were calculated and were presented as error bars in the Figures.

Key Research Accomplishments

1. This research project has addressed many of the tasks listed in the "Statement of Work", generated three papers published in "The Journal of Biological Chemistry", one "Cancer Research" paper, and one "Biochemical Journal paper". The grant also supported training of research students and postdoctoral associates.

2. This work has verified a putative biochemical mechanism by which endometase/matrilysin-2/matrix metalloproteinase-26 (MMP-26) may promote human prostate cancer cell invasion.

3. We showed that the levels of MMP-26 protein in human prostate carcinomas from multiple patients were significantly higher than those in prostatitis, benign prostate hyperplasia, and normal prostate glandular tissues. Statistical analyses have been performed.

4. MMP-26 was capable of activating pro-MMP-9 by cleavage at the Ala^{93}-Met^{94} site of the prepro-enzyme. This activation proceeded in a time- and dose-dependent manner, facilitating the efficient cleavage of fibronectin by MMP-9. The activated MMP-9 products generated by MMP-26 appeared more stable than those cleaved by MMP-7 under the conditions tested.

5. To investigate the contribution of MMP-26 to cancer cell invasion via the activation of MMP-9, highly invasive and metastatic human prostate carcinoma cells, androgen-repressed prostate cancer (ARCaP) cells, were selected as a working model. ARCaP cells express both MMP-26 and MMP-9. Specific anti-MMP-26 and anti-MMP-9 functional blocking antibodies both reduced the invasiveness of ARCaP cells across fibronectin or type IV collagen.

6. The introduction of MMP-26 antisense cDNA into ARCaP cells reduced the MMP-26 protein level in these cells and strongly suppressed the invasiveness of ARCaP cells.

7. Double immunofluorescence staining and confocal laser scanning microscopic images revealed that MMP-26 and MMP-9 were co-localized in parental and MMP-26 sense-transfected ARCaP cells. Moreover, MMP-26 and MMP-9 proteins were both expressed in the same human prostate carcinoma tissue samples examined.

8. These results indicate that MMP-26 may be a physiological and pathological activator of pro-MMP-9, and the activation of pro-MMP-9 by MMP-26 may be an important mechanism contributing to the invasive capabilities of prostate carcinomas.

9. Peptide libraries were used to profile the substrate specificity of MMP-26 from the P4 to P4′ sites. The optimal cleavage motifs for MMP-26 were Lys-Pro-Ile/Leu-Ser (P1)-Leu/Met (P1′)-Ile/Thr-Ser/Ala-Ser.

10. The strongest preference was observed at the P1′ and P2 sites where hydrophobic residues were favored. Proline was preferred at P3 and Serine at P1. The overall specificity was similar to that of other MMPs except that more flexibility was observed at P1, P2′, and P3′.

11. Synthetic inhibitors of gelatinases and collagenases inhibited MMP-26 with similar efficacy. A pair of stereoisomers had a only 40-fold difference in K_i^{app} values against MMP-26 compared to a 250-fold difference against neutrophil collagenase, indicating that MMP-26 is less stereo-selective for its inhibitors.

12. MMP-26 auto-digested itself during the folding process; two of the major autolytic sites were Leu^{49}-Thr^{50} and Ala^{75}–Leu^{76}, which still left the cysteine switch sequence (PH**C**^{82}GVPD) intact. This suggests that Cys^{82} may not play a role in the latency of the zymogen.

13. MMP-26 cleaved Phe^{352}–Leu^{353} and Pro^{357}–Met^{358} in the reactive loop of alpha 1 proteinase inhibitor and His^{140}–Val^{141} in insulin-like growth factor binding protein-1, likely rendering these substrates inactive.

14. Among the fluorescent peptide substrates analyzed, Mca-Pro-Leu-Ala-Nva-Dpa-Ala-Arg-NH_2 displayed the highest specificity constant (30000 / Molar second) with MMP-26.

15. The intermediate S1' pocket of the endometase active site has been revealed by enzyme inhibition kinetic studies using our novel MMP inhibitors, protein sequence analyses, and molecular modeling/computational biochemistry.

16. Potent and selective inhibitors of endometase have been identified and tested in biochemical experiments, and some preliminary data were also obtained for the inhibition of human prostate cancer cell invasion by one of the potent inhibitors.

17. Transgenic human prostate cancer cell lines (both androgen-repressed and androgen-dependent) have been made and MMP-26 over-expression cells, knock out cells, and dominant-negative catalytically inactive mutants have been generated and tested. The degree of invasiveness of these human prostate cancer cell lines were correlated with the expression levels of MMP-26 protein. These results verified our hypotheses.

18. Human breast cancer tissues were examined as controls for prostate cancer studies. Breast carcinoma *in situ* also expressed high levels of MMP-26 and MMP-26 may play a role in the initiation of invasion of human breast cancers.

19. Tissue inhibitors of metalloproteinases TIMP-2 and TIMP-4 are potent inhibitors of MMP-26 and they have inhibited the activation of pro-MMP-9 by MMP-26.

20. MMP-26 gene is expressed by human breast carcinoma/epithelial cancer cells as examined by *in situ* hybridization, confirming MMP-26 is expressed by epithelial cells

and its epithelial origin. These data have been reported in the "Cancer Research" paper. Please see attached reprints.

21. This report proposes a working model for the future studies of proMMP-26 activation, the design of inhibitors, and the identification of optimal physiological and pathological substrates of MMP-26 *in vivo*.

22. This report showed the relative stability and efficacy of some of the novel inhibitors in inhibiting human prostate cancer cell invasion. These inhibitors blocked the activities of matrix metalloproteinases under cell culture conditions.

23. Almost all the major tasks have been accomplished and more promising data are still generated.

24. This report demonstrates that the PI's laboratory has been very productive and produced exceptional results beyond what have been described in the Statement of Work. Twelve scientific research papers related to this project have been published and additional manuscripts are in progress and under preparation.

Reportable Outcomes

A. Published papers and manuscripts submitted and in preparation:

1. H.I. Park, B.E. Turk, F.E. Gerkema, L.C. Cantley, and **Q.-X. Sang*** (2002) Peptide substrate specificities and protein cleavage sites of human endometase/matrilysin-2/matrix metalloproteinase-26. *J. Biol. Chem.* **277,** 35168-35175.

2. T.-B. Kang, Y.-G. Zhao, D. Pei, J.F. Sucic, and **Q.-X. Sang*** (2002) Intracellular activation of human adamalysin 19/disintegrin and metalloproteinase 19 by furin occurs via one of the two consecutive recognition sites. *J. Biol. Chem.* **277,** 25583-25591.

3. T. Kang, H. I., Park, Y. Suh, Y.-G. Zhao, H. Tschesche, and **Q.-X. Sang*** (2002) Autolytic Processing at Glu(586)-Ser(587) within the Cysteine-rich Domain of Human Adamalysin 19/Disintegrin-metalloproteinase 19 is Necessary for its Proteolytic Activity. *J. Biol. Chem.* **277,** 48514-48522

4. Y.-G. Zhao, A. Xiao, R.G. Newcomer, H.I. Park, T. Kang, L.W.K. Chung, M.G. Swanson, H. E. Zhau, J. Kurhanewicz, and **Q.-X. Sang*** (2003) Activation of Pro-Gelatinase B by Endometase/Matrilysin-2 Promotes Invasion of Human Prostate Cancer Cells. *J. Biol. Chem.* **278,** 15056-15064.

5. H.I. Park, Y. Jin, D.R. Hurst, C.A. Monroe, S. Lee, M.A. Schwartz, and **Q.-X. Sang*** (2003) The intermediate S1' pocket of the endometase/matrilysin-2 active site revealed by enzyme inhibition kinetic studies, protein sequence analyses, and homology modeling. *J. Biol. Chem.*, 278:51646-51653.

6. X. Liao, J.B. Thrasher, J. Pelling, J. Holzbeierlein, Q.-X. Sang, and B. Li (2003) Androgen stimulates matrix metalloproteinase-2 expression in human prostate cancer. *Endocrinology.* **144,** 1656-1663.

7. D. R. Hurst, M.A. Schwartz, M.A. Ghaffari, Y. Jin, H. Tschesche, G.B. Fields, and **Q.-X. Sang*** (2004) Catalytic- and ecto-domains of membrane type 1-matrix metalloproteinase have similar inhibition profiles but distinct endopeptidase activities. *Biochem. J.* **377,** 775-779.

8. Y.-G. Zhao, A.-Z. Xiao, H.I. Park, R.G. Newcomer, M. Yan, Y.-G. Man, S.C. Heffelfinger, and **Q.-X. Sang*** (2004) Endometase/matrilysin-2 in human breast ductal carcinoma *in situ* and its inhibition by tissue inhibitors of metalloproteinases-2 and -4: a putative role in the initiation of breast cancer invasion. *Cancer Res.* **64,** 590-598.

9. T. Kang, H. Tschesche, and **Q.-X. Sang*** (2004) Evidence for Disulfide Involvement in the Regulation of Intramolecular Autolytic Processing by Human Adamalysin19/ADAM19. *Exp. Cell Res.* **298,** 285-295.

10. Y.-G. Man* and **Q.-X. Sang*** (2004) The Significance of Focal Myoepithelial Cell Layer

Disruptions in Human Breast Tumor Invasion: a Paradigm Shift from the "Protease-centered" Hypothesis. *Exp. Cell Res.* **301,** 103-118.

11. W. Qiu, S.-X. Bai, M.-R. Zhao, X.-Q. Wu, Y.-G. Zhao, **Q.-X. Sang**, Y.-L. Wang (2005) Spatio-temporal expression of matrix metalloproteinase-26 in human placental trophoblasts and fetal red cells during normal placentation. *Biol. Reprod.* **72,** 954-959 [Epub ahead of print, 2004 Dec 15].

12. Y.-G. Man, T. Shen, Y.-G. Zhao, and **Q.-X. Sang** (2005) Focal prostate basal cell layer disruptions and leukocyte infiltration are correlated events: A potential mechanism for basal cell layer disruptions and tumor invasion. *Cancer Detect. Prevent.* In press.

13. Y.-G. Man, T. Shen, **Q.-X. Sang**, P.E. Berg, and A.M. Schwartz (2005) Cell clusters in a subset of *in situ* breast tumors show an unusual growth pattern: implications for invasion and metastasis. *Cancer Detect. Prevent.* Accept pending satisfactory revision.

14. Y.-G. Man*, **Q.-X. Sang***, C. Zhao, C. Mannion, and W.A. Gardner (2005) Focal Basal Cell Degeneration with T-lymphocyte and Mast Cell Infiltration is Associated with Onset of Human Prostate Tumor Invasion. *Exp. Cell Res.* Submitted.

15. D. Wildeboer, S. Naus, **Q.-X. Sang**, J.W. Bartsch, and A. Pagenstecher (2005) Distinct expression levels and activities of human metalloproteinase-disintegrins including ADAM8 and ADAM19 in primary brain tumors. *Am. J. Pathol.* Submitted.

16. D.R. Hurst, M.A. Schwartz, Y.-H. Jin, M.A. Ghaffari, and **Q.-X. Sang*** (2005). Inhibition characteristics of membrane type 1-matrix metalloproteinase with novel mercaptosulfide inhibitors. *Biochem. J.* In preparation.

17. S. Lee, H.I. Park, and **Q.-X. Sang*** (2005) Structural and functional role of calcium ions in Human Endometase/Matrilysin 2/MMP-26. *J. Biol. Chem.* In preparation.

18. K. K. Desai, R.G. Newcomer, K.A. Iczkowski, Y.-G. Zhao, W.W. Tan, K.J. Wu, M.D. Roycik, and **Q.-X. Sang*** (2005) TIMP-4 in Human Prostate: Its correlation with the malignant potential of HGPIN and coordination with MMP-26. *Biochem. Biophy. Res. Commun.* In preparation.

B. In addition to the Principal Investigator, Dr. Sang, the following students and research associates at Professor Sang's laboratory have been partially funded by this grant.

Douglas R. Hurst, Graduate Student Research Assistant
Robert G. Newcomer, Graduate Student Assistant
Mark Dru Roycik, Graduate Student Assistant
Megan E. Moruski, Undergraduate Student Assistant
Jennifer Walker, Undergraduate Student Assistant
Kevin K. Desai, Undergraduate Student Assistant

Dr. Hyun I. Park, Postdoctoral Research Associate
Dr. Yunge Zhao, Postdoctoral Research Associate
Margaret Mary Coryn, Student Assistant
Sara C. Monroe, Research Assistant
Dr. Tiebang Kang, Postdoctoral Research Associate
Dr. Aizhen Xiao, Postdoctoral Research Associate

Conclusions

The spread of prostate cancer cells to other parts of the body is the leading cause of patient death. In 2000, we reported the discovery, cloning, and characterization of human matrix metalloproteinase-26 (MMP-26), **endometase**. We have been testing three specific hypotheses: 1) The expression levels of MMP-26 is correlated with the metastatic potentials and the degrees of malignancy of human prostate cells; 2) MMP-26 has unique structure and enzymatic function; 3) MMP-26 enhances prostate cancer invasion by digesting extracellular matrix proteins and inactivating serine proteinase inhibitors, and specific inhibitors of MMP-26 block prostate cancer invasion. We have showed that the levels of MMP-26 protein in human prostate carcinomas from multiple patients were significantly higher than those in prostatitis, benign prostate hyperplasia, and normal prostate glandular tissues. High levels of MMP-26 is also expressed by human breast ductal carcinoma *in situ*. Both MMP-26 gene and protein are expressed by the carcinoma cells confirming its epithelial origin. MMP-26 promoted prostate cancer invasion via activation of pro-gelatinase B/MMP-9. Functional blocking antibodies against either MMP-26 or MMP-9 blocked human prostate cancer cell invasion. Furthermore, antisense cDNA of MMP-26 and catalytically inactive mutant MMP-26 also inhibited prostate cancer cell invasion. The over-expression of MMP-26 cDNA in both androgen-dependent and independent cells lines enhanced the invasiveness of these cells. Tissue inhibitors of metalloproteinases TIMP-2 and TIMP-4 are also potent inhibitors of MMP-26. The endometase active site structure and function have been investigated and revealed to have an intermediate S1' pocket using synthetic metalloproteinase inhibitors, protein sequence analyses and homology modeling studies. These findings may aid in rational inhibitor/potential drug design for the development of more potent and selective inhibitors of MMP-26. Optimal peptide substrate specificity and protein cleavage sites have been identified in both peptide libraries and potentially physiologically relevant proteins. These results suggest that endometase/MMP-26 may promote human prostate and breast cancer cell invasion and it is specifically expressed in human prostate and breast cancer tissues. Some of these inhibitors have been tested for their stability in cell culture media and ability in invasion through extracellular matrix proteins using modified Boyden invasion chamber model. Those inhibitors are relatively stable and effective in inhibiting human prostate cancer cell invasion. We have also examined the endometase expression pattern in human prostate and breast cancer tissues and clinical specimens and studied its pathological role in human prostate and breast cancers. Interestingly, high grade prostate intraepithelial neoplasia (HGPIN) has the highest expression levels of MMP-26, indicating that MMP-26 may play a significant role in the conversion of non-invasive tumor to invasive cancer. This project may identify a novel marker for prostate cancer detection and a new target for prostate cancer treatment. Almost all the major tasks have been accomplished and more promising data are still generated. This report demonstrates that the PI's laboratory has been very productive and produced exceptional results beyond what have been described in the Statement of Work. Twelve scientific research papers related to this project have been published and additional manuscripts are in progress and under preparation. This project has been extended for one more year to complete all the tasks under a Federal Demonstration, No-cost Extension for 12-month Agreement.

References

Please see references cited in the following 9 papers and appendices:

1. H.I. Park, B.E. Turk, F.E. Gerkema, L.C. Cantley, and **Q.-X. Sang*** (2002) Peptide substrate specificities and protein cleavage sites of human endometase/matrilysin-2/matrix metalloproteinase-26. *J. Biol. Chem.* **277,** 35168-35175.

2. Y.-G. Zhao, A. Xiao, R.G. Newcomer, H.I. Park, T. Kang, L.W.K. Chung, M.G. Swanson, H. E. Zhau, J. Kurhanewicz, and **Q.-X. Sang*** (2003) Activation of Pro-Gelatinase B by Endometase/Matrilysin-2 Promotes Invasion of Human Prostate Cancer Cells. *J. Biol. Chem.* **278,** 15056-15064.

3. H.I. Park, Y. Jin, D.R. Hurst, C.A. Monroe, S. Lee, M.A. Schwartz, and **Q.-X. Sang*** (2003) The intermediate S1' pocket of the endometase/matrilysin-2 active site revealed by enzyme inhibition kinetic studies, protein sequence analyses, and homology modeling. *J. Biol. Chem.*, 278:51646-51653.

4. X. Liao, J.B. Thrasher, J. Pelling, J. Holzbeierlein, Q.-X. Sang, and B. Li (2003) Androgen stimulates matrix metalloproteinase-2 expression in human prostate cancer. *Endocrinology.* **144,** 1656-1663.

5. D. R. Hurst, M.A. Schwartz, M.A. Ghaffari, Y. Jin, H. Tschesche, G.B. Fields, and **Q.-X. Sang*** (2004) Catalytic- and ecto-domains of membrane type 1-matrix metalloproteinase have similar inhibition profiles but distinct endopeptidase activities. *Biochem. J.* **377,** 775-779.

6. Y.-G. Zhao, A.-Z. Xiao, H.I. Park, R.G. Newcomer, M. Yan, Y.-G. Man, S.C. Heffelfinger, and **Q.-X. Sang*** (2004) Endometase/matrilysin-2 in human breast ductal carcinoma *in situ* and its inhibition by tissue inhibitors of metalloproteinases-2 and -4: a putative role in the initiation of breast cancer invasion. *Cancer Res.* **64,** 590-598.

7. T. Kang, H. Tschesche, and **Q.-X. Sang*** (2004) Evidence for Disulfide Involvement in the Regulation of Intramolecular Autolytic Processing by Human Adamalysin19/ADAM19. *Exp. Cell Res.* **298,** 285-295.

8. Y.-G. Man* and **Q.-X. Sang*** (2004) The Significance of Focal Myoepithelial Cell Layer Disruptions in Human Breast Tumor Invasion: a Paradigm Shift from the "Protease-centered" Hypothesis. *Exp. Cell Res.* **301,** 103-118.

9. Y.-G. Man, T. Shen, Y.-G. Zhao, and **Q.-X. Sang** (2005) Focal prostate basal cell layer disruptions and leukocyte infiltration are correlated events: A potential mechanism for basal cell layer disruptions and tumor invasion. *Cancer Detect. Prevent.* In press.

Appendices

Appendix 1. Effects of Novel Matrix Metalloproteinase Inhibitors on Human Prostate Cancer Cell Invasion (attached below)

Appendix 2. Eleven papers/reprints are attached.

1. H.I. Park, B.E. Turk, F.E. Gerkema, L.C. Cantley, and **Q.-X. Sang*** (2002) Peptide substrate specificities and protein cleavage sites of human endometase/matrilysin-2/matrix metalloproteinase-26. *J. Biol. Chem.* **277,** 35168-35175.

2. T.-B. Kang, Y.-G. Zhao, D. Pei, J.F. Sucic, and **Q.-X. Sang*** (2002) Intracellular activation of human adamalysin 19/disintegrin and metalloproteinase 19 by furin occurs via one of the two consecutive recognition sites. *J. Biol. Chem.* **277,** 25583-25591.

3. T. Kang, H. I., Park, Y. Suh, Y.-G. Zhao, H. Tschesche, and **Q.-X. Sang*** (2002) Autolytic Processing at Glu(586)-Ser(587) within the Cysteine-rich Domain of Human Adamalysin 19/Disintegrin-metalloproteinase 19 is Necessary for its Proteolytic Activity. *J. Biol. Chem.* **277,** 48514-48522

4. Y.-G. Zhao, A. Xiao, R.G. Newcomer, H.I. Park, T. Kang, L.W.K. Chung, M.G. Swanson, H. E. Zhau, J. Kurhanewicz, and **Q.-X. Sang*** (2003) Activation of Pro-Gelatinase B by Endometase/Matrilysin-2 Promotes Invasion of Human Prostate Cancer Cells. *J. Biol. Chem.* **278,** 15056-15064.

5. H.I. Park, Y. Jin, D.R. Hurst, C.A. Monroe, S. Lee, M.A. Schwartz, and **Q.-X. Sang*** (2003) The intermediate S1' pocket of the endometase/matrilysin-2 active site revealed by enzyme inhibition kinetic studies, protein sequence analyses, and homology modeling. *J. Biol. Chem.*, 278:51646-51653.

6. X. Liao, J.B. Thrasher, J. Pelling, J. Holzbeierlein, Q.-X. Sang, and B. Li (2003) Androgen stimulates matrix metalloproteinase-2 expression in human prostate cancer. *Endocrinology.* **144,** 1656-1663.

7. D. R. Hurst, M.A. Schwartz, M.A. Ghaffari, Y. Jin, H. Tschesche, G.B. Fields, and **Q.-X. Sang*** (2004) Catalytic- and ecto-domains of membrane type 1-matrix metalloproteinase have similar inhibition profiles but distinct endopeptidase activities. *Biochem. J.* **377,** 775-779.

8. Y.-G. Zhao, A.-Z. Xiao, H.I. Park, R.G. Newcomer, M. Yan, Y.-G. Man, S.C. Heffelfinger, and **Q.-X. Sang*** (2004) Endometase/matrilysin-2 in human breast ductal carcinoma *in situ* and its inhibition by tissue inhibitors of metalloproteinases-2 and -4: a putative role in the initiation of breast cancer invasion. *Cancer Res.* **64,** 590-598.

9. T. Kang, H. Tschesche, and **Q.-X. Sang*** (2004) Evidence for Disulfide Involvement in the Regulation of Intramolecular Autolytic Processing by Human Adamalysin19/ADAM19. *Exp. Cell Res.* **298,** 285-295.

10. Y.-G. Man* and **Q.-X. Sang*** (2004) The Significance of Focal Myoepithelial Cell Layer Disruptions in Human Breast Tumor Invasion: a Paradigm Shift from the "Protease-centered" Hypothesis. *Exp. Cell Res.* **301,** 103-118.

11. Y.-G. Man, T. Shen, Y.-G. Zhao, and **Q.-X. Sang** (2005) Focal prostate basal cell layer disruptions and leukocyte infiltration are correlated events: A potential mechanism for basal cell layer disruptions and tumor invasion. *Cancer Detect. Prevent.* In press.

Appendix 1

Effects of Novel Synthetic Matrix Metalloproteinase Inhibitors on Human Prostate Cancer Cell Invasion

Yunge Zhao, Aizhen Xiao, and Qing-Xiang Amy Sang*

MATERIALS AND METHODS

1. **Stability assay** of YHJ-132 and YHJ-294 in cell culture media was performed:
   Enzyme: MT1-MMP CD domain (Final Concentration 2 nM)

   Substrate: M1895 (Final Concentration 1 uM)

   Assay buffer: (50 mM HEPES, 150 mM NaCl, 10 mM CaCL2, 0.02% Brij-35).

   Temperature: 25C (consistent)

   Media: DMEM (low glucose) +10% FBS or serum free DMEM media.

   Excitation Wavelength: 328 nm

   Emission Wavelength: 393 nm

   Incubation time: 15-20 minutes

2. **ARCaP cell invasion assay**: Modified Boyden Chamber Model.

   The invasiveness of ARCaP cells cultured in the presence of MMP inhibitors through reconstructed ECM was determined. The concentration of YHJ-132 or YHJ-294 was 1, 5, 10, 25, 50 and/or 100 μM. 0.5% ethanol was used as control. Because YHJ-132 is very stable in cell culture media, added every 24 hours. YHJ-294 is not very stable in cell culture media, added every 8-10 hours. The same amount of ethanol was also added into the ethanol control wells at the same time. Briefly, modified Boyden chambers containing polycarbonate filters with 8-μm pores (Becton Dickinson, Boston, MA) were coated with 100 μl (0.5 mg/ml) human plasma FN (Gibco, Carlsbad, California) or (0.5mg/ml) type IV collagen (Sigma) or Matrigel. Three hundred μl of prepared cell suspension (1×10^6 cells/ml) in serum-free medium was added to each insert, and 500 μl of media containing 10% fetal bovine serum was added to the lower chamber. After 48 hours of incubation, invasive cells that had passed through the filters to the lower surface of the membrane were fixed in 4% paraformaldehyde (PFA) (Sigma, St. Louis, Missouri). The cells were then stained with 0.1% Crystal Violet solution and photographed with an Olympus DP10 digital camera (Melville, NY) under a Nikon FX microscope (Melville, NY). The cells were then counted by Integrated Morphometry Analysis (IMA).

3. Gelatin Zymography: Media from each insert was collected for gelatin zymogram analyses according to standard method that we described on our JBC and Cancer Research papers.

RESULTS

YHJ-1323 is a very stable MMPI in cell culture system. It keeps stable up to 24 even 48 hours. While YHJ-294 is less stable, which only last 6 hours in cell culture system. These indicate that YHJ-294 has to be added every 6-10 hour to keep effect in the cell culture system.

Please see the attached results sheets for details.

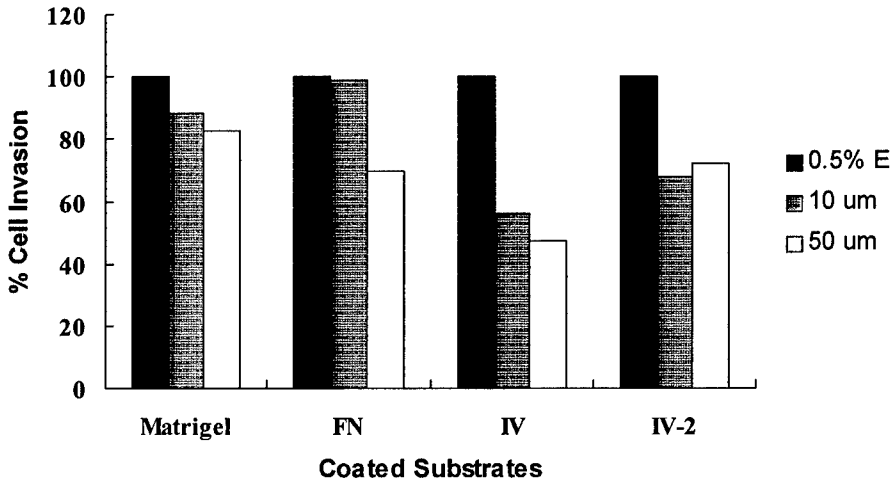

Inhibition of ARCaP Cell Invasion by YHJ-132

(FN, fibronectin; IV, type IV collagen, IV-2, type IV collagen repeat, E, ethanol)
Notice: The YHJ-132 concentration in IV and IV-2 is 25 μM instead of 10 μM.

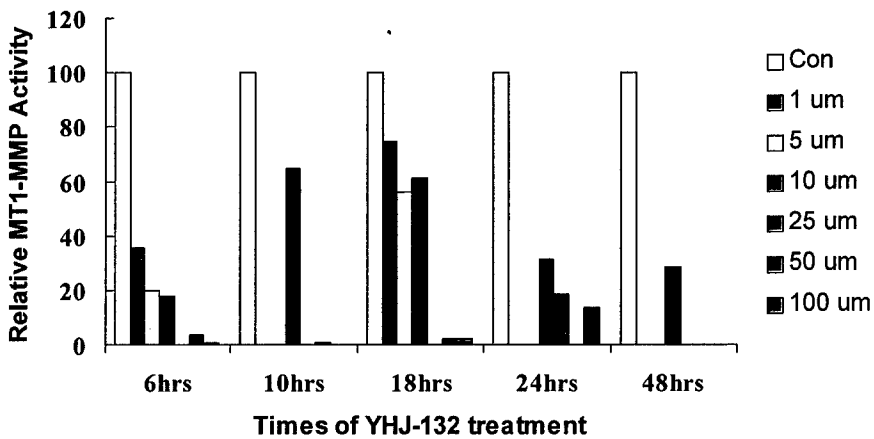

Stability of YHJ-132 in Cell Culture Media

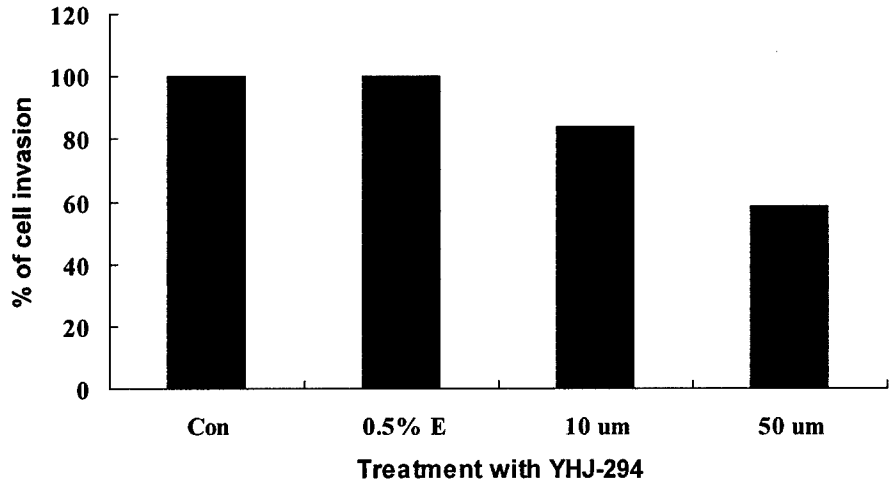

YHJ-294 Inhibits ARCaP cells invasion through Matrigel

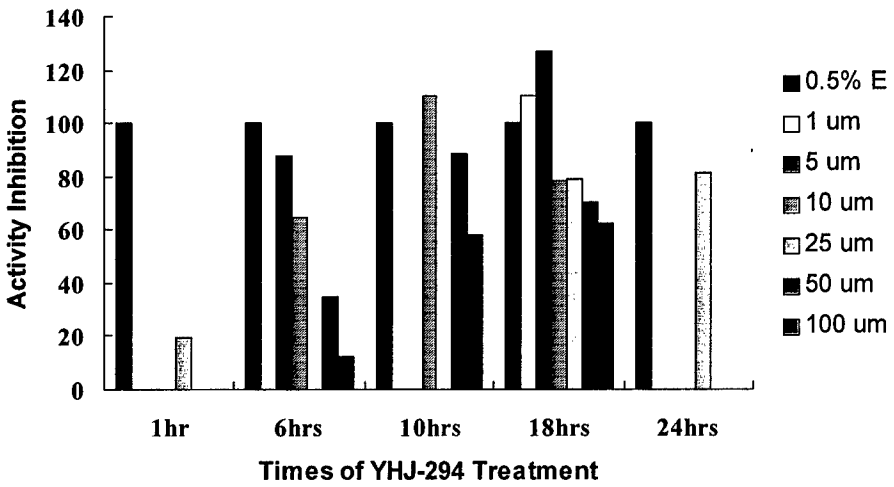

Stability of YHJ-294 in Cell Culture Media
(Con, Control; E, ethanol; YHJ-294, MMPI)

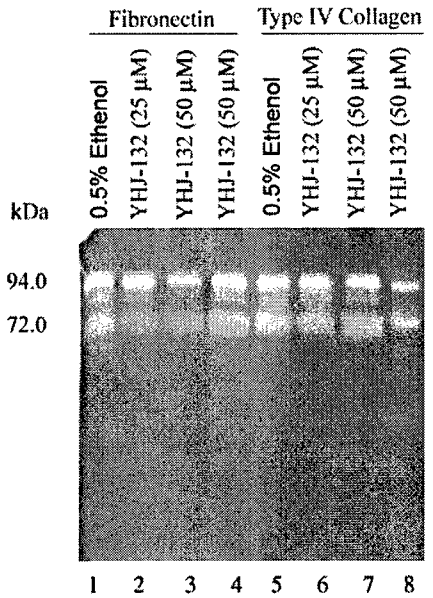

Zymography Analysis of ARCaP Invasion Media with or without YHJ-132 Treatment

THE JOURNAL OF BIOLOGICAL CHEMISTRY
Vol. 277, No. 38, Issue of September 20, pp. 35168–35175, 2002
Printed in U.S.A.

Peptide Substrate Specificities and Protein Cleavage Sites of Human Endometase/Matrilysin-2/Matrix Metalloproteinase-26*

Received for publication, May 23, 2002, and in revised form, July 5, 2002
Published, JBC Papers in Press, July 15, 2002, DOI 10.1074/jbc.M205071200

Hyun I. Park‡, Benjamin E. Turk§, Ferry E. Gerkema‡, Lewis C. Cantley§, and Qing-Xiang Amy Sang‡¶

From the ‡Department of Chemistry and Biochemistry and Institute of Molecular Biophysics, Florida State University, Tallahassee, Florida 32306-4390 and the §Department of Medicine, Harvard Medical School, Beth Israel Deaconess Medical Center, Boston, Massachusetts 02215

Human endometase/matrilysin-2/matrix metalloproteinase-26 (MMP-26) is a novel epithelial and cancer-specific metalloproteinase. Peptide libraries were used to profile the substrate specificity of MMP-26 from the P4–P4′ sites. The optimal cleavage motifs for MMP-26 were Lys-Pro-Ile/Leu-Ser(P1)-Leu/Met(P1′)-Ile/Thr-Ser/Ala-Ser. The strongest preference was observed at the P1′ and P2 sites where hydrophobic residues were favored. Proline was preferred at P3, and Serine was preferred at P1. The overall specificity was similar to that of other MMPs with the exception that more flexibility was observed at P1, P2′, and P3′. Accordingly, synthetic inhibitors of gelatinases and collagenases inhibited MMP-26 with similar efficacy. A pair of stereoisomers had only a 40-fold difference in K_i^{app} values against MMP-26 compared with a 250-fold difference against neutrophil collagenase, indicating that MMP-26 is less stereoselective for its inhibitors. MMP-26 autodigested itself during the folding process. Two of the major autolytic sites were Leu^{49}–Thr^{50} and Ala^{75}–Leu^{76}, which still left the cysteine switch sequence ($PHC^{82}GVPD$) intact. This suggests that Cys^{82} may not play a role in the latency of the zymogen. Interestingly, inhibitor titration studies revealed that only ~5% of the total MMP-26 molecules was catalytically active, indicating that the thiol groups of Cys^{82} in the active molecules may be dissociated or removed from the active site zinc ions. MMP-26 cleaved Phe^{352}–Leu^{353} and Pro^{357}–Met^{358} in the reactive loop of α_1-proteinase inhibitor and His^{140}–Val^{141} in insulin-like growth factor-binding protein-1, probably rendering these substrates inactive. Among the fluorescent peptide substrates analyzed, Mca-Pro-Leu-Ala-Nva-Dpa-Ala-Arg-NH_2 displayed the highest specificity constant (30,000/molar second) with MMP-26. This report proposes a working model for the future studies of pro-MMP-26 activation, the design of inhibitors, and the identification of optimal physiological and pathological substrates of MMP-26 *in vivo*.

Matrix metalloproteinases (MMPs)[1] share a conservative metal binding sequence of HE*X*GH*XX*G*XX*HS and a turn containing methionine (1). Evidence suggests that MMPs may play important roles in extracellular matrix (ECM) remodeling in physiological processes (2, 3). Excessive breakdown of the ECM by MMPs is observed in pathological conditions including periodontitis, rheumatoid arthritis, and osteoarthritis. MMPs also participate in tumor cell invasion and metastasis by degrading the basement membrane and other ECM components and allowing the cancer cells to gain access to blood and lymphatic vessels (4). Analyses of a large number of peptide and protein substrates and more recent work with phage display and synthetic peptide libraries have led to the identification of consensus cleavage site motifs for a number of different MMPs (5–13). The substrate specificities of MMPs are quite similar to each other, showing strong preferences for hydrophobic residues at P1′. Although distinct MMPs often prefer the same type of amino acid residues at corresponding positions surrounding the cleavage site, differences in the orders of preference for specific residues at each position may more precisely determine MMP specificity for substrates.

Endometase (matrilysin-2/MMP-26) is the smallest member of the MMP family, with a molecular mass of 28 kDa (14–17). Sequence homology calculations identified metalloelastase (MMP-12) and stromelysin-1 (MMP-3) as the closest relatives. Nevertheless, the specificity constant profile of peptide substrates with MMP-26 was quite different from that with MMP-12 and MMP-3 (14). According to protein substrate studies *in vitro*, MMP-26 might process matrix proteins such as fibronectin, vitronectin, fibrinogen, type IV collagen, gelatinase B (MMP-9), and gelatin (14–17).

MMP-26 has been found to be highly expressed in several cancer cell lines. A significant level of expression in normal tissues was found only in the uterus and placenta. The limited occurrence of MMP-26 in normal tissues suggests that the production of this enzyme may be strictly regulated during specific events, such as implantation, and that MMP-26 could be a target enzyme for the treatment of cancer and other pathological conditions.

The biological function and substrate specificity of MMP-26 are not yet fully understood. According to the protein substrate

* This work was supported in part by a Department of Defense, U. S. Army Prostate Cancer Research Program Grant DAMD17-02-1-0238; a grant from the American Cancer Society, Florida Division F01FSU-1, the National Institutes of Health Grant CA78646; a grant from the Florida State University Research Foundation (to Q.-X. A. S.); National Science Foundation Postdoctoral Training Grant DBI 9602233 (to H. I. P.); National Institutes of Health Grant GM56203 (to L. C. C. and B. E. T.); and National Institutes of Health NRSA Fellowship GM19895 (to B. E. T.). The costs of publication of this article were defrayed in part by the payment of page charges. This article must therefore be hereby marked "*advertisement*" in accordance with 18 U.S.C. Section 1734 solely to indicate this fact.

¶ To whom correspondence should be addressed: Dept. of Chemistry and Biochemistry, Florida State University, Chemistry Research Bldg. (DLC), Rm. 203, Tallahassee, FL 32306-4390. Tel.: 850-644-8683; Fax: 850-644-8281; E-mail: qxsang@chem.fsu.edu; Website: www.chem.fsu.edu/editors/sang/sang.html.

[1] The abbreviations used are: MMP, matrix metalloproteinase; α_1-PI, α_1-protease inhibitor; Brij-35, polyoxyethylene lauryl ether; IGFBP-1, insulin-like growth factor binding protein-1; MALDI-TOF MS, matrix-assisted laser desorption ionization time-of-flight mass spectrometry; ECM, extracellular matrix; Tricine, *N*-[2-hydroxy-1,1-bis(hydroxymethyl)ethyl]glycine; Dnp, 2,4-dinitrophenyl; Dpa, *N*-3-(2,4-dinitrophenyl)-L-2,3-diaminopropionyl; Mca, (7-methoxycoumarin-4-yl)acetyl; Nva, non-valine.

studies *in vitro*, it may participate in ECM degradation. In this study, we take a step forward toward understanding the biochemical properties and functions of MMP-26 by identifying the cleavage sites of protein and peptide substrates, characterizing the substrate specificities of MMP-26 and measuring the potencies of synthetic inhibitors.

EXPERIMENTAL PROCEDURES

Materials—Dnp-Pro-Leu-Gly-Met-Trp-Ser-Arg-OH, Dnp-Pro-Leu-Ala-Tyr-Trp-Ala-Arg-OH, Mca-Pro-β-cyclohexylalanyl-Gly-Nva-His-Ala-Dpa-NH_2, Mca-Pro-Leu-Ala-Nva-Dpa-Ala-Arg-NH_2, insulin-like growth factor binding protein-1 (IGFBP-1), and MMP-specific synthetic inhibitors were purchased from Calbiochem, and Dnp-Pro-Leu-Gly-Leu-Trp-Ala-D-Arg-NH_2 and Mca-Arg-Pro-Lys-Pro-Val-Glu-Nva-Trp-Arg-Lys(Dnp)-NH_2 were purchased from Bachem. Hydroxamic acid derivatives of amino acids, buffers, cysteine, α_1-protease inhibitor (α_1-PI), and 1,10-phenanthroline were purchased from Sigma. Metal salts, Brij-35, sodium dodecyl sulfate, dithioerythreitol, and 2-mercaptoethanol were purchased from Fisher. Peptide libraries were synthesized at the Tufts University Core Facility (Boston, MA) as described previously (12).

Preparation of Partially Active MMP-26—MMP-26 was expressed in the form of inclusion bodies from transformed *E. coli* cells as described previously (14). The inclusion bodies were isolated and purified using B-PER™ bacterial protein extraction reagent according to the manufacturer's instructions. The insoluble protein was dissolved in 8 M urea to ~5 mg/ml. The protein solution was diluted to ~100 μg/ml in 8 M urea and 10 mM dithiothreitol for 1 h, dialyzed in 4 M urea, 1 mM dithiothreitol, 50 mM HEPES, or Tricine, pH 7.5, for at least 1 h and then folded by dialysis in buffer containing 50 mM HEPES or Tricine, 0.2 M NaCl, 10 mM $CaCl_2$, 20 μM $ZnSO_4$, 0.01% Brij-35, pH 7.5, for 16 h. To enhance the activity of MMP-26, the folded enzyme was dialyzed twice for 24 h at 4 °C in the folding buffer without Zn^{2+} ion. The total enzyme concentration was measured by UV absorption using ϵ_{280} = 57130 M^{-1} cm^{-1}, which was calculated by Genetics Computer Group software.

Peptide Library Methods—The methods were performed as described previously (12). To determine the specificity for the primed positions (18), an amino-terminally acetylated dodecamer peptide mixture (1 mM) consisting of a roughly equimolar mixture of the 19 naturally occurring L-amino acids excluding cysteine at each site was incubated with MMP-26 in 50 mM HEPES, pH 7.4, 200 mM NaCl, 5 mM $CaCl_2$ at 37 °C until 5–10% of the peptides were digested. An aliquot (10 μl) of the mixture was subjected to automated amino-terminal peptide sequencing. The data in each sequencing cycle were normalized to the total molar amount of amino acids in that cycle so that a value of 1 indicated the average value. Undigested peptides and the amino-terminal fragments of digested peptides are amino-terminally blocked and therefore do not contribute to the sequenced pool.

The specificity of the unprimed side was determined by libraries with the sequence MAXXXXXLRGAARE(K-biotin) for the P3 site and MAX-XPXXLRGGGEE(K-biotin) for other sites, where X represents a degenerate position, K-biotin is ε-(biotinamidohexanoyl)lysine, and the amino terminus is unblocked. Libraries were partially digested with MMP-26 as described above, quenched with EDTA (10 mM), and treated in batch with 400 μl of avidin-agarose resin (Sigma). The mixture was transferred to a column, which was washed with 25 mM ammonium bicarbonate. The unbound fraction was evaporated to dryness under reduced pressure, suspended in water, and sequenced. Data were normalized as described above.

Kinetic Assays—Assays of fluorescent peptide substrates were performed by following the procedures reported in the literature (14, 29). For substrates containing the tryptophan residue, the fluorescence was observed at an excitation wavelength of 280 nm and emission wavelength of 360 nm, and for substrates containing 3-methoxycoumarin, fluorescence was measured at an excitation wavelength of 328 nm and emission wavelength of 393 nm. All of the kinetic experiments were conducted in 50 mM HEPES buffer containing 10 mM $CaCl_2$, 0.2 M NaCl, and 0.01% Brij-35. To assess inhibition potency for tight binding inhibitors, the apparent inhibitor dissociation constants (K_i^{app} values) were calculated by fitting the data to Morrison's equation (19). The inhibitor dissociation constants (K_i values) were determined by Dixon's plot (20) for less potent inhibitors. The inhibition assays were performed with a peptide substrate (1 μM), Mca-Pro-Leu-Gly-Leu-Dpa-Ala-Arg-NH_2, and 5–10 different inhibitor concentrations. The substrate stock solutions were prepared in Me_2SO and then further diluted to 50% Me_2SO in water. The final Me_2SO concentration in the assays was 1%. The inhibitors were dissolved in Me_2SO to 5 or 2 mM and diluted with methanol with the exception of inhibitor IV (Calbiochem catalogue number: 444250), which was dissolved in assay buffer. The final methanol concentration in the inhibition assays was 5% (v/v). The specificity constants (k_{cat}/K_m values) were determined by the equation $V = (k_{cat}/K_m)[E][S]$, which is modified from the Michaelis-Menten equation when $[S] \ll K_m$.

The enzyme became a mixture of several states after partial activation by dialysis. The total concentration of 400 nM MMP-26 was measured by absorption at 280 nm and calculated using a molar extinction coefficient of 57,130 M^{-1} cm^{-1}. The enzyme was titrated with MMP inhibitor I (GM-6001) to determine the concentration of catalytically active MMP-26. The titration analysis revealed the concentration of active MMP-26 to be 21 nM, which was ~5% of the total protein concentration after dialysis. For an accurate titration, the concentration of an enzyme is required to be at least 100-fold more than the inhibition constant of the titrant (21). To avoid the depletion of substrate by a high MMP-26 concentration, a less specific substrate, Mca-Arg-Pro-Lys-Pro-Val-Glu-Nva-Trp-Arg-Lys(Dnp)-NH_2, designed for MMP-3 (22), was used for detection of the initial rate. The cleavage of this substrate by MMP-26 was the slowest among peptide substrates studied in our laboratory (14).

IGFBP-1 and α_1-PI Digestion by MMP-26—IGFBP-1, α_1-PI, and MMP-26 solutions were diluted or dissolved in 50 mM HEPES buffer at pH 7.5 containing 10 mM $CaCl_2$, 0.2 M NaCl, and 0.01% Brij-35. IGFBP-1 (4 μg) and MMP-26 (0.63 μg) in a total volume of 50 μl were incubated for 2 days at room temperature. Each day, 10 μl of reaction mixture was taken, and the reaction was stopped by boiling for 5 min after 2× SDS-PAGE sample buffer containing 2% SDS, 100 mM dithiothreitol, and 50 mM EDTA was added. The cleaved products were separated by a 12% acrylamide gel and detected by silver staining. For cleavage of α_1-PI, 90 μg of α_1-PI were incubated with 1.3 μg of MMP-26 in a total volume of 100 μl. The samples were collected after 1 h, 1day, and 2 days. The cleaved products were separated by a 15% SDS-PAGE and detected by silver staining.

Determination of Cleavage Products by Matrix-assisted Laser Desorption Ionization Time-of-Flight Mass Spectrometry (MALDI-TOF MS)—The cleavage sites of fluorogenic peptide substrates and α_1-PI were determined by measuring the mass of the cleavage products with a Bruker protein time-of-flight mass spectrometer. The reaction mixture was mixed with an equivalent volume of α-cyano-4-hydroxycinamic acid (4.5 mg/ml in 50% CH_3CN, 0.05% trifluoroacetic acid) matrix solution containing synthetic peptide calibrants. Because the high salt concentration increased the noise in the mass spectra, the digestion reaction was performed with 10 mM HEPES buffer containing 5 mM $CaCl_2$ overnight at room temperature. For fluorogenic substrates, MMP-9 was used as a positive control.

RESULTS

Substrate Specificities of MMP-26—The substrate specificity of MMP-26 was investigated using a recently described peptide library method (12). Data are shown in Fig. 1. The residues preferred at each site from P4–P4′ are summarized in Table I. The strongest selectivity was seen at the P1′ site where large hydrophobic residues were preferred. Small residues, alanine and serine, were preferred at the P3′ site. Although P2′ and P4′ displayed indistinct specificity compared with the P1′ site, a lack of a preference for a basic residue (Arg or Lys) at the P2′ site was unique to MMP-26 (Table I). Among the unprimed positions, the P3 site showed the highest selectivity preferring proline and valine. The P1 site was not as selective as the P3 site, although small residues such as serine were preferred. The preference of MMP-26 for proline at P3, hydrophobic residues at P2 and P1′ sites, and serine at P1 is similar to that of other MMPs (5–13).

Inhibition of MMP-26 by Synthetic Inhibitors—Inhibition constants for several inhibitors designed for collagenases and gelatinases were measured with MMP-26, and these values are shown in Fig. 2. Among the four inhibitors tested, inhibitor I (23) was the most potent for MMP-26 with a K_i^{app} of 0.36 nM. Inhibitor II inhibited MMP-26 with a K_i^{app} of 1.5 nM, which is similar to the inhibition constant with neutrophil collagenase MMP-8 (4 nM) (24). Inhibitor III is a less potent stereoisomer of inhibitor II, and MMP-8 discriminates between the two with a 250-fold difference in their inhibition constants (1000 *versus* 4

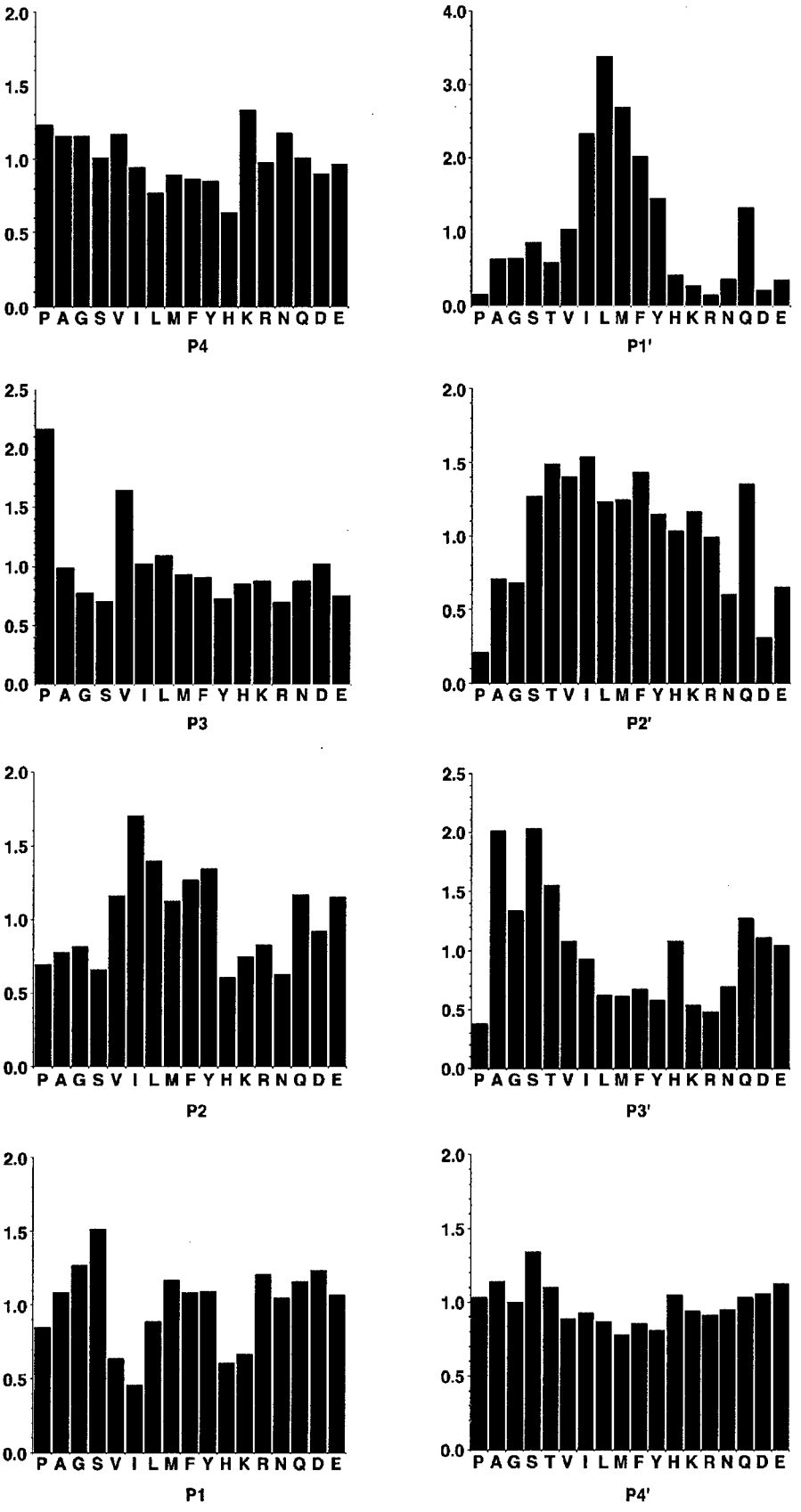

FIG. 1. **Cleavage site specificity of MMP-26 (endometase).** The *figures* on the *right* represent the relative distribution of amino acid residues at positions COOH terminus (P1′–P4′) to the MMP-26 cleavage site determined by sequencing the cleavage fragments of a random dodecamer (Ac-*XXXXXXXXXXXX*). Data are normalized so that a value of 1 corresponds to the average quantity per amino acid in a given sequencing cycle and would indicate no selectivity. Tryptophan was not included in the analysis because of poor yield during sequencing. The *figures* on the *left* represent specificity of positions amino terminus to the MMP-26 cleavage site. For the P3 position, data shown were obtained using the library MA*XXXXX*LRGAARE(K-biotin). For all other positions, the P3 proline library MG*XX*P*XX*LRGGGEE(K-biotin) was used. Glutamine and threonine were omitted in some cycles because of high background on the sequencer. Data were normalized as for the primed sites.

nM). There was a 40-fold difference between the K_i^{app} values of the pair of stereoisomers with MMP-26 (60 *versus* 1.5 nM). Inhibitor IV inhibited MMP-26 with a K_i^{app} of 2.9 μM and an IC_{50} value of 3.4 μM. This IC_{50} value is similar to the IC_{50} values with interstitial collagenases MMP-1 and MMP-8 (both are 1 μM) (25).

TABLE I
Cleavage site motifs for MMP-26[a] compared with those of six other MMPs[b]

Enzyme	Cleavage position							
	P4	P3	P2	P1	P1′	P2′	P3′	P4′
MMP-26	Lup (1.3)	Pro (2.2) Val (1.6)	Ile (1.7) Leu (1.4) Tyr (1.3)	Ser (1.5)	Leu (3.4) Met (2.7) Ile (2.3) Phe (2.0) Tyr (1.5) Gln (1.3)	Ile (1.5) Iwe (1.5) Phe (1.4) Gln (1.4)	Ser (2.0) Ada (2.0) Thr (1.6) Gly (1.3)	Ser (1.3)
MMP-1	Val	Pro	Met	Ser	Met	Met	Ala	
MMP-2	Ile	Pro	Val	Ser	Leu	Arg	Ser	
MMP-3	Lys	Pro	Phe	Ser	Met	Met	Met	
MMP-7	Val	Pro	Leu	Ser	Leu	Val	Met	
MMP-9	Val	Pro	Leu	Ser	Leu	Arg	Ser	
MMP-14	Ile	Pro	Glu	Ser	Leu	Arg	Met	
MMP	Val	Pro	Leu	Ser	Leu	Arg	Ala	
Consensus[c]		Val	Tyr		Met Ile	Ile		

[a] Quantities were determined from sequencing data as described for Fig. 1, and values ≥1.3 are listed. All primed sites were obtained using the library Ac-*XXXXXXXXXXX*. MA*XXXXX*LRGAARE(K-biotin) and MG*XXPXX*LRGGGEE(K-biotin) were used to produce the data at the unprimed sites.

[b] Data from Turk *et al.* (12). A series of consensus peptides/optimal cleavage site motifs were selected and listed for each MMP.

[c] Data summarized from Turk *et al.* (12). These listed residues were selected among amino acids that appeared at least in 5 of the 6 MMPs with values ≥1.3.

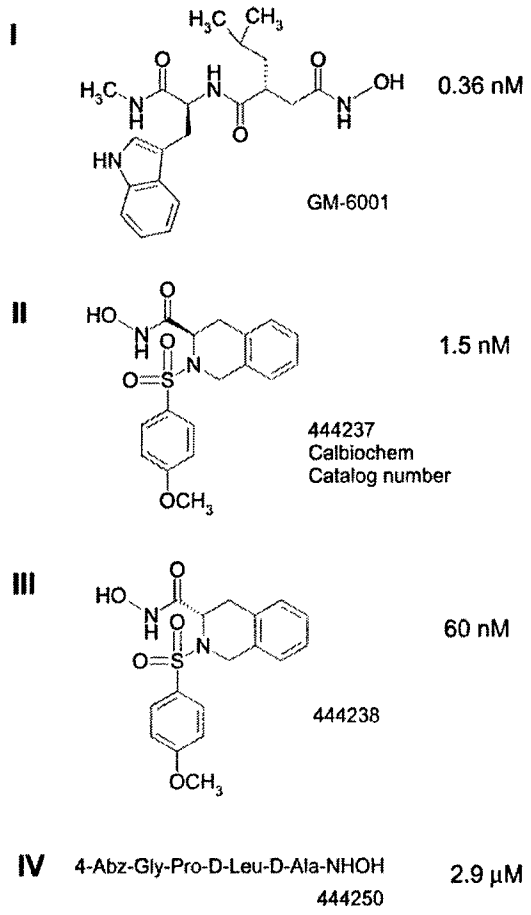

FIG. 2. **The structures of MMP inhibitors and their inhibitor dissociation constants with MMP-26.** The apparent inhibition constants (K_i^{app} values) were determined by Morrison's equation for tight binding inhibitors (compounds *I*, *II*, and *III*) (19), and the inhibition constant (K_i value) was determined by Dixon's plot for a less potent inhibitor (compound *IV*) (20). The values were 0.36, 1.5, 60, and 2900 nM for compounds I, II, III, and IV, respectively.

Autocleavage Sites of Recombinant MMP-26—Dialysis of the folded pro-form of MMP-26 results in an increase in activity because of autolysis of the prodomain. MMP-26 was collected after two 24-h dialyses with fresh buffer at 4 °C (further dialysis or incubation gradually reduced the activity). Partially activated MMP-26 was compared with the zymogen form on a silver-stained polyacrylamide gel (Fig. 3). The band near 30 kDa was confirmed to be pro-MMP-26 by amino-terminal sequencing (Fig. 3, *lane 2*) (14). Several bands below 30 kDa appeared after the dialysis, three of which were located between 20 and 25 kDa (Fig. 3, *lane 3*). One or more of the three cleavage products may be active forms of MMP-26 and was analyzed by amino-terminal sequencing. Only the top two bands were successfully sequenced. The top band resulted from cleavage of a peptide bond between Leu^{49} and Thr^{50}, and the band below it was a product of cleavage between Ala^{75} and Leu^{76} (sequence based on Ref. 14). The cleavage at either site does not remove the cysteine switch sequence PHC^{82}GVPDGSD.

Cleavage of Fluorogenic Substrates by MMP-26—Initial screening of a number of fluorogenic peptide substrates revealed that gelatinase and collagenase peptide substrates were most efficiently cleaved by MMP-26 (14, 17). Therefore, we chose peptide substrates designed for gelatinases or collagenases for further study, three of which contained Trp and two of which contained 7-methoxy coumarin as the fluorogenic group, respectively (26–30). The active MMP-26 concentration was determined by active site titration with inhibitor I (Fig. 4) using the least efficient substrate tested as described under "Experimental Procedures." The titration analysis revealed the concentration of active MMP-26 to be ~5% of the total enzyme concentration (21 of 400 nM). The cleavage sites of the six fluorogenic peptide substrates were determined by identifying the mass of the products by mass spectrometry. Mass spectra of the cleavage products revealed that the cleavage sites of the substrates by MMP-26 and MMP-9 were identical as shown in the example of peptide III (Fig. 5). The specificity constants (k_{cat}/K_m) of these six peptide substrates with MMP-26 were measured and calculated as shown in Table II. MMP-26 hydrolyzed peptide V with the highest specificity constant (3.0×10^4 M^{-1} s^{-1}), which is still 10-fold lower than the specificity constant with MMP-2 (3.97×10^5 M^{-1} s^{-1}) (26).

Cleavage Site of α_1-PI and IGFBP-1—MMP-26 cleaved α_1-PI near the COOH terminus to produce a COOH-terminal fragment of approximately 5 kDa (Fig. 6, *lanes 6* and *7*). This fragment was detected by silver staining of a 15% SDS-PAGE gel run under optimized conditions to identify proteins of molecular masses <10 kDa as described previously (31). A 24-h

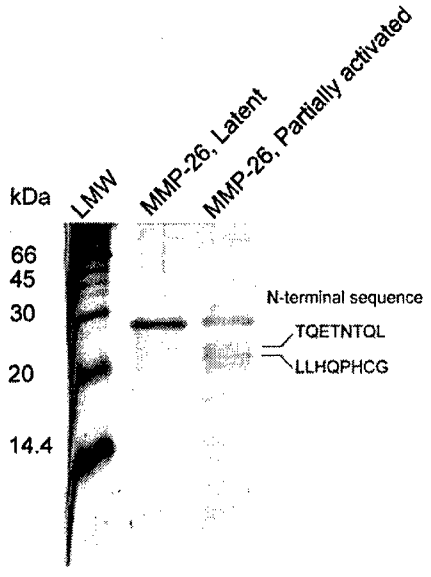

FIG. 3. **Autolysis of MMP-26 during dialysis.** *Lanes 1–3* were low molecular weight markers and the folded MMP-26 before and after dialysis at 4 °C for 24 h, respectively. The cleavage sites of MMP-26 that formed the two major bands around 20 kDa were revealed to be The^{51}–Gln^{52} and Ala^{75}–Leu^{76} by amino-terminal sequencing.

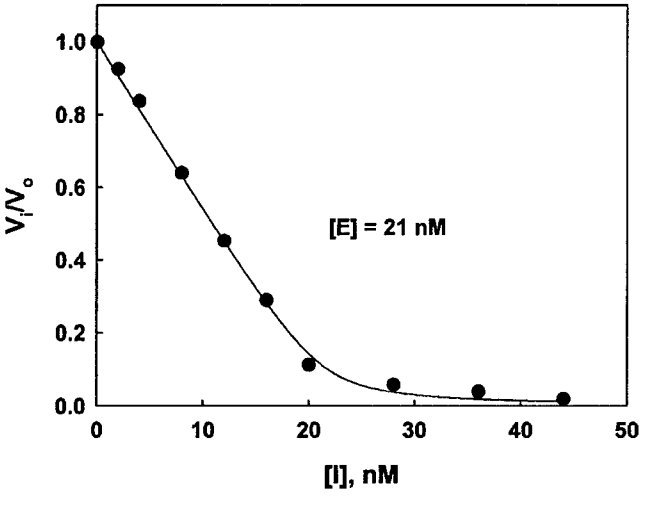

FIG. 4. **Determination of the active MMP-26 concentration by titration of MMP-26 with inhibitor I.** Total MMP-26 concentration was estimated to be 400 nM by molar absorptivity. The estimated active concentration was 21 nM by fitting the titration data into Morrison's equation (19). The assays were performed as described under "Experimental Procedures" with 1 μM of the substrate.

incubation of α_1-PI with MMP-26 at room temperature led to the formation of a fragment below 14.4 kDa (*lane 6*), which was not cleaved any further after 2 days of incubation (*lane 7*). The mass spectrum of the α_1-PI and MMP-26 mixture (Fig. 7*B*) exhibited two new peaks located at 4260 and 4774, which were not observed in the spectrum of α_1-PI alone (Fig. 7*A*). Based on molecular mass analysis, the cleavage sites resulting in these fragments should be Phe^{352}–Leu^{353} (~4774 Da) and Pro^{357}–Met^{358} (~4260 Da) near the COOH terminus of α_1-PI.

A comparison of *lanes 2* and *7* in Fig. 8 indicated that there was no detectable proteolysis of IGFBP-1 without MMP-26. The dark band around 30 kDa (IGFBP-1) disappeared, and a band below 14.4 kDa appeared when IGFBP-1 was incubated with MMP-26 for 1 or 2 days (*lanes 4* and *5*, respectively). The amino-terminal sequence of this band was determined to be Val-The-Asn-Ile-Lys-Lys-Trp-Lys, demonstrating that it arises

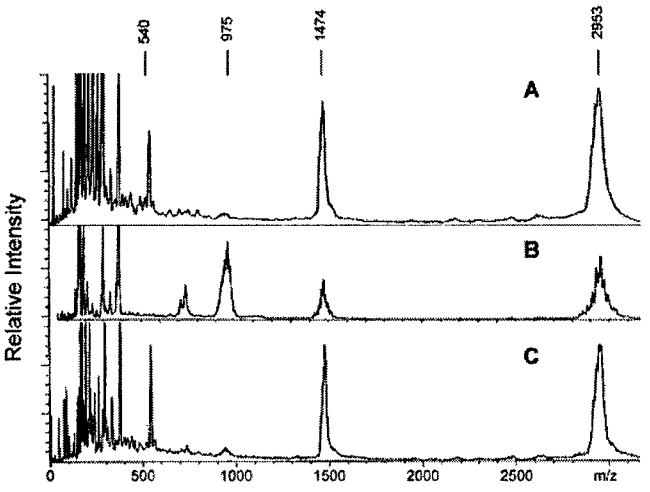

FIG. 5. **An example of the determination of fluorogenic peptide cleavage sites by MALDI TOF mass spectrometry.** 80 μM peptide substrate III (Table II), Dnp-Pro-Leu-Gly-Leu-Trp-Ala-(D)-Arg-OH) was incubated overnight with 5 nM MMP-9 (human neutrophil gelatinase) (*A*), alone (*B*), and with 20 nM endometase (*C*), pH 7.5, and 10 mM HEPES containing 5 mM $CaCl_2$ at room temperature. The two peaks observed at *m/z* 1474 and 2953 were internal synthetic peptide mass calibrants. The peaks at *m/z* 975 and 542 were the substrate and the cleaved peptide fragment, Leu-Trp-Ala-(D)-Arg-OH, produced by cleavage of the Gly–Leu peptide bond by MMP-9 and endometase, respectively.

TABLE II
Peptide substrates of MMP-26[a]

Fluorogenic substrate cleavage sites[b]	k_{cat}/K_m
	$s^{-1}\ M^{-1}$
P3 P2 P1 P1′ P2′ P3′ P4′	
Dnp-Pro-Leu-Gly-Met-Trp-Ser-Arg-OH (I)	9.4×10^3
Dnp-Pro-Leu-Ala-Tyr-Trp-Ala-Arg-OH (II)	3.5×10^3
Dnp-Pro-Leu-Gly-Leu-Trp-Ala-(D)Arg-OH (III)	4.9×10^3
Mca-Pro-Cha-Gly-Nva-His-Ala-Dpa-NH_2 (IV)	1.7×10^4
Mca-Pro-Leu-Ala-Nva-Dpa-Ala-Arg-NH_2 (V)	3.0×10^4
Mca-Pro-Leu-Gly-Leu-Dpa-Ala-Arg-NH_2 (VI)	2.2×10^4

[a] All of the assays were performed in pH 7.5 buffer containing 50 mM HEPES, 0.2 M NaCl, 0.01 M CaCl2, 0.01% Brij-35 at 25°C. The range of substrate concentrations used were 1μM, and the active MMP-26 concentration used was 2 nM for the substrates containing the Mca group and 10 nM for the substrates containing the Trp residue.

[b] The cleavage sites of the substrates were determined by mass spectrometry as described under "Experimental procedures" and Fig. 5.

from cleavage at the same site (His^{140}–Val^{141}) as stromelysin-3 (MMP-11), which produces an inactive 9-kDa fragment (32).

DISCUSSION

The results obtained from peptide library studies indicate that MMP-26 substrate specificities are similar to those of other MMPs where hydrophobic residues are preferred at P1′and P2, proline is preferred at P3, and serine is preferred at P1. The optimal cleavage motifs/consensus peptide sequences for MMP-26 were Lys-Pro-Ile/Leu-Ser(P1)-Leu/Met(P1′)-Ile/Thr-Ser/Ala-Ser (Table I), which are not identical to those of MMP-1, MMP-2, MMP-3, MMP-7, MMP-9, and MMP-14 (12). Based on this sequence specificity knowledge, new fluorescence resonance energy transfer substrates more specific for MMP-26 will be designed and developed. These data may provide critical information applicable to the design of new MMP-26-specific inhibitors and to the identification of novel physiological and pathological substrates of MMP-26 *in vivo*.

The inhibition constants of four synthetic inhibitors with MMP-26 were comparable to those with gelatinases and collagenases, the enzymes for which the inhibitors were designed. This corroborates the findings that the substrate specificity of

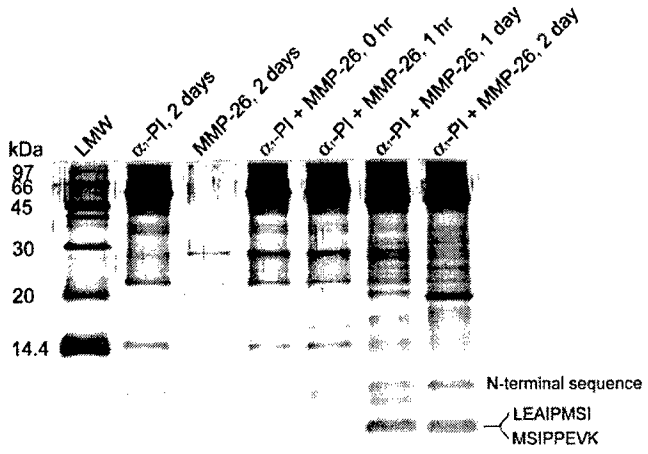

FIG. 6. **Cleavage of human α_1-PI by MMP-26.** After incubation of an α_1-PI (900 μg/ml) and MMP-26 (13 μg/ml) mixture for 1 day (*lane 6*) and 2 days (*lane 7*) at room temperature, the COOH-terminal cleavage products were detected by silver staining a 15% SDS-PAGE gel. Samples containing α_1-PI were overloaded to detect the bands of around 4.5 kDa in *lanes 6* and *7*, which might be 4.8- and 4.2-kDa fragments produced by MMP-26 proteolysis of α_1-PI. The two amino-terminal sequences were deduced from the mass spectrometry results shown in Fig. 6 compared with the primary structure of human α_1-PI.

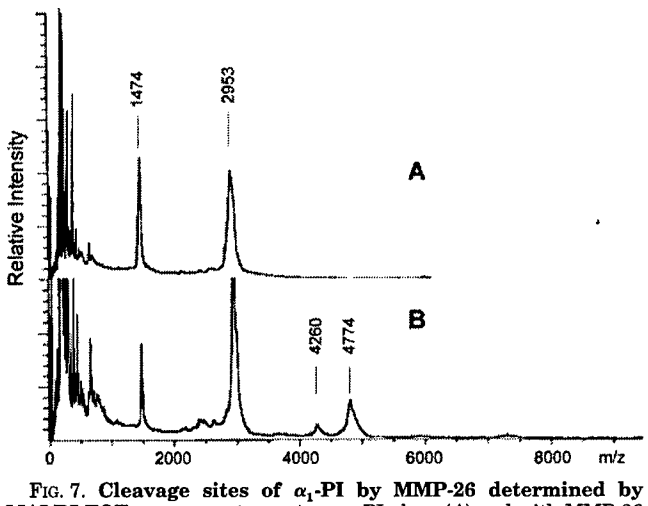

FIG. 7. **Cleavage sites of α_1-PI by MMP-26 determined by MALDI TOF mass spectrometry.** α_1-PI alone (*A*) and with MMP-26 (*B*) were incubated for 1 day in 10 mM HEPES buffer at pH 7.5 containing 5 mM $CaCl_2$. The peaks at *m/z* 1474 and 2953 were two internal calibrants. The two peaks observed at *m/z* 4260 and 4774 were produced from α_1-PI cleavage by MMP-26 at the sites Pro^{357}–Met^{358} and Phe^{352}–Leu^{353}.

MMP-26 is quite close to that of other MMPs. Inhibitor I/GM6001 was the most potent inhibitor of MMP-26 tested with a K_i^{app} of 0.36 nM. GM6001 also potently inhibits MMP-2 (K_i = 0.5 nM) and MMP-8 (K_i = 0.1 nM) but is less effective against MMP-3 (K_i = 27 nM) (23). Inhibitor III is a less potent stereoisomer of inhibitor II, and MMP-8 discriminates between the two with a 250-fold difference in their inhibition constants. There was only 40-fold difference between the K_i^{app} values of the stereoisomers with MMP-26, indicating that MMP-26 is less stereoselective for its inhibitors. Inhibitor IV was more selective for MMP-1 and MMP-8 (IC_{50} = 1 μM against both enzymes) than MMP-9 (IC_{50} = 30 μM) and MMP-3 (IC_{50} = 150 μM) (25). This inhibitor has an IC_{50} value of 3.4 μM with MMP-26, similar as that with MMP-1 and MMP-8.

A survey of known protein cleavage sites determined *in vitro* for MMP-26 is summarized in Table III. The survey indicates that hydrophobic residues are preferred at P1′ and appear in

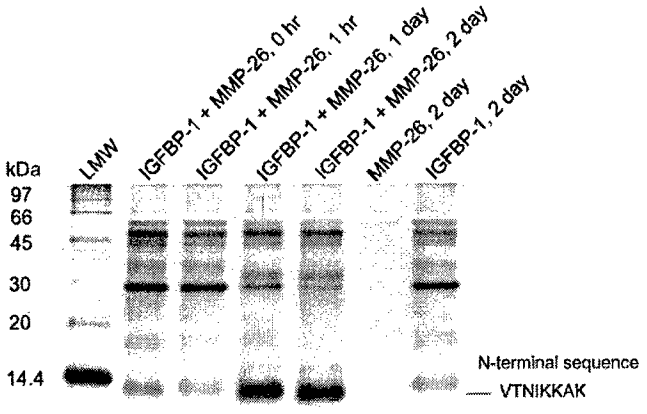

FIG. 8. **Cleavage of IGFBP-1 by MMP-26.** IGFBP-1 (80 μg/ml) was incubated with MMP-26 (13 μg/ml) for 0 h (*lane 2*), 1 h (*lane 3*), 1 day (*lane 4*), and 2 days (*lane 5*). The dense band below 14.4 kDa observed after 1 day (*lane 4*) was the product of IGFBP-1 cleavage by MMP-26 at the His^{140}–Val^{141} site.

TABLE III
Protein sequences hydrolyzed by MMP-26

Proteins	Cleavage sites[a]
α_1-PI[a]	GAMF-LEAI
	EAIP-MSIP
MMP-26 (autolysis)[b]	QMHA-LLHQ
	SPLL-TQET
MMP-26 (autolysis)[c]	QLLQ-QFHR
IGFBP-1[b]	KALH-VTNI
Fibronectin[d]	SPVA-VSQS
Vitronectin[d]	KPEG-IDSR
Fibrinogen[d]	SKPN-MIDA
	HTEK-LVTS
	GDKE-LRTG

[a] A line is inserted in the cleavage site.
[b] Data from this study.
[c] Data from Marchenko *et al.* (41).
[d] Data from Marchenko *et al.* (17).

almost all of the substrates. Residues occurring at other positions that agree with the consensus from the peptide libraries include proline (3 times) at P3, hydrophobic residues (6 times) at P2, and Ser, Ala, and Thr (4 times) at P3′. Residues at the other positions seem random and do not coincide with residue predictions by the peptide libraries, although the libraries do indicate less stringent selectivity at these positions. Accordingly, no individual protein cleavage site precisely matches the consensus motif determined by the peptide library studies, suggesting that the cleavage sites in these protein substrates are probably suboptimal for cleavage by MMP-26. The folding topology of the protein may be a contributing factor to the enzyme-substrate interactions. Although the protein cleavage site may not be the optimal sequence, the peptide chain might assume a conformation that is easily accessible to a protease active site; for example, an exposed loop is found in the bait region of α_2-macroglobulin (33), and the reactive loop is found in the bait region of α_1-PI (34). Alternatively, the cleavage of a suboptimal site may be promoted by recruitment to the enzyme via a substrate-binding exosite. In addition, the presence of unfavorable residues around the cleavage site may slow down the rate of digestion by a protease, regulating the degradation process.

MMP-26 has been shown to digest several components of the extracellular matrix, such as fibronectin, collagens, fibrinogen, and vitronectin, but not any of several plasma proteins tested with the exception of α_1-PI (14, 17). It has been reported that the cleavage of the reactive loop residues around 350–365 in α_1-PI by MMP-1 and MMP-3 inactivates the inhibitor (34–36). The digestion of α_1-PI by MMP-26 generates two major peaks

that originate from the cleavage at two sites near the COOH-terminal region, Phe^{352}–Leu^{353} (~4774 Da) and Pro^{357}–Met^{358} (~4260 Da). These are the same cleavage sites for MMP-1 (35). In addition, MMP-3 cleaves the Pro^{357}–Met^{358} bond (34). MMP-11 cleaves the Ala^{350}–Met^{351} bond (36), a site distinct from those of MMP-26 and MMP-1. Interestingly, direct evidence showed that α_1-PI was a critical substrate for MMP-9 *in vivo* in a mouse model of the autoimmune disease *bullous pemphigoid* (37). Thus, MMP-26 may inactivate α_1-PI like the other MMPs to promote serine proteinase activity, enhancing extracellular matrix degradation in cancers or other pathological processes.

The insulin-like growth factors, IGFBPs, and IGFBP proteases are involved in the regulation of somatic growth and cellular proliferation. The level of free insulin-like growth factor in a system is modulated by rates of insulin-like growth factor production and clearance and the degree of binding to IGFBPs (38). IGFBP-1 inhibits IGF-I-induced proliferation of the MCF-7 human breast adenocarcinoma (32). Through their inactivation of IGFBP-1, MMPs were able to promote cell growth and survival by the increase of the effective insulin-like growth factor concentration in the surrounding medium (32). MMP-26 cleaves the His^{140}–Val^{141} bond in IGFBP-1 as does MMP-11. Therefore, the cleavage of IGFBP-1 by MMP-26 to produce the 9-kDa inactive form may sustain the survival of cancer cells, increasing the chance of metastasis.

The cleavage sites in the fluorogenic substrates seem in good agreement with the motifs determined by the peptide library approach. Although the six commercial fluorogenic peptide substrates tested were not designed for the specificity of MMP-26, some of them resemble closely to the consensus sequences of peptide substrates for MMP-26 determined by the peptide library studies, proline at P3, a hydrophobic residue at P2, P1′, and P2′, and small residues at P3′, with the exception that serine is preferred at P1 and P4′, Lys is preferred at P4, but a basic residue is not preferred at P2′. The best substrate tested for MMP-26 was peptide V, Mca-Pro-Leu-Ala-Nva-Dpa-Ala-Arg-NH_2. This peptide appears to be very close to optimal sequences determined by the peptide library studies where there is a selected residue at essentially every position (see Fig. 1 and Table I) with the exception that the peptide libraries do not have Nva at P1′.

The cleavage sites in the protein substrates tested do not match exactly the optimal motifs identified by the peptide library approach; however, upon close examination of the protein cleavage site data presented in Table III, it seems that the amino acid residues at P1 and P4′ are less selective. This is in good agreement with the peptide library data. Furthermore, P1′ is more selective, and Leu, Met, and Ile are preferred at P1′ (Fig. 1). This finding is consistent with the protein cleavage site data shown in Table III in which 7 of the 11 residues (64%) at P1′ are these residues. Moreover, two Lys residues are found at the P4, and two Ser residues are found at P4′ of the protein cleavage sites, which is also unique to MMP-26 according to the library data.

The relative rates of cleavage in the six fluorogenic substrates also correspond to the peptide library data relatively well. The best substrate is peptide V with a specificity constant of $3.0 \times 10^4\ M^{-1}\ s^{-1}$. In addition to peptide V, peptides IV and VI are also relatively good substrates for MMP-26 with specificity constants of $1.7 \times 10^4\ M^{-1}\ s^{-1}$ and $2.2 \times 10^4\ M^{-1}\ s^{-1}$, respectively (Table II). The worst substrate of MMP-26 in Table II is peptide II with a specificity constant ~10 times slower than peptide V. Neither Ala at P1 nor Tyr at P1′ in the peptide II is preferred. On the other hand, the rate of cleavage of peptide V, the best peptide of MMP-26 in Table II, is 10 times slower than the rate of substrate cleavage by MMP-2 ($3.97 \times 10^5\ M^{-1}\ s^{-1}$) (26). The slower rate of peptide and protein digestion by MMP-26 suggests that this enzyme is not the most powerful MMP catalytically or the optimal substrates for MMP-26 have not been identified.

It is also possible that a manageable rate of MMP-26 catalysis may be required in biological processes such as normal implantation where tight control of substrate degradation is highly desirable. In the latter scenario, the function of MMP-26 may not be limited to the direct degradation of ECM. MMP-26 may play a more critical role in controlling the activities of growth factors or proteases that mediate such processes. Consequently, biologically significant substrates of MMP-26 may be growth factor-binding proteins, receptors, zymogens, and enzyme inhibitors.

MMP-26 is not only unique in terms of its tissue and cell-specific expression as reported by us and others (14–17) but also because of its unique cysteine switch sequence (P**H**^{81}CGVPDGSD) and thus its unique pathway of proenzyme activation. Many members of the MMP family follow the classic cysteine-switch activation model (39, 40). The inactivity of a pro-MMP is generally attributable to a complex between the sulfhydryl group of a cysteine residue in the cysteine switch sequence (P**R**CGVPDV) of the prodomain and the active site zinc atom in the catalytic domain. The activation of a pro-MMP can be achieved proteolytically by hydrolysis of the propeptide on the carboxyl-terminal side of the cysteine switch residue near the border between the propeptide and catalytic domains. This proteolytic step may be catalyzed by another proteinase or it may be an autolytic step (39, 40). However, Marchenko *et al.* (41) have challenged the cysteine-switch model. Their report showed that the activating cleavage site of pro-MMP-26 occurs at Gln^{59}–Gln^{60}, leaving the putative cysteine switch sequence intact. It was suggested that the Arg to His substitution existing in the unique P**H**^{81}CGVPDGSD cysteine-switch motif of pro-MMP-26 abolishes the ability of Cys^{82} to interact with the zinc ion of the catalytic domain (41).

We have identified two of the major autolytic sites in MMP-26 to be Leu^{49}–Thr^{50} and Ala^{75}–Leu^{76}. Although different from the Gln^{59}–Gln^{60} site, the cleavage at these two sites also does not remove the cysteine switch sequence (PHC^{82}GVPD) from the enzyme, suggesting that Cys^{82} may not play a role in the latency of the zymogen, which is consistent with the hypothesis proposed by Marchenko *et al.* (41). Alternatively, the thiol group of Cys^{82} could be transiently dissociated from the zinc ion at the active site, allowing a water molecule to bind to the zinc ion and the enzyme to exhibit catalytic activity. Our inhibitor titration data demonstrated that ~5% of the total enzyme molecules was active. This observation may support the concept that the thiol groups of Cys^{82} in the active enzyme molecules are dissociated or removed from the active site zinc ions and the thiol groups of the Cys^{82} in remaining 95% of the total enzyme molecules are still coordinated with the zinc ions at the active sites, forming a steady-state equilibrium between the active enzyme molecules and the zymogen molecules. However, this hypothesis and the detailed activation mechanisms of pro-MMP-26 remain to be thoroughly investigated (42). In summary, this work provides new knowledge on the MMP-26 substrate specificity to build a working model for the future design of MMP-26 inhibitors, studies of pro-MMP-26 activation, and identification of optimal physiological and pathological substrates of MMP-26 *in vivo*.

Acknowledgments—We thank Margaret Seavy at the Bioanalytical Facility for protein amino-terminal sequencing and Sara C. Monroe for editorial assistance with manuscript preparation at the Florida State University. We appreciate Dr. Jian Ni at the Human Genome Sciences Inc. for previous collaboration on the human MMP-26 project.

REFERENCES

1. Hooper, N. M. (1994) *FEBS Lett.* **354,** 1–6
2. Shapiro, S. D. (1998) *Curr. Opin. Cell Biol.* **10,** 602–608
3. Nagase, H., and Woessner, J. F. (1999) *J. Biol. Chem.* **271,** 28509–28515
4. Johansson, N., Ahonen, M., and Kähäri, V. M. (2000) *Cell. Mol. Life Sci.* **57,** 5–15
5. Netzel-Arnett, S., Sang, Q.-X., Moore, W. G., Narve, M. Birkedal-Hansen, H., and Van Wart, H. E. (1993) *Biochemistry* **32,** 6427–6432
6. McGeehan, G. M., Bickett, D. M., Green, M., Kassel, D., Wiseman, J. S., and Berman, J. (1994) *J. Biol. Chem.* **269,** 32814–32820
7. Smith, M. M., Shi, Lihong, and Narve, M. (1995) *J. Biol. Chem.* **270,** 6440–6449
8. Nagase, H., and Fields, G. B. (1996) *Biopolymers* **40,** 399–416
9. Ohkubo, S., Miyadera, K., Sugimoto, Y., Matsuo, K., Wierzba, K., and Yamada, Y. (1999) *Biochem. Biophys. Res. Commun.* **266,** 308–313
10. Deng, S., Bickett, D. M., Mitchell, J. L., Lambert, M. H., Blackburn, R. K., Carter, H. L., III, Neugebauer, J., Pahel, G., Weiner, M. P., and Moss, M. L. (2000) *J. Biol. Chem.* **275,** 31422–31427
11. Kridel, S. J., Chen, E., Kotra, L. P., Howard, E. W., Mobashery, S., and Smith, J. W. (2001) *J. Biol. Chem.* **276,** 20572–20578
12. Turk, B. E., Huang, L. L., Piro, E. T., and Cantley, L. C. (2001) *Nature Biotechnol.* **19,** 661–667
13. Chen, E. I., Kridel, S. J., Howard, E. W., Li, W., Godzik, A., and Smith, J. W. (2002) *J. Biol. Chem.* **277,** 4485–4491
14. Park, H. I., Ni, J., Gerkema, F. E., Liu, D., Belozerov, V. E., and Sang, Q.-X. A. (2000) *J. Biol. Chem.* **275,** 20540–20544
15. Uría, J. A., and López-Otín, C. (2000) *Cancer Res.* **60,** 4745–4751
16. de Coignac, A. B., Elson, G., Delneste, Y., Magistrelli, G., Jeannin, P., Aubry, J.-P. Berthier, O., Schmitt, D., Bonnefoy, J.-Y., and Gauchat, J.-F. (2000) *Eur. J. Biochem.* **267,** 3323–3329
17. Marchenko, G. N., Ratnikov, B. I., Rozanov, D. V., Godzik, A., Deryugina, E. I., and Strongin, A. Y. (2001) *Biochem. J.* **356,** 705–718
18. Schechter, I., and Berger, A. (1967) *Biochem. Biophys. Res. Comm.* **27,** 157–162
19. Morrison, J. F. (1969) *Biochim. Biophys. Acta* **185,** 269–286
20. Cornish-Bowden, A. (1974) *Biochem. J.* **137,** 143–144
21. Copeland, R. A. (2000) in *Enzymes: a Practical Introduction to Structure, Mechanism, and Data Analysis.* 2nd Ed., pp. 305–349, Wiley-VCH, Inc., New York
22. Nagase, H., Fields, C. G., and Fields, G. B. (1994) *J. Biol. Chem.* **269,** 20952–20957
23. Galardy, R. E., Cassabonne, M. E., Giese, C., Gilbert, J. H., Lapierre, F., Lopez, H., Schaefer, M. E., Stack, R., Sullivan, M., and Summers, B. (1994) *Ann. N. Y. Acad. Sci.* **732,** 315–323
24. Matter, H., Schwab, W., Barber, D., Billen, G., Haase, B., Neises, B., Schudok, M., Thorwart, W., Schreuder, H., Brachvogel, V., Lönze, P., and Weithmann, K. U. (1999) *J. Med. Chem.* **42,** 1908–1920
25. Odake, S., Morita, Y., Morikawa, T., Yoshida, N., Hori, H., and Nagai, Y. (1994) *Biochem. Biophys. Res. Comm.* **199,** 1442–1446
26. Murphy, G., Nguyen, Q., Cockett, M. I., Atkinson, S. J., Allan, J. A., Knight, C. G., Willenbrock, F., and Docherty, A. J. P. (1994) *J. Biol. Chem.* **269,** 6632–6636
27. Knäuper, V., López-Otín, C., Smith, B., Knight, G., and Murphy, G. (1996) *J. Biol. Chem.* **271,** 1544–1550
28. Knight, C. G., Willenbrock, F., and Murphy, G. (1992) *FEBS Lett.* **296,** 263–266
29. Netzel-Arnett, S., Mallya, S. K., Nagase, H., Birkedal-Hansen, H., and Van Wart, H. E. (1991) *Anal. Biochem.* **195,** 86–92
30. Stack, M. S., and Gray, R. D. (1989) *J. Biol. Chem.* **264,** 4277–4281
31. Schägger, H., and Jagow, G. (1987) *Anal. Biochem.* **166,** 368–379
32. Manes, S., Mira, E., Barbacid, M. M., Cipres, A., Fernandez-Resa, P., Buesa, J. M., Merida, I., Aracil, M., Marquez, G., and Martinez-A. C. (1997) *J. Biol. Chem.* **272,** 25706–25712
33. Sottrup-Jensen, L. (1989) *J. Biol. Chem.* **264,** 11539–11542
34. Mast, A. E., Enghild, J. J., Nagase, H., Suzuki, K., Pizzo, S. V., and Salvesen, G. (1991) *J. Biol. Chem.* **266,** 15810–15816
35. Desrochers, P. E., Jeffrey, J. J., and Weiss, S. J. (1991) *J. Clin. Invest.* **87,** 2258–2265
36. Pei, D., Majmudar, G., and Weiss, S. J. (1994) *J. Biol. Chem.* **269,** 25849–25855
37. Liu, Z., Zhou, X., Shapiro, S. D., Shipley, J. M., Twining, S. S., Diaz, L. A., Senior, R. M., and Werb, Z. (2000) *Cell* **102,** 647–655
38. Ferry, R. J., Jr., Katz, L. E. L., Grimberg, A., Cohen, P., and Weinzimer, S. A. (1999) *Horm. Metab. Res.* **31,** 192–202
39. Springman, E. B., Angleton, E. L., Birkedal-Hansen, H., and Van Wart, H. E. (1990) *Proc. Natl. Acad. Sci. U. S. A.* **87,** 364–368
40. Van Wart, H. E., and Birkedal-Hansen, H. (1990) *Proc. Natl. Acad. Sci. U. S. A.* **87,** 5578–5582
41. Marchenko, N. D., Marchenko, G. N., and Strongin, A. Y. (2002) *J. Biol. Chem.* **277,** 18967–18972
42. Sang, Q. X. (2002) in *Handbook of Proteolytic Enzymes* (Barrett, A. J., Rawlings, N. D., and Woessner, J. F., eds) 2nd Ed., Academic Press, Orlando, FL, in press

THE JOURNAL OF BIOLOGICAL CHEMISTRY
Vol. 277, No. 28, Issue of July 12, pp. 25583–25591, 2002
Printed in U.S.A.

Intracellular Activation of Human Adamalysin 19/Disintegrin and Metalloproteinase 19 by Furin Occurs via One of the Two Consecutive Recognition Sites*

Received for publication, April 12, 2002, and in revised form, April 29, 2002
Published, JBC Papers in Press, May 2, 2002, DOI 10.1074/jbc.M203532200

Tiebang Kang‡, Yun-Ge Zhao‡, Duanqing Pei§, Joseph F. Sucic¶, and Qing-Xiang Amy Sang‡‖

From the ‡Department of Chemistry and Biochemistry and Institute of Molecular Biophysics, Florida State University, Tallahassee, Florida 32306-4390, the §Department of Pharmacology, University of Minnesota, Minneapolis, Minnesota 55455, and the ¶Biology Department, University of Michigan, Flint, Michigan 48502-1950

Adamalysin 19 (a disintegrin and metalloproteinase 19, ADAM19, or meltrin β) is a plasma membrane metalloproteinase. Human ADAM19 zymogen contains two potential furin recognition sites (RX(K/R)R), ^{196}KRPR^{200}R and ^{199}RRMK^{203}R, between its pro- and catalytic domains. Protein N-terminal sequencing revealed that the cellular mature forms of hADAM19 started at ^{204}EDLNSMK, demonstrating that the preferred furin cleavage site was the ^{200}RMK^{203}R↓^{204}EDLN. Those mature forms were catalytically active. Both Pittsburgh mutant of α_1-proteinase inhibitor and dec-Arg-Val-Lys-Arg-chloromethyl ketone, two specific furin inhibitors, blocked the activation of hADAM19. Activation of hADAM19 was also blocked by brefeldin A, which inhibits protein trafficking from the endoplasmic reticulum to the Golgi, or A23187, a calcium ionophore known to inhibit the autoactivation of furin. When ^{202}KR were mutated to AA, the proenzyme was also activated, suggesting that ^{197}RPRR is an alternative activation site. Furthermore, only pro-forms of hADAM19 were detected in the ^{199}RR to AA mutant, which abolished both furin recognition sites. Moreover, the zymogens were not converted into their active forms in two furin-deficient mammalian cell lines; co-expression of hADAM19 and furin in these two cell lines restored zymogen activation. Finally, co-localization between furin and hADAM19 was identified in the endoplasmic reticulum-Golgi complex and/or the trans-Golgi network. This report is the first thorough investigation of the intracellular activation of adamalysin 19, demonstrating that furin activated pro-hADAM19 in the secretory pathway via one of the two consecutive furin recognition sites.

The adamalysin, ADAM[1] (for a disintegrin and metalloprotease), or metalloprotease/disintegrin/cysteine-rich family includes proteins containing disintegrin- and metalloprotease-like domains. These proteinases are involved in diverse processes, such as development, cell-cell interaction, and protein ectodomain shedding (1–5). For example, ADAM10/kuzbanian (KUZ) and ADAM17/tumor necrosis factor-α convertase play key roles in the processing of both Notch1 receptor, which is critical in development, and amyloid precursor protein, which is related to the pathogenesis of Alzheimer's disease (3, 4, 6). Six different ADAMs, ADAM2, -9, -12, -15, -23, and -28, are able to interact with integrins such as $\alpha_6\beta_1$, $\alpha_v\beta_3$, $\alpha_9\beta_1$, $\alpha_v\beta_5$, $\alpha_5\beta_1$, and $\alpha_4\beta_1$, regulating cell-cell interactions in normal and pathological processes (7, 8). In the prodomain of ADAMs, there is a cysteine switch sequence similar to the motif found in matrix metalloproteases (MMPs) (9, 10), keeping ADAMs in latent forms (2, 3, 11, 12). There are one or more furin cleavage sites between the pro- and metalloprotease domains of almost all members of the ADAM family discovered (2, 13–15), but only several ADAM precursors, including ADAM1, -9, -12, -15, and -17 and ADAMTS1, -4, and -12, have been shown to be activated by furin or furin-like proprotein convertases (16–23).

Adamalysin 19/ADAM19, a type 1 membrane protein containing an intact zinc-binding site in its metalloprotease domain, was cloned from mice (24, 25) and humans (26, 27). Human adamalysin 19 was recently demonstrated to be an active metalloproteinase through its cleavage of α_2-macroglobulin (α_2-M) *in vitro* (27). The endopeptidase activity of adamalysin 19 was blocked by specific antibodies against its catalytic and disintegrin domain peptides (28). Mouse ADAM19 cleaved intracellular neuregulin, a member of the epidermal growth factor (EGF) family *in vivo* (29). Human ADAM19 and its mouse homolog are highly similar, sharing 80.6% identity in nucleotide sequences and 84.1% identity in amino acid sequences (24, 27). Among its many roles, hADAM19 may be important in osteoblast differentiation (24), as a marker for the differentiation and characterization of dendritic cells, in the distinction between macrophages and dendritic cells (26), and in the intracellular processing of neuregulin (29). ADAM19 is synthesized as a zymogen, and its mechanism of activation has not been thoroughly investigated.

* This work was supported in part by National Institutes of Health Grant CA78646; by Department of Defense United States Army Medical Research Acquisition Activity Grant DAMD17-02-1-0238; by American Cancer Society, Florida Division Grant F01FSU-1; and by a grant from the Florida State University Research Foundation (to Q.-X. A. S.), as well as by National Institutes of Health Grant CA76308 (to D. P.). The costs of publication of this article were defrayed in part by the payment of page charges. This article must therefore be hereby marked "*advertisement*" in accordance with 18 U.S.C. Section 1734 solely to indicate this fact.

‖ To whom correspondence should be addressed: Dept. of Chemistry and Biochemistry, 203 DLC, Chemistry Research Bldg., Rm. 203, Florida State University, Tallahassee, FL 32306-4390. Tel.: 850-644-8683; Fax: 850-644-8281; E-mail: sang@chem.fsu.edu.

[1] The abbreviations used are: ADAM, a disintegrin and metalloproteinase; ADAMTS, ADAM with thrombospondin-like motifs; α_2-M, α_2-macroglobulin; BACE, β-amyloid-converting enzyme; BFA, brefeldin A; decRVKR-CMK, dec-Arg-Val-Lys-Arg-chloromethyl ketone; DMEM, Dulbecco's modified Eagle's medium; EGF, epidermal growth factor; ER, endoplasmic reticulum; FBS, fetal bovine serum; MDCK, Madin-Darby canine kidney; MMP, matrix metalloproteinase; MT-MMP, membrane-type MMP; pAT, α_1-antitrypsin or α_1-proteinase inhibitor; α_1-PI, α_1-proteinase inhibitor; pATp, Pittsburgh mutant of α_1-antitrypsin/proteinase inhibitor; PACE4, paired basic amino acid-converting enzyme 4; PBS, phosphate-buffered saline; PC, proprotein convertase; 7.P15 cell, furin-deficient monkey kidney COS-7 strain cell; RIPA, radioimmune precipitation buffer; RPE.40 cell, furin-deficient Chinese hamster ovary-K1 strain cell; TGN, trans-Golgi network.

The proprotein convertases (PCs) are a large family of serine proteinases that recognize dibasic or RX(K/R)R motifs and cleave the peptide bond on the carboxyl side (30–32). As a major proprotein convertase, furin is concentrated in the trans-Golgi network (TGN) and cycles between this compartment and the cell surface through the endocytic pathway. The autoactivation and intracellular trafficking of furin are well characterized. Numerous studies have shown that furin activates a large number of proproteins in multiple compartments (30–32). For instance, furin has been demonstrated to mediate the activation of proenzymes, such as β-amyloid-converting enzyme (BACE), some matrix metalloproteinases (MMPs), including MMP-11, -14, -16, and -24, and some ADAMs, including ADAM1, -9, -12, -15, and -17 and ADAMTS1, -4, and -12 (16–23, 30, 31, 33–40). However, the molecular mechanism and pathway by which the cells regulate the potentially important interactions between these proenzymes and the proprotein convertase in cells are not fully understood. In this report, we present evidence that furin is responsible for the activation of hADAM19 and this activation can occur via one of the two consecutive recognition sites and that furin is co-localized with the substrate in the ER-Golgi complex and/or TGN.

EXPERIMENTAL PROCEDURES

Chemicals, Cell Lines, Cell Culture, and Immunological Reagents—All common laboratory chemicals, proteinase inhibitors, brefeldin A (BFA), anti-FLAG-M2 monoclonal antibody, and its agarose conjugates were purchased from Sigma. Anti-furin antibodies were from Affinity Bioreagents, Inc.(Golden, CO). Protein A/G PLUS agarose was from Santa Cruz Biotechnology, Inc. (Santa Cruz, CA). The CMK-based furin inhibitor dec-Arg-Val-Lys-Arg-chloromethyl ketone (decRVKR-CMK); a calcium ionophore, A23187; and a matrix metalloproteinase inhibitor, ilomastat (GM6001), were from BACHEM (Philadelphia, PA). Restriction enzymes were from Promega or Invitrogen. COS1, Madin-Darby canine kidney (MDCK), and derivative cells were maintained as described (40–43). The furin-deficient Chinese hamster ovary-K1 strain RPE.40 and furin-deficient COS-7 cell strain 7.P15 were cultured as described (44). Dulbecco's modified Eagle's medium (DMEM), fetal bovine serum (FBS), penicillin G, and streptomycin were from Invitrogen. α_2-M was from Roche Molecular Biochemicals. Goat anti-mouse conjugated with fluorescein isothiocyanate and goat anti-rabbit-conjugated rhodamine red were from Jackson Immunoresearch Laboratory, Inc. (West Grove, PA). Rabbit polyclonal hADAM19 antibodies pAb361 (anti-metalloproteinase domain) and pAb362 (anti-disintegrin domain) were generated by our laboratory as reported (28).

PCR Primers, Mutagenesis, and Expression Constructs—pCR3.1uni-ADAM19 wild type and mutants with or without the FLAG tag were generated by high fidelity polymerase chain reaction with *Pfu* polymerase (Stratagene) as described (40–43). The primer sequences for wild type ADAM19 were 5′-ACC ATG CCA GGG GGC GCA GGC GCC-3′ (forward primer) and 5′-GAT TTT CGA GCT AAT CAT CCC TCC-3′ (reverse primer). For deletion from the transmembrane domain to the cytoplasmic domain, sequences were 5′-ACC ATG CCA GGG GGC GCA GGC GCC-3′ (forward primer) and 5′-AGG ACC CAC ACT CTC AGG GGG-3′ (reverse primer). For ^{196}KR to AA mutant, sequences were 5′-CAG ACC AAG **GCG GCA** CCT CGC AGG-3′ (forward primer) and 5′-CCT GCG AGG **TGC CGC** CTT GGT CTG-3′ (reverse primer). For ^{199}RR to AA mutant, sequences were 5′-G AAG CGA CCT **GCC GCG** ATG AAA AGG-3′ (forward primer) and 5′-CCT TTT CAT **CGC GGC** AGG TCG CTT C-3′ (reverse primer). For ^{202}KR to AA mutant, sequences were 5′-CGC AGG ATG **GCA GCG** GAA GAT TTA AAC-3′ (forward primer) and 5′-GTT TAA ATC TTC **CGC TGC** CAT CCT GCG-3′ (reverse primer). Expression constructs for the wild type full-length form and the truncation form were named F46 and D52, respectively. The ^{196}KR to AA, ^{199}RR to AA, and ^{202}KR to AA mutants of full-length and truncation forms were called ^{196}RA-F, ^{196}RA-D, ^{199}RA-F, ^{199}RA-D, ^{202}RA-F, ^{202}RA-D, respectively. All constructs were confirmed by DNA sequencing. The expression vectors for furin and its soluble form, paired basic amino acid-converting enzyme 4 (PACE4), α_1-PI (pAT), and Pittsburgh mutant of α_1-PI (pATp) were constructed as previously described (37).

DNA Transfection and Generation of Stable hADAM19 Expression Cell Lines—LipofectAMINE 2000-mediated DNA transfections into MDCK cells were performed following the instructions provided by Invitrogen. Stable lines were selected in the presence of G418 (400 μg/ml) and screened by Western blotting as described (40–42).

Western Blotting—The experiments were carried out as described previously (40, 41). Briefly, cells were grown to 80% confluence and were treated as indicated. After centrifugation at 14,000 × *g* for 15 min at 4 °C to clear any debris, the serum-free media were prepared for SDS-PAGE. The cells were lysed with RIPA (50 mM Tris, pH 7.5, 150 mM NaCl, 0.25% sodium deoxycholate, 0.1% Nonidet P-40, 1 mM phenylmethylsulfonyl fluoride, 2.5 μM GM6001, 10 μg/ml aprotinin, 10 μg/ml E64, and 10 μg/ml pepstatin A) for 15 min in ice. The supernatant was collected after centrifugation at 14,000 × *g* for 20 min at 4 °C. After electrophoresis, the proteins were transferred onto nitrocellulose membranes and probed with anti-FLAG-M2 or anti-hADAM19 and developed as described (40, 41).

Purification of Soluble hADAM19 and Protein N-terminal Sequencing—All proteins were purified on anti-FLAG-M2 affinity columns as described (42, 43). Briefly, cells stably expressing wild type soluble hADAM19 (D52-5) or ^{199}RR to AA mutant (^{199}RA-D-6) were grown to 100% confluence, then washed with PBS twice and incubated for 48 h in serum-free medium containing GM6001 (to prevent the degradation of hADAM19). The conditioned media were collected, centrifuged to clear debris, and loaded onto an anti-M2 immuno-affinity column (1 ml of resuspended agarose) prewashed with Tris-buffered saline. The bound materials were extensively washed with Tris-buffered saline, eluted with FLAG peptides, and collected in 200-μl fractions. The fractions were analyzed by Western blot using anti-hADAM19 antibodies or anti-FLAG-M2. The fraction containing the highest hADAM19 protein concentration was prepared for protein N-terminal sequencing. After separation by SDS-PAGE, the samples were transferred to a polyvinylidene difluoride membrane and stained with Coomassie Blue R-250. After destaining, the hADAM19 bands were excised and sent to the Bioanalytical Core Facility at the Florida State University for N-terminal amino acid sequencing.

α_2-M Trapping Assay to Determine Endopeptidase Activity of hADAM19 Species—The detailed experimental procedure was previously reported (27, 28). Briefly, 10 μl of the fraction containing purified soluble hADAM19 was mixed with 24 μl of α_2-M (0.2 unit/ml), adjusted to a total volume of 100 μl by adding HEPES buffer (50 mM HEPES, pH 7.5, 200 mM NaCl, 10 mM $CaCl_2$, 25 μM $ZnCl_2$, 0.05% Brij-35), and incubated at 37 °C for 1–5 days. A 20-μl aliquot of the mixture was removed daily, put into 2× SDS-PAGE sample buffer, and boiled. Following SDS-PAGE, the protein bands in the gels were visualized by silver staining.

Transient Transfection into COS1, RPE.40, or 7.P15 Cells—COS1, RPE.40 or 7.P15 cells were seeded in 24- or 6-well plates for 16–24 h at 80% confluence prior to transfection. The cells were then transfected with the indicated plasmids using LipofectAMINE 2000. After 6–10 h, serum-free or 5% FBS DMEM containing 2.5 μM GM6001, with or without CMK, BFA, or A23187 at indicated concentrations, were added for another 24 h. The conditioned media and cell lysates were analyzed by Western blotting. For co-transfection experiments in these cells, the indicated plasmid was transfected alone as a control and then co-transfected with expression plasmids directing the production of furin, PACE4, pAT, pATp, furin and pAT, or furin and pATp. After 6–10 h, serum-free or 5% FBS DMEM containing GM6001 (2.5 μM) was added to the transfected cells for 16–24 h. Then, the conditioned media and cell lysates were analyzed by Western blotting as described above.

Glycosylation Analysis—*N*-Glycosylation *in vitro* was investigated by endoglycosidase F treatment as described previously (40, 41). Briefly, transfected cells were grown to 80% confluence and incubated in serum-free medium for 24 h. The conditioned media were then collected, and the cells were lysed with RIPA. After centrifugation, the conditioned media or the supernatant from RIPA were treated with glycosidase F (5 units, Roche Molecular Biochemicals) for 20 h at 37 °C and analyzed by Western blotting.

Confocal Microscopy—The procedures have been described in detail previously (38, 40). Briefly, MDCK cells expressing hADAM19 wild type or ^{199}RA mutant were grown on coverslips in six-well plates with or without treatment with CMK, BFA, or A23187. After fixing with Lina's fixation buffer for 30 min, the cells were permeabilized with buffer A (0.3% Triton X-100, 1% neutral detergent solution, 1% bovine serum albumin, and 0.01% NaN_3 in PBS) for 1 h and incubated for 3 h with anti-furin and anti-FLAG-M2 (1:100 dilution in buffer A) for double staining. After washing with PBS three times, secondary antibodies conjugated with either fluorescein isothiocyanate or rhodamine red were added to the cells for 1 h, followed by four washes with PBS. Confocal microscopy experiments were performed at the Biological Science Imaging Resource Facility at Florida State University.

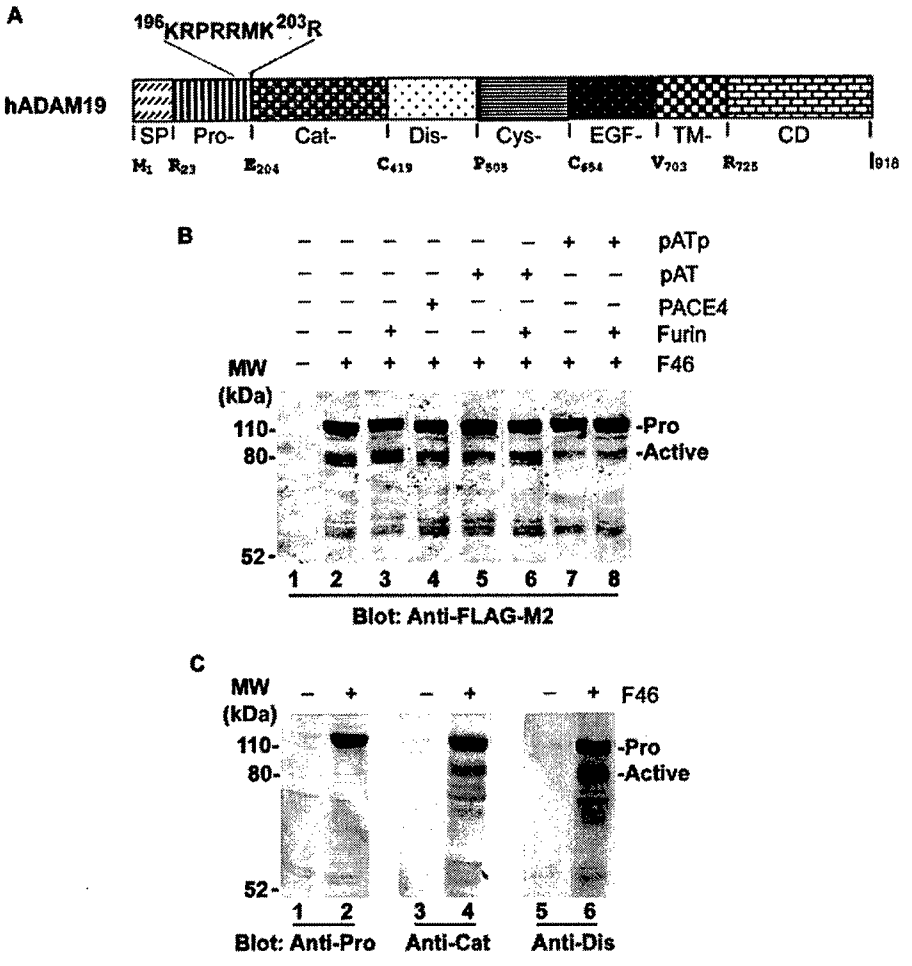

FIG. 1. **The prodomain removal of hADAM19 by furin.** *A*, a schematic diagram of the hADAM19 domain structure. The furin recognition sequence is shown *above* the border between the pro- and catalytic domains. *SP*, signal peptide; *Pro-*, prodomain; *Cat-*, catalytic domain; *Dis-*, disintegrin domain; *Cys-*, cysteine-rich domain; *EGF-*, EGF-like domain; *TM*, transmembrane domain; *CD*, cytoplasmic domain. *B*, detection of hADAM19 by Western blotting with anti-FLAG-M2 monoclonal antibody. Cell lysates from COS1 cells transfected with the blank vector (*lane 1*), pCR3.1-hADAM19 (F46) alone (*lane 2*), or co-transfected with plasmid encoding furin (*lane 3*), PACE4 (*lane 4*), pAT (*lane 5*), pAT and furin (*lane 6*), pATp (*lane 7*), or pATp and furin (*lane 8*). The pro- and active forms of hADAM19 are indicated. *C*, characterization of hADAM19 using polyclonal antibodies against different domains of hADAM19. Cell lysates from *lanes 1* and *2* in *B* were analyzed by Western blotting with the following hADAM19 polyclonal antibodies: anti-prodomain (*Pro*) (*lanes 1* and *2*), anti-catalytic domain (*Cat*) (*lanes 3* and *4*), or anti-disintegrin domain (*Dis*) (*lanes 5* and *6*).

RESULTS

Removal of the hADAM19 Prodomain Is Dependent on Furin Activity—The sequence of hADAM19 contains two potential furin recognition sites (R*X*(K/R)R), ^{196}KRPRRMK^{203}R, between its pro- and catalytic domains (Fig. 1*A*). To ascertain the role of furin in the cleaving of the hADAM19 prodomain, wild type hADAM19 (F46) with a C-terminal FLAG tag was transfected into COS1 cells alone or co-transfected with furin, PACE4, α_1-proteinase inhibitor (pAT), both furin and pAT, Pittsburgh mutant of α_1-proteinase inhibitor (pATp, a specific inhibitor of furin) (37, 45), or both furin and pATp. As shown in Fig. 1*B*, active hADAM19 forms were increased by the introduction of furin, but not PACE4. Furthermore, pATp blocked the processing of hADAM19; furin could not restore this processing when cells were co-transfected with furin and pATp (*lane 8*). pAT had little effect on endogenous or furin-induced processing of hADAM19 (*lanes 2*, *3*, *5*, and *6*). Because pATp did not completely block the hADAM19 processing, the low levels of endogenous processing may also be meditated by other proprotein convertases in addition to furin (*lanes 7* and *8*).

Interestingly, both the pro- and active forms of hADAM19 were doublets. These doublets may be differentially glycosylated forms. According to protein sequence analyses, hADAM19 has five potential glycosylation sites (27). Indeed, endoglycosidase F converted the doublets into a single pro- or active form, respectively (data not shown). To verify that the active hADAM19 lacks a prodomain, hADAM19 antibodies against the pro-, catalytic, or disintegrin domains (28) were used to probe the proteins in the cell lysates. The results in Fig. 1*C* clearly showed that the processed 80-kDa hADAM19 came from the removal of its prodomain because it was not recognized by the antibody against the prodomain peptide; however, it was detected with antibodies against its catalytic and disintegrin domains, respectively. These data showed that furin activity played a major role for the intracellular removal of hADAM19 prodomain.

To further demonstrate a direct role for furin in the activation of the hADAM19 zymogen, COS1 cells transfected with wild type hADAM19 (F46) were incubated with dec-Arg-Val-Lys-Arg-CMK (decRVKR-CMK), a widely used inhibitor of furin (17, 38, 40, 46, 47). As shown in Fig. 2*A*, decRVKR-CMK blocked the activation of hADAM19 in a dose-dependent manner. Because furin is mainly localized in TGN and the autoactivation of furin is calcium-dependent (48), we investigated whether hADAM19 activation occurred in the trans-Golgi network and required calcium. COS1 cells transfected with wild type hADAM19 were treated with BFA, which blocks protein trafficking from the ER to the Golgi apparatus (48, 49), or A23187, a calcium ionophore known to inhibit the maturation of furin (48). As shown in Fig. 2*B*, only the pro-forms of hADAM19 were detected upon treatment with either BFA or A23187. These results are consistent with furin-mediated activation of hADAM19.

Deletion of the Transmembrane Domain and the Cytoplasmic Tail of hADAM19 Does Not Alter the Processing of the Prodomain by Furin—To isolate soluble hADAM19 protein for enzyme activity assays, a construct encoding the extracellular domain (ectodomain) of hADAM19 containing a C-terminal FLAG tag was generated; this construct was called D52 and lacked the transmembrane domain and cytoplasmic domain

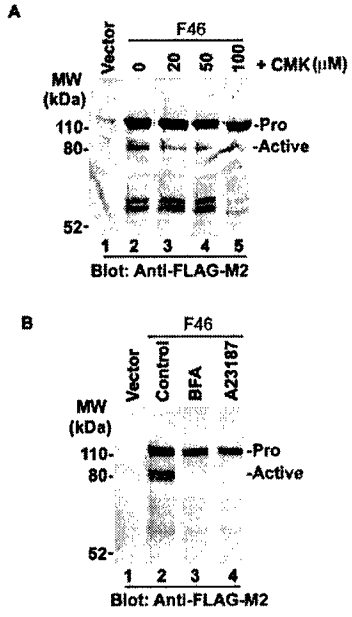

FIG. 2. **Blocking hADAM19 processing with CMK, BFA, or A23187.** *A*, dose-dependent inhibition of hADAM19 processing by decRVKR-CMK. COS1 cells transfected with the blank vector (*lane 1*) or pCR3.1hADAM19 (F46, *lanes 2–5*) were grown in 24-well plates with 0.1% methanol (v/v) (*lanes 1* and *2*) or CMK at 20 μM (*lane 3*), 50 μM (*lane 4*), or 100 μM (*lane 5*) for 24 h. The cell lysates were analyzed by Western blotting with anti-FLAG-M2. *B*, prevention of the hADAM19 prodomain removal by BFA and A23187. COS1 cells were transfected with the blank vector (*lane 1*) or F46 (*lanes 2–4*). Cells were grown in 24-well plates without (*lanes 1* and *2*) or with either 10 μg/ml BFA (*lane 3*) or 0.5 μM A23187 (*lane 4*) for 24 h. The cell lysates were analyzed as in *A*.

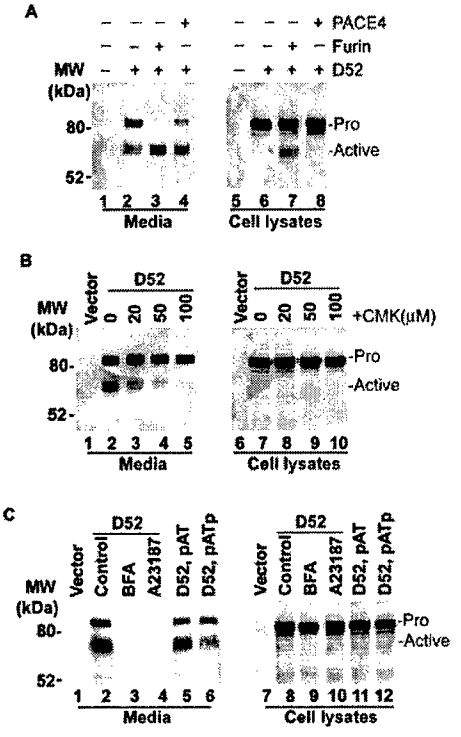

FIG. 3. **Activation of the ectodomain of hADAM19.** *A*, enhancement of the processing of soluble hADAM19 by furin. COS1 cells were transfected with the blank vector (*lanes 1* and *5*), or vector expressing soluble hADAM19 (D52) alone (*lanes 2* and *6*), or co-expressing with furin (*lanes 3* and *7*), or with PACE4 (*lanes 4* and *8*). Both conditioned media and cell lysates (*lanes 5–8*) were analyzed by Western blotting with anti-FLAG-M2. *B*, dose-dependent inhibition of the processing of soluble hADAM19 by CMK. The conditioned media (*lanes 1–5*) and cell lysates (*lanes 6–10*) were from COS1 cells transfected with the blank vector (*lanes 1* and *6*) or D52 (*lanes 2–5* and *7–10*). Cells were grown in 24-well plates with 0.1% methanol (v/v) (*lanes 1, 2, 6,* and *7*) or CMK at 20 μM (*lanes 3* and *8*), 50 μM (*lanes 4* and *9*), and 100 μM (*lanes 5* and *10*) for 12–16 h followed by incubation in serum-free media for 24 h. Samples were analyzed by Western blotting as in *A*. *C*, processing of soluble hADAM19 in the secretory pathway. COS1 cells were grown in 24-well plates overnight and then transfected with the blank vector (*lanes 1* and *7*) or D52 alone (*lanes 2–4* and *8–10*), or co-transfected with plasmids encoding either pAT (*lanes 5* and *11*) or pATp (*lanes 6* and *12*). The next day, cells were treated with either 10 μg/ml BFA (*lanes 3* and *9*) or 0.5 μM A23187 (*lanes 4* and *10*) in serum-free medium for 24 h. The conditioned media (*lanes 1–6*) or cell lysates (*lanes 7–12*) were analyzed as in *A*.

(Fig. 4*A*). This hADAM19 ectodomain construct was transfected into COS1 cells. As shown in Fig. 3*A*, only the active forms of soluble hADAM19 were detected in the media from COS1 cells co-expressing the hADAM19 ectodomain and furin. Both pro- and active forms were detected in the media from the cells co-transfected with PACE4 or transfected with the ectodomain construct alone. Additionally, the active forms were detected in the cell lysates only when cells were co-transfected with furin (Fig. 3*A*, *lanes 5–8*).

A dose-dependent inhibition of soluble hADAM19 activation by decRVKR-CMK was observed (Fig. 3*B*). However, there was no significant effect of decRVKR-CMK on the intracellular levels of hADAM19. Furthermore, there was no secretion of soluble hADAM19 in the transfected cells treated with either BFA or A23187 (Fig. 3*C*). Also, pATp dramatically decreased the amount of active forms in the medium when it was expressed in COS1 cells, but pAT failed to do so (Fig. 3*C*). Once again, no significant differences were seen in response to these treatments in the cell lysates (Fig. 3*C*). These results show that the soluble forms of hADAM19 were processed in the same manner as the full-length form and are consistent with furin-mediated activation of hADAM19.

There Are Two Alternative Furin Recognition Sites between the Pro- and Catalytic Domain of hADAM19—Upon the examination of the hADAM19 protein sequence, two consecutive furin recognition sites (R*X*(K/R)R), ^{196}KRPR^{200}R and ^{199}RRMK^{203}R, were found (Fig. 1*A*). We hypothesized that these two furin recognition sites are alternatively used for the intracellular activation of pro-ADAM19 by furin. To test this hypothesis, three mutants were generated in full-length and ectodomain hADAM19, which converted the ^{196}KR, ^{199}RR, and ^{202}KR into AA, respectively. These were named as ^{196}RA-F, ^{196}RA-D, ^{199}RA-F, ^{199}RA-D, ^{202}RA-F, and ^{202}RA-D, respectively, indicating that one (^{196}RA-F, ^{196}RA-D, ^{202}RA-F, or ^{202}RA-D) or no (^{199}RA) furin recognition site existed in the hADAM19 mutants (Fig. 4*A*).

All of the plasmids were transfected into COS1 cells to compare the levels of activated hADAM19 for the wild type and RA mutants in both the full-length (RA-F) and ectodomain forms (RA-D). As shown in Fig. 4 (*B* and *C*), no active forms of ^{199}RA mutants were detected as a result of the absence of a furin cleavage motif, whereas almost equivalent amounts of the active forms of the ^{196}RA and ^{202}RA mutants were detected. The wild type, full-length hADAM19 (Fig. 4*B*) and ectodomain form (Fig. 4*C*) were studied in parallel with the mutants. In addition, the protein levels of hADAM19 were almost equal among the cell lysates from these transfectants (Fig. 4, *B* and *C*). These results strongly supported the hypothesis that processing of the prodomain of hADAM19 was dependent on the presence of either one of the two consecutive furin recognition sites between the pro- and catalytic domains.

To further confirm that furin processed hADAM19 via one of the two alternative furin recognition sites, samples of the media from the four cell lines in Fig. 4*C* were incubated with the medium containing soluble furin, which was obtained from the

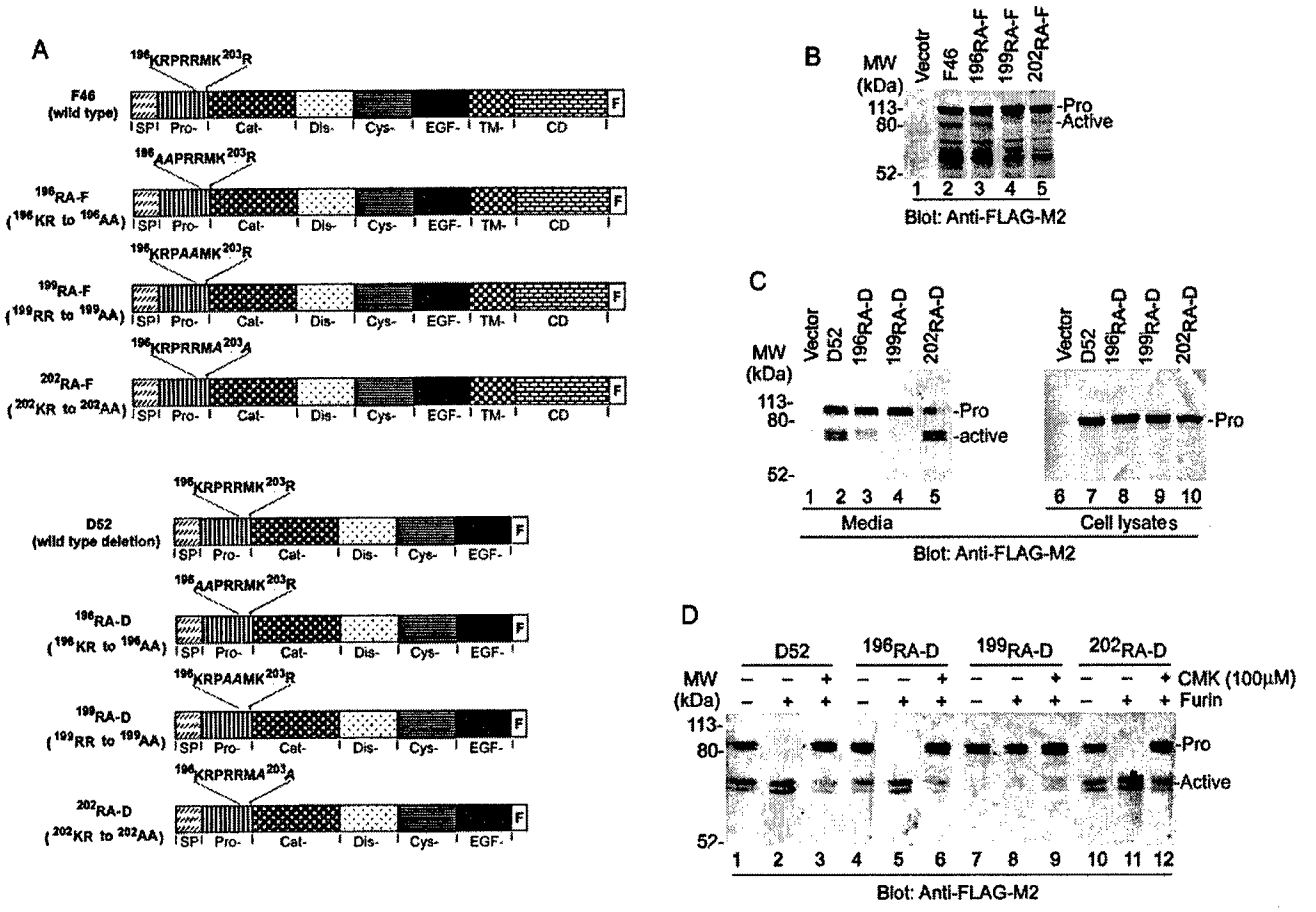

FIG. 4. **Requirement of furin motifs between the pro- and catalytic domains for the activation of hADAM19.** *A*, a schematic illustration for the wild type expression vector pCR3.1hADAM19 and its mutant constructs. All the constructs have a C-terminal FLAG tag. *SP*, signal peptide; *Pro-*, prodomain; *Cat-*, catalytic domain; *Dis-*, disintegrin domain; *Cys-*, cysteine-rich domain; *EGF-*, EGF-like domain; *TM*, transmembrane domain; *CD*, cytoplasmic domain; *F*, FLAG tag. *B*, processing of hADAM19 in the ^{199}RR to AA mutant is abolished. COS1 cells were transfected with the blank vector (*lane 1*), F46 (*lane 2*), ^{196}RA-F (*lane 3*), ^{199}RA-F (*lane 4*), or ^{202}RA-F (*lane 5*), and grown in 24-well plates for 24–36 h. The cells were lysed with RIPA followed by SDS-PAGE and Western blotting with anti-FLAG-M2. *C*, inhibition of the processing of the hADAM19 ectodomain in the ^{199}RR to AA mutant. The conditioned media (*lanes 1–5*) and cell lysates (*lanes 6–10*) were from COS1 cells transfected with the blank vector (*lanes 1* and *6*), D52 (*lanes 2* and *7*), ^{196}RA-D (*lanes 3* and *8*), ^{199}RA-D (*lanes 4* and *9*), or ^{202}RA-D (*lanes 5* and *10*) overnight, followed by incubation in serum-free medium for 24 h. The samples were analyzed by Western blotting with anti-FLAG-M2. *D*, activation of the soluble hADAM19 by exogenous soluble furin. The condition media from *lanes 2–4* in *C* were mixed with equal volumes of conditioned serum-free media from COS1 cells transfected with the blank vector (*lanes 1, 4, 7,* and *10*) or soluble furin (*lanes 2, 3, 5, 6, 8, 9, 11,* and *12*). After being incubated with (*lanes 3, 6, 9,* and *12*) or without 50 μM CMK (*lanes 1, 2, 4, 5, 7, 8, 10,* and *11*) at 37 °C for 24 h, the samples were analyzed by Western blotting as in *C*.

furin-transfected COS1 cell culture. The medium from COS1 cells transfected with a blank vector was used as a negative control. As shown in Fig. 4*D*, soluble furin did not process the ^{199}RA mutant of the soluble hADAM19. However, the wild type and the mutant soluble proteins containing a furin recognition motif were cleaved by furin. This furin-mediated processing was sensitive to decRVKR-CMK inhibition, consistent with the intracellular processing results obtained earlier (Figs. 3*A* and 4*C*). These results demonstrated that furin could activate hADAM19 at both furin cleavage sites between the prodomain and the catalytic domain of the zymogen.

Removal of the Prodomain Was Required for hADAM19 to Exert Its Proteolytic Activity—In our previous reports, an *in vitro* assay was established using α_2-M to test the activity of hADAM19 (27, 28). To assess the importance of zymogen activation to the proteolytic activity of hADAM19, stable lines of wild type hADAM19 and its ^{199}RA mutants were generated in MDCK cells, in which the endogenous furin activity is high (38, 40, 50). One stable line was chosen from each group as a representative to be treated with CMK, BFA, or A23187 and to examine whether hADAM19 would display the same processing as it did in COS1 cells. As predicted, CMK, BFA, or A23187 blocked the activation of wild type hADAM19 in the stably transfected MDCK cells called F46-4 (Fig. 5*A*). MDCK cells stably expressing the full-length ^{199}RA (^{199}RA-F-9) showed no conversion of the pro-hADAM19 to its active form (Fig. 5*A*). Furthermore, as shown in Fig. 5*B*, the active forms were only detected in the medium from MDCK cells stably expressing soluble hADAM19 (D52-5). When D52-5 cells were treated with decRVKR-CMK for 24 h, the pro-forms of soluble hADAM19 were predominantly detected from the cell culture medium. There were no active forms detected in the medium from the ^{199}RA-D6 mutant cells, which were MDCK cells stably expressing soluble hADAM19 with the ^{199}RA mutation (Fig. 5*B*).

Soluble hADAM19 proteins were purified from conditioned media of D52-5 and ^{199}RA-D6 cells. The endopeptidase activity of the purified metalloproteinases was tested using an α_2-M trapping and cleaving assay. As shown in Fig. 5*C*, only the wild type proteins could complex with α_2-M and generate two cleaved products. This activity was completely blocked by EDTA. The ^{199}RA mutant proteins were inactive, likely because the prodomain containing the cysteine switch residue

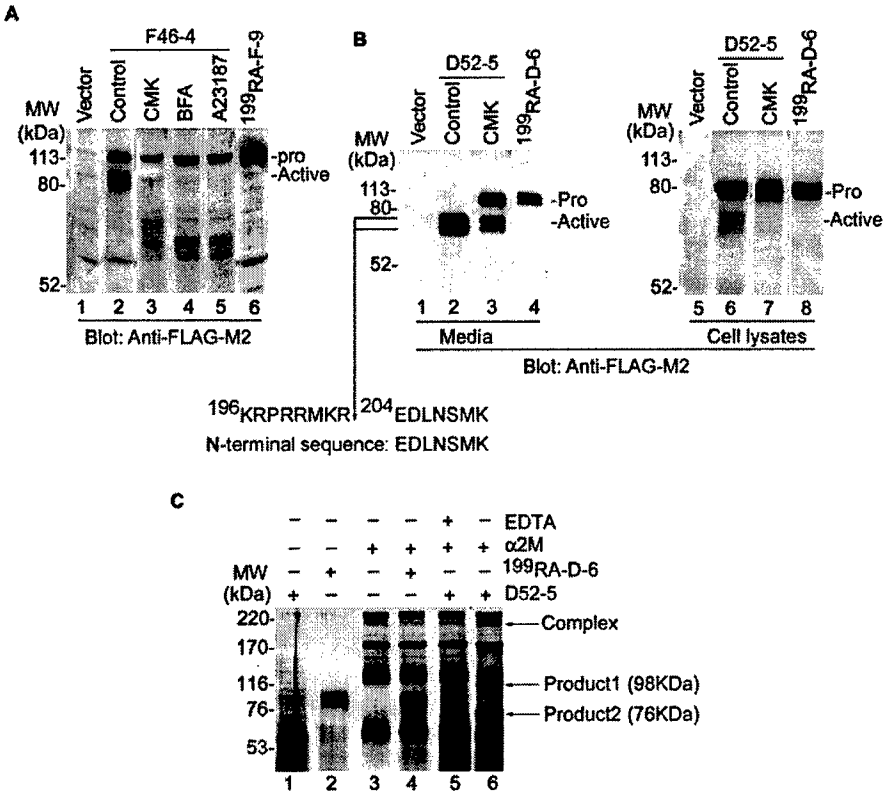

FIG. 5. **Requirement of the zymogen activation for the proteolytic activity of hADAM19.** *A*, processing of hADAM19 in stably transfected MDCK cells. MDCK cells stably expressing wild type hADAM19 (F46-4; *lanes 2–5*) or ^{199}RA mutant (^{199}RA-F-9; *lane 6*) were seeded in six-well plates at 50% confluence. The next day, cells were treated with CMK (100 μM, *lane 3*), BFA (10 μg/ml, *lane 4*), or A23187 (0.5 μM, *lane 5*). *Lanes 2* and *6* represent untreated controls. The cells were lysed with RIPA followed by analysis of Western blotting using anti-FLAG-M2. MDCK cells stably transfected with the blank vector were an additional control (*lane 1*). *B*, the requirement of furin in the processing of soluble hADAM19 in stably transfected MDCK cells. MDCK cells stably expressing soluble hADAM19 (D52-5) (*lanes 2, 3, 6,* and *7*) or soluble ^{199}RA mutant (^{199}RA-D-6) (*lanes 4* and *8*) were grown in 24-well plates to 100% confluence. Cells were incubated in serum-free media without (*lanes 1, 2, 4, 5, 6,* and *8*) or with CMK (100 μM, *lanes 3* and *7*) for 24 h. Both conditioned media (*lanes 1–4*) and lysates (*lanes 5–8*) were analyzed by Western blotting as in *A*. MDCK cells stably transfected with the blank vector is a control (*lane 1*). *C*, the proteolytic activity of soluble mature hADAM19. Purified soluble hADAM19 from D52-5 and ^{199}RA-D6 were incubated in reaction buffer alone (*lanes 1* and *2*) or with α_2-M in the absence (*lanes 4* and *5*) or presence of EDTA (*lane 5*) for 48 h. α_2-M in reaction buffer alone (48 h) was a control (*lane 3*). The α_2-M·hADAM19 complex and the cleavage products of α_2-M by hADAM19 are labeled on the *right*. Note that pro-soluble hADAM19 (^{199}RA-D-6) did not form the complex with α_2-M.

was not removed by furin (Fig. 5*B*). These results suggest that hADAM19 activation also obeys the cysteine-switch mechanism for zymogen latency and activation. Furthermore, N-terminal sequences of the purified hADAM19 proteins from the media revealed that the processed doublets (Fig. 5*B*, *lane 2*) had the identical N-terminal sequences of ^{204}EDLNSMK, suggesting that furin prefers to cleave hADAM19 using the recognition site of ^{200}RMK^{203}R rather than ^{197}RPR^{200}R. The doublets have different glycosylation patterns as verified by endoglycosidase F treatment experiments (data not shown). These results confirmed the prediction that hADAM19 was activated by furin through cleavage of the ^{203}R-^{204}E peptide bond at the sequence ^{199}RRMKR ↓ ^{204}EDLNSMK.

Two Furin-deficient Cell Strains (RPE.40 and 7.P15) Do Not Activate Pro-hADAM19, and the Introduction of Furin into These Cells Restores Zymogen Activation—To further confirm that furin activity was required for the intracellular activation of pro-hADAM19, the wild type of full-length and soluble forms of hADAM19 (F46 and D52) were transfected into RPE.40 cells and 7.P15 cells, two furin-deficient cell strains (44, 51). Processing of hADAM19 to its mature forms was negligible in these cell lines. However, the active forms were clearly detectable when cells co-expressed furin (data not shown). As shown in Fig. 6, there were barely detectable levels of the active forms of soluble hADAM19 in the media of the two D52-transfected cell lines. High levels of active forms were only detected in the media when the cells co-expressed furin, although PACE4 also increased the amount of active forms when it was co-expressed with D52 (Fig. 6, *A* and *B*). Curiously, the active forms were only detected in the lysates of cells co-expressing D52 and furin. These data further confirm that furin was responsible for the intracellular activation of hADAM19.

Furin Was Co-localized with hADAM19 in the ER-Golgi Complex and/or TGN—To verify that hADAM19 was a physiologically relevant substrate of furin, the cellular localization of furin and hADAM19 was examined by confocal microscopy using MDCK cells stably expressing hADAM19 (Fig. 7). Untreated cells are marked as F46-4 (control) (Fig. 7, *top panels*). Co-localization of hADAM19 and furin was clearly observed, and was consistent with ER-Golgi complex and/or TGN localizations (*top, middle panel*). Furthermore, hADAM19 was also seen at the edges of the plasma membrane (*right lane, top panel*) where furin was rare (*left lane, top panel*). Interestingly, a similar pattern of co-localization between the ^{199}RA mutant and furin was also observed (Fig. 7, *bottom panels*), suggesting that the co-localization was independent of the recognition sites for furin in hADAM19. To test whether the agents that block the activation of hADAM19 could prevent co-localization between furin and hADAM19 (Fig. 5*A*), the cells were treated with CMK, BFA, or A23187. None of these treatments interfered with the co-localization pattern of furin and hADAM19 (Fig. 7), suggesting that furin may be co-localized with

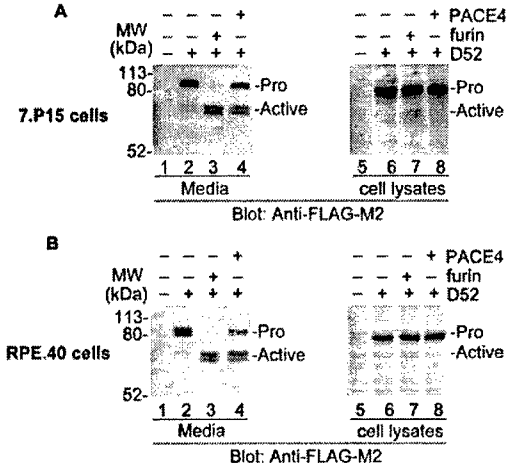

FIG. 6. **Processing the hADAM19 prodomain in furin-deficient mammalian cell lines.** *A*, hADAM19 in 7.P15 cells. 7.P15 cells were transfected with the blank vector (*lanes 1* and *5*) or D52 alone (*lanes 2* and *6*) or co-transfected with D52 and plasmids encoding furin (*lanes 3* and *7*) or PACE4 (*lanes 4* and *8*). Cells were grown in 24-well plates for 12–16 h followed by incubation in serum-free medium for 24 h. Conditioned media (*lanes 1–4*) and cell lysates (*lanes 5–8*) were analyzed by Western blotting with anti-FLAG-M2. *B*, hADAM19 in RPE.40 cells. RPE.40 cells were transfected with the blank vector (*lanes 1* and *5*) or D52 alone (*lanes 2* and *6*) or were co-transfected either D52 and plasmids encoding furin (*lanes 3* and *7*) or PACE4 (*lanes 4* and *8*). Cells were grown in 24-well plates overnight followed by incubation in serum-free media for 24 h. Conditioned media (*lanes 1–4*) and cell lysates (*lanes 5–8*) were analyzed by Western blotting as in *A*.

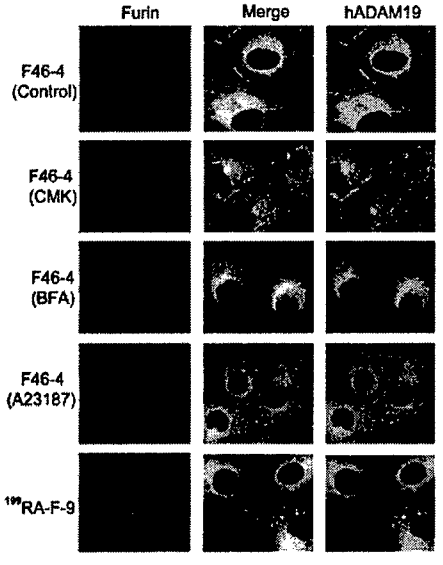

FIG. 7. **Co-localization of hADAM19 and furin.** MDCK cells stably expressing wild type hADAM19 (F46-4) or ^{199}RA mutant (^{199}RA-F-9) grown on coverslips in six-well plates were treated with nothing (control), 100 μM CMK, 10 μg/ml BFA, or 0.5 μM A23187 for 24 h. The fixed slides were stained for both hADAM19 with anti-FLAG-M2 (*right panels*) and furin with anti-furin (*left panels*). The merged pictures for both hADAM19 and furin are presented in the *middle column*. Note that hADAM19 is co-localized with furin, independent on furin motif, with neither CMK, BFA, nor A23187 altering the staining pattern.

hADAM19 in perinuclear ER-Golgi complex and/or TGN independent of the furin catalytic activity.

DISCUSSION

Proteolysis of the extracellular matrix and cell surface proteins mediated by metalloproteases, including MMPs and ADAMs, is of vital importance for tissue-remodeling processes during normal and pathological conditions, such as tissue morphogenesis, wound healing, inflammation, and tumor cell invasion and metastasis (3–7, 52, 53). Metalloproteases are synthesized as inactive proenzymes or zymogens, and their latency is maintained by a cysteine-switch residue in the propeptide domain in which the thiol group is coordinated to the active site zinc (II) (2, 9–12). To display any proteolytic activities, the prodomain located N-terminal to the catalytic domain must be removed from the zymogen in most cases. Recently, PCs, such as furin and or furin-like serine peptidases, have been recognized as very important enzymes for the zymogen activation, although various mechanisms have been proposed for the activation of pro-MMPs and pro-ADAMs. Furin or furin-like PCs mediate zymogen activation by recognizing a conserved R*X*(K/R)R motif in the boundary between pro- and catalytic domains. This motif is present in almost all ADAMs and nine MMPs (2, 13, 53). By analyzing the intracellular activation of hADAM19, we have demonstrated that both furin activity and one of the two consecutive sites in ^{197}RPRRMK^{203}R in ADAM19 are required for activation, which is dependent on calcium and proper secretory pathway trafficking. Furthermore, we have provided direct evidence that furin is co-localized with hADAM19 in ER-Golgi complex and/or TGN. This colocalization between furin and hADAM19 is independent of the furin recognition site and is resistant to a variety of treatments, such as CMK, BFA, and A23187, that inhibit furin activity, vesicular trafficking, and calcium signal, respectively. These findings are consistent with the report published recently showing that furin was co-localized with MMP16 independent of their apparent enzyme-substrate relationship (40).

Latency and Activation of ADAMs—The classic cysteine switch mechanism for pro-MMP latency and activation was originally proposed for MMPs (10) and may be applied for many MMPs discovered with the exception of MMP-3, MMP-23, and MMP-26 (41, 54–58). The activation of pro-MMP-3 by a mercurial compound was triggered by a perturbation of the conformation of the precursor rather than a direct disruption of the Cys-zinc interaction (54). A salt bridge in pro-MMP-3 might also contribute to the latency of the proenzyme (55). Organomercurial treatment failed to activate pro-MMP-26 with a unique cysteine-switch motif, P**H**^{81}CG*XX*D, and when the conserved cysteine-switch sequence, P**R**^{81}CG*XX*D, in the prodomain of pro-MMP-26 was restored by mutagenesis, the cysteine-switch activation mechanism was not induced (58).

Regarding the ADAM family members, the active ADAMs, such as ADAM1, -9, -10, -12, -15, -17, -19, -28, and ADAMTS1, -4, and -12, contain a catalytic site consensus sequence (HE*XX*H) in their metalloprotease domains (2, 11–14, 16–21, 27–29, 53, 59–61). They may also have a putative cysteine-switch residue in their prodomain to keep them inactive (9). For example, the investigation by Leochel *et al.* (11) demonstrated that the latency and activation mechanism of ADAM12 was similar to the cysteine switch model proposed for MMPs. ADAM9, -15, and -17 showed catalytic activity against their substrates only after their prodomains were removed (12, 21, 22). However, for many ADAMs, including ADAM19, no direct evidence has been provided to support the hypothesis that the Cys-zinc coordination is required for latency. For ADAM17/tumor necrosis factor-α convertase, the prodomain was not only an inhibitor of the catalytic domain, but also appeared to act like a chaperone, facilitating secretion, folding, or both of the ADAM protein (12). In this report, we have demonstrated that, after the removal of the prodomain of hADAM19 by furin, the enzyme has endopeptidase activity against α_2-M. However, furin is unable to cleave the prodomain of the ^{199}RR to AA hADAM19 mutant lacking a furin recognition site in the boundary of the pro- and catalytic domains. This mutant has no

proteolytic activity using an α_2-M trapping assay. These results demonstrate that at least one of the furin recognition sites is required for the removal of the propeptide domain by furin to activate pro-hADAM19. The detailed mechanism of pro-ADAM19 latency and activation and the role of the cysteine-switch sequence remain to be further investigated.

For the activation of ADAM zymogens, two mechanisms have been reported. One is the removal of the prodomain by autolysis, but it was shown only in ADAM28 (60). The predominant mechanism for the activation of ADAMs is mediated by furin or furin-like PCs in the secretory pathway. This mechanism has been shown in many ADAMs, including ADAM1, -9, -12, -15, -17, and -19, and ADAMTS1, -4, and -12, using N-terminal sequencing, specific inhibitors of furin, blockers of protein trafficking from ER to Golgi, exogenous soluble furin *in vitro*, furin-deficient cell lines, and mutagenesis at the furin recognition site(s) (R*X*(K/R)R) between the pro- and catalytic domain (Refs. 16–23; this report). In the present report, we provide a thorough investigation of ADAM zymogen activation mediated by furin (Figs. 1–6) and evidence that furin is co-localized with ADAMs in the ER-Golgi complex and/or TGN (Fig. 7), showing that ADAMs are similar to MMPs in these respects (38, 40).

There Are Two Consecutive Furin Recognition Sites in the Boundary of the Pro- and Catalytic Domains of hADAM19—The minimal furin recognition sequence requires basic residues at P_1 and P_4 (R*X*XR) and in some cases, at the P_1 position, an amino acid with a hydrophobic aliphatic side chain is not suitable (31). Typically, there is only one furin recognition site between the pro- and catalytic domain of the substrates of furin as found in most members of the ADAM family, seven MMPs, pro-BACE, and Notch1 receptor (2, 13–15, 30, 31, 33–40, 53, 62). In this report, we present evidence for the first time that there are two consecutive furin recognition sites, ^{197}RPR^{200}R and ^{200}RMK^{203}R, between the pro- and catalytic domain in hADAM19, which adhere to the rules for efficient cleavage by furin (31). Only pro-forms were detectable in the ^{199}RA mutant, which lacked a furin recognition site between its pro- and catalytic domain, whereas the mutants of both ^{196}RA and ^{202}RA, which possessed recognition sites, were converted into the active forms. Thus, the Arg residue at the P_4 site is required for the intracellular hADAM19 maturation mediated by furin (Figs. 4 and 5*B*). Interestingly, N-terminal sequencing of wild type mature forms (Fig. 5) confirmed that the preferred intracellular cleavage site for hADAM19 activation is the one nearer to the catalytic domain, ^{200}RMK^{203}R, as predicted before (26, 27). This motif is conserved in mice as ^{201}RMK^{204}R (24). The distal motif, ^{197}RPR^{200}R in humans, however, is replaced with ^{198}QPR^{201}R in mice, which is not efficiently cleaved by furin.

A notion that pro-hADAM19 activation by furin may be sequential, *i.e.* ^{200}R^{201}M is cleaved first followed by ^{203}R^{204}E, seems to be consistent with the partially activated soluble species seen for ^{196}RA-D compared with ^{202}RA-D data in Fig. 4*C*; however, it does not agree with the data shown in Fig. 4*B*, where it is seen that the presence of furin with the full-length ^{196}RA-F leads to more activated species than ^{202}RA-F. The delicate changes in the interactions between furin and the different mutants that have subtle structural and conformational differences might be partially responsible for the different activation levels observed. Moreover, among all the protein N-terminal sequence data of wild type hADAM19 activated species, only ^{204}EDLNSMK was found; the alternative cleavage site product of ^{201}MKRED was not detected. Most importantly, the minimal furin recognition sequence requires basic residues at P_1 and P_4 (R*X*XR) and the Arg residue at the P_4 site is required for the intracellular hADAM19 maturation mediated by furin (Figs. 4 and 5*B*). It may not be possible for furin, an endopeptidase, to effectively cleave the product of the ^{200}R-^{201}M cleavage because the ^{201}MK^{203}R-^{204}ED sequence lacks the required Arg at the P_4 site. Thus, our data suggest that the ^{203}R-^{204}E site is the predominant cleavage site and ^{200}R-^{201}M is an alternative cleavage site by furin when the predominant site is missing. This is consistent with the model proposed for wild type MT1-MMP, in which the pro-MT1-MMP is processed primarily at the ^{108}RRKR site to generate the active proteinase and the secondary site within ^{86}K*XX*RR*X*R is cleaved only when the primary ^{108}RRKR motif was mutated (39).

Notably, there are two potential consecutive furin recognition sites in other metalloproteinase zymogens, including ADAM11 (AB009675, ^{292}RLRRK^{297}R), ADAM22 (AF155382, ^{219}RPKRSK^{225}R), ADAMTS4 (AF148213, ^{206}RPRRAK^{212}R), MT2-MMP (NM_002428, ^{126}RRRRK^{131}R), and MT5-MMP (AJ010262, ^{118}RRRRNK^{224}R). The ones nearer to the catalytic domains are conserved in different species, whereas the distal ones might be acquired later during evolution. Although the significance of the two alternative recognition sites in these precursors remains poorly understood, we may speculate that the processing of these zymogens are crucial for some biological events; the zymogens may be activated by furin at a different cleavage site even if the primary site is abolished by mutation.

Significance of Furin and Its Related PC Pathways in the Processing of Precursors—Furin and its related PCs have been demonstrated as the major enzymes responsible for the maturation of many precursors, such as some ADAMs and MMPs (Refs. 16–23 and 37–40; this report). Furthermore, zymogens of BACE, a major enzyme related to Alzheimer's disease, and some growth factors and cell surface receptors, such as transforming growth factor β, insulin-like growth factor, hepatocyte growth factor receptor, and Notch1 receptor, are converted into their active forms by these PC pathways (30, 31, 33–36, 62). Thus, this activation mechanism by a PC may play key roles in many physiological and pathological events. In fact, furin knockout mice are embryonic lethal (63), and inhibition of furin results in absent or decreased invasion and tumorigenicity of human cancer cells (64, 65). The inability to activate many types of proproteins, including some pro-ADAMs and pro-MMPs, in furin null mice may contribute to the abnormal phenotypes during early development and morphogenesis in those mice. On the other hand, the design and synthesis of furin specific inhibitors may lead to a new strategy in the treatment of cancer and other diseases, such as Alzheimer's disease, in the human adult.

Acknowledgments—We thank Kim Riddle and Joe Ekman for excellent assistance in confocal microscopy at Biological Science Imaging Facility, Margaret Seavy at the Bioanalytical Facility for protein N-terminal sequencing, and Sara C. Monroe for editorial assistance with the manuscript preparation at the Florida State University. We appreciate Dr. Ping Wei at Human Genome Sciences Inc. for previous collaboration on the human ADAM19 project.

REFERENCES

1. Wolfsberg, T. G., and White, J. M. (1996) *Dev. Biol.* **180,** 389–401
2. Stone, A. L., Kroeger, M., and Sang, Q. X. (1999) *J. Protein Chem.* **18,** 447–465
3. Schlondorff, J., and Blobel, C. P. (1999) *J. Cell Sci.* **112,** 3603–3617
4. Blobel, C. P. (2000) *Curr. Opin. Cell Biol.* **12,** 606–612
5. Kheradmand, F., and Werb, Z. (2002) *Bioessays* **24,** 8–12
6. Esler, W. P., and Wolfe, M. S. (2001) *Science* **293,** 1449–1454
7. Evans, J. P. (2001) *Bioessays* **23,** 628–639
8. Bridges, L. C., Tani, P. H., Hanson, K. R. Roberts, C. M., Judkins, M. B., and Bowditch, R. D. (2002) *J. Biol. Chem.* **277,** 3784–3792
9. Grams, F., Huber, R., Kress, L. F., Moroder, L., and Bode W. (1993) *FEBS Lett.* **335,** 76–80
10. Van Wart, H. E., and Birkedal-Hansen, H. (1990) *Proc. Natl. Acad. Sci. U. S. A.* **87,** 5578–5582
11. Loechel, F., Overgaad, M. T., Oxvig, C., Albrechtsen, R., and Wewer, U. M. (1999) *J. Biol. Chem.* **274,** 13427–13433
12. Milla, M. E., Leesnitzer M. A., Moss. M. L., Clay, W. C. Carter, H. L., Miller, A. B., Su, J., Lambert, M. H., Willard, D. H., Sheeley, D. M., Kost, T. A., Burkhart, W., Moyer, M., Blackburn, R. K., Pahel, G. L., Mitchell, J. L., Hoffman, C. R., and Becherer, J. D. (1999) *J. Biol. Chem.* **274,** 30563–30570

13. Primakoff, P., and Myles, D. G. (2000) *Trends Genet.* **16,** 83–87
14. Tortorella, M. D., Burn, T. C., Pratta, M. A., Abbaszade, I., Hollis, J. M., Liu, R., Rosenfeld, S. A., Copeland, R. A., Decicco, C. P., Wynn, R., Rockwell, A., Yang, F., Duke, J. L., Solomon, K., George, H., Bruckner, R., Nagase, H., Itoh, Y., Ellis, D. M., Ross, H., Wiswall, B. H., Murphy, G., Hillman, M. C., Jr., Hollis, G. F., Newton, R. C., Magolda, R. L., Trzaskos, J. M., and Arner, E. C. (1999) *Science* **284,** 1664–1666
15. Yoshinaka, T., Nishii, K., Yamada, K., Sawada, H., Nishiwaki, E., Smith, K., Yoshino, K., Ishiguro, H., and Higashiyama, H. (2002) *Gene (Amst.)* **282,** 227–236
16. Cal, S., Arguees, J. M., Fernandez, P. L., and Lopez-Otin, C. (2001) *J. Biol. Chem.* **276,** 17932–17940
17. Gao, G., Westling, J., Thompson, V. P., Howell, T. D., Gottschall, P. E., and Sandy, J. D. (2002) *J. Biol. Chem.* **277,** 11034–11041
18. Kuno, K., Terashima, Y., and Matsushima, K. (1999) *J. Biol. Chem.* **274,** 18821–18826
19. Loechel, F., Gilpin, B. J., Engvall, E., Albrechtsen, R., and Wewer, U. M. (1998) *J. Biol. Chem.* **273,** 16993–16997
20. Lum, L., and Blobel, C. P. (1997) *Dev. Biol.* **191,** 131–145
21. Lum, L., Reid, M. S., and Blobel, C. P. (1998) *J. Biol. Chem.* **273,** 26236–26247
22. Roghani, M., Becherer, J. D., Moss, M. L., Atherton, R. E., Erdjument-Bromage, H., Arribas, J., Blackburn, R. K., Weskamp, G., Tempst, P., and Blobel, C. P. (1999) *J. Biol. Chem.* **274,** 3531–3540
23. Schlondorff, J., Becherer, J. D., and Blobel, C. P. (2000) *Biochem. J.* **347,** 131–138
24. Inoue, D., Reid, M., Lum, L., Kratzschmar, J., Weskamp, G., Myung, Y. M., Baron, R., and Blobel, C. P. (1998) *J. Biol. Chem.* **273,** 4180–4187
25. Kurohara, K., Masuda, Y., Nagabukuro, N., Tsuji, A., Amagasa, T., and Fujisawa-Sehara, (2000) *Biochem. Biophys. Res. Commun.* **270,** 522–527
26. Fritsche, J., Moser, M., Faust, S., Peuker, A., Buttner, R., Andreesen, R., and Kreutz, M. (2000) *Blood* **96,** 732–739
27. Wei, P., Zhao, Y.-G., Zhuang, L., Ruben, S., and Sang, Q.-X. (2001) *Biochem. Biophys. Res. Commun.* **280,** 744–755
28. Zhao, Y., Wei, P., and Sang, Q.-X. (2001) *Biochem. Biophys. Res. Commun.* **289,** 288–294
29. Shirakabe, K., Wasuda, S., Kurisaki, T., and Fujisawa-Sehara, A. (2001) *J. Biol. Chem.* **276,** 9352–9358
30. Molloy, S. S., Anderson, E. D., Jean, F., and Thomas, G. (1999) *Trends Cell Biol.* **9,** 28–35
31. Nakayama, K. (1997) *Biochem. J.* **327,** 625–635
32. Steiner, D. F. (1998) *Curr. Opin. Chem. Biol.* **848,** 45–62
33. Benjannet, S., Elagoz, A., Wickham, L., Mamarbachi, M., Munzer, J. S., Basak, A., Lazure, C., Cromlish, J. A., Sisodia, S., Chretien, M., and Seidah, N. G. (2001) *J. Biol. Chem.* **276,** 10879–10887
34. Bennett, B. D., Denis, P., Haniu, M., Teplow, D. B., Kahn, S., Louis, J. C., Citron, M., and Vassar, R. (2000) *J. Biol. Chem.* **275,** 37712–37717
35. Capell, A., Steiner, H., Willem, M., Kaiser, H., Meyer, C., Walter, J., Lammich, S., Multhaup, G., and Haass, C. (2000) *J. Biol. Chem.* **275,** 130849–130854
36. Creemers, J. W., Dominguez, D. I., Plets, E., Serneels, L., Taylor, N. A., Multhaup, G., Craessaaerts, K., Annaert, W., and De Strooper, B. (2001) *J. Biol. Chem.* **276,** 4211–4217
37. Pei, D., and Weiss, S. J. (1995) *Nature* **375,** 244–247
38. Wang, X., and Pei, D. (2001) *J. Biol. Chem.* **276,** 35953–35960
39. Yana, I., and Weiss, S. J. (2000) *Mol. Biol. Cell* **11,** 2387–2401
40. Kang, T., Nagase, H., and Pei, D. (2002) *Cancer Res.* **62,** 675–681
41. Kang, T., Yi, J., Yang, W., Wang, X., Jiang, A., and Pei, D. (2000) *FASEB J.* **14,** 2559–2568
42. Pei, D., Kang, T., and Qi, H. (2000) *J. Biol. Chem.* **275,** 33988–33997
43. Kang T, Yi, J., Guo, A., Wang, X., Overall, C. M., Jiang, W., Elde, R., Borregaard, N., and Pei, D. (2001) *J. Biol. Chem.* **276,** 21960–21968
44. Inocencio, N. M., Sucic, J. F., Moehring, J. M., Sepence, M. J., and Moehring, T. J. (1997) *J. Biol. Chem.* **272,** 1344–1348
45. Wasley, C. L., Rehemtulla, A., and Kaufman, R. J. (1993) *Curr. Opin. Biotechnol.* **3,** 560–565
46. Angliker, H., Wikstrom, P., Shaw, E., Brenner, C., and Fuller, R. S. (1993) *Biochem. J.* **293,** 75–81
47. Vey, M., Schafer, W., Berghofer, S., Klenk, H. D., and Garten, W. (1994) *J. Cell Biol.* **127,** 1829–1842
48. Fujiwara, T., Oda, T. K., Yokota, S., Takatsuki, A., and Ikehara, Y. (1988) *J. Biol. Chem.* **263,** 18545–18552
49. Hallenberger, S., Bosch, V., Angliker, H., Shaw, E., Klenk, H. D., and Garten, W. (1992) *Nature* **360,** 358–361
50. Shapiro, J., Sciaky, N., Lee, J., Bosshart, H., Angeletti, R. H., and Bonifacino, J. S. (1997) *J. Histochem. Cytochem.* **45,** 3–12
51. Bass, J., Turck, C., Rouard, M., and Steiner, D. F. (2000) *Proc. Natl. Acad. Sci. U. S. A.* **97,** 11905–11909
52. Chang, C., and Werb, Z. (2001) *Trends Cell Biol.* **11,** S37–S45
53. Vu, T. H., and Werb, Z. (2000) *Genes Dev.* **14,** 2123–2133
54. Chen, L. C., Noelken, M. E., and Nagase, H. (1993) *Biochemistry* **32,** 10289–10295
55. Galazka, G., Windsor, L. J., Birkedal-Hansen, H., and Engler, J. A. (1996) *Biochemistry* **35,** 11221–11227
56. Pei, D. (1999) *FEBS Lett.* **457,** 262–270
57. Velasco, G., Pendas, A. M., Fueyo, A., Knauper, V., Murphy, G., and Lopez-Otin, C. (1999) *J. Biol. Chem.* **274,** 4570–4576
58. Marchenko, N. D., Marchenko, G. N., and Strongin, A. Y. (2002) *J. Biol. Chem.* **277,** 18967–18972
59. Howard, L., Zhang, Y., Horrocks, M., Maciewicz, R. A., and Blobel, C. P. (2001) *FEBS Lett.* **498,** 82–86
60. Howard, L., Maciewicz, R. A., and Blobel, C. P. (2000) *Biochem. J.* **348,** 21–27
61. Lopez-Perez, E., Zhang, Y., Frank, S. J., Creemers, J., Seidah, N., and Checler, F. (2001) *J. Neurochem.* **76,** 1532–1539
62. Logeat, F., Bessia, C., Brou, C., LeBail, O., Jarrianlt, S., Seidah, N. G., and Israel, A. (1998) *Proc. Natl. Acad. Sci. U. S. A.* **95,** 8108–8112
63. Roebroek, A. J., Umans, L., Pauli, I. G., Robertson, E. J., van Leuven, F., Van de Ven, W. J., and Constam, D. B. (1998) *Development* **125,** 4863–4876
64. Bassi, D. E., De Cicco, R. L., Mahloogi, H., Zucker, S., Thomas, G., and Klei-Szanto, A. J. P. (2001) *Proc. Natl. Acad. Sci. U. S. A.* **98,** 10326–10331
65. Khatib, A.-M., Siegfried, G., Prat, A., Lius, J., Chretien, M., Metrakos, P., and Seidah, N. G. (2001) *J. Biol. Chem.* **276,** 30686–30693

THE JOURNAL OF BIOLOGICAL CHEMISTRY
Vol. 277, No. 50, Issue of December 13, pp. 48514–48522, 2002
Printed in U.S.A.

Autolytic Processing at Glu^{586}-Ser^{587} within the Cysteine-rich Domain of Human Adamalysin 19/Disintegrin-Metalloproteinase 19 Is Necessary for Its Proteolytic Activity*

Received for publication, September 3, 2002, and in revised form, October 15, 2002
Published, JBC Papers in Press, October 18, 2002, DOI 10.1074/jbc.M208961200

Tiebang Kang‡§, Hyun I. Park‡, Yewseok Suh‡, Yun-Ge Zhao‡, Harald Tschesche§, and Qing-Xiang Amy Sang‡¶

From the ‡Department of Chemistry and Biochemistry and Institute of Molecular Biophysics, Florida State University, Tallahassee, Florida 32306-4390 and the §Department of Biochemistry, Faculty of Chemistry, University of Bielefeld, Bielefeld 33615, Germany

We investigated the regulation of the proteolytic activity of human adamalysin 19 (a disintegrin and metalloproteinase 19, hADAM19). It was processed at Glu^{586}(P1)-Ser^{587}(P1′) site in the cysteine-rich domain as shown by protein N-terminal sequencing. This truncation was autolytic as illustrated by its R199A/R200A or E346A mutation that prevented the zymogen activation by furin or abolished the catalytic activity. Reagents that block furin-mediated activation of pro-hADAM19, decRVKR-CMK, A23187, and brefeldin A abrogated this processing. The sizes of the side chains of the P1 and P1′ residues are critical for the processing of hADAM19. The amount of processing product in the E586Q or S587A mutant with a side chain almost the same size as that in the wild type was almost equal. Conversely, very little processing was observed when the size of the side chain was changed significantly, such as in the E586A, E586G, or S587F mutants. Two mutants with presumably subtle structural distinctions from wild type hADAM19, E586D and S587T, displayed rare or little processing and had very low capacities to cleave α2-macroglobulin and a peptide substrate. Therefore, this processing is necessary for hADAM19 to exert its proteolytic activities. Moreover, a new peptide substrate, Ac-RPLE-SNAV, which is identical to the processing site sequence, was cleaved at the E-S bond by soluble hADAM19 containing the catalytic and disintegrin domains. This enzyme cleaved the substrate with K_m, k_{cat}, and k_{cat}/K_m of 2.0 mM, 2.4/min, and 1200 M^{-1} min^{-1}, respectively, using a fluorescamine assay. Preliminary studies showed that a protein kinase C activator, phorbol 12-myristate 13-acetate, promoted the cellular processing of hADAM19; however, three calmodulin antagonists, trifluoperazine, W7, and calmidazolium, impaired this cleavage, indicating complex signal pathways may be involved in the processing.

Ectodomain shedding is a process in which a wide variety of transmembrane proteins, such as growth factors and growth factor receptors, cytokines and their receptors, amyloid precursor protein (APP),[1] adhesion molecules, and enzymes, proteolytically release their extracellular domains. It is believed to play key roles in normal development, arthritis, inflammation, and tumorigenesis (1–5). Although the signal pathways regulating ectodomain shedding remain poorly understood, numerous studies have shown that structurally different proteins share common pathways (5–8). For example, phorbol 12 myristate 13-acetate (PMA), a protein kinase C (PKC) activator, is generally a potent inducer of ectodomain shedding. Other signals, such as calcium, calmodulin (CaM), tyrosine kinase, mitogen-activated protein kinase (MAPK), and phosphatase, also play roles in certain shedding processes (9–23). On the other hand, the shedding process, in most cases, is hindered by hydroxamate-based inhibitors of metalloproteinases, such as BB94, GM6001, and tumor necrosis factor-α proteinase inhibitor (TAPI) (5–8, 19, 24–26).

Inhibitor studies have shown that TIMP-3, not TIMP-1 or TIMP-2, impairs many shedding processes, indicating that the proteins comprising the a disintegrin and metalloprotease (ADAM)/adamalysin/metalloprotease, disintegrin, cysteine-rich (MDC) family, rather than the matrix metalloproteinase (MMP) family, are the predominant sheddases (27–30). Indeed, five ADAMs have been implicated in shedding processes so far. ADAM17/TACE, a major sheddase, has a role in the shedding of tumor necrosis factor-α (TNF-α), transforming growth factor-α (TGF-α), L-selectin, both TNF receptors, interleukin-1 receptor II, HER4, Notch, and TNF-related activation-induced cytokine (TRANCE). It also acts as a PMA-induced APP α-secretase (1–6, 31). ADAM10/Kuzbanian, another major sheddase, is required for Notch signaling. It can cleave the Notch ligand Delta, heparin-binding epidermal growth factor (HB-EGF), TNF-α, L1 adhesion molecule, and ephrin A2 and is

* This work was supported by National Institutes of Health Grant CA78646, by Department of Defense, U.S. Army Medical Research Acquisition Activity Grant DAMD17-02-1-0238, by American Cancer Society, Florida Division Grant F01FSU-1, by the Florida State University Research Foundation (to Q.-X. A. S.), and by the Deutsche Forschungsgemeinschaft (DFG), Bonn (SFB 549, project A05 and DFG Grant Ts 8-35/3) (to H. T.). The costs of publication of this article were defrayed in part by the payment of page charges. This article must therefore be hereby marked "*advertisement*" in accordance with 18 U.S.C. Section 1734 solely to indicate this fact.

¶ To whom correspondence should be addressed: Dept. of Chemistry and Biochemistry, Florida State University, 203 DLC, Chemistry Research Bldg., Rm. 203, Tallahassee, FL 32306-4390. Tel.: 850-644-8683; Fax: 850-644-8281; E-mail: sang@chem.fsu.edu.

[1] The abbreviations used are: APP, amyloid precursor protein; Ab, antibody; ADAM, a disintegrin and metalloproteinase; ADAMTS, a disintegrin and metalloproteinase with thrombospondin-like motifs; α2-M, α2-macroglobulin; CaM, calmodulin; decRVKR-CMK, decanoyl-Arg-Val-Lys-Arg-chloromethyl ketone; mAb, monoclonal antibody; MAPK, mitogen-activated protein kinase; MDC, metalloprotease/disintegrin/cysteine-rich; MDCK, Madin-Darby canine kidney; MMPs, matrix metalloproteinases; MT-MMPs, membrane-type MMPs; NRG, neuregulin; PKC, protein kinase C; PMA, phorbol 12-myristate 13-acetate; TACE, tumor necrosis factor α convertase; TAPI, tumor necrosis factor-α proteinase inhibitor; TIMPs, tissue inhibitors of metalloproteinases; TGF-α, transforming growth factor-α; TNF-α, tumor necrosis factor- α; TRANCE, TNF-related activation-induced cytokine; W7, *N*-(6-aminohexyl)-5-chloro-1-naphthalenesulfonamide.

an APP α-secretase (1–5, 32, 33). ADAM9 is believed to participate in the PMA-stimulated shedding of HB-EGF (34) and can function as an APP α-secretase (35). ADAM19/MDC β has been linked to shedding of the epidermal growth factor receptor-ligand neuregulin-β1 (36). ADAM12/MDC α has recently been shown to be responsible for endogenous shedding of HB-EGF in the heart (37). In addition, MMP7 has a functionally relevant role in shedding of TNF-α and FasL (38, 39), and MT1-MMP can be autolytically shed and is an enzyme capable of releasing both CD44 and TRANCE (21, 40, 41). However, not many proteinases responsible for ectodomain shedding of proteins have been identified.

Adamalysin 19/ADAM19/MDC β, cloned from mice (42, 43) and humans (44, 45), is a type I membrane-bound protein containing the basic domains of ADAMs, such as the prodomain, metalloprotease and disintegrin domain, cysteine-rich domain, transmembrane domain, and cytoplasmic domain (3). In addition to the processing of neuregulin (NRG) (36), human adamalysin 19 (hADAM19) is believed to play a role in osteoblast differentiation, in the distinction between macrophages and dendritic cells, and as a marker for the differentiation and characterization of dendritic cells (44). Recently, we demonstrated that hADAM19 is activated by furin in the secretory pathway and that the intracellular removal of the prodomain is required for its proteolytic activity, which was assessed with an α2-macroglobulin (α2-M) trapping assay *in vitro* (46). Emerging evidence indicates that metalloproteinase activity is regulated by the process of shedding or truncation, as in the cases of MT1-MMP, MT5-MMP, ADAM13, and ADAMTS4 (40, 47–49). Here we show that autolytic processing at $Glu^{586} \downarrow Ser^{587}$ of hADAM19 within its cysteine-rich domain is required for its endopeptidase activity and that efficient processing of hADAM19 is mainly dependent on the sizes of both Glu^{586} and Ser^{587}. We also show that PKC, CaM, and calcium signals may regulate the hADAM19 processing, which is not sensitive to GM6001 or TIMP-3. Moreover, we present a peptide substrate that mimics the processing site and may be used to determine the activity of soluble hADAM19 by a fluorescamine assay.

MATERIALS AND METHODS

Chemicals, Cell Lines, Cell Culture, and Immunological Reagents—All common laboratory chemicals, proteinase inhibitors, PMA, trifluoperazine, *N*-(6-aminohexyl)-5-chloro-1-naphthalenesulfonamide (W7), calmidazolium, PD98059, wortmannin, LY290042, pervanadate, and anti-FLAG-M2 monoclonal antibody (mAb) and its agarose conjugates were purchased from Sigma Chemical Co. (St. Louis, MO). The CMK-based furin inhibitor, dec-Arg-Val-Lys-Arg-chloromethyl ketone (decRVKR-CMK), and a matrix metalloproteinase inhibitor, ilomastat (GM6001), were purchased from Bachem (Philadelphia, PA). TIMP-3 was purchased from R & D Systems (Minneapolis, MN). Restriction enzymes were purchased from Promega (Madison, WI) or Invitrogen (Gaithersburg, MD). COS1 and Madin-Darby canine kidney (MDCK) cells and its derivatives were maintained as described (45). Dulbecco's modified Eagle's medium was purchased from Invitrogen (Gaithersburg, MD). Fetal bovine serum, penicillin G, and streptomycin were purchased from Invitrogen (Rockville, MD). α2-M was purchased from Roche Molecular Biochemicals (Indianapolis, IN). Rabbit polyclonal hADAM19 antibodies pAb361 (anti-metalloproteinase domain, anti-Cat) and pAb362 (anti-disintegrin domain, anti-Dis) were generated by our laboratory as reported previously (50).

PCR Primers, Mutagenesis, and Expression Constructs—All inserts tagged with FLAG at their C terminus were cloned into pCR3.1uni, including wild type hADAM19 (F46), soluble hADAM19 (D52), ^{199}RA-D (described in Ref. 46), and all mutants used in this study. The primer sequences for full-length (E346A-F) and soluble (E346A-D) $Glu^{346} \rightarrow$ Ala mutants were: forward primer, 5′-C ATG GCC CAC **GCG** ATG GGC CAC-3′; reverse primer, 5′-GTG GCC CAT **CGC** GTG GGC CAT G-3′. For deletion from the cysteine-rich domain to the end of the C terminus (D-CR): forward primer, 5′-ACC ATG CCA GGG GGC GCA GGC GCC-3′; reverse primer, 5′-GGT ACC ATC CAT CTG GTA GAA G-3′. For the soluble $Glu^{586} \rightarrow$ Ala mutant (E586A-D): forward primer, 5′-CGG CCC CTG **GCG** TCC AAC GCG-3′; reverse primer, 5′-CGC GTT GGA **CGC** CAG GGG CCG-3′. For the soluble $Glu^{586} \rightarrow$ Gly mutant (E586G-D): forward primer, 5′-CGG CCC CTG **GGG** TCC AAC GCG-3′; reverse primer, 5′-CGC GTT GGA **CCC** CAG GGG CCG-3′. For the soluble $Glu^{586} \rightarrow$ Asp mutant (E586D-D): forward primer, 5′-CGG CCC CTG **GAC** TCC AAC GCG-3′; reverse primer, 5′-CGC GTT GGA **GTC** CAG GGG CCG-3′. For the soluble $Glu^{586} \rightarrow$ Gln mutant (E586Q-D): forward primer, 5′-CGG CCC CTG **CAG** TCC AAC GCG-3′; reverse primer, 5′-CGC GTT GGA **CTG** CAG GGG CCG-3′. For the soluble $Ser^{587} \rightarrow$ Ala mutant (S587A-D): forward primer, 5′-CCC CTG GAG **GCC** AAC GCG GTG-3′; reverse primer, 5′-CAC CGC GTT **GGC** CTC CAG GGG-3′. For the soluble $Ser^{587} \rightarrow$ Thr mutant (S587T-D): forward primer, 5′-CCC CTG GAG **ACC** AAC GCG GTG-3′; reverse primer, 5′-CAC CGC GTT **GGT** CTC CAG GGG-3′. For the soluble $Ser^{587} \rightarrow$ Phe mutant (S587F-D): forward primer, 5′-CCC CTG GAG **TTC** AAC GCG GTG-3′; reverse primer, 5′-CAC CGC GTT **GAA** CTC CAG GGG-3′. All constructs were confirmed by DNA sequencing.

DNA Transfection and Generation of Stable Cell Lines—COS1 cells were seeded into 24-well plates for 16–24 h at 80% confluence and transfected with the indicated plasmids using LipofectAMINE2000 according to the instructions provided by Invitrogen (Gaithersburg, MD). After 6–10 h, serum-free Dulbecco's modified Eagle's medium and the indicated reagents were added, and the mixture was incubated for another 24 h. The conditioned media and cell lysates were then analyzed by Western blotting (46). The same transfection procedure was performed to generate stable MDCK cell lines, and the selection for hADAM19 was begun in the presence of G418 (400 μg/ml) after transfection for 24 h. The conditioned media and/or cell lysates of the clones were subjected to Western blotting to confirm the expression of hADAM19 (46).

Western Blotting—The experiments were carried out as described previously (46). Briefly, cells were grown to 80% confluence and were treated as indicated. After centrifugation for 15 min at 14,000 × *g* and 4 °C to clear any debris, the serum-free media were collected and prepared for SDS-PAGE. The cells were lysed with RIPA buffer (50 mM Tris, pH 7.5, 150 mM NaCl, 0.25% sodium deoxycholate, 0.1% Nonidet P-40, 1 mM phenylmethylsulfonyl fluoride, 2.5 μM GM6001, 10 μg/ml aprotinin, 10 μg/ml E64, and 10 μg/ml pepstatin A) for 15 min on ice. The supernatant was collected after centrifugation for 20 min at 14,000 × *g* and 4 °C. After electrophoresis, the proteins were transferred onto nitrocellulose membranes, probed with anti-FLAG-M2 or anti-hADAM19, and developed as before (46).

Purification of Soluble hADAM19 and N-terminal Sequencing—All proteins were purified on anti-FLAG-M2 affinity columns as described previously (46); however, HEPES buffer (50 mM HEPES, pH 7.5, 200 mM NaCl, 10 mM $CaCl_2$, 25 μM $ZnCl_2$, 0.05% Brij-35) was used instead of TBS buffer for the purpose of determining the activity of hADAM19 by a fluorescamine assay. Briefly, cells from stable lines expressing soluble hADAM19, D52-5, E586D-D, S587T-D, and D-CR, were grown to 100% confluence, washed twice with phosphate-buffered saline, and incubated for 48 h. in serum-free media. The conditioned media were collected, centrifuged to clear any debris, and loaded onto an anti-M2 immunoaffinity column (1 ml of resuspended agarose) that had been prewashed with HEPES buffer. The bound materials were extensively washed with HEPES buffer, eluted with FLAG peptides, and collected in 500-μl fractions. The fractions were analyzed by Western blot using anti-hADAM19 antibodies or anti-FLAG-M2, and the protein was quantified by its UV absorbance at 280 nm. The fractions containing the most wild type or mutant hADAM19 proteins were used for the α2-M trapping assay and fluorescamine assay. In the case of D52-5, the most concentrated fraction was also prepared for protein N-terminal sequencing to determine the shedding site. After separation by SDS-PAGE, the samples were transferred to a PVDF membrane and stained with Coomassie Blue R-250. After destaining, the hADAM19 bands were excised and sent to Margaret Seavy at the Bioanalytical Core Facility at the Florida State University for N-terminal amino acid sequencing.

α2-M Trapping Assay—The detailed experimental procedure was previously reported (46, 50). Briefly, equal amounts of purified wild type and mutated soluble hADAM19 were mixed with 24 μl of α2-M (0.2 unit/ml), respectively, adjusted to a total volume of 100 μl with HEPES buffer, and incubated at 37 °C for the indicated times. A 20-μl aliquot of the mixture was removed at the indicated times, put in 2× SDS-PAGE sample buffer, and boiled. Following SDS-PAGE, the protein bands in the gels were visualized by silver staining.

Determination of Kinetic Parameters of hADAM19 Using a New Peptide Assay—The N-terminal acetylated peptide (Ac-RPLESNAV) was synthesized by Dr. Umesh Goli at the Biochemical Analysis, Synthesis,

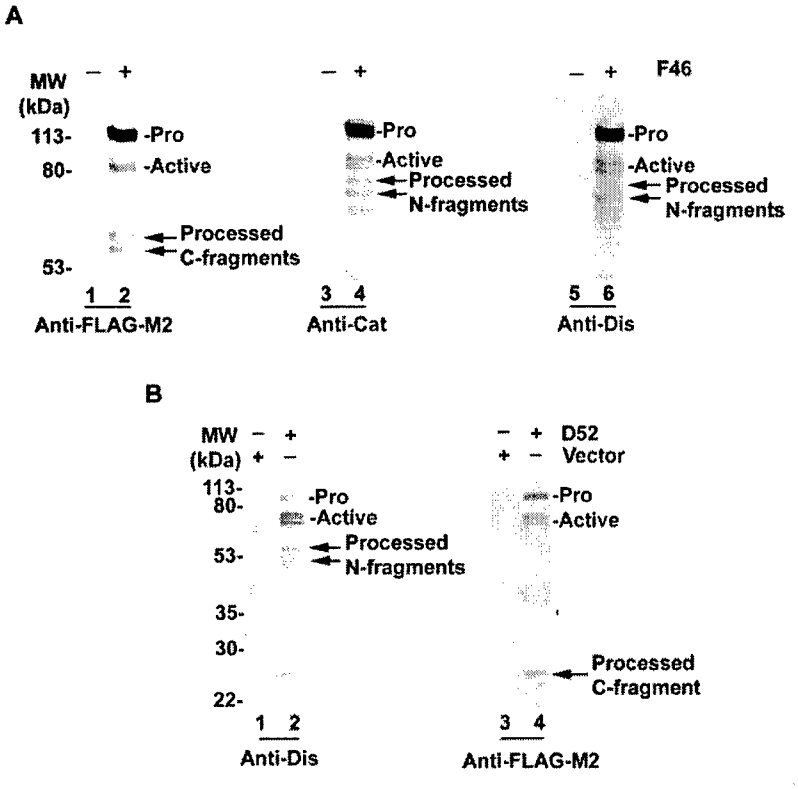

FIG. 1. **hADAM19 is processed within the cysteine-rich domain in COS1-transfected cells.** *A*, detection of hADAM19 by Western blotting with anti-FLAG-M2 mAb (*lanes 1* and *2*), anti-catalytic domain pAb (Anti-Cat) (*lanes 3* and *4*), or anti-disintegrin domain polyclonal antibody (Anti-Dis) (*lanes 5* and *6*). Cell lysates with radioimmune precipitation assay buffer from COS1 cells transfected with the blank vector (*lanes 1*, *3*, and *5*) or pCR3.1hADAM19 (F46) (*lanes 2*, *4*, and *6*). The pro, active, and processed forms of hADAM19 are indicated. *B*, characterization of soluble hADAM19. COS1 cells were transfected with the blank vector (*lanes 1* and *3*) or soluble hADAM19 (D52) (*lanes 2* and *4*). The conditioned media were analyzed by Western blotting using anti-disintegrin domain Ab (Anti-Dis) (*lanes 1* and *2*) and anti-FLAG-M2 mAb (*lanes 3* and *4*).

and Sequence Service Laboratory at Florida State University. The stock solutions of the peptide substrates were prepared in 0.05 M HEPES, pH 7.5, 0.2 M NaCl, 0.01 M $CaCl_2$, and 0.01% Brij-35. The peptide concentrations ranged from 0.2 to 4.0 mM, and the enzyme concentration was 160 nM. N-terminal sequencing for this released peptide was performed after overnight hydrolysis by the enzyme. Hydrolysis of the peptide by the enzyme was monitored by measuring fluorescence intensity (51). After incubation for the indicated times, the hydrolytic reaction was quenched by adding 20 μl of 100 mM 1,10-phenanthroline into 100 μl of reaction mixture. For the control sets, the 1,10-phenanthroline solution was added at the start of incubation. After the reaction was quenched, 100 μl of 0.1% fluorescamine in 10% Me_2SO/90% assay buffer was added into each reaction mixture. Relative fluorescence of the product coupled with fluorescamine was determined on a PerkinElmer Life Sciences LS-50B spectrofluorometer using an excitation wavelength of 386 nm and an emission wavelength of 477 nm. Excitation and emission slit widths were both 10 nm. Relative fluorescence was converted to nanomoles of product using a standard curve obtained with arginine. The final solution was diluted further with the assay buffer, if it was necessary. The values of k_{cat} and K_m were determined by fitting the data to the Michaelis-Menten equation. A molar extinction coefficient of 33,120 M^{-1} cm^{-1}, which was calculated by using Genetic Computer Group (GCG) software, was used to determine the concentration of soluble hADAM19.

RESULTS

hADAM19 Is Processed within the Cysteine-rich Domain—Shedding or truncation is increasingly being recognized as a key regulator of the activity of some metalloproteinases (40, 47–49). It was intriguing to investigate the possibility of shedding or truncation in hADAM19. As shown in Fig. 1*A*, in addition to the pro and active forms of hADAM19, we detected a doublet of protein of about 58 kDa by anti-FLAG-M2 in the lysate of the transfected COS1 cells expressing full-length hADAM19 with C-terminal FLAG tags (F46). We did not detect the doublet using antibodies against the catalytic and disintegrin domains of hADAM19, indicating that the 58-kDa protein is the processed C-terminal fragment lacking the metalloproteinase and disintegrin domains of hADAM19. On the other hand, another doublet of around 72 kDa was detected in the same lysate by these two hADAM19 antibodies but not anti-FLAG-M2 (Fig. 1*A*), suggesting that the 72-kDa protein is the processed N-terminal fragment containing the metalloproteinase and disintegrin domains of hADAM19. Taken together, a cellular processing occurs in hADAM19 after its disintegrin domain in the COS1-transfected cells. Notably, the doublets result from different forms of glycosylation as verified by glycosidase F treatment (Ref. 46 and data not shown). To probe the domain in which the processing occurs, we made two deletion forms of hADAM19 with C-terminal FLAG tags, soluble hADAM19 (D52), which lacked the transmembrane domain and cytoplasmic domain, and a form that lacked the cysteine-rich domain through the cytoplasmic domain (D-CR) (see Fig. 4). When D52 and D-CR were transfected into COS1 cells, we were able to detect several proteins in the conditioned media using both anti-FLAG-M2 and the antibody against the disintegrin domain, including the soluble pro and active forms of hADAM19. However, a 26-kDa protein in the conditioned medium from D52-transfected cells was clearly detectable using anti-FLAG-M2, but not the disintegrin domain antibody, suggesting that the 26-kDa protein is the processed C-terminal fragment of soluble hADAM19. In contrast, a doublet at 60–65 kDa was detected in the medium by the anti-disintegrin domain antibody, but not anti-FLAG-M2, indicating that the 60- to 65-kDa protein is the processed N-terminal fragment of soluble hADAM19 (Fig. 1*B*). There were no additional proteins detectable in the conditioned medium from the cells transfected with D-CR (data not shown); therefore, the processing of hADAM19 might be accounted for by shedding within its cysteine-rich domain.

PMA Up-regulates Processing of Full-length but Not Soluble hADAM19—PMA is a potent inducer of ectodomain shedding of many transmembrane proteins (5, 8–12, 14, 16, 19, 20, 34). To examine the effect of PMA on the processing of hADAM19, the COS1 cells transfected with F46 were treated with PMA overnight. As shown in Fig. 2*A*, PMA obviously enhanced hADAM19 processing in the COS1-transfected cells as detected under reducing conditions. Interestingly, we failed to detect the

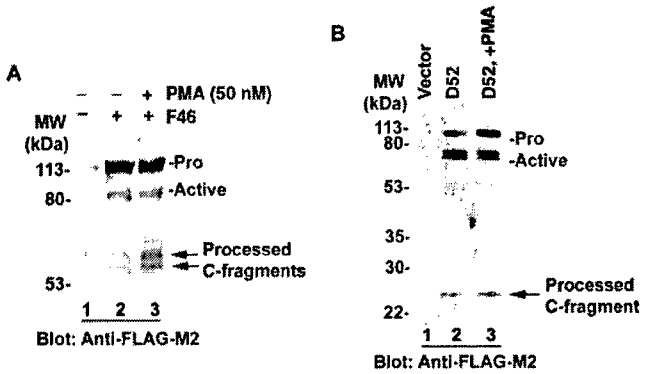

FIG. 2. **PMA enhances the processing at cysteine-rich domain of full-length, but not soluble, hADAM19.** *A*, enhancement of the processing at cysteine-rich domain of full-length hADAM19 by PMA. COS1 cells were transfected with the blank vector (*lane 1*) or F46 (*lanes 2* and *3*). After treated without (*lanes 1* and *2*) or with PMA (50 nM) (*lane 3*) overnight, the cells were lysed and probed with anti-FLAG-M2 mAb. *B*, PMA had no effect on the processing at cysteine-rich domain of soluble hADAM19. The conditioned media were collected from COS1 cells transfected with the blank vector (*lane 1*) or D52 (*lanes 2* and *3*) after overnight treatment with 50 nM PMA. The results were obtained from Western blots using anti-FLAG-M2 mAb.

processed N-terminal fragments in the conditioned media from the F46-transfected COS1 cells, even after PMA treatment (data not shown), suggesting that the processed N-terminal fragment may be still associated with the remaining C-terminal fragment or full-length of hADAM19 via one or more disulfide bonds. Therefore, according to the definition of ectodomain shedding, membrane-bound proteins release their soluble forms and the processing of hADAM19 within its cysteine-rich domain is not technically a form of shedding. To test if PMA-enhanced processing relies on the transmembrane and cytoplasmic domains, we treated the COS1 cells expressing D52 with PMA. As shown in Fig. 2*B*, PMA had a negligible effect on the processing of soluble hADAM19, suggesting that PMA might enhance the processing of hADAM19 via interaction with the cytoplasmic domain, transmembrane domain, or both. As a note, we used the processed C-terminal fragment at 26 kDa as a marker for the processing of soluble hADAM19 throughout this study.

The Processing at Glu^{586} ↓ Ser^{587} within the Cysteine-rich Domain Occurs by an Autolytic Mechanism—A recent report showed that ADAM13 shedding is dependent on its own metalloproteinase activity (48). We therefore hypothesized that the metalloproteinase activity of hADAM19 is also involved in its processing. To test this hypothesis, we used several independent approaches. As shown in Fig. 3*A*, rare processing was detected in the conditioned media from D52-transfected COS1 cells that were treated with decRVKR-CMK, which blocks the activation of hADAM19 (46). This indicates that prodomain removal is necessary for the processing at its cysteine-rich domain of hADAM19. Furthermore, ^{199}RA-D, an inactive mutant of soluble hADAM19 resistant to furin-mediated removal of its prodomain (46), displayed no processing, confirming that the soluble pro-form of hADAM19 lacks the capacity to process at its cysteine-rich domain (Fig. 3*A*). (The total protein level in the media was comparable to that in the media of the D52 cells.) We also generated another soluble inactive form of hADAM19 (E346A-D), in which the active residue Glu at 346 in the metalloproteinase domain was mutated to Ala, and transfected it into COS1 cells. Obviously, no processing at its cysteine-rich domain was observed in the media of these cells. Once again, the total protein level in the media was almost equal to that in the media of the D52 cells (Fig. 3*A*). These results strongly argue that the processing at its cysteine-rich domain of soluble hADAM19 depends on its own metalloproteinase activity. However, neither GM6001 nor TIMP-3, inhibitors that typically block sheddase activity (26–30), inhibited the autolytic processing of hADAM19 at its cysteine-rich domain (data not shown).

To further confirm that autolytic processing at its cysteine-rich domain occurs in soluble hADAM19, we generated stable MDCK cell lines called D52-5, ^{199}RA-D-6, and E346A-D-17, which expressed soluble D52, ^{199}RA, and E346A, respectively. As we expected, the 26-kDa-processed fragment was clearly detectable in the conditioned media from D52-5; the processing was dramatically inhibited by decRVKR-CMK (Fig. 3*B*). Furthermore, there was no processing at the cysteine-rich domain in ^{199}RA-D-6 and E346A-D-17 (Fig. 3*B*). (The total amount of soluble protein was comparable among the conditioned media of these cell lines). Once again, PMA, GM6001, and TIMP-3 failed to affect the processing of D52-5 (Figs. 2*B* and 3*B*, data not shown).

N-terminal sequencing revealed that the starting sequence of the purified 26-kDa protein was SNAVPIDT, which is identical to ^{596}SNAVPIDT^{594} within the cysteine-rich domain of hADAM19. This suggests that the processing of hADAM19 occurs at Glu^{586} ↓ Ser^{587} within its cysteine-rich domain (Fig. 3*B*).

The Sizes of Glu^{586} and Ser^{587} Are Critical for the Processing at Glu^{586} ↓ Ser^{587} of Soluble hADAM19—To examine the importance of the Glu^{586} (P1) and Ser^{587} (P1′) sites in the processing at Glu^{586} ↓ Ser^{587} of soluble hADAM19, we changed the size, charge, and polarity of these two residues by mutagenesis. The constructs are shown in Fig. 4. Shown in Fig. 5*A*, there was no or little detectable processing in the COS1 cells transfected with either E586D-D or S587T-D, suggesting that subtle changes in the sizes of residues at the P1 and P1′ positions can dramatically impair the processing. Furthermore, rare or little processing was observed when significant changes were made to the side chains of the residues at these sites, as in the cases of the Glu^{586} to Ala or Gly, and Ser^{587} to Phe mutants (Fig. 5*A*). On the other hand, the amount of processing product in the E586Q-D or S587A-D mutant, in which the side chain of the amino acid residue was almost the same size as that in wild type soluble hADAM19, was almost equal (Fig. 5*A*).

To further confirm the fate of processing at Glu^{586} ↓ Ser^{587} upon changes at the P1 and P1′ sites, we chose mutants with subtle changes and, presumably, structural similarities, Glu^{586} to Asp and Ser^{587} to Thr, to generate stable transfectants in MDCK cells. Shown in Fig. 5*B*, rare or little processing was detectable in the conditioned media from these stable MDCK transfectants, confirming that both soluble E586D-D and S587T-D have undetectable or little ability to process, even if they are cleaved by furin in the MDCK transfectants. (There were no significant differences in protein levels among the transfectants.)

The Signals of CaM and Calcium May Be Involved in the Processing at Glu^{586} ↓ Ser^{587} of hADAM19—In addition to the PKC pathway, there are several other signal pathways, involving tyrosine kinase, MAPKs, phosphatase, phosphatidylinositol 3-kinase, calcium, and CaM, which regulate the ectodomain-shedding process (10, 13–19, 21–23). Specific inhibitors were used to determine whether or not these signal pathways regulate the processing at Glu^{586} ↓ Ser^{587} of hADAM19. As shown in Fig. 6, only CaM inhibitors impaired the processing of soluble hADAM19. The other inhibitors, including genistein, PD98059, pervanadate, wortmannin, and LY290042, had no significant effects on the processing of soluble or full-length hADAM19 (data not shown). In addition, both A23187 and brefeldin A block the activation of both soluble and full-length

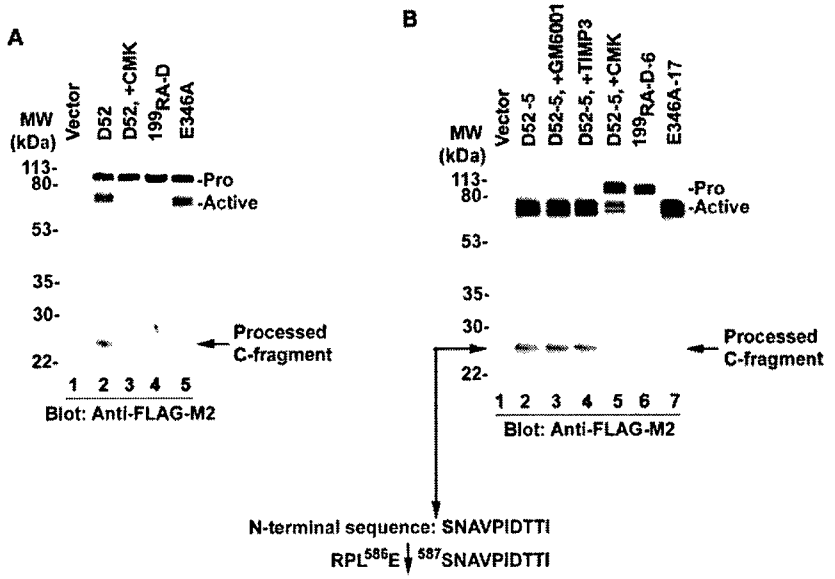

FIG. 3. **hADAM19 autolytically process at Glu^{586} ↓ Ser^{587} within the cysteine-rich domain.** *A*, autolytic processing at the cysteine-rich domain of soluble hADAM19 in COS1-transfected cells. COS1 cells were transfected with the blank vector (*lanes 1*), D52 (*lanes 2* and *3*), soluble mutant with ^{199}RR to ^{199}AA (^{199}RA-D) (*lane 4*), or soluble inactive mutant (E346A-D) (*lane 5*) and incubated without (*lanes 1, 2, 4,* and *5*) or with 100 μM CMK (*lane 3*) for 16 h. The conditioned media were analyzed by Western blotting with anti-FLAG-M2 mAb. *B*, processing at cysteine-rich domain of soluble hADAM19 in the stable MDCK transfectants. MDCK cells stably expressing soluble hADAM19 (D52-5) (*lanes 2–5*), soluble ^{199}RA mutant (^{199}RA-D-6) (*lane 6*), or the soluble inactive mutant (E346A-D-17) (*lane 7*) were treated without (*lanes 1, 2, 6,* and *7*) or with 5 μM GM6001 (*lane 3*), 100 nM TIMP-3 (*lane 4*), or 100 μM CMK (lane 5) overnight. The conditioned media were analyzed by Western blotting using anti-FLAG-M2 mAb. MDCK cells transfected with the blank vector were used as a control (*lane 1*). The sequence for the shed C-terminal protein is shown at the *bottom*.

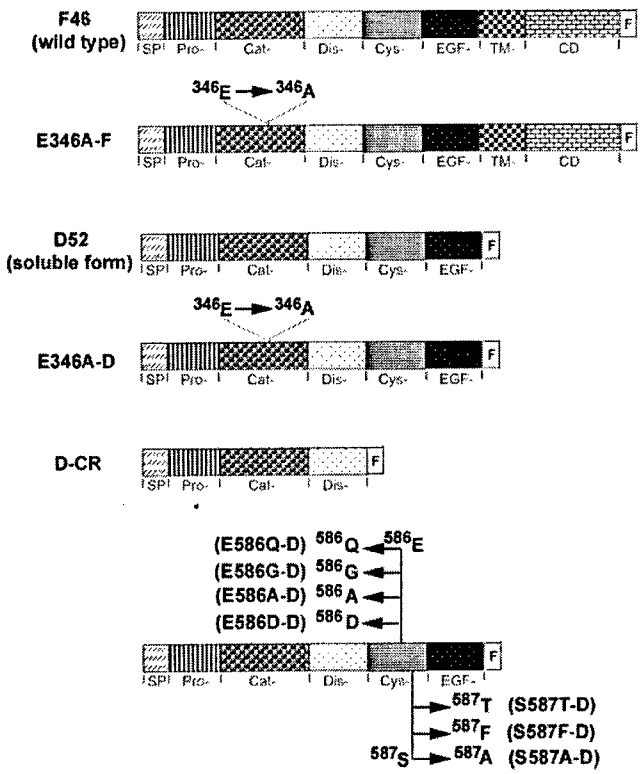

FIG. 4. **A schematic illustration of the wild type expression vector pCR3.1hADAM19 and its mutant constructs.** All of the constructs have a C-terminal FLAG tag. *SP*, signal peptide; *Pro-*, prodomain; *Cat-*, catalytic domain; *Dis-*, disintegrin domain; *Cys-*, cysteine-rich domain; *EGF-*, EGF-like domain; *TM*, transmembrane domain; *CD*, cytoplasmic domain; *F*, FLAG tag.

hADAM19 (46). There was no processing at Glu^{586} ↓ Ser^{587} detectable under the treatment of either A23187 or brefeldin A (data not shown), indicating that hADAM19 is activated and processed in the secretory pathway. Taken together, our results suggest that PKC, CaM, and calcium signal pathways may be related to the processing at Glu^{586} ↓ Ser^{587} of hADAM19.

The Processing at Glu^{586} ↓ Ser^{587} Is Necessary for hADAM19 to Exert Its Proteolytic Activity against α2-M—To assess the significance of the processing at Glu^{586} ↓ Ser^{587} of hADAM19, we purified the proteins from D52-5, E586D-D, and S587T-D, respectively. Intriguingly, the processed N-terminal fragments, containing the metalloproteinase, disintegrin, and parts of the cysteine-rich domain, were detected as mature forms using anti-disintegrin antibody (data not shown). This suggests that the processed N-terminal segments bind with unprocessed soluble forms or processed C-terminal-soluble fragments by one or more disulfide bonds, consistent with the results obtained early from the full-length hADAM19 (data not shown). When we probed the purified proteins with anti-FLAG-M2, as shown in Fig. 7*A*, S587T-D displayed relatively more processing than E586D-D, in which a very low level of processing was detected. D52-5 showed much more processing than E586D-D and S587T-D. As shown in Fig. 7*B*, D52-5 protein had a much greater ability to form a complex with α2-M and generate two products compared with both E586D-D and S587T-D proteins, which displayed much lower activities. Obviously, S587T-D had a relatively higher activity than E586D-D, which showed very low activity. These results perfectly coincide with the Western blot shown in Fig. 7*A*, indicating that the more that hADAM19 processed at Glu^{586} ↓ Ser^{587}, the more proteolytic activity it exerted against α2-M *in vitro*.

Ac-RPLE-SNAV Is Cleaved by Active hADAM19—To test hADAM19 activity, we synthesized a new peptide, Ac-RPLE-SNAV, which encompasses the processing site of hADAM19 and is conserved among humans and mice (42, 45). Because the processing at Glu^{586} ↓ Ser^{587} is mediated by its own metalloproteinase activity (Fig. 3), we were able to use this peptide to assay soluble hADAM19 activity and obtained the similar results as from the α2-M assay (Fig. 7*B*). Once again, the highest

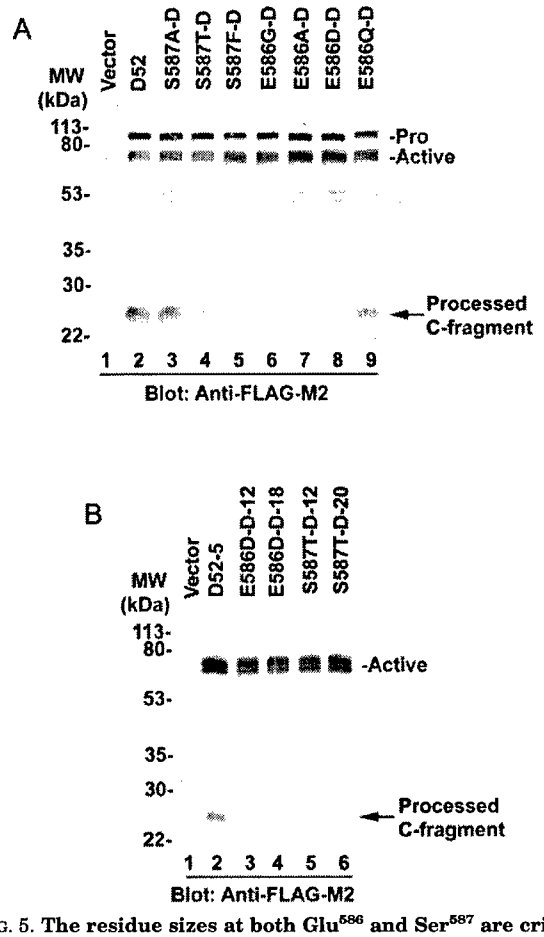

FIG. 5. **The residue sizes at both Glu^{586} and Ser^{587} are critical for the processing at Glu^{586} ↓ Ser^{587} of hADAM19.** *A*, processing profile at Glu^{586} ↓ Ser^{587} of soluble mutants in COS1-transfected cells. COS1 cells were transfected with the blank vector (*lane 1*), D52 (*lane 2*), soluble mutants with Ser^{587} to Ala (S587A-D) (*lane 3*), Thr (S587T-D) (*lane 4*), or Phe (S587F-D) (*lane 5*), or Glu^{586} → Gly (E586G-D) (*lane 6*), Ala (E586A-D) (*lane 7*), Asp (E586D-D) (*lane 8*), or Gln (E586Q-D) (*lane 9*). The conditioned media were subjected to SDS-PAGE and Western blotting with anti-FLAG-M2 mAb. *B*, detection of the processing at Glu^{586} ↓ Ser^{587} of hADAM19 in MDCK cells stably expressing soluble hADAM19 mutants. Four MDCK cells stably expressing soluble hADAM19 with Glu^{586} → Asp (E586D-D-12 and E586D-D-18) (*lanes 3* and *4*) or Ser^{587} to Ala (S587A-D-12 and S587A-D-20) (*lanes 5* and *6*) were prepared in serum-free media overnight. The conditioned media were analyzed by Western blotting using anti-FLAG-M2 mAb. MDCK cells transfected with the blank vector (*lane 1*) and D52-5 cells (*lane 2*) were used as controls.

activity was seen in D52-5 with 1% cleavage after incubation overnight. E586D-D and S587T-D only showed 30 and 10% the activity exerted by D52-5, respectively (data not shown). As we knew, the activity at 1% was not enough for a fluorescence assay. However, given that D52-5 was not fully processed (maybe 25% of the mature hADAM19 got processed according to the Western blotting result as shown in Fig. 7*A*), we decided to generate another stable line in MDCK cells expressing D-CR (Fig. 4). The reason we deleted the whole cysteine-rich domain is that we surmised that this domain has a potential interaction with the metalloproteinase domain, disintegrin domain, or both that might decrease the activity. Fortunately, purified D-CR from the MDCK transfectants had a higher activity for cleaving our new peptide substrate, and the cleavage product detected by N-terminal sequencing was peptide SNAV, confirming that the peptide substrate was cleaved at the E-S bond, which is identical to the processing site in the hADAM19 protein. Furthermore, as shown in Fig. 8, the k_{cat}, K_m, and k_{cat}/K_m values for 150-min incubation were 2.4 min^{-1}, 2.0 mM, and

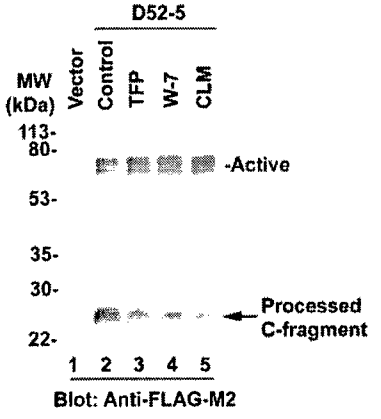

FIG. 6. **Processing at Glu^{586} ↓ Ser^{587} of hADAM19 is inhibited by calmodulin inhibitors.** MDCK cells stably expressing soluble hADAM19 (D52-5) (*lanes 2–5*) were treated without (*lanes 1* and *2*) or with 100 μM trifluoperazine (*lane 3*), 25 μM W7 (*lane 4*), or 50 μM calmidazolium (*lane 5*) for 16 h. The conditioned media were then analyzed by Western blotting using anti-FLAG-M2 mAb. MDCK cells transfected with the blank vector were used as a control (*lane 1*).

1200 M^{-1} min^{-1}, respectively. Thus, we developed a peptide substrate for determining soluble hADAM19 activity by a fluorescamine assay.

DISCUSSION

In the current report, we have demonstrated that processing of hADAM19 occurs at Glu^{586} ↓ Ser^{587} within the cysteine-rich domain by its own metalloproteinase activity and is a necessary step to display its proteolytic activity against both a peptide substrate and α2-M *in vitro*. We have also revealed that the processing at Glu^{586} ↓ Ser^{587} of hADAM19 is regulated by a unique pathway, distinguishable from those shown for other ADAMs, MT-MMPs, and other membrane-bound proteins.

Shedding or Processing of Metalloproteinases—Growing evidence suggests that shedding is of vital importance for the regulation of metalloproteinase activity. For MT-MMPs, Pei's group reported that MT5-MMP is shed by furin, down-regulating its activity, and that interleukin-8 triggers the signal for both release and activation of MT6-MMP by an unknown mechanism (47, 52). The activity of MT1-MMP can be autolytically terminated directly on the cell surface or via production of a soluble functional fragment, consequently down-regulating enzyme activity on the cell surface (40). Among ADAMs, ADAM13 is the only one that has been shown to shed its ectodomain intracellularly by an autolytic mechanism, producing an active enzyme able to bind with α2-M and integrins (48). In addition, truncation of mature ADAMTS4 at its C terminus is required for its aggrecanase activity (49). In this report, we demonstrate that hADAM19 carries out processes within its cysteine-rich domain, resulting in an active enzyme shown by both α2-M and peptide substrate assays *in vitro* (Figs. 3, 7, and 8). It might, therefore, be a general regulatory mechanism that MT-MMPs, such as MT1-MMP and MT5-MMP, are down-regulated by shedding to release active forms from the cell surface, whereas ADAMs must shed, carry out process, or become truncated at the C terminus to exert their functions, such as acting as a sheddase, binding with integrins on the cell surface, or digesting components of the extracellular matrix.

Regulation of the Processing at Glu^{586} ↓ Ser^{587} of hADAM19—The signal pathways involved in shedding or truncation processes, especially of ADAMs, are poorly understood. In the present report, we provide unique characteristics of the regulation of the processing at Glu^{586} ↓ Ser^{587} of hADAM19. We found that PMA, a common inducer of shedding, also enhances the processing at Glu^{586} ↓ Ser^{587} of hADAM19 (Fig.

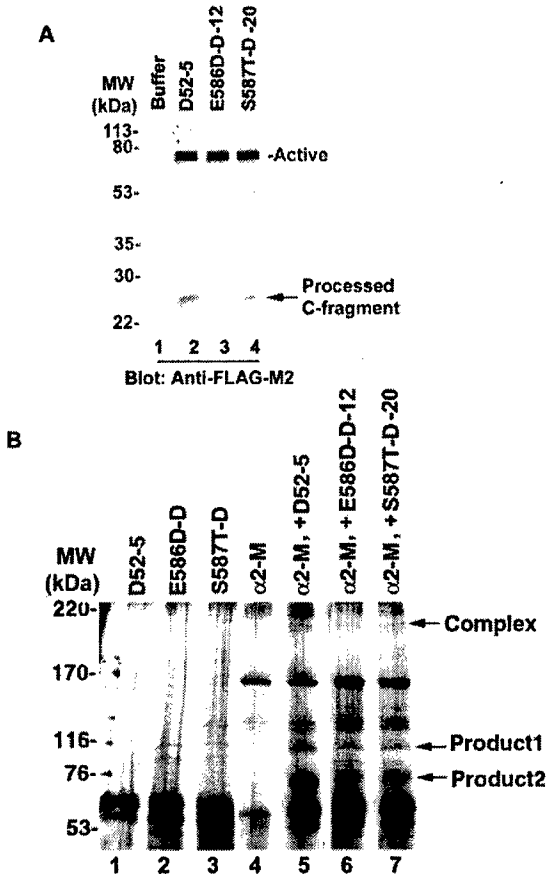

FIG. 7. **Requirement of the processing at Glu^{586} ↓ Ser^{587} for the proteolytic activity of hADAM19.** *A*, processing status at Glu^{586} ↓ Ser^{587} of purified proteins from the stable MDCK transfectants. MDCK cells stably expressing soluble hADAM19 (D52-5) (*lane 2*), soluble Glu^{586} → Asp (E586D-D-12) (*lane 3*), or soluble Ser^{587} to Ala (S587A-D-20) (*lane 4*) were prepared for purification as described under "Materials and Methods." Western blots using anti-FLAG-M2 mAb were performed on equal amounts of these purified proteins. *B*, the proteolytic activity of soluble hADAM19 using α2-M *in vitro*. The purified hADAM19 from D52-5 (*lanes 1* and *5*), E586D-D-12 (*lanes 2* and *6*), or S587A-D-20 (*lanes 3* and *7*) were normalized and incubated in reaction buffer alone (*lanes 1–3*) or with α2-M (*lanes 5–7*) for 24 h. α2-M in reaction buffer alone (24 h) was a control (*lane 3*). The α2-M·hADAM19 complex and the cleavage products of α2-M by hADAM19 are labeled on the *right*.

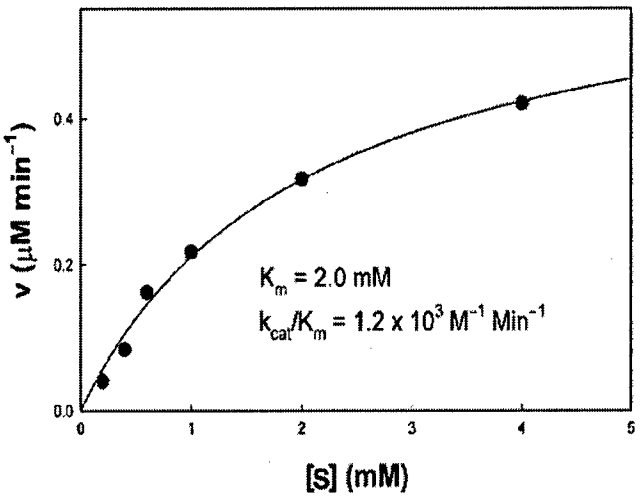

FIG. 8. **The hydrolysis of Ac-RPLE-SNAV by hADAM19.** The peptide (Ac-RPLE-SNAV) (0.2–4.0 mM), which mimics the processing site of hADAM19, was incubated with 0.26 μM soluble, active ADAM19 for 150 min. The formation of product was measured by monitoring the coupling of fluorescamine with the amino group newly formed from the cleavage. The nonlinear regression analysis of the data indicates k_{cat} = 2.4 min^{-1}, K_m = 2.0 mM, and k_{cat}/K_m = 1200 M^{-1} min^{-1}.

2*A*). The mechanism probably involves the cytoplasmic domain, transmembrane domain, or both, because PMA did not alter the processing of soluble hADAM19 (Fig. 2*B*). This is consistent with reports showing that the cytoplasmic domain of ADAM9 is required for PMA-induced shedding (34) and that the membrane anchor of TACE is necessary for its processing of TNF-α (53, 54). In addition, there are a few reports that have demonstrated the requirement of the cytoplasmic tail for shedding of pro-NRG, APP, pro-TGF, and L1 adhesion molecules (17, 55, 56). However, in most cases, endogenous and/or inducer-mediated shedding is independent of the cytoplasmic domain (Fig. 2*B*) (14, 17, 19, 22, 24). Calcium ionophore, A23187, is another potent inducer of most protein-shedding processes (13–16). Nevertheless, we found that A23187 and brefeldin A block the activation of both full-length and soluble hADAM19. Subsequently, no processing at Glu^{586} ↓ Ser^{587} was detectable, suggesting that hADAM19 is activated and processed in the secretory pathway (46, data not shown). Inhibitors of CaM have been shown to stimulate the shedding of several proteins, including MT1-MMP, pro-TGFα, pro-NRG, and APP, by a mechanism independent of both PKC and calcium (17–20). However, in our study, a reverse result was obtained; the processing at Glu^{586} ↓ Ser^{587} was inhibited by the CaM inhibitors (Fig. 6). Finally, we found that tyrosine kinase, MAPK, phosphatase, or phosphatidylinositol 3-kinase do not seem to play roles in the processing at Glu^{586} ↓ Ser^{587} of hADAM19 (data not shown), although they have been previously shown to participate in some shedding processes (9–12, 21–23, 29).

In addition, the proteinases responsible for the shedding of many cell surface molecules seem to have broad sequence specificity as revealed by mutational analysis of residues around the cleavage site of pro-TGFα, APP, IL-6 receptor, L-selectin, and pro-TNFα (57–61). In this report, we used mutagenesis to show that the residue sizes of the side chains at both the Glu^{586} and Ser^{587} sites are extremely important for normal processing at Glu^{586} ↓ Ser^{587} of hADAM19. Even delicate changes, such as Glu^{586} → Asp and Ser^{587} → Thr, caused dramatic decreases in the processing. Notably, many studies have shown that some potent synthetic inhibitors of metalloproteinases, such as TAPI, BB94, and GM6001, can block most, if not all, shedding processes and that many shedding processes are sensitive to TIMP-3, a matrix-associated TIMP that preferably inhibits ADAMs (5–8, 19, 24–30). However, neither GM6001 nor TIMP-3 inhibits the autolytic processing at Glu^{586} ↓ Ser^{587} of hADAM19 (Fig. 3*B*), which is consistent with some reports showing that the shedding of MT5-MMP, MT6-MMP, and IL-6 receptor is not affected by metalloproteinase inhibitors (47, 52, 62). One possibility, we speculate, is that shedding, in most cases, occurs at membrane-proximal regions on the cell surface, which are easily accessible to hydroxamate-based inhibitors and TIMP-3 (5, 25, 60, 63). Human ADAM19 processing takes place at a region distal from the transmembrane domain in the secretory pathway, which is less accessible to GM6001 and TIMP-3 (Fig. 3*B*). How hADAM19 initiates the processing at Glu^{586} ↓ Ser^{587} and what the roles for the disintegrin- and cysteine-rich domains are during the processing at Glu^{586} ↓ Ser^{587} remain to be uncovered. Perhaps dimerization through the disintegrin- and/or cysteine-rich domains is the key step for the processing as proposed for other ADAMs (3). This might also be an explanation for the fact that the processed N-terminal fragments, containing the metalloproteinase, disintegrin, and parts of the cysteine-rich domain, were not detected in the conditioned medium from the transfected COS1 cells with full-

length hADAM19 and were present among the purified soluble hADAM19 proteins (data not shown).

A New Peptide Substrate Based on the Processing Site Sequence for hADAM19—The peptide substrates currently used to measure MMP activity are synthesized based on the cleavage sites of protein substrates. Because hADAM19 processes at $Glu^{586} \downarrow Ser^{587}$ by its own metalloproteinase activity, we surmised that a peptide encompassing the processing site would be an ideal substrate. Indeed, this peptide, Ac-RPLE-SNAV, was suitable for a fluorescamine assay of enzyme activity and was cleaved at the *E*-S site as determined by peptide N-terminal sequencing. Although the wild type hADAM19 showed a minimally detectable activity by this method, D-CR, containing the metalloproteinase and disintegrin domains, displayed a higher activity to determine kinetic parameters after incubation for 150 min using our fluorescamine assay (Fig. 8). The kinetic parameters, k_{cat}, K_m, and k_{cat}/K_m, were 2.4 min^{-1}, 2.0 mM, and 1200 M^{-1} min^{-1}, respectively, demonstrating that this is a poor substrate and will have a limited usage. It is necessary that the peptide substrates will be optimized by creating analogs that are hydrolyzed more efficiently by hADAM19 in the near future. Our preliminary data show that TIMP-3 can inhibit hADAM19 activity in this peptide-based assay,[2] which is similar to the results for ADAM10, -12, and -17 and ADAMTS4 and -5 *in vitro* (64–67), and confirm that the TIMP-3 we used was active. However, TIMP-3 had no effect on the cellular processing at $Glu^{586} \downarrow Ser^{587}$ of soluble hADAM19 (Fig. 3*B*), indicating that this processing occurred intracellularly, to where TIMP-3 molecules might not be accessible. Interestingly, ADAMTS4 is truncated at $Glu^{373} \downarrow Ala^{374}$, the site for the cleavage of ADAMTS4 and ADAMTS5, not MMPs. In contrast, the truncation site at $Asn^{341} \downarrow Phe^{342}$ is mediated by MMPs, not aggrecanases (49, 68). Our mutational data showed that the $Glu^{586} \downarrow Ala^{587}$ processing site was also optimal for autolytic processing of hADAM19 (Fig. 5*B*), indicating that our peptide substrate might be useful to determine the activity of other ADAMs, such as aggrecanases. This peptide substrate may also be used for testing metalloproteinase inhibitors against hADAM19 and other ADAMs.

Acknowledgments—We thank Sara C. Monroe at Florida Statue University for her editorial assistance with the manuscript preparation and Dr. Jörg-Walter Bartsch at the University of Bielefeld for his critical review of the manuscript.

REFERENCES

1. Schlondorff, J., and Blobel, C. P. (1999) *J. Cell Sci.* **112,** 3603–3617
2. Kheradmand, F., and Werb, Z. (2002) *Bioessays* **24,** 8–12
3. Primakoff, P., and Myles, D. G. (2000) *Trends Genet.* **16,** 83–87
4. Blobel, C. P. (2000) *Curr. Opin. Cell Biol.* **12,** 606–612
5. Hooper, N. M., Karran, E. H., and Turner, A. J. (1997) *Biochem. J.* **321,** 265–279
6. Peschon, J. J., Slack, J. L., Reddy, P., Stocking, K. L., Sunnarborg, S. W., Lee, D. C., Russell, W. E., Castner, B. J., Johnson, R. S., Fitzner, J. N., Boyce, R. W., Nelson, N., Kozlosky, C. J., Wolfson, M. F., Rauch, C. T., Cerretti, D. P., Paxton, R. J., March, C. J., and Black, R. A. (1998) *Science* **282,** 1281–1284
7. Arribas, J., Coodly, L., Vollmer, P., Kishimoto, T. K., Rose-John, S., and Massague, J. (1996) *J. Biol. Chem.* **271,** 11376–11382
8. Mullberg, J., Rauch, C. T., Wolfson, M. F., Castner, B., Fitzner, J. N., Otten-Evans, C., Mohler, K. M., Cosman, D., and Black, R. A. (1997) *FEBS Lett.* **401,** 235–238
9. Desdouits-Magnen, J., Desdouits, F., Takeda, S., Syu, L. J., Saltiel, A. R., Buxbaum, J. D., Czernik, A. J., Nairn, A. C., and Greengard, P. (1998) *J. Neurochem.* **70,** 524–530
10. Gutwein, P., Oleszewski, M., Mechtersheimer, S., Agmon-Levin, N., Krauss, K., and Altevogt, P. (2000) *J. Biol. Chem.* **275,** 15490–15497
11. Fan, H., and Derynck, R. (1999) *EMBO J.* **18,** 6962–6972
12. Gechtman, Z., Alonso, J. L., Raab, G., Ingber, D. E., and Klagsbrun, M. (1999) *J. Biol. Chem.* **274,** 28828–28835
13. Vecchi, M., Baulida, J., and Carpenter, G. (1996) *J. Biol. Chem.* **271,** 18989–18995
14. Dethlefsen, S. M., Raab, G., Moses, M. A., Adam, R. M., Klagsbrun, M., and Freeman, M. R. (1998) *J. Cell. Biochem.* **69,** 143–153
15. Yee, N. S., Langen, H., and Besmer, P. (1993) *J. Biol. Chem.* **268,** 14189–14201
16. Pandiella, A., and Massague, J. (1991) *J. Biol. Chem.* **266,** 5769–5773
17. Kahn, J., Walcheck, B., Migaki, G. I., Jutila, M. A., and Kishimoto, T. K. (1998) *Cell* **92,** 809–812
18. Annabi, B., Pilorget, A., Bousquet-Gagnon, N., Gingras, D., and Beliveau, R. (2001) *Biochem. J.* **359,** 325–333
19. Diaz-Rodriguez, E., Esparis-Ogando, A., Montero, J. C., Yuste, L., and Pandiella, A. (2000) *Biochem. J.* **346,** 359–367
20. Fors, B. P., Goodarzi, K., and von Andrian, U. H. (2001) *J. Immunol.* **167,** 3642–3651
21. Schlondorff, J., Lum, L., and Blobel, C. P. (2001) *J. Biol. Chem.* **276,** 14655–14674
22. Vecchi, M., Rudolph-Owen, L. A., Brown, C. L., Dempsey P. J., and Carpenter, G. (1998) *J. Biol. Chem.* **273,** 20589–20595
23. Manna, S. K., and Aggarwal, B. B. (1998) *J. Biol. Chem.* **273,** 33333–33341
24. Crowe, P. D., Walter, B. N., Mohler, K. M., Otten-Evans, C., Black, R. A., and Ware, C. F. (1995) *J. Exp. Med.* **181,** 1205–1210
25. Arribas, J., Lopez-Casillas, F., and Massague, J. (1997) *J. Biol. Chem.* **272,** 17160–17165
26. Ilan, N., Mohsenin, A., Cheung, L., and Madri, J. A. (2001) *FASEB J.* **15,** 362–372
27. Borland, G., Murphy, G., and Ager, A. (1999) *J. Biol. Chem.* **274,** 2810–2815
28. Fitzgerald, M. L., Wang, Z., Park, P. W., Murphy, G., and Bernfield, M. (2000) *J. Cell Biol.* **148,** 811–824
29. Nath, D., Williamson, N. J., Jarvis, R., and Murphy, G. (2001) *J. Cell. Sci.* **114,** 1213–1220
30. Hargreaves, P. G., Wang, F., Antcliff, J., Murphy, G., Lawry, J., Russell, R. G., and Croucher, P. I. (1998) *Br. J. Haematol.* **101,** 694–702
31. Lum, L., Wong, B. R., Josien, R., Becherer, J. D., Erdjument-Bromage, H., Schlondorff, J., Tempst, P., Choi, Y., and Blobel, C. P. (1999) *J. Biol. Chem.* **274,** 13613–13618
32. Mechtersheimer, S., Gutwein, P., Agmon-Levin, N., Stoeck, A., Oleszewski, M., Riedle, S., Fogel, M., Lemmon, V., and Altevogt, P. (2001) *J. Cell Biol.* **155,** 661–673
33. Hattori, M., Osterfied, M., and Flanagan, J. (2000) *Science* **289,** 1360–1365
34. Izumi, Y., Hirata, M., Hasuwa, H., Iwamoto, R., Umata, T., Miyado, K., Tamai, Y., Kurisaki, T., Sehara-Fujisawa, A., Ohno, S., and Mekada, E. (1998) *EMBO J.* **17,** 7260–7272
35. Koike, H., Tomioka, S., Sorimachi, H., Saido, T. C., Maruyama, K., Okuyama, A., Fujisawa-Sehara, A., Ohno, S., Suzuki, K., and Ishiura, S. (1999) *Biochem. J.* **343,** 371–375
36. Shirakabe, K., Wakatsuki, S., Kurisaki, T., and Fujisawa-Sehara, A. (2001) *J. Biol. Chem.* **276,** 9352–9358
37. Asakura, M., Kitakaze, M., Takashima, S., Liao, Y., Ishikura, F., Yoshinaka, T., Ohmoto, H., Node, K., Yoshino, K., Ishiguro, H., Asanuma, H., Sanada, S., Matsumura, Y., Takeda, H., Beppu, S., Tada, M., Hori, M., and Higashiyama, S. (2002) *Nat. Med.* **8,** 35–40
38. Haro, H., Crawford, H. C., Fingleton, B., Shinomiya, K., Spengler, D. M., and Matrisian, L. M. (2000) *J. Clin. Invest.* **105,** 143–150
39. Powell, W. C., Fingleton, B., Wilson, C. L., Boothby, M., and Matrisian, L. M. (1999) *Curr. Biol.* **9,** 1441–1447
40. Toth, M., Hernandez-Barrantes, S., Osenkowski, P., Bernardo, M. M., Gervasi, D. C., Shimura, Y., Meroueh, O., Kotra, L. P., Galvez, B. G., Arroyo, A. G., Mobashery, S., and Fridman, R. J. (2002) *J. Biol. Chem.* **277,** 26340–26350
41. Kajita, M., Itoh, Y., Chiba, T., Mori, H., Okada, A., Kinoh, H., and Seiki, M. (2001) *J. Cell Biol.* **153,** 893–904
42. Inoue, D., Reid, M., Lum, L., Kratzschmar, J., Weskamp, G., Myung, Y. M., Baron, R., and Blobel, C. P. (1998) *J. Biol. Chem.* **273,** 4180–4187
43. Kurohara, K., Matsuda, Y., Nagabukuro, A., Tsuji, A., Amagasa, T., and Fujisawa-Sehara, A. (2000) *Biochem. Biophys. Res. Commun.* **270,** 522–527
44. Fritsche, J., Moser, M., Faust, S., Peuker, A., Buttner, R., Andreesen, R., and Kreutz, M. (2000) *Blood* **96,** 732–739
45. Wei, P., Zhao, Y.-G., Zhuang, L., Ruben, S., and Sang, Q.-X. (2001) *Biochem. Biophys. Res. Commun.* **280,** 744–755
46. Kang, T., Zhao, Y. G., Pei, D., Sucic, J. F., and Sang, Q. X. (2002) *J. Biol. Chem.* **277,** 25583–25591
47. Wang, X., and Pei, D. (2001) *J. Biol. Chem.* **276,** 35953–35960
48. Gaultier, A., Cousin, H., Darribere, T., and Alfandari, D. (2002) *J. Biol. Chem.* **277,** 23336–23344
49. Gao, G., Westling, J., Thompson, V. P., Howell, T. D., Gottschall, P. E., and Sandy, J. D. (2002) *J. Biol. Chem.* **277,** 11034–11043
50. Zhao, Y. G., Wei, P., and Sang Q. X. (2001) *Biochem. Biophys. Res. Commun.* **289,** 288–294
51. Netzel-Arnett, S., Sang, Q.-X., Moore, W. G. I., Narve, M., Birkedal-Hansen, H., and Van Wart, H. E. (1993) *Biochemistry* **32,** 6427–6432
52. Kang, T., Yi, J., Guo, A., Wang, X., Overall, C. M., Jiang, W., Elde, R., Borregaard, N., and Pei, D. (2001) *J. Biol. Chem.* **276,** 21960–21968
53. Reddy, P., Slack, J. L., Davis, R., Cerretti, D. P., Kozlosky, C. J., Blanton, R. A., Shows, D., Peschon, J. J., and Black, R. A. (2000) *J. Biol. Chem.* **275,** 14608–14614
54. Itai, T., Tanaka, M., and Nagata, S. (2001) *Eur. J. Biochem.* **268,** 2074–2082
55. Bosenberg, M. W., Pandiella, A., and Massague, J. (1992) *Cell* **71,** 1157–1165
56. Liu, X., Hwang, H., Cao, L., Wen, D., Liu, N., Graham, R. M., and Zhou, M. (1998) *J. Biol. Chem.* **273,** 34335–34340
57. Wong, S. T., Winchell, L. F., McCune, B. K., Earp, H. S., Teixidó, J., Massagué, J., Herman, B., and Lee, D. C. (1989) *Cell* **56,** 495–506
58. Sisodia, S. S. (1992) *Proc. Natl. Acad. Sci. U. S. A.* **89,** 6075–6079
59. Müllberg, J., Oberthür, W., Lottspeich, F., Mehl, E., Dittrich, E., Graeve, L., Heinrich, P. C., and Rose-John, S. (1994) *J. Immunol.* **152,** 4958–4968
60. Migaki, G. I., Kahn, J., and Kishimoto, T. K. (1995) *J. Exp. Med.* **182,** 549–557
61. Tang, P., Hung, M. C., and Klostergaard, J. (1996) *Biochemistry* **35,** 8226–8233

[2] T. Kang, H. Park, and Q. X. Sang, unpublished data.

62. Mullberg, J., Durie, F. H., Otten-Evans, C., Alderson, M. R., Rose-John, S., Cosman, D., Black, R. A., and Mohler, K. M. (1995) *J. Immunol.* **155,** 5198–5205
63. Alfalah, M., Parkin, E. T., Jacob, R., Sturrock, E. D., Mentele, R., Turner, A. J., Hooper, N. M., and Naim, H. Y. (2001) *J. Biol. Chem.* **276,** 21105–21109
64. Amour, A., Knight, C. G., Webster, A., Slocombe, P. M., Stephens, P. E., Knauper, V., Docherty, A. J., and Murphy, G. (2000) *FEBS Lett.* **473,** 275–279
65. Amour, A., Slocombe, P. M., Webster, A., Butler, M., Knight, C. G., Smith, B. J., Stephens, P. E., Shelley, C., Hutton, M., Knauper, V., Docherty, A. J., and Murphy, G. (1998) *FEBS Lett.* **435,** 39–44
66. Loechel, F., Fox, J. W., Murphy, G., Albrechtsen, R., and Wewer, U. M. (2000) *Biochem. Biophys. Res. Commun.* **278,** 511–515
67. Kashiwagi, M., Tortorella, M., Nagase, H., and Brew, K. (2001) *J. Biol. Chem.* **276,** 12501–12504
68. Westling, J., Fosang, A. J., Last, K., Thompson, V. P., Tomkinson, K. N., Hebert, T., McDonagh, T., Collins-Racie, L. A., LaVallie, E. R., Morris, E. A., and Sandy, J. D. (2002) *J. Biol. Chem.* **277,** 16059–16066

THE JOURNAL OF BIOLOGICAL CHEMISTRY
Vol. 278, No. 17, Issue of April 25, pp. 15056–15064, 2003
Printed in U.S.A.

Activation of Pro-gelatinase B by Endometase/Matrilysin-2 Promotes Invasion of Human Prostate Cancer Cells*

Received for publication, October 28, 2002, and in revised form, February 10, 2003
Published, JBC Papers in Press, February 13, 2003, DOI 10.1074/jbc.M210975200

Yun-Ge Zhao‡, Ai-Zhen Xiao‡, Robert G. Newcomer‡, Hyun I. Park‡, Tiebang Kang‡, Leland W. K. Chung§, Mark G. Swanson¶, Haiyen E. Zhau§, John Kurhanewicz¶, and Qing-Xiang Amy Sang‡‖

From the ‡Department of Chemistry and Biochemistry and Institute of Molecular Biophysics, Florida State University, Tallahassee, Florida 32306-4390, the §Molecular Urology and Therapeutics Program, Emory University Winship Cancer Institute, Atlanta, Georgia 30322, and the ¶Magnetic Resonance Science Center, University of California, San Francisco, California 94143-1290

This work has explored a putative biochemical mechanism by which endometase/matrilysin-2/matrix metalloproteinase-26 (MMP-26) may promote human prostate cancer cell invasion. Here, we showed that the levels of MMP-26 protein in human prostate carcinomas from multiple patients were significantly higher than those in prostatitis, benign prostate hyperplasia, and normal prostate glandular tissues. The role of MMP-26 in prostate cancer progression is unknown. MMP-26 was capable of activating pro-MMP-9 by cleavage at the Ala^{93}–Met^{94} site of the prepro-enzyme. This activation proceeded in a time- and dose-dependent manner, facilitating the efficient cleavage of fibronectin by MMP-9. The activated MMP-9 products generated by MMP-26 appeared more stable than those cleaved by MMP-7 under the conditions tested. To investigate the contribution of MMP-26 to cancer cell invasion via the activation of MMP-9, highly invasive and metastatic human prostate carcinoma cells, androgen-repressed prostate cancer (ARCaP) cells were selected as a working model. ARCaP cells express both MMP-26 and MMP-9. Specific anti-MMP-26 and anti-MMP-9 functional blocking antibodies both reduced the invasiveness of ARCaP cells across fibronectin or type IV collagen. Furthermore, the introduction of *MMP-26* antisense cDNA into ARCaP cells significantly reduced the MMP-26 protein level in these cells and strongly suppressed the invasiveness of ARCaP cells. Double immunofluorescence staining and confocal laser scanning microscopic images revealed that MMP-26 and MMP-9 were co-localized in parental and *MMP-26* sense-transfected ARCaP cells. Moreover, MMP-26 and MMP-9 proteins were both expressed in the same human prostate carcinoma tissue samples examined. These results indicate that MMP-26 may be a physiological and pathological activator of pro-MMP-9.

During the initial phases of carcinoma cell invasion, as tumor cells begin to spread and infiltrate into the surrounding normal tissues, these cells must first degrade the basement membrane and other elements of the extracellular matrix (ECM),[1] including type IV collagen, laminin, and fibronectin (FN) (1). Multiple protease families, including the matrix metalloproteinases (MMPs), serine proteases, and cysteine proteases, are suspected of contributing to the invasive and metastatic abilities of a variety of malignant tumors (2–5), but the specific biochemical mechanisms that facilitate these invasive behaviors remain elusive.

More than 23 human *MMPs*, and numerous homologues from other species, have been reported (5), and matrix metalloproteinase-26 (*MMP-26*)/endometase/matrilysin-2 is a novel member of this enzyme family that was recently cloned and characterized by our group (6) and others (7–9). *MMP-26* mRNA is primarily expressed in epithelial cancers, such as lung, breast, endometrial, and prostate carcinomas, in their corresponding cell lines (6–9), and in a very limited number of normal adult tissues, such as the uterus (6, 8), placenta (7, 8), and kidney (9). Recently, we have found that the levels of *MMP-26* gene and protein expression are higher in a malignant choriocarcinoma cell line (JEG-3) than in normal human cytotrophoblast cells (10). Our preliminary studies indicate that expression of *MMP-26* may be correlated with the malignant transformation of human prostate and breast epithelial cells. The specific expression of *MMP-26* in malignant tumors and the proteolytic activity of this enzyme against multiple components of the ECM, including fibronectin, type IV collagen, vitronectin, gelatins, and fibrinogen, as well as non-ECM proteins such as insulin-like growth factor-binding protein 1 and α1-protease inhibitor (6–9), indicate that MMP-26 may possess an important function in tumor progression.

Another member of the *MMP* family considered to be an important contributor to the processes of invasion, metastasis, and angiogenesis exhibited by tumor cells is gelatinase B (*MMP-9*) (11–14). Uría and López-Otín (8) have demonstrated that MMP-26 is able to cleave MMP-9, and here we examine the possibility that MMP-26 facilitates tumor cell invasion through the activation of pro-MMP-9. The highly invasive and metastatic cell line utilized for this study, an androgen-re-

* This work was supported in part by Department of Defense/United States Army Prostate Cancer Research Program Grant DAMD17-02-1-0238, National Institutes of Health Grant CA78646, American Cancer Society, Florida Division, Grant F01FSU-1, the Florida State University Research Foundation (to Q.-X. A. S.), and National Institutes of Health Grants CA82739 and CA76620 (to H. E. Z. and L. W. K. C., respectively). The costs of publication of this article were defrayed in part by the payment of page charges. This article must therefore be hereby marked "*advertisement*" in accordance with 18 U.S.C. Section 1734 solely to indicate this fact.

‖ To whom correspondence should be addressed: Dept. of Chemistry and Biochemistry, Florida State University, 203 DLC, Chemistry Research Bldg., Rm. 203, Tallahassee, FL 32306-4390. Tel.: 850-644-8683; Fax: 850-644-8281; E-mail: sang@chem.fsu.edu.

[1] The abbreviations used are: ECM, extracellular matrix; ANOVA, analysis of variance; ARCaP, androgen repressed prostate cancer cells line; BPH, benign prostate hyperplasia; FN, fibronectin; IMA, integrated morphometry analysis; MMP-7, matrix metalloproteinase-7/matrilysin; MMP-9, matrix metalloproteinase-9/gelatinase B; MMP-26, matrix metalloproteinase-26/endometase/matrilysin-2; MMPs, matrix metalloproteinases; CAPS, 3-cyclohexylamino-1-propanesulfonic acid.

pressed human prostate cancer (ARCaP), was derived from the ascites fluid of a patient with advanced prostate cancer that had metastasized to the lymph nodes, lungs, pancreas, liver, kidneys, and bones (15). This cell line produces high levels of MMP-9 and gelatinase A (MMP-2) (15, 16).

In this study, we provide evidence that MMP-26 is capable of activating pro-MMP-9, and that once activated, MMP-9 cleaves fibronectin, type IV collagen, and gelatin with great efficiency. Both the MMP-26 and MMP-9 proteins were highly expressed in the ARCaP cells, and co-localization of their expression patterns was consistently observed. The invasiveness of ARCaP cells through FN or type IV collagen was significantly decreased in the presence of antibodies specifically targeting MMP-26 or MMP-9. In addition, cells transfected with antisense *MMP-26*, showing significant reduction of MMP-26 at the protein level, exhibited a reduction of invasive potential *in vitro* in addition to a significant diminution in observed levels of active MMP-9 protein. These results support the hypothesis that activation of MMP-9 by MMP-26 may promote the *in vitro* invasiveness of ARCaP cells through FN or type IV collagen, whereas the co-expression of MMP-26 and MMP-9 in many human prostate carcinoma tissues indicates that this relationship may also occur *in vivo*.

MATERIALS AND METHODS

Cell Culture—ARCaP, DU145, PC-3, and LNCaP, which are all established human prostate carcinoma cell lines, were routinely grown in low-glucose Dulbecco's modified Eagle's medium supplemented with 10% fetal bovine serum, 100 units/ml penicillin, and 100 μg/ml streptomycin in a humidified atmosphere containing 5% CO_2 at 37 °C.

Silver Stain and Gelatin Zymography—Purified recombinant MMP-26 (6) or MMP-7 were incubated with purified pro-MMP-9 (17) or pro-MMP-2 (18) in HEPES buffer (50 mM HEPES, pH 7.5, 200 mM NaCl, 10 mM $CaCl_2$, and 0.01% Brij-35) at 37 °C. For the dosage dependence of MMP-9 activation, MMP-9 (0.2 μM, final concentration) was incubated with MMP-7 and MMP-26 at the indicated molar concentration ratio (2:1, 4:1, and 8:1) for 24 h. The MMP-9 activation was quenched by 2× SDS-PAGE sample buffer containing 50 mM EDTA. The resulting solution was further diluted five times and 5 μl of the diluted sample was loaded onto SDS-polyacrylamide gels (8%). For the time dependence of MMP-9 activation, MMP-9 (0.2 μM) was incubated with MMP-7 (0.05 μM) and MMP-26 (0.05 μM) for the indicated time periods (0, 4, 8, 24 and 48 h) before quenching with the sample buffer. For FN cleavage assays, 2 μl of FN (0.25 mg/ml) were incubated with 30 μl of MMP-26 (final concentration 0.05 μM), pro-MMP-9 (final concentration 0.2 μM), or MMP-26-activated MMP-9 solutions in 1× HEPES buffer at 37 °C for 18 h. For silver staining, the reaction was stopped by adding 4× reducing sample buffer (6% SDS, 40% glycerol, 200 mM Tris-HCl, pH 6.8, 5% β-mercaptoethanol, 200 mM EDTA, and 0.08% bromphenol blue) and boiled for 5 min. Following electrophoresis on a 9% SDS-polyacrylamide gel, the protein bands were visualized by silver staining (19). For gelatin zymogram, the gel was incubated for 3 h at 37 °C before it was stained with 0.1% Coomassie Blue solution (17, 20, 21).

Protein N-terminal Sequencing—Samples were separated by SDS-PAGE and transferred to ProBlott™ polyvinylidene difluoride membranes (Applied Biosystems) using CAPS buffer (10 mM CAPS, pH 11, 0.005% SDS). Proteins were visualized by staining with Coomassie Brilliant Blue R-250 solution (0.1% Coomassie Brilliant Blue R-250, 40% methanol, 1% acetic acid) and excised fragments were sent for sequencing. N-terminal sequencing was performed at the Bioanalytical Core Facility, Florida State University.

Reverse Transcriptase-PCR Analysis—RNA was extracted from the original cells by Trizol according to manufacturer protocols (Invitrogen, Carlsbad, CA), and 2 μg of total RNA were subjected to reverse transcriptase-PCR according to the standard protocol provided with the PCR kit (Invitrogen Corp., Carlsbad, CA). The *MMP-26* forward primer was 5′-ACCATGCAGCTCGTCATCTTAAGAG-3′; the reverse primer was 5′-AGGTATGTCAGATGAACATTTTTCTCC-3′; for glyceraldehyde-3-phosphate dehydrogenase the forward primer was 5′-ACGGATTTGGTCGTATTGGG-3′; the reverse primer was 5′-TGATTTTGGAGGGATCTCGC-3′. PCR reactions were performed using a Biometra Personal Cycler (Biometra, Germany) with 30 thermal cycles of 10 s at 94 °C denaturing, 30 s at 60 °C annealing, and 1 min at 72 °C elongation. Ten μl of the amplified PCR products were then electrophoresed on a 1.0% agarose gel containing 0.5 mg/ml ethidium bromide for analysis of size differences. To confirm the amplification of the required cDNA sequences, PCR products were digested with a restriction enzyme as directed by the manufacturer.

Generation and Characterization of Polyclonal Antibodies—Specific antigen peptides corresponding to unique sequences in the pro-domain and metalloproteinase domain of MMP-26 were synthesized by Dr. Umesh Goli at the Biochemical Analysis, Synthesis and Sequencing Services Laboratory of the Department of Chemistry and Biochemistry, Florida State University (Tallahassee, FL). The sequence selected from the pro-domain was Thr^{50}-Gln-Glu-Thr-Gln-Thr-Gln-Leu-Leu-Gln-Gln-Phe-His-Arg-Asn-Gly-Thr-Asp^{67}, and the sequence selected from the metalloproteinase domain was Asp^{188}-Lys-Asn-Glu-His-Trp-Ser-Ala-Ser-Asp-Thr-Gly-Tyr-Asn^{201} of the prepro-enzyme. Using the BLAST search method at the National Center for Biotechnology Information web site against all of the sequences in the data banks, no peptide with >45% level of identity was found (6), predicting the antibodies directed against these two peptides should be specific. The purity of these peptides was verified by reverse-phase high performance liquid chromatography and mass spectrometry. Rabbit anti-human antibodies were then generated, purified, and characterized as described previously (19, 21). Western blot analyses have demonstrated that these two antibodies are highly specific for MMP-26 because they do not cross-react with human matrilysin (MMP-7), stromelysin (MMP-3), gelatinase A (MMP-2), gelatinase B (MMP-9), and some other proteins tested (data not shown).

Western Blotting—Western blotting for MMP-26 was performed by lysing the cells with Tris-buffered saline (50 mM Tris and 150 mM NaCl, pH 7.4) containing 1.5% (v/v) Triton X-114 as described previously (21). Aliquots (20 μl) of cell lysate and media containing equal volumes (20 μl) from each treatment treated with SDS sample buffer were then loaded onto an SDS-polyacrylamide gel. Samples were electrophoresed and then electroblotted onto a nitrocellulose membrane. Immunoreactive MMP-26 bands were visualized using a horseradish peroxidase or alkaline phosphatase-conjugated secondary antibody (Jackson ImmunoResearch, West Grove, PA). Western blot analysis for MMP-9 was performed with a 1 μg/ml dilution of polyclonal anti-MMP-9 antibody (Oncogene Science, Cambridge, MA). MMP-9 bands were visualized using an alkaline phosphatase-conjugated secondary antibody (Jackson ImmunoResearch) followed by the addition of 5-bromo-4-chloro-3-indoyl phosphate and nitro blue tetrazolium. The blot membranes were then scanned, and the signal intensities were measured by integrated morphometry analysis (IMA) (Metamorph System, version 4.6r8, Universal Imaging Corporation, Inc., West Chester, PA). The signal intensities obtained were expressed as integrated optical density (the sum of the optical densities of all pixels that make up the object). All the bands used the same exclusive threshold for analysis.

Immunocytochemistry and Immunohistochemistry—Cells were fixed in 50% methanol, 50% acetone for 15 min and permeated with 1% Triton X-100 in Tris-buffered saline for 15 min. Formalin-fixed paraffin-embedded human prostate cancer tissues were sectioned to 4 μm thickness and fixed on slides. The sections were dewaxed with xylene and rehydrated in 100 and 95% ethanol. Nonspecific antibody binding in cells and sections was blocked with blocking buffer (0.2% Triton X-100, 5% normal goat serum, and 3% bovine serum albumin in Tris-buffered saline) for 1 h at room temperature prior to overnight incubation with affinity-purified specific rabbit anti-human MMP-26 antibody in the same buffer (5 μg/ml for immunocytochemistry and 10 μg/ml for inmmunohistochemistry) or goat anti-human MMP-9 antibody (25 μg/ml for immunohistochemistry, R&D Systems, Minneapolis, MN) at 4 °C. Cells and sections were incubated with alkaline phosphatase-conjugated secondary antibody (Jackson ImmunoResearch) diluted (1:5000) in the blocking buffer for 4 h at room temperature. The signals were detected by adding Fast-Red (Sigma). Purified preimmune IgGs from the same animal were used as negative controls for MMP-26. Normal goat serum was used as a negative control for MMP-9. The sections were counterstained lightly with hematoxylin for viewing negatively stained cells.

Preparation of MMP-26 Constructs—Full-length cDNA of *MMP-26* was amplified by PCR according to published sequences (6) and cloned into modified mammalian expression vector pCR™3.1-Uni with a FLAG tag at its C-terminal as described (22). Following confirmation of cDNA sequencing, plasmids containing correct inserts were used as sense vectors and plasmids with reversibly inserted cDNA were used as antisense vectors (22).

Transfections of ARCaP Cells and Isolation of MMP-26 Sense and Antisense Construct Stably Transfected Clones—ARCaP cells were

transfected with sense and antisense *MMP-26* cDNA-containing vectors using LipofectAMINE 2000 (Invitrogen) as described earlier (22, 23). Sense- and antisense-transfected cell lines were treated identically with regard to transfection conditions and maintenance in the selection medium. Stable transfectants were selected by growing the cells in 400 μg/ml Geneticin (G418; Invitrogen). Cells that survived were then expanded in the absence of G418 for additional studies. Stable transfectants were screened on the basis of FLAG and MMP-26 expression. Clones with *MMP-26* sense- and antisense-integrated constructs were selected and analyzed for MMP-26 expression, invasive capabilities in modified Boyden chamber invasion assays, and co-localization with MMP-9. Parental ARCaP cells served as controls.

Cell Invasion Assay—The invasiveness of ARCaP cells cultured in the presence of MMP-26 or MMP-9 functional blocking antibodies, parental ARCaP cells, sense *MMP-26*- and antisense *MMP-26*-transfected cells through reconstructed ECM was determined as per our previous report (24). The final concentrations of MMP-26 antibody were 10 and 50 μg/ml. The preimmune IgG from the same animal was used as control for MMP-26 antibody, and the final concentration was 50 μg/ml. The mouse anti-human MMP-9 monoclonal antibody is Ab-1, clone 6-6B, which is a functional neutralizing antibody that inhibits the enzymatic activity of MMP-9 (25) (Oncogene Research Products, CalBiochem, La Jolla, CA). The final concentrations of MMP-9 monoclonal antibody were 10 and 25 μg/ml. The preimmune mouse IgG (Alpha Diagnostic Intl. Inc., San Antonio, TX) was used as control, and the concentration was 25 μg/ml. Briefly, modified Boyden chambers containing polycarbonate filters with 8-μm pores (Becton Dickinson, Boston, MA) were coated with 0.5 mg/ml human plasma FN (Invitrogen) or 0.5 mg/ml type IV collagen (Sigma). Three-hundred μl of prepared cell suspension (1×10^6 cells/ml) in serum-free medium was added to each insert, and 500 μl of media containing 10% fetal bovine serum was added to the lower chamber. After 60 h of incubation, invasive cells that had passed through the filters to the lower surface of the membrane were fixed in 4% paraformaldehyde (Sigma). The cells were then stained with 0.1% crystal violet solution and photographed with an Olympus DP10 digital camera (Melville, NY) under a Nikon FX microscope (Melville, NY). The cells were then counted by IMA. For statistical analyses, the number of invasive cells treated with preimmune IgG was assumed to reflect 100% cell invasion. The ratio of the number of invaded cells that were treated with antibody or the *MMP-26* gene-transfected cells to preimmune IgG or parental cells, respectively, was used for subsequent comparative analyses by analysis of variance (ANOVA). Media from each insert was collected for Western blot and gelatin zymogram analyses.

Immunofluorescence and Confocal Laser Scanning Microscopy—Cells were cultured on 8-well slides for 24 h, then fixed in fresh 4% paraformaldehyde for 15 min at room temperature and permeabilized with 0.2% Triton X-100 in 10% normal goat serum in phosphate-buffered saline. The fixed, permeabilized cells were stained for 1 h at room temperature with anti-human MMP-26 (25 μg/ml) or a goat anti-human antibody targeting MMP-9 (R&D Systems, Minneapolis, MN) (1:200 dilution). Secondary rhodamine red-X-conjugated mouse anti-rabbit IgG for MMP-26 or fluorescein-conjugated donkey anti-goat IgG (Jackson ImmunoResearch) for MMP-9 were subsequently applied at a 1:200 dilution for 1 h at room temperature. Slow Fade mounting medium was added to the slides, and fluorescence was analyzed using a Zeiss LSM510 laser scanning confocal microscope (Carl Zeiss, Germany) equipped with a multiphoton laser according to our previous report (23). Images were processed for reproduction using Photoshop software version 6.0 (Adobe Systems, Mountainview, CA). Purified preimmune IgGs from the same animal were used as negative controls for MMP-26, and normal goat serum was used as a negative control for MMP-9.

Densitometric and Statistical Analysis—Samples were simultaneously stained with antibody and preimmune IgG on the same slide, and the areas of MMP-26 immunostaining were quantified by IMA. Four photographs were taken from each sample with an Olympus DP10 digital camera under a Nikon FX microscope. An appropriate color threshold was determined (color model, HSI; hue, 230–255; saturation and intensity, full spectrum), the glandular epithelia from each image was isolated into closed regions, and all areas of staining in compliance with these specific parameters were measured by IMA. The total area of these closed regions was determined by region measurement, and the ratio of signal area to total area was then determined. The average of the four ratios obtained from each sample was then used for subsequent analysis. The same color threshold was maintained for all samples. The preimmune staining ratio was subtracted from the antibody-staining ratio, and this value was then divided by the preimmune staining ratio to yield the reduced signal to background ratios used for subsequent comparative analyses by ANOVA. Statistical analysis of all samples was performed with the least significant difference correction of ANOVA for multiple comparisons. Data represent the mean ± S.D. from three experiments where differences with $p < 0.05$ were considered to be significant.

RESULTS

Activation of Pro-MMP-9 by MMP-26 and Cleavage of Substrates by Activated MMP-9—Gelatin zymography was utilized for determination of MMP-9 activity levels following cleavage by MMP-26. Zymography revealed that pro-MMP-9 presented as 225-, 125-, and 94-kDa gelatinolytic bands under non-reducing conditions (Fig. 1, *A*, *lane 1*, and *B*, *lanes 1* and *6*). The 225-kDa band is a homodimer of pro-MMP-9, the 125-kDa band is a heterodimer of pro-MMP-9 and neutrophil gelatinase-associated lipocalin, and the 94-kDa band is a monomer of pro-MMP-9 (17, 26, 27). New 215-, 115-, and 86-kDa bands were generated after incubation with MMP-26 (Fig. 1, *A* and *B*), and their activities were increased in a dose- and time-dependent manner (Fig. 1, *A* and *B*). Compared with MMP-7, the cleavage products generated by MMP-26 at the concentrations tested appear more stable (Fig. 1, *A* and *B*). However, pro-MMP-2 was not activated after incubation with identical concentrations of MMP-26 (data not shown).

MMP-26 cleaved pro-MMP-9 (94 kDa) to yield a new 86-kDa band on a silver-stained gel under reducing conditions (Fig. 1*C*, *lane 4*). N-terminal sequencing showed that the 86-kDa protein had the sequence of MRTPRXG, which is the same N terminus as reported during activation of pro-MMP-9 by $HgCl_2$ (28), human fibroblast-type collagenase (MMP-1) (17), phenylmercuric acid (29), and aminophenylmercuric acid (30). For further confirmation of MMP-9 activity, digestive assays were performed utilizing FN as a substrate. MMP-26 alone demonstrated weak cleavage of FN (Fig. 1*C*, *lane 6*), whereas pro-MMP-9 exhibited no cleavage of FN (Fig. 1*C*, *lane 7*). Once activated by MMP-26, MMP-9 cleaved FN very effectively, generating at least 6 new bands (Fig. 1*C*, *lane 8*).

Expression of MMP-26 in Human Prostate Gland and ARCaP Cells—Immunohistochemistry staining revealed that the intensity of MMP-26 staining was the highest in human prostate carcinoma (15 patient cases, Gleason grades 5–7), was low in prostatitis (9 cases), and was very low in benign prostate hyperplasia (BPH) (12 cases) and normal prostate gland tissues (7 cases) (Fig. 2*A*). Densitometric and statistical analysis (Fig. 2*B*) showed that the intensities of the immunostaining signals were significantly different between normal prostate gland and prostate cancer samples ($p = 0.0007$), between BPH and prostate cancer ($p = 0.0025$), and also between prostatitis and prostate cancer ($p = 0.0043$). However, there were no significant differences between normal and BPH ($p > 0.05$), normal and prostatitis ($p > 0.05$), or BPH and prostatitis tissues ($p > 0.05$) (Fig. 2*B*).

For selection of a prostate cancer cell line that expressed *MMP-26* for use as a working model, reverse transcriptase-PCR and Western blot analyses were used to detect MMP-26 expression in four human prostate cancer cell lines. *MMP-26* mRNA was identified in the ARCaP, DU145, and LNCaP cell lines, but not in the PC-3 cell line (Fig. 3*A*). Whereas the 20-kDa form of MMP-26 was detected in the ARCaP detergent phase, a doublet between 30 and 40 kDa of pro-MMP-26 was located in the ARCaP aqueous phase (Fig. 3*B*). This doublet might be two *N*-glycosylated forms of pro-MMP-26 predicted according to the ScanProsite program, with two possible *N*-glycosylation sites at $N^{64}GTD^{67}$ and $N^{221}QSS^{224}$. MMP-26 may have *N*-linked sugars according to the results obtained from *N*-glycosidase F (PNGase F, Roche Molecular Biochemicals) digestion experiments (data not shown). MMP-26 protein was

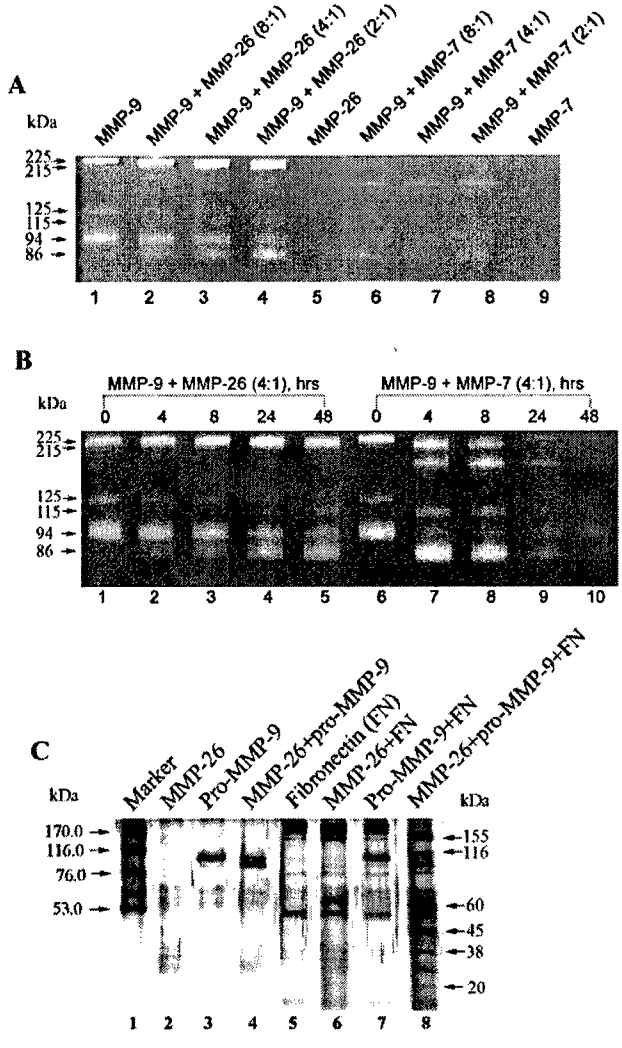

FIG. 1. **Activation of pro-MMP-9 by MMP-26.** *A* and *B*, gelatin zymogram of MMP-9 activity before and after activation of pro-MMP-9 by MMP-26 under non-reducing conditions. The 225-kDa band is a homodimer of pro-MMP-9, the 125-kDa band is a heterodimer of pro-MMP-9 and neutrophil gelatinase-associated lipocalin, and the 94-kDa band is a monomer of pro-MMP-9 (17, 26, 27). The activation reactions were incubated at 37 °C. *A*, dose-dependent analysis of pro-MMP-9 activation by MMP-26 (*lanes 1–4*) and MMP-7 (*lanes 6–8*). The activation reaction was incubated 37 °C for 24 h. The gelatin zymogram reaction was incubated at 37 °C for 3 h. The 86-kDa band was sequenced and the sequence is MRTPRXG, which is a product cleaved at the Ala^{93}–Met^{94} site. *B*, time-dependent analysis of pro-MMP-9 activation by MMP-26 (*lanes 1–5*) and MMP-7 (*lanes 6–10*). The gelatin zymogram reaction was incubated at 37 °C for 3 h. The ratio labeled in *A* and *B* is the molar concentration ratio. *C*, pro-MMP-9 activated by MMP-26 and cleavage of FN by MMP-26 and MMP-9 as detected by a silver-stained gel under reducing conditions. The molar concentration ratio for pro-MMP-9:MMP-26 is 4:1 and the reaction was incubated at 37 °C for 24 h. The molecular mass standards are labeled on the *left* and the estimated molecular masses of the FN cleavage products are labeled on the *right*.

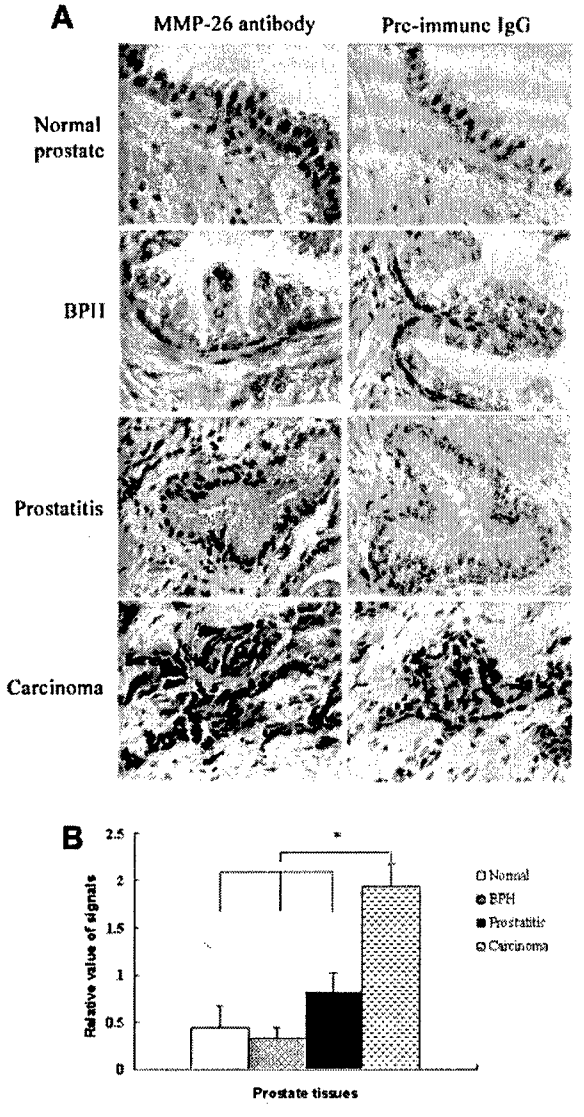

FIG. 2. **Comparison of MMP-26 expression in human normal and pathological prostate tissues.** *A*, immunohistochemistry and localization of MMP-26 in human prostate carcinoma (15 patient cases), prostatitis (9 cases), benign prostate hyperplasia (12 cases), and normal prostate gland tissues (7 cases). Cells stained *red* indicate MMP-26 expression. Photographs were taken under a microscope with ×400 magnification. *B*, densitometric analysis of MMP-26 expression in human prostate tissues. The quantification analysis was described under "Materials and Methods." Four pictures were taken from each sample with ×200 magnification. The epithelial regions were selected and the staining area and total selected area were obtained by IMA and analyzed by one-way ANOVA with LSD correction. Data shown are the mean ± S.D. values from the different prostate tissues. *, $p < 0.01$. *BPH*, benign prostate hyperplasia; *Normal*, normal prostate tissue; *Carcinoma*, prostate adenocarcinoma.

not detected in the DU145, LNCaP, or PC-3 cell lines (Fig. 3*B*), or in the ARCaP media under these experimental conditions (data not shown). Immunocytochemistry data confirmed that MMP-26 was localized inside the ARCaP cells (Fig. 3*C*) in a polarized manner.

Inhibitory Effects of Anti-MMP-26 and Anti-MMP-9 Antibodies on the Invasiveness of ARCaP Cells—To determine the role of MMP-26 and MMP-9 in ARCaP cell invasiveness, antibodies targeting the metalloproteinase domain of MMP-26 and targeting MMP-9 were utilized during *in vitro* cell invasion assays. We found significant ($p < 0.01$) reduction in the invasive potential of ARCaP cells through FN at concentrations of 10 (62.4%) and 50 μg/ml (46.0%) for the MMP-26 antibody (Fig. 4*A*), and at concentrations of 10 (55.9%) and 25 μg/ml (53.1%) for the MMP-9 antibody (Fig. 4*B*), when compared with the preimmune IgGs. We also found significantly ($p < 0.01$) reduced invasive potential in the movement of ARCaP cells through type IV collagen at concentrations of 10 (29.3%) and 50 μg/ml (18.8%) for the MMP-26 antibody (Fig. 4*A*), and at concentrations of 10 (52.2%) and 25 μg/ml (28.0%) for the MMP-9 antibody (Fig. 4*B*), when compared with the preimmune IgG. Antibody targeting the pro-domain of MMP-26 also significantly decreased the invasive potential of ARCaP cells through

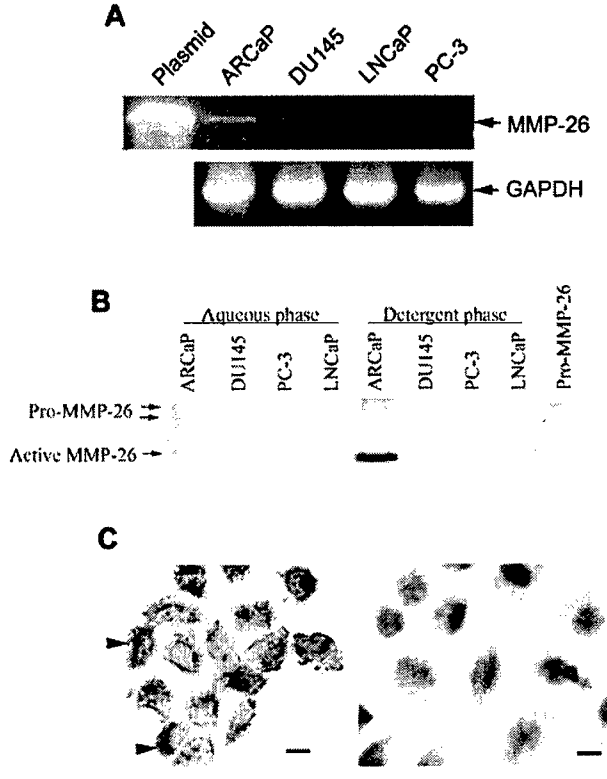

FIG. 3. ***MMP-26* mRNA and protein expression in ARCaP cells.** *A*, reverse transcriptase-PCR analysis of *MMP-26* mRNA in ARCaP, DU145, LNCaP, and PC-3 cell lines. MMP-26 plasmid is used as control (*top panel*, *lane 1*). The mRNA levels of a glycolysis pathway enzyme, glyceraldehyde-3-phosphate dehydrogenase (*GAPDH*), are shown in the *bottom panel* as a positive control to normalize cellular mRNA concentration. *B*, Western blot analysis of MMP-26 protein in ARCaP, DU145, LNCaP, and PC-3 cell lines. The *last lane* is recombinant pro-MMP-26 as a control. *C*, immunocytochemistry localization of MMP-26 in ARCaP cells. *Left panel*, the primary antibody is rabbit anti-MMP-26 antibody; *right panel*, the primary antibody is preimmune IgG from the same rabbit. *Red* staining indicates MMP-26 expression. *Scale bars* = 12 μm. *Arrows* show the positive staining signals. The cells were counterstained with hematoxylin for viewing of negatively stained cells (*purple*).

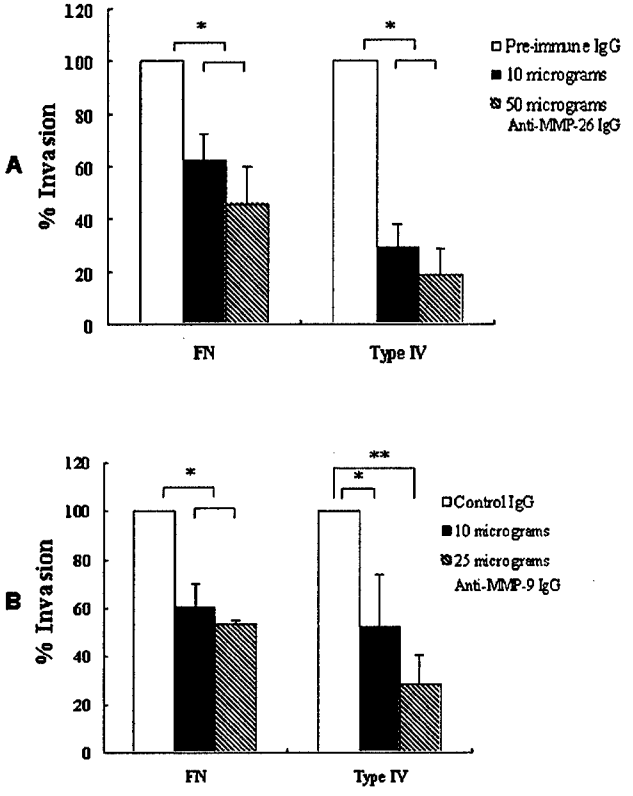

FIG. 4. **Blocking of ARCaP cell invasion through FN and type IV collagen by MMP-26 and MMP-9 antibodies.** The invasion assay was performed with modified Boyden chambers. The MMP-26 antibody is a rabbit anti-human MMP-26 metallo-domain antibody. The MMP-9 antibody is a mouse anti-human MMP-9 monoclonal antibody. The percentage of invading cells was quantified as described under "Materials and Methods." *A*, comparison of the invaded cell number in the presence of MMP-26 antibody/preimmune IgG. *Control*, preimmune rabbit IgG and the final concentration is 50 μg/ml. Ten and 50 μg of IgG means the final concentrations are 10 and 50 μg/ml, respectively. *B*, comparison of the invaded cell number in the presence of MMP-9 antibody/preimmune IgG. *Control*, preimmune mouse IgG and the concentration is 25 μg/ml. Ten and 25 μg of IgG means that the concentrations are 10 and 25 μg/ml, respectively. The invaded cell numbers of the preimmune IgG treatment were used as the 100% invasiveness. *Type IV*, type IV collagen. Data shown are the mean ± S.D. values from four separate experiments for each group. *, $p < 0.01$; **, $p < 0.001$.

FN and type IV collagen (data not shown). These results show that both anti-MMP-26 and anti-MMP-9 antibodies significantly inhibit ARCaP cell invasion through FN and type IV collagen.

MMP-26 Protein Expression in Stable Transfectants by Immunocytochemistry and Western Blotting—To further confirm the role of MMP-26 in ARCaP cell invasion, we transfected pCR 3.1 vectors containing full-length *MMP-26* cDNA in both sense and antisense orientations into ARCaP cells. Immunocytochemistry and Western blotting were performed to determine MMP-26 protein expression levels in the parental cells in addition to the sense and antisense *MMP-26* construct-transfected cells. Immunocytochemistry showed very strong MMP-26 staining in both the parental ARCaP and sense *MMP-26* construct-transfected cells, whereas the antisense *MMP-26* construct-transfected cells exhibited only minimal staining for MMP-26 (Fig. 5*A*). Western blotting revealed strong MMP-26 bands in the parental ARCaP and sense *MMP-26* construct-transfected cells, whereas only a very faint band was detected in the antisense *MMP-26* construct-transfected cells. No MMP-26 was detected in the cell culture media (Fig. 5*B*).

Reduction of Invasiveness of MMP-26 Antisense Stable Transfectants—Both the parental ARCaP and sense *MMP-26* construct-transfected cell lines invaded through either FN or type IV collagen *in vitro* during cell invasion assays (Fig. 6*A*), but without a marked difference ($p > 0.05$) in their invasive potentials (Fig. 6*B*). Antisense *MMP-26* construct-transfected cells showed a significant ($p < 0.01$) decrease in invasive potential through the same materials (44.0 and 23.5%, respectively) when compared with parental ARCaP cells (Fig. 6, *A* and *B*). A significant ($p < 0.01$) difference between the sense and antisense *MMP-26* construct-transfected cells was also noted (Fig. 6, *A* and *B*).

Reduced Levels of Active MMP-9 in MMP-26 Antisense Stably Transfected Cells—To determine the role of MMP-26-mediated MMP-9 activation in ARCaP cell invasion, the level of MMP-9 in conditioned media samples collected from the Boyden chambers during *in vitro* cell invasion assays was detected. Western blotting revealed a strong 86-kDa band of active MMP-9 in the conditioned media from parental ARCaP and sense *MMP-26* construct-transfected cells. A similar band, but of weaker intensity, was detected in the conditioned media collected from the antisense *MMP-26* construct-transfected cells (Fig. 7*A*). Semiquantitative analysis revealed that the active form of MMP-9 was significantly decreased ($p < 0.01$) in both the FN and type IV collagen invasive assay media from the antisense *MMP-26* construct-transfected cells (Fig. 7*B*).

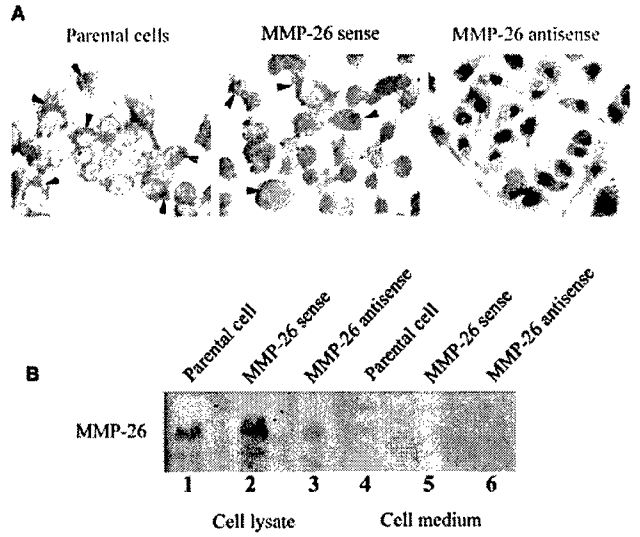

FIG. 5. **MMP-26 protein expression in parental ARCaP, sense *MMP-26* construct, and antisense *MMP-26* construct stably transfected cells.** *A*, immunocytochemistry of MMP-26 expression in parental ARCaP, sense *MMP-26* construct, and antisense *MMP-26* construct stably transfected cells. *Red* staining indicates MMP-26 expression. *Arrows* show examples of the positive staining signals. The cells were counterstained with hematoxylin for viewing of MMP-26 negative cells (*purple*). *B*, Western blot analysis of MMP-26 protein expression. Parental ARCaP, sense *MMP-26* construct, and antisense *MMP-26* construct stably transfected cells were cultured utilizing an equivalent number of cells. Conditioned medium samples were collected prior to cell lysis.

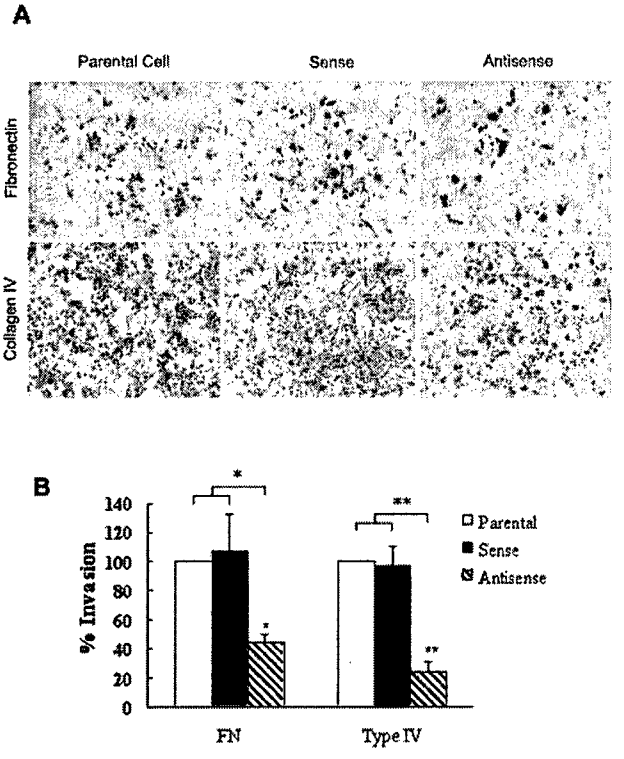

FIG. 6. **Invasion of parental ARCaP, sense, or antisense *MMP-26* construct stably transfected cells through FN and type IV collagen.** *A*, cells that invaded to the lower surface of the membrane were photographed under a microscope with ×40 magnification. *B*, the percentage of invading cells in parental and *MMP-26* sense or antisense construct stably transfected ARCaP cells. The cell numbers of the invaded parental cells were used as 100% invasiveness. The cells were counted and analyzed as described under "Materials and Methods." Data shown are the mean ± S.D. values from three separate experiments for each group. *, $p < 0.01$; **, $p < 0.001$.

Co-localization of MMP-26 with MMP-9 in Parental and MMP-26 Sense Gene Stably Transfected ARCaP Cells, and Co-expression of MMP-26 and MMP-9 in Human Prostate Carcinoma Tissue Samples—Double immunofluorescence experiments were performed in parental ARCaP and *MMP-26* stably transfected cells with human *MMP-26* sense or antisense genes. The red color indicates MMP-26 and the green color indicates MMP-9 protein staining. Merged images show a color shift to orange-yellow, indicating co-localization between MMP-26 and MMP-9. Confocal laser scanning microscopic analysis revealed co-localization of both proteins in the cytoplasm of parental ARCaP (Fig. 8*A*, *a–d*) and sense-transfected cells (Fig. 8*A*, *e–h*), but not in the antisense-transfected cells (Fig. 8*A*, *i–l*). Very weak signals were detected in parental ARCaP control cells using purified preimmune IgG for the detection of MMP-26 and nonimmune goat sera for the detection of MMP-9 (Fig. 8*A*, *m–p*). MMP-26 and MMP-9 proteins were also found to be co-expressed in human prostate carcinoma tissue samples (Fig. 8*B*).

DISCUSSION

MMP-26 is able to activate MMP-9 by cleavage at the Ala^{93}–Met^{94} site of the prepro-MMP-9, which is the same cleavage site detected previously during activation with $HgCl_2$ (28), human fibroblast-type collagenase (17), phenylmercuric acid (29), and aminophenylmercuric acid (30). This activation was confirmed by the effective cleavage of FN using MMP-9 activated by MMP-26. These results indicate that the zymogen form of MMP-9 can be transiently activated without the proteolytic loss of the cysteine (Cys^{99})-switch residue, even though these findings may appear to be in conflict with the original Cys-switch hypothesis (31). The 86-kDa form of MMP-9 may also be further activated to produce lower molecular mass active species similar to the process activated by other MMPs (17). Among all the MMPs, matrilysin (MMP-7) and MMP-26 share domain structures with pro- and metalloproteinase domains only and are both expressed in epithelial cells (6–9). Therefore, MMP-26 is also named as matrilysin-2 (8). Both MMP-26 and MMP-7 could activate MMP-9 but their cleavage sites in pro-MMP-9 are different. Matrilysin cleaved MMP-9 at two sites, Glu^{59}–Met^{60} and Arg^{106}–Phe^{107} of the prepro-MMP-9 (17). Our current results also demonstrated that the MMP-9 activation mediated by MMP-26 is much slower than that mediated by MMP-7, but the activation products are much more stable when compared with the products of activation by MMP-7. This indicates that activation of MMP-9 by MMP-26 is prolonged but persistent, which is consistent with the process of tumor cell invasion. MMP-26 did not cleave pro-MMP-2, another gelatinase, indicating that pro-MMP-9 activation by MMP-26 is highly selective. MMP-9 is a powerful enzyme, and is considered to be an important contributor to the processes of invasion, metastasis, and angiogenesis in various tumors (11–14, 32–36).

This work has tested the hypothesis that MMP-26 may enhance human prostate cancer cell invasion via the activation of pro-MMP-9 using an ARCaP cell line as a working model. The ARCaP cell line is a highly invasive and metastatic human prostate cancer cell line that expresses both MMP-9 (15) and MMP-26. We found that *MMP-26* mRNA was detected in the ARCaP cell line and two other human prostate carcinoma cell lines, DU145 and LNCaP, but the MMP-26 protein was only detected in ARCaP cells. More importantly, high levels of MMP-26 protein were also detected in human prostate carcinoma cells by immunohistochemistry, but only low expression was seen in prostatitis, benign prostate hyperplasia, and normal prostate tissues. This is in agreement with reports of

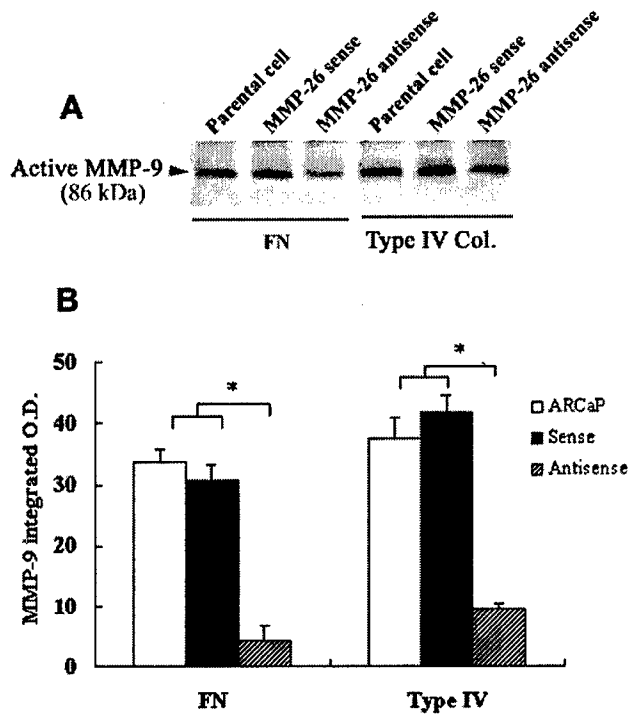

FIG. 7. **Detection of MMP-9 in the invasive assay media from parental ARCaP, sense *MMP-26* construct, or antisense *MMP-26* construct stably transfected cells.** *A*, Western blot of the invasive assay media. Media samples were collected from the upper compartments of Boyden chambers during cell invasion assays. *B*, densitometry scanning and semiquantitative analysis of the levels of MMP-9 in the invasive assay media. Data shown are the mean ± S.D. values from four separate experiments for each group. *, $p < 0.001$.

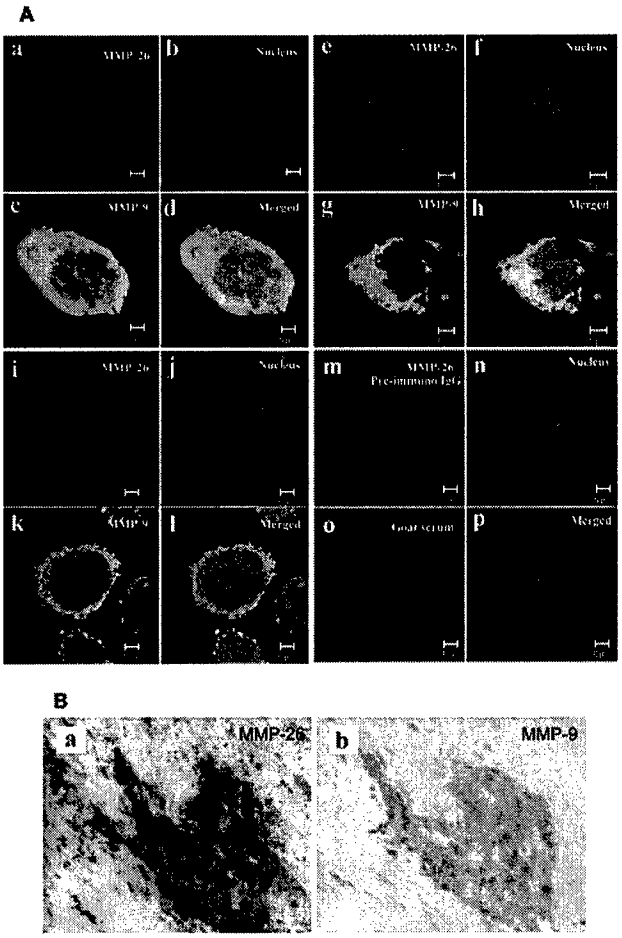

FIG. 8. **Co-localization of MMP-26 and MMP-9 in parental and sense *MMP-26*-transfected ARCaP cells and an example of MMP-26 and MMP-9 co-expression in the same human prostate carcinoma tissues.** *A*, double immunofluorescence staining and confocal laser scanning micrographs of parental, sense, and antisense *MMP-26*-transfected ARCaP cells. *Red* indicates MMP-26 signals and *green* indicates MMP-9 signals. *Yellow* reveals the co-localization of MMP-26 and MMP-9. *Blue* fluorescence represents the nuclei. *a–d*, parental ARCaP cells. *e–h*, sense *MMP-26* construct-transfected cells. *i–l*, antisense *MMP-26* construct-transfected cells. *m–p*, parental ARCaP cells with preimmune IgG and goat sera as controls. *Scale bars* = 5 μm. *B*, an example of co-expression of MMP-26 and MMP-9 proteins in the same human prostate carcinoma tissues. *a*, strong positive MMP-26 protein staining in epithelial cells of human prostate carcinoma (Gleason grade 3 + 3). *b*, positive MMP-9 protein staining in epithelial cells of the same human prostate carcinoma. Cells stained *red* indicate MMP-26 and MMP-9 expression. The sections were counterstained with hematoxylin for viewing negatively stained cells. Photographs were taken under a microscope with ×400 magnification.

MMP-26 gene expression in epithelial cancers (6–9). We have previously reported that the levels of *MMP-26* gene and protein expression are increased in a malignant choriocarcinoma cell line (JEG-3) to levels that are well in excess of that found in normal human cytotrophoblast cells (10). The majority of MMP-26 protein detected was in the detergent phase of the ARCaP cell lysates, not in the conditioned media, and only low levels were observed in the aqueous phase. This is in accordance with recent studies demonstrating that *MMP-26*-transfected COS-7 and HEK293 cells secrete the protein poorly (7–9). As MMP-26 was found in the detergent phase of the ARCaP cell lysates, it is possible that MMP-26 may be associated with cell membrane components via an unidentified mechanism. Membrane-associated MMP-26 may participate directly in degradation of the ECM, activating pro-enzymes, and releasing growth factors, partially accounting for the inhibition of ARCaP cell invasion by the MMP-26 antibody tested. These reports converge to suggest that MMP-26 may play an important role in human carcinoma invasion and tumor progression.

MMP-26 exhibits wide substrate specificity, and is capable of degrading many components of the basement membrane and other ECM components (6–9, 37). Although MMP-26 can cleave type IV collagen, fibronectin, and other proteins, it is a catalytically less powerful enzyme than gelatinase B/MMP-9. The inhibition of ARCaP cell invasion by MMP-26-specific antibodies suggests that MMP-26 may contribute to ARCaP cell invasion by cleaving ECM components directly and/or by activating pro-MMP-9 to cleave the ECM. Our FN cleavage assays with MMP-26 alone and MMP-26-activated MMP-9 show that once activated by MMP-26, MMP-9 cleaves FN more efficiently. This indicates that the activation of MMP-9 may be a major pathway for MMP-26 promotion of ARCaP cell invasion. Indeed, this hypothesis was further verified by ARCaP cell invasion inhibition in the presence of MMP-9 functional blocking antibodies. When the proteolytic activity of MMP-26 is combined with that of activated MMP-9, which digests ECM and basement membrane proteins in an even more aggressive fashion than MMP-26 alone, this hints at an amplification mechanism by which MMP-26 might contribute significantly to the processes of tumor cell invasion and subsequent metastasis.

Several lines of evidence have demonstrated that biochemical activation of pro-MMP-9 by MMP-26 may be a physiologically and pathologically relevant event. Our results demonstrated that antibodies directed against MMP-26 catalytic domain and prodomain both blocked the ARCaP cell invasion. Equally as significant, a function blocking monoclonal antibody that inhibits MMP-9 catalytic activity (25, 38) also prevented the invasion of ARCaP cells in patterns similar to a MMP-26 antibody. These results verify our hypothesis that activation of

pro-MMP-9 by MMP-26 promotes invasion of human prostate cancer cells.

Recently, our group has also determined that MMP-26 autodigested itself during the folding process. Two of the major autolytic sites were Leu^{49}–Thr^{50} and Ala^{75}–Leu^{76}, which left the "cysteine-switch" sequence ($PHC^{82}GVPD$) intact (37), and suggests that Cys^{82} may not play a role in the latency of the zymogen form. Another group has demonstrated that autolytic activation of MMP-26 occurred at $LLQ^{59} \downarrow Q^{60}FH$, which is upstream from the cysteine residue known to be responsible for the latency of many other MMPs (39). Interestingly, our pro-domain antigen peptide mimics the Thr^{50} to Asp^{67} region of MMP-26, and the resultant antibody complex shields the autocleavage sites (data not shown). This fortunate circumstance may account for the decreased invasiveness of ARCaP cells treated with our antibody targeting the pro-domain, while also suggesting that the catalytic activity of MMP-26 may not require the highly conserved cysteine-switch activation mechanism.

To further confirm the role of MMP-26 during ARCaP cell invasion, we generated stably transfected ARCaP cells with vectors containing full-length *MMP-26* cDNA in both the sense and antisense orientations. Our results show that transfection of the ARCaP cells with antisense *MMP-26* constructs leads to decreased levels of MMP-26 protein expression when compared with parental and sense controls, suggesting that this antisense construct is responsible for the observed decrease in MMP-26 protein expression, resulting in profound biological consequences. In cell invasion assays, antisense-transfected cells show a marked reduction in invasiveness over those of parental ARCaP and *MMP-26* sense gene-transfected ARCaP cells, suggesting that the modulation of *MMP-26* in ARCaP cells altered the invasive potential of these cells in our experimental model system, lending support to the hypothesis that MMP-26 activity may play a crucial role in facilitating the invasion of ARCaP cells through the ECM.

Western blotting of conditioned media collected from the upper compartments of the Boyden chambers during invasion assays reveals that the 86-kDa active form of MMP-9 is present in parental ARCaP and sense *MMP-26*-transfected ARCaP cell media, but very little active MMP-9 is present in the antisense *MMP-26*-transfected ARCaP cell media. These findings suggest that MMP-26 activated MMP-9 in parental ARCaP and sense *MMP-26*-transfected ARCaP cells, while very little activation took place in the antisense *MMP-26*-transfected ARCaP cells. When present, active MMP-9 accumulates in the cytosol of human endothelial cells, where it is eventually utilized by invading pseudopodia (40), and it is possible that endogenous, self-activated MMP-26 acts as an activator for intracellular pro-MMP-9. The active form of MMP-9 may then be stored inside the cell, ready for rapid release when it is required to facilitate the invasion of ARCaP cells.

Consistent with the above data, double immunofluorescence labeling and confocal laser scanning microscopy reveal that MMP-26 and MMP-9 were co-localized in parental ARCaP and sense *MMP-26*-transfected ARCaP cells, affording them ample opportunity to interact. Co-localization was not observed in antisense *MMP-26*-transfected ARCaP cells, as MMP-26 was not expressed in these cells. Immunohistochemistry revealed a similar relationship in human prostate tissue samples, demonstrating that MMP-26 and MMP-9 were also co-expressed in prostate carcinomas. Recently, Nemeth *et al.* (36) have reported that both *MMP-9* mRNA and protein were expressed in biopsy specimens from patients with documented, bone-metastatic prostate cancer. Thus, the biochemical activation mechanism of pro-MMP-9 that we observed *in vitro* might well be applicable to prostate cancer *in vivo*.

Although direct degradation of the ECM by MMP-26 may contribute to the processes of cell invasion and tumor metastasis, as the consequential relationship between MMP-26 and MMP-9 begins to emerge, we find evidence of coordination and a proteolytic cascade (activation of MMP-9) that may be a major pathway to promote the invasion of human prostate carcinoma. The specific expression of MMP-26 and its potential role in the invasion of cancer cells suggest that MMP-26 may be a new marker for certain types of prostate carcinomas, and perhaps a new therapeutic molecular target for prostate cancer.

Acknowledgments—We gratefully acknowledge Dr. Jian Ni at Human Genome Sciences Inc. for previous collaboration pertaining to *MMP-26* cloning and Sara C. Monroe and Margie Coryn for editorial assistance with manuscript preparation. We are grateful to Dr. Umesh Goli in our department for synthesis of the peptide antigens, Margaret Seavy at the Bioanalytical Core facility for performing the N-terminal sequencing, and Kimberly Riddle and Jon Ekman at the Department of Biological Sciences Imaging Facility for excellent assistance with confocal microscopy.

REFERENCES

1. Matrisian, L. M. (1992) *Bioessays* **14,** 455–463
2. Goldfarb, R. H., and Liotta, L. A. (1986) *Semin. Thromb. Hemostasis* **12,** 294–307
3. McCawley, L. J., and Matrisian, L. M. (2000) *Mol. Med. Today* **6,** 149–156
4. Sternlicht, M. D., and Werb, Z. (2001) *Annu. Rev. Cell Dev. Biol.* **17,** 463–516
5. Egeblad, M., and Werb, Z. (2002) *Nat. Rev. Cancer* **2,** 163–176
6. Park, H. I., Ni, J., Gerkema, F. E., Liu, D., Belozerov, V. E., and Sang, Q.-X. (2000) *J. Biol. Chem.* **275,** 20540–20544
7. de Coignac, A. B., Elson, G., Delneste, Y., Magistrelli, G., Jeannin, P., Aubry, J. P., Berthier, O., Schmitt, D., Bonnefoy, J. Y., and Gauchat, J. F. (2000) *Eur. J. Biochem.* **267,** 3323–3329
8. Urría, J. A., and López-Otín, C. (2000) *Cancer Res.* **60,** 4745–4751
9. Marchenko, G. N., Ratnikov, B. I., Rozanov, D. V., Godzik, A., Deryugina, E. I., and Strongin, A. Y. (2001) *Biochem. J.* **356,** 705–718
10. Zhang, J., Cao, Y. J., Zhao, Y.-G., Sang, Q.-X., and Duan, E.-K. (2002) *Mol. Hum. Reprod.* **8,** 659–666
11. Scorilas, A., Karameris, A., Arnogiannaki, N., Ardavanis, A., Bassilopoulos, P., Trangas, T., and Talieri, M. (2001) *Br. J. Cancer.* **84,** 1488–1496
12. Hrabec, E., Strek, M., Nowak, D., and Hrabec, Z. (2001) *Respir. Med.* **95,** 1–4
13. Sakamoto, Y., Mafune, K., Mori, M., Shiraishi, T., Imamura, H., Mori, M., Takayama, T., and Makuuchi, M. (2000) *Int. J. Oncol.* **17,** 237–243
14. Shen, K. H., Chi, C. W., Lo, S. S., Kao, H. L., Lui, W. Y., and Wu, C. W. (2000) *Anticancer Res.* **20,** 1307–1310
15. Zhau, H. Y., Chang, S. M., Chen, B. Q., Wang, Y., Zhang, H., Kao, C., Sang, Q. A., Pathak, S. J., and Chung, L. W. (1996) *Proc. Natl. Acad. Sci. U. S. A.* **93,** 15152–15157
16. Matsubara, S., Wada, Y., Gardner, T. A., Egawa, M., Park, M. S., Hsieh, C. L., Zhau, H. E., Kao, C., Kamidono, S., Gillenwater, J. Y., and Chung, L. W. K. (2001) *Cancer Res.* **61,** 6012–6019
17. Sang, Q.-X., Birkedal-Hansen, H., and Van Wart, H. E. (1995) *Biochim. Biophys. Acta* **1251,** 99–108
18. Sang, Q. A., Bodden, M. K., and Windsor, L. J. (1996) *J. Protein Chem.* **15,** 243–253
19. Zhao, Y. G., Wei, P., and Sang, Q.-X. (2001) *Biochem. Biophys. Res. Commun.* **289,** 288–294
20. Zhao, Y.-G., Xiao, A. Z., Cao, X. M., and Zhu, C. (2002) *Mol. Reprod. Dev.* **62,** 149–158
21. Li, H., Bauzon, D. E., Xu, X., Tschesche, H., Cao, J., and Sang, Q.-X. (1998) *Mol. Carcinog.* **22,** 84–94
22. Kang, T., Yi, J., Yang, W., Wang, X., Jiang, A., and Pei, D. (2000) *FASEB J.* **14,** 2559–2568
23. Kang, T., Zhao, Y.-G., Pei, D., Sucic, J. F., and Sang, Q.-X. (2002) *J. Biol. Chem.* **277,** 25583–25591
24. Sang, Q.-X., Jia, M.-C., Schwartz, M. A., Jaye, M. C., Kleinman, H. K., Ghaffari, M. A., and Luo, Y.-L. (2000) *Biochem. Biophys. Res. Commun.* **274,** 780–786
25. Ramos-DeSimone, N., Moll, U. M., Quigley, J. P., and French, D. L. (1993) *Hybridoma* **12,** 349–363
26. Tschesche, H., Zolzer, V., Triebel, S., and Bartsch, S. (2001) *Eur. J. Biochem.* **268,** 1918–1928
27. Yan, L., Borregaard, N., Kjeldsen, L., and Moses, M. A. (2001) *J. Biol. Chem.* **276,** 37258–37265
28. Triebel, S., Blaser, J., Reinke, H., Knauper, V., and Tschesche, H. (1992) *FEBS Lett.* **298,** 280–284
29. Wilhelm, S. M., Collier, I. E., Marmer, B. L., Eisen, A. Z., Grant, G. A., and Goldberg, G. I. (1989) *J. Biol. Chem.* **264,** 17213–17221
30. Okada, Y., Gonoji, Y., Naka, K., Tomita, K., Nakanishi, I., Iwata, K., Yamashita, K., and Hayakawa, T. (1992) *J. Biol. Chem.* **267,** 21712–21719
31. Van Wart, H. E., and Birkedal-Hansen, H. (1990) *Proc. Natl. Acad. Sci. U. S. A.* **87,** 5578–5582
32. Arlt, M., Kopitz, C., Pennington, C., Watson, K. L., Krell, H. W., Bode, W., Gansbacher, B., Khokha, R., Edwards, D. R., and Kruger, A. (2002) *Cancer Res.* **62,** 5543–5550

33. Li, Y., and Sarkar, F. H. (2002) *Cancer Lett.* **186,** 157–164
34. Mase, K., Iijima, T., Nakamura, N., Takeuchi, T., Onizuka, M., Mitsui, T., and Noguchi, M. (2002) *Lung Cancer* **36,** 271–276
35. Singer, C. F., Kronsteiner, N., Marton, E., Kubista, M., Cullen, K. J., Hirtenlehner, K., Seifert, M., and Kubista, E. (2002) *Breast Cancer Res. Treat.* **72,** 69–77
36. Nemeth, J. A., Yousif, R., Herzog, M., Che, M., Upadhyay, J., Shekarriz, B., Bhagat, S., Mullins, C., Fridman, R., and Cher, M. L. (2002) *J. Natl. Cancer Inst.* **94,** 17–25
37. Park, H. I., Turk, B. E., Gerkema, F. E., Cantley, L. C., and Sang, Q.-X. (2002) *J. Biol. Chem.* **277,** 35168–35175
38. Seftor, R. E., Seftor, E. A., Koshikawa, N., Meltzer, P. S., Gardner, L. M., Bilban, M., Stetler-Stevenson, W. G., Quaranta, V., and Hendrix, M. J. (2001) *Cancer Res.* **61,** 6322–6327
39. Marchenko, N. D., Marchenko, G. N., and Strongin, A. Y. (2002) *J. Biol. Chem.* **277,** 18967–18972
40. Nguyen, M., Arkell, J., and Jackson, C. J. (1998) *J. Biol. Chem.* **273,** 5400–5404

THE JOURNAL OF BIOLOGICAL CHEMISTRY
Vol. 278, No. 51, Issue of December 19, pp. 51646–51653, 2003
Printed in U.S.A.

The Intermediate S_1' Pocket of the Endometase/Matrilysin-2 Active Site Revealed by Enzyme Inhibition Kinetic Studies, Protein Sequence Analyses, and Homology Modeling*

Received for publication, September 11, 2003
Published, JBC Papers in Press, October 7, 2003, DOI 10.1074/jbc.M310109200

Hyun I. Park, Yonghao Jin, Douglas R. Hurst, Cyrus A. Monroe, Seakwoo Lee, Martin A. Schwartz, and Qing-Xiang Amy Sang‡

From the Department of Chemistry and Biochemistry and Institute of Molecular Biophysics, Florida State University, Tallahassee, Florida 32306-4390

Human matrix metalloproteinase-26 (MMP-26/endometase/matrilysin-2) is a newly identified MMP and its structure has not been reported. The enzyme active site S_1' pocket in MMPs is a well defined substrate P_1' amino acid residue-binding site with variable depth. To explore MMP-26 active site structure-activity, a series of new potent mercaptosulfide MMP inhibitors (MMPIs) with Leu or homophenylalanine (Homophe) side chains at the P_1' site were selected. The Homephe side chain is designed to probe deep S_1' pocket MMPs. These inhibitors were tested against MMP-26 and several MMPs with known x-ray crystal structures to distinguish shallow, intermediate, and deep S_1' pocket characteristics. MMP-26 has an inhibition profile most similar to those of MMPs with intermediate S_1' pockets. Investigations with hydroxamate MMPIs, including those designed for deep pocket MMPs, also indicated the presence of an intermediate pocket. Protein sequence analysis and homology modeling further verified that MMP-26 has an intermediate S_1' pocket formed by Leu-204, His-208, and Tyr-230. Moreover, residue 233 may influence the depth of an MMP S_1' pocket. The residue at the equivalent position of MMP-26 residue 233 is hydrophilic in intermediate-pocket MMPs (*e.g.* MMP-2, -8, and -9) and hydrophobic in deep-pocket MMPs (*e.g.* MMP-3, -12, and -14). MMP-26 contains a His-233 that renders the S_1' pocket to an intermediate size. This study suggests that MMPIs, protein sequence analyses, and molecular modeling are useful tools to understand structure-activity relationships and provides new insight for rational inhibitor design that may distinguish MMPs with deep *versus* intermediate S_1' pockets.

Matrix metalloproteinases (MMPs,[1] matrixins) are believed to participate in angiogenesis, embryonic development, morphogenesis, reproduction, tissue resorption and remodeling, and tumor growth, progression, invasion, and metastasis through breakdown of the extracellular matrix, cell surface proteins, and processing growth factors, cytokines, and chemokines (1–3). Recently, human MMP-26 (endometase/matrilysin 2) was identified and its mRNA expression was detected in normal tissues of the human uterus and placenta, and in many types of malignant tumors (4–7). Characterization of the MMP-26 promoter suggests that this proteinase may be expressed in cancer cells of epithelial origin (8). MMP-26 may play an important role in human prostate and breast cancer invasion (9–10).

MMP-26 cleaves type I gelatin, α_1-proteinase inhibitor, fibrinogen, fibronectin, vitronectin, type IV collagen, and insulin-like growth factor binding protein-1 (4, 7, 11). Studies of MMP-26 indicate that it has substrate specificity similar to other MMPs, with the exception of a preference for Ile at the P_2 and P_2' positions, for small residues at the P_3' and P_4' positions, and Lys at the P_4 position (11). MMP-26 also hydrolyzes several synthetic fluorogenic peptide substrates designed for stromelysin-1, gelatinases, collagenases, and tumor necrosis factor-α converting enzyme (4, 11). According to these peptide substrate studies, MMP-26 may be capable of cleaving a broad range of substrates, although it has less catalytic efficiency than other MMPs.

X-ray crystal structures of MMPs illustrate that overall topology and secondary structures are conserved (12–18). The S_1' pocket, a hydrophobic pocket of variable depth, is a well defined substrate P_1'-binding site in MMPs. Three types of S_1' pockets can be distinguished from the available structures of MMPs (19–20). One type is a shallow pocket, as found in MMP-1 (human fibroblast collagenase; 13) and MMP-7 (matrilysin; 16), where the pockets are limited by the side chains of Arg and Tyr, respectively, crossing the pockets. Many of the structurally known MMPs possess Leu at the corresponding site, and its side chain forms the top of the pocket rather than crossing the pocket. These Leu-containing MMPs may be further classified as deep and intermediate S_1' pocket MMPs. A deep, tunnel-like pocket is found in MMP-3 (stromelysin-1; 12), MMP-12 (metalloelastase; 17), and MMP-14 (MT1-MMP; 21), whereas MMP-2 (gelatinase A; 22), MMP-8 (human neutrophil collagenase; 15), and MMP-9 (gelatinase B; 23) possess an intermedi-

* This work was supported by Department of Defense/U. S. Army Prostate Cancer Research Program Grant DAMD17-02-1-0238, National Institutes of Health Grant CA78646, the American Cancer Society, Florida Division F01FSU-1, and the Florida State University Research Foundation (to Q.-X. A. S.), a grant from the Molecular Design and Synthesis (MDS) Research Foundation (to M. A. S.), National Science Foundation Postdoctoral Training Grant DBI 9602233 (to H. I. P.), Department of Defense/U. S. Army Breast Cancer Research Program Predoctoral Fellowship DAMD17-00-1-0243 (to D. R. H.), and a Pfizer Summer Undergraduate Student Research Fellowship (to C. A. M.). The costs of publication of this article were defrayed in part by the payment of page charges. This article must therefore be hereby marked "*advertisement*" in accordance with 18 U.S.C. Section 1734 solely to indicate this fact.

‡ To whom correspondence should be addressed: Dept. of Chemistry and Biochemistry, Florida State University, Chemistry Research Bldg. DLC, Rm. 203, Tallahassee, FL 32306-4390. Tel.: 850-644-8683; Fax: 850-644-8281; E-mail: sang@chem.fsu.edu.

[1] The abbreviations used are: MMP, matrix metalloproteinase; Boc, *tert*-butoxycarbonyl; Brij-35, polyoxyethylene lauryl ether; Homophe, homophenylalanine; Mca, (7-methoxycoumarin-4-yl)acetyl; Dpa, *N*-3-(2,4-dinitrophenyl)-2,3-diaminopropionyl; MMPI, matrix metalloproteinase inhibitor.

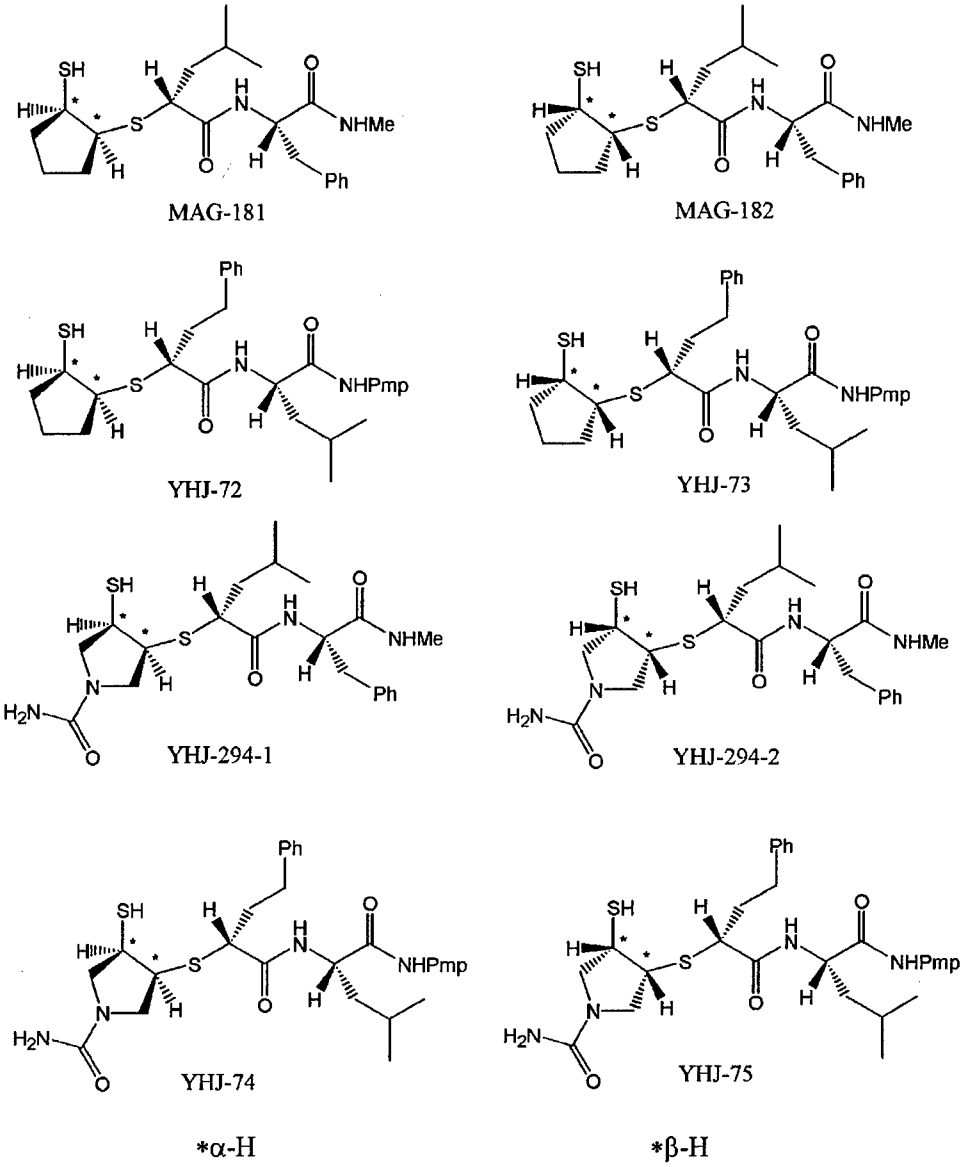

Abbreviations: Me, Methyl; Ph, Phenyl; Pmp, *p*-methoxyphenyl.

FIG. 1. **Structures of new mercaptosulfide MMP inhibitors.** The diastereomer notation in the ring system is started from the α carbon of the mercapto group.

TABLE I
Inhibition of human MMPs by mercaptosulfide MMP inhibitors

Inhibitor	K_i^{app}								
	Shallow		Deep			Intermediate			
	MMP-1	MMP-7	MMP-3	MMP-12	MMP-14	MMP-2	MMP-8	MMP-9	MMP-26
	nM			*nM*				*nM*	
MAG-181	680	710	2500	1,300	259	85	4.1	44	81
MAG-182	49	40	470	130	24	1.1	0.89	0.57	17
YHJ-72	$>12 \times 10^3$	5,500	150	130	380	930	530	180	160
YHJ-73	$>12 \times 10^3$	1,000	100	13	16	20	70	8.6	28
YHJ-294–1	5,200	3,500	$>40 \times 10^3$	16,000	3,000	430	130	550	450
YHJ-294–2	100	26	360	93	13	6.1	1.2	1.2	2.8
YHJ-74		3600	270	117	20	88	300	220	82
YHJ-75	2400	300	21	5.6	3.7	6.9	44	3.0	8.6

ate-sized pocket, which is neither deep nor shallow. An enzyme with a shallow pocket prefers large, aliphatic residues in the P_1' position, such as Leu and Met (24–25). The remainder of the MMPs can accommodate larger amino acid derivatives, such as homophenylalanine, in the P_1' position (26).

MMP-26, composed of 261 amino acid residues and lacking a hemopexin-like domain, represents the smallest member of the MMP family. The primary structure of MMP-26 can be divided into three regions that include a signal peptide, a propeptide domain, and a catalytic domain. MMP-26 identification, ex-

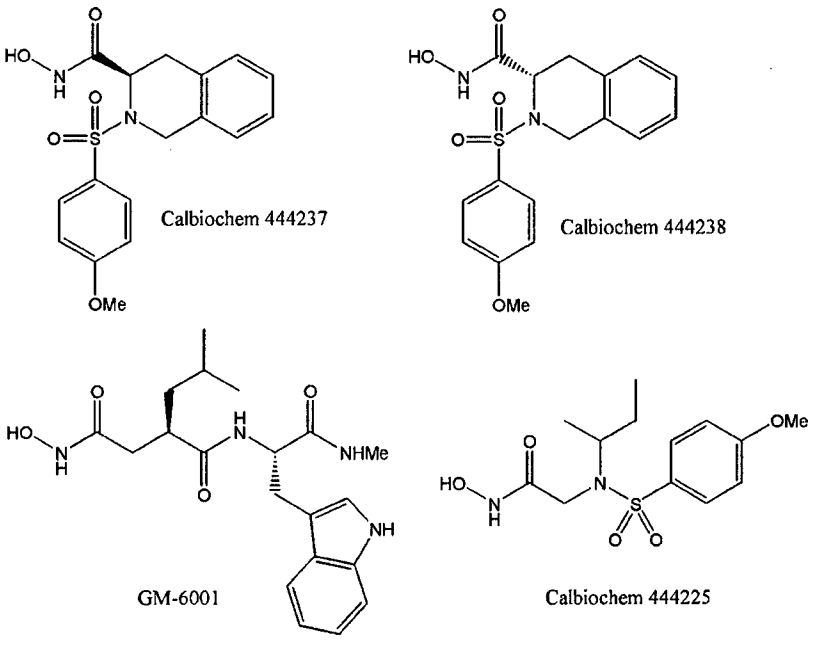

FIG. 2. **Structures of commercially available hydroxamate MMP inhibitors.** Calbiochem 444237, 444238, and 444225 are three known inhibitors of deep S_1' pocket MMPs.

TABLE II
Inhibition of MMP-26, MMP-7, and MMP-12 by hydroxamate MMP inhibitors

Inhibitor	K_i^{app}		
	MMP-26	MMP-7	MMP-12
		nM	
GM6001	0.36[a]	3.7	3.6
444237	1.5[a]	225	0.20
444238	60[a]	5.7×10^3	36
444225	43	2100	3.4

[a] Values from Ref. 11.

```
Shallow S1' Pocket MMPs
      203                                   235
MMP-1   HRVAAHELGH SLGLSHSTDI GALMYPSYTFSGD
MMP-7   LYAATHELGH SLGMGHSSDP NAVMYPTYGNGDP

Deep S1' Pocket MMPs
MMP-3   FLVAAHEIGH SLGLFHSANT EALMYPLYHSLTD
MMP-12  FLTAVHEIGH SLGLGHSSDP KAVMFPTYKYVDI
MMP-14  FLVAVHELGH ALGLEHSSDP SAIMAPFYQWMDT

Intermediate S1' Pocket MMPs
MMP-2   FLVAAHEFGH AMGLEHSQDP GALMAPIYTYTKN
MMP-8   FLVAAHEFGH SLGLAHSSDP GALMYPNYAFRET
MMP-9   FLVAAHEFGH ALGLDHSSVP EALMYPMYRFTEG
MMP-26  FLVATHEIGH SLGLQHSGNQ SSIMYPTYWYHDP
```

FIG. 3. **The sequence alignment of eight MMPs.** The alignment was determined using the Genetic Computer Group (Wisconsin Package, version 10, Madison, WI, 2002) program PILEUP with a default gap weight of 8 and a gap length weight of 2 based on the full protein sequences without propeptide regions. *Boldface* amino acid residues form the S_1' pocket. *Italicized* sequences are metal binding consensus sequences. *Underlined* residues may determine S_1' pocket characteristics. To align MMP-2 and MMP-9, the 183-residue insert of fibronectin type II-like modules were deleted before the alignment. The residue numbering system is based on the sequence of MMP-26 (4).

pression, and substrate specificity have been explored by several groups (4–11). However, the S_1' pocket characteristics of MMP-26 are unknown because of the absence of an MMP-26 x-ray crystallographic structure. Therefore, in this study we have utilized previously characterized and newly developed mercaptosulfide MMPIs (27–29) together with protein sequence analyses and molecular modeling to understand the S_1' pocket characteristics of MMP-26.

EXPERIMENTAL PROCEDURES

Materials—The fluorescent peptide substrates for MMPs used in this study were purchased from Bachem Chemical Co. The metal salts and Brij-35 were purchased from Fisher Scientific Inc. The hydroxamate MMPIs 444237, 444238, 444225, and GM6001 were purchased from Calbiochem. All other chemicals were purchased from Sigma.

The mercaptosulfide inhibitors were prepared and characterized as previously described (27–29). *cis*-1-Acetylthio-2-*tert*-butoxycarbonylthiocyclopentane and *cis*-3-acetylthio-4-*tert*-butoxycarbonylthio-*N*-*tert*-butoxycarbonylpyrrolidine were synthesized (29) and *S*-alkylated with (2*S*)-2-bromo-4-methylpentanoic acid or (2*S*)-2-bromo-4-phenylbutanoic acid; the latter bromoacids were derived from L-leucine and L-homophenylalanine, respectively (27). Subsequent coupling with L-PheNHMe or L-leucine-*p*-methoxyanilide (27) afforded the *S*-Boc and *N*-Boc protected inhibitors as mixtures of two diastereomers. The *N*-Boc group was selectively removed and replaced by the other acyl groups (29). The diastereomers were separated by flash chromatography on silica gel or by reverse-phase preparative high performance liquid chromatography on a C18 column. The slower-eluting *S*-Boc protected diastereomer exhibited the more potent MMP inhibition in each case. Its stereochemistry was assigned by ^{1}H NMR NOE analysis (MAG-182), x-ray crystallography (YHJ-294-2) (29), or by analogy. Finally, the *S*-Boc protecting groups were removed by brief treatment with 2 *N* HCl in acetic acid and the mercaptosulfide inhibitors were isolated by lyophilization of the reaction mixture.

MAG-181: m.p. 174–176 °C; $[\alpha]^{25}_D$ + 11.2° (*c* = 0.4, MeOH); analysis (CHNS). *S*-Boc derivative: m.p. 118–119 °C; $[\alpha]^{25}_D$ + 33.5° (*c* = 0.49, MeOH); analysis (CHNS).

MAG-182: m.p. 173–174 °C; $[\alpha]^{25}_D$ + 98.6° (*c* = 0.45, MeOH); analysis (CHNS). *S*-Boc derivative: m.p. 159–160 °C; $[\alpha]^{25}_D$ + 63.4 (*c* = 0.52, MeOH); analysis (CHNS).

YHJ-72: m.p. 136–137 °C; $[\alpha]^{20}_D$ − 67.9° (*c* = 0.14, $CHCl_3$); analysis (CHNS). *S*-Boc derivative: m.p. 94–95 °C; $[\alpha]^{25}_D$ +0.4° (*c* = 0.24, $CHCl_3$); analysis (CHNS).

YHJ-73: m.p. 145–146 °C; $[\alpha]^{20}_D$ − 0.7° (*c* = 0.14, $CHCl_3$); analysis (CHNS). *S*-Boc derivative: m.p. 126–127 °C; $[\alpha]^{25}_D$ − 8.8° (*c* = 0.25, $CHCl_3$); HRMS.

YHJ-294-1: m.p. 98–100 °C; $[\alpha]^{20}_D$ + 54.4° (*c* = 0.50, MeOH); analysis (CHNS). *S*-Boc derivative: m.p. 123–124 °C; $[\alpha]^{20}_D$ + 11.5° (*c* = 0.55, MeOH); analysis (CHNS).

YHJ-294-2: m.p. 128–130 °C; $[\alpha]^{20}_D$ + 38.5° (*c* = 0.40, MeOH); analysis (CHNS). *S*-Boc derivative: m.p. 173–175 °C; $[\alpha]^{20}_D$ + 82.6° (*c* = 0.50, MeOH); analysis (CHNS).

YHJ-74: m.p. 174–175 °C; $[\alpha]^{20}_D$ + 2.4° (*c* = 0.50, $CDCl_3$); HRMS. *S*-Boc derivative: m.p. 112–113 °C; $[\alpha]^{20}_D$ − 42.1° (*c* = 0.24, $CHCl_3$); analysis (CHNS).

YHJ-75: m.p. 105–106 °C; $[\alpha]^{20}_D$ − 35.4° (*c* = 0.24, $CHCl_3$); analysis (CHNS). *S*-Boc derivative: m.p. 171–172 °C; $[\alpha]^{20}_D$ + 17.2° (*c* = 0.25, $CHCl_3$); HRMS.

Enzyme Preparation and Folding of the Denatured Protein—MMP-7/matrilysin, MMP-3/stromelysin-1 (30), and MMP-12/metalloelastase (4) were kindly provided by Dr. Harold E. van Wart (Roche Diagnostics),

Professor L. Jack Windsor (Indiana University), and Dr. C. Bruun Schiødt (OsteoPro A/S), respectively. MMP-1/human fibroblast collagenase, MMP-2/human fibroblast gelatinase, MMP-8/human neutrophil collagenase, and MMP-9/human neutrophil gelatinase were described previously (30, 31). The catalytic domain of MT1-MMP/MMP-14 was provided by Professor Harald Tschesche (Bielefeld University) (32). MMP-26 was prepared as described previously (4, 11). Briefly, MMP-26 was expressed as inclusion bodies from a transformed BL-21 DE3 strain. After bacterial insoluble body preparation with B-Per™ reagent, the isolated insoluble protein was folded by following the procedures previously outlined (4–11). The total MMP-26 concentration was measured by UV absorption and calculated with the molar extinction coefficient $\epsilon_{280} = 57130\ M^{-1}\ cm^{-1}$. The active concentration of MMP-26 was determined by titration with GM6001, a tight-binding inhibitor, as described previously (11).

Kinetic Assays and Inhibition of Endometase—The substrate Mca-PLGLDpaAR-NH_2 was used to measure inhibition constants (11, 33). Enzymatic assays were performed at 25 °C in 50 mM HEPES buffer at pH 7.5 in the presence of 10 mM $CaCl_2$, 0.2 M NaCl, and 0.01 or 0.05% Brij-35 with substrate concentrations of 1 μM. The release of product was monitored by measuring fluorescence (excitation and emission wavelengths of 328 and 393 nm, respectively) with a PerkinElmer luminescence spectrophotometer LS 50B connected to a temperature controlled water bath. All stock solutions of inhibitors were in methanol. For inhibition assays, 10 μl of inhibitor stock solution, 176 μl of assay buffer, and 10 μl of enzyme stock solution were mixed and incubated for 30 to 60 min prior to initiation of the assay, which was accomplished by adding and mixing 4 μl of the substrate stock solution. Enzyme concentrations ranged from 0.2 to 7 nM during the assay. Apparent inhibition constant (K_i^{app}) values were calculated by fitting the kinetic data to the Morrison equation for tight-binding inhibitors (34, 35), where v_i and v_0 are the initial rates with and without inhibitor, respectively, and $[E]_o$ and $[I]_o$ are the initial (total) enzyme and inhibitor concentrations, respectively.

$$\frac{v_i}{v_o} = \frac{[E]_o - [I]_o - K_i^{app} + \sqrt{([I]_o + K_i^{app} - [E]_o)^2 + 4[E]_o K_i^{app}}}{2[E]_o} \quad \text{(Eq. 1)}$$

Determination of Mercaptosulfide Inhibitor Concentration—The active inhibitor concentrations were estimated by titrating the mercapto group with 5,5′-dithiobis(2-nitrobenzoic acid) (Ellman's reagent) as described previously (36, 37). Briefly, the reaction of 5,5′-dithiobis(2-nitrobenzoic acid) with the mercapto group produces 2-nitro-5-thiobenzoic acid. The concentration of 2-nitro-5-thiobenzoic acid is then measured by monitoring the absorbance at 412 nm. Cysteine was used to generate the standard curve with a molar extinction coefficient of $14{,}000 \pm 500\ M^{-1}\ cm^{-1}$, which is close to the value in the literature (37).

Computational Protein Sequence Analyses and Homology Modeling Structure of MMP-26—The sequence alignment of MMP catalytic domains was performed by the PILEUP program in Genetics Computer Group (GCG) software (Wisconsin Package version 10), with a default gap weight of 8 and gap length weight of 2. To align MMP-2 and -9, the 183-residue inserts of fibronectin type II-like modules were deleted before the alignment. The homology modeling structure of the MMP-26 catalytic domain was constructed using the Swiss Model program (38–40) with the crystal structure of the MMP-12-inhibitor complex (Protein Data Bank number 1JK3) (17) as a template. The mercaptosulfide inhibitors were computationally docked into the active site of MMP-26 with MacroModel version 7.2 (41, 42). Global minimization calculations were performed by the Monte Carlo molecular mechanical minimization method (43) with the Amber force field modified to include parameters for zinc and calcium. Residues within 7 Å of the inhibitor were included in the minimizations. All modeling was performed using the continuum solvent model. The crystallographic structures of MMP-1 (Protein Data Bank number 1HFC) (44), MMP-7 (Protein Data Bank number 1MMQ) (16), MMP-8 (Protein Data Bank number 1BZS) (45), MMP-12 (Protein Data Bank number 1JK3) (17), and MMP-14 (Protein Data Bank number 1BUV) (21) were used for comparison of the S_1' pocket.

RESULTS

Inhibition of MMPs with Mercaptosulfide MMPIs—An inhibitor set consisting of eight mercaptosulfide inhibitors was chosen to evaluate the S_1' pocket of MMP-26 (Fig. 1). These inhibitors contain P_1' and P_2' residues and have a mercapto and a sulfide group as a possible bidentate metal-binding moiety. The inhibitors contain a Leu side chain (MAG-181 and -182 and YHJ-294-1 and -2) or a Homophe side chain (YHJ-72, -73, -74, and -75) at the P_1' site. These inhibitors were tested against MMPs with known pocket characteristics (MMP-1–3, -7–9, -12, and -14). The inhibition potency of this class of inhibitors for the MMPs is significantly enhanced with a *β-H* configuration at the five-membered ring containing the mercapto and sulfide groups. The inhibitors with a Leu side chain are more potent against the shallow pocket MMPs, MMP-1/human fibroblast collagenase, and MMP-7/matrilysin than those with a Homophe side chain. Inhibitors with a Homophe side chain (YHJ-72, -73, 74, and -75) were more potent against the known deep-pocket MMPs such as MMP-3, -12, and -14 than those

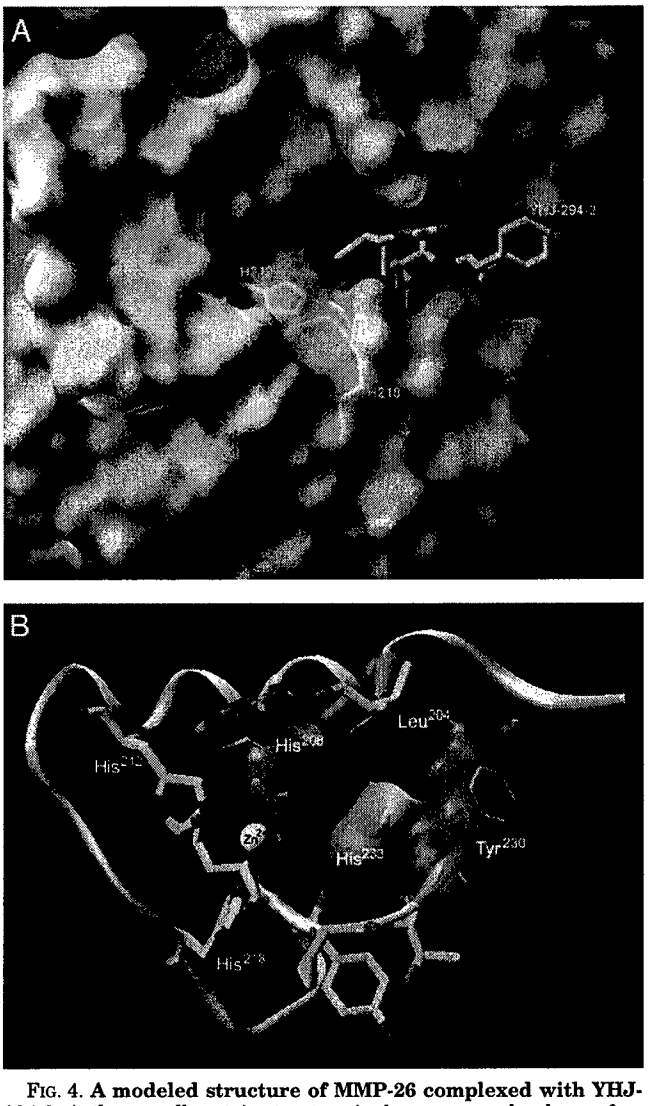

FIG. 4. **A modeled structure of MMP-26 complexed with YHJ-294-2.** *A*, the overall protein structure is shown as a molecular surface and the residues coordinating the catalytic Zn(II) (*magenta sphere*) are represented as *brown sticks* (His-208, His-212, and His-218). The inhibitor YHJ-294-2 is represented as a tube with atoms colored as follows: *green*, carbon; *red*, oxygen; *blue*, nitrogen; and *yellow*, sulfur. *B*, a close-up view of the S_1' pocket reveals that Leu-204, His-208, and Tyr-230 may be involved in formation of the pocket walls represented as *pink* molecular surfaces. The depth of the pocket may be limited by His-233 (*light blue* molecular surface). The three His residues coordinating the Zn(II) (*blue sphere*) are represented by tubes colored as described in *A*. The homology-modeled structure of MMP-26 was generated with the Swiss Model program (38–40) using the x-ray crystallographic structure of a cd-MMP-12-inhibitor complex as a template (Protein Data Bank code 1JK3) (17). The resulting MMP-26 structure was docked with YHJ-294-2 and energy-minimized as described under "Experimental Procedures."

FIG. 5. **The x-ray crystallographic structure MMP-8 (Protein Data Bank number 1BZS) (45) and homology modeled MMP-26 structure are shown after superimposition of zinc (*black sphere*) and histidine N ligands with MacroModel version 7.2.** The proteins are represented by a *flat ribbon* (MMP26) or by a *line ribbon* (MMP-8). Arg-233 and His-233 from MMP-8 and -26, respectively, may limit the depth of the S_1' pocket and are represented by *gray* and *black sticks*.

with Leu side chain. The inhibitors with the Leu side chain at the P_1' site (MAG-182 and YHJ-294-2) inhibit MMP-7 (40 and 26 nM, respectively) and MMP-12 (130 and 93 nM, respectively) without significant differences in K_i^{app} values. However, the presence of Homophe at the P_1' site dramatically distinguishes MMP-12 from MMP-7. YHJ-73 efficiently inhibits MMP-12 (13 nM), however, the potency is decreased to 1 μM against MMP-7. This trend is also displayed by YHJ-75, which has a high nM K_i^{app} value against MMP-7 (300 nM) but retains potency against MMP-12 (5.6 nM). This dramatic change of potency because of changes in the P_1' site of the inhibitors is consistently observed with the remaining shallow- and deep-pocket MMPs.

MMPs with an intermediate pocket can also accommodate the Homophe at the P_1' residue. However, the difference in inhibitor potency observed with Leu or Homophe at the P_1' residue is not as remarkable as that in the shallow- and deep-pocket MMPs. Inhibitors containing Leu at the P_1' site (MAG-182 and YHJ-294-2) are only slightly more potent against MMP-2 and MMP-9 than inhibitors with Homophe (YHJ-73 and -75). These Homophe inhibitors are still potent against MMP-8 with K_i^{app} values in the low nanomolar range. In general, these results indicate that mercaptosulfide inhibitors are suitable for characterizing the S_1' pocket of MMPs.

Characteristics of the S_1' Pocket of MMP-26 as Probed by Mercaptosulfide MMPIs—Inhibition constants for the inhibitors in Fig. 1 were measured with MMP-26 (Table I). YHJ-294-2 is the most potent inhibitor of MMP-26 among the mercaptosulfide inhibitors tested, with a K_i^{app} value of 2.8 nM. MMP-26 also favors the β-*H* configuration at the cyclopentyl or pyrrolidine ring moiety in the inhibitor. Addition of the urea-substituted pyrrolidine ring in place of the cyclopentyl ring (YHJ-294-1 and -2; YHJ-74 and -75) enhances the stereoselectivity for the β-*H* configuration. Importantly, MMP-26 prefers Leu over Homophe at the S_1' site, similar to the intermediate pocket MMPs, MMP-2, -8, and -9.

Characterization of MMP-26 S_1' Pocket Using Commercial Hydroxamate MMPIs—The S_1' site of MMP-26 was further investigated with commercially available inhibitors (Fig. 2). MMP-7/matrilysin was selected as a representative member of the shallow S_1' pocket MMPs and MMP-12/metalloelastase as one of the deep S_1' pocket MMPs for comparison purposes. The K_i^{app} values of the inhibitors with MMP-7, MMP-12, and MMP-26 are summarized in Table II. GM6001 is a broad-spectrum and potent inhibitor of MMPs (K_i^{app} = 0.4 nM for MMP-1, 0.5 nM for MMP-2, 27 nM for MMP-3, 0.1 nM for MMP-8, and 0.2 nM for MMP-9) (46). It is also the most potent synthetic MMP-26 inhibitor tested, with a K_i^{app} value of 0.36 nM. It contains a Leu residue at the P_1' site, and inhibits MMP-7 (3.7 nM) and MMP-12 (3.6 nM) with similar K_i^{app} values as observed in the mercaptosulfide inhibitors with a Leu side chain at the P_1' site. The potent inhibitor 444237 of deep S_1' pocket MMPs and its less potent stereoisomer 444238 were designed for human MMP-8 (IC_{50} = 4 nM and 1 μM, respectively; 45). Inhibitor 444225 was designed to be a potent deep S_1' pocket inhibitor of MMP-3 (K_i = 130 nM; 47). The 4-methoxybenzenesulfonyl group of these inhibitors binds at the deep S_1' pocket according to the crystallographic structure (45) and the structure-activity relationship of several derivatives (47). They inhibit MMP-7 and MMP-12 with at least 150-fold lower K_i^{app} values for MMP-12 than MMP-7. These deep S_1' pocket inhibitors effectively inhibited MMP-26 with at least 90-fold lower K_i^{app} values than those of MMP-7, but were more potent against MMP-12. These results are consistent with MMP-26 having an intermediate S_1' pocket.

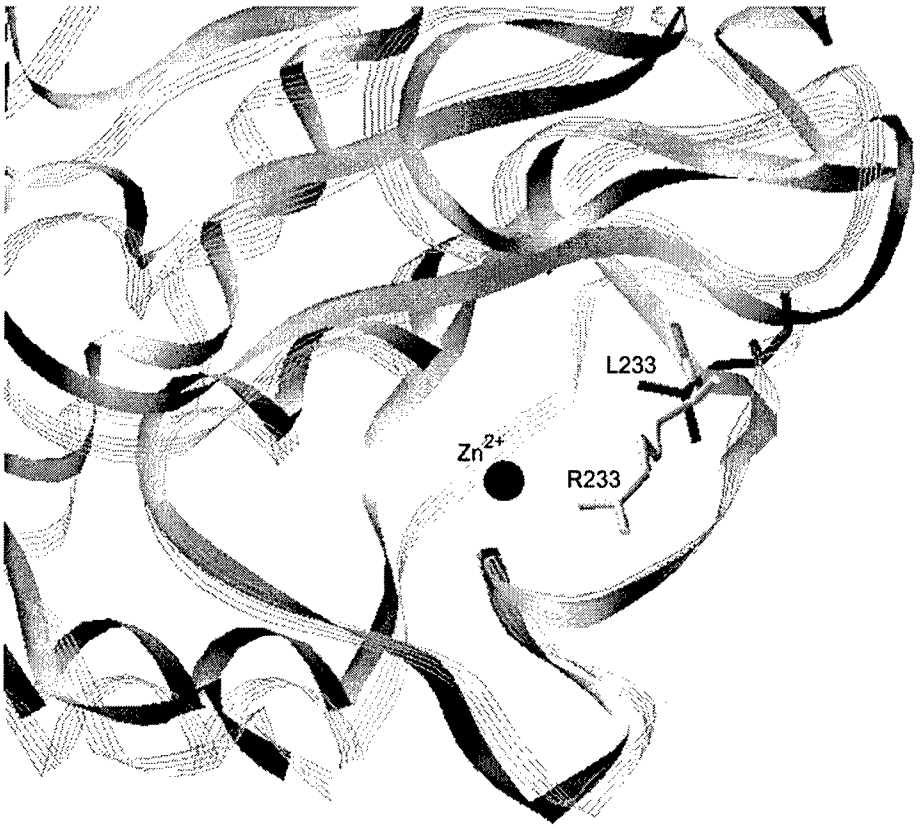

FIG. 6. **The x-ray crystallographic structures MMP-3 (Protein Data Bank number 1CIZ) (48) and MMP-8 (Protein Data Bank number 1BZS) (45) are shown after superimposition of zinc (*black sphere*) and histidine N ligands with MacroModel version 7.2.** The proteins are represented by a *flat ribbon* (MMP-8) or by a *line ribbon* (MMP-3). The Arg-233 in MMP-8 limits the depth of the S_1' pocket that is not restricted in MMP-3 by Leu-233.

Sequence Alignment and Homology Modeling Structure of MMP-26—The folding topology and patterns of all MMP catalytic domains are quite similar (19). Thus, homology modeling and protein sequence alignment may be useful tools to predict key residues involved in forming the S_1' pocket of MMP-26. Protein sequence alignment in Fig. 3 reveals a plausible explanation for residues participating in the formation of the S_1' pocket of MMP-26. According to the alignment, Leu-204, His-208, and Tyr-230 may be key residues in forming the S_1' pocket of MMP-26. To evaluate the prediction from the alignment, a homology modeled structure of the MMP-26 catalytic domain was constructed using the Swiss Model program (38–40) and the crystal structure of the MMP-12-inhibitor complex (Protein Data Bank number 1JK3) (17) as a template. The mercaptosulfide inhibitors were docked into the modeled MMP-26 structure using MacroModel version 7.2. The docked structures were further energy minimized as described under "Experimental Procedures." The overall MMP-26 structure complexed with YHJ-294-2 is shown in Fig. 4*A*. Consistent with other MMP family members (19), the non-primed (left) side of the MMP-26 active site is relatively flat. The primed (right) side extends deeper into the surface and the well defined S_1' pocket is clearly visible. The pocket that is formed by Leu-204, His-208, and Tyr-230 is illustrated in Fig. 4*B*. Interestingly, the depth of the pocket may be limited by His-233, consistent with the intermediate size prediction.

DISCUSSION

The inhibition characteristics of MMP-26 with mercaptosulfide inhibitors (Table I) and hydroxamate inhibitors (Table II) indicate that MMP-26 does not have a shallow S_1' pocket. According to the protein sequence alignment in Fig. 3 and the crystallographic structures of MMP-7 (16) and MMP-1 (13), Leu-204 in MMP-26 is substituted for Tyr and Arg at the equivalent position in MMP-7 and MMP-1, respectively. The side chains of Tyr and Arg terminate the S_1' pockets in these shallow-pocket MMPs. In the structure of MMP-26 (Fig. 4*B*), the side chain of Leu-204 forms the top wall of the S_1' pocket as found in most MMPs. Thus, MMP-26 appears to satisfy the requirement for a deep-pocket MMP. However, the inhibition profile of MMP-26 indicates a difference in the S_1' pocket of MMP-26 from those of other deep-pocket MMPs. The inhibitors with Homophe at the S_1' site (YHJ-73 and -75) do not show better potency than those with Leu (MAG-182 and YHJ-294-2). For the deep-pocket MMPs, the inhibition constants are consistently lower for the Homophe inhibitors than Leu inhibitors. The inhibition profile of MMP-26 with mercaptosulfide inhibitors is more similar to intermediate-pocket MMPs (MMP-2, -8, and -9) than deep-pocket MMPs (MMP-3, -12, and -14). These results suggest that MMP-26 may possess an intermediate pocket similar to those of MMP-2, MMP-8, and MMP-9.

A structural comparison of MMP-26 with MMP-8 further supports the similarity between the S_1' pockets of these two enzymes. The overlapping structures of MMP-8 (Protein Data Bank number 1BZS) (45) and MMP-26 at the S_1' pocket are displayed in Fig. 5. In MMP-8, it is known that the depth of the S_1' pocket is restricted by the Arg-233 side chain projecting toward the catalytic Zn(II) (14). In MMP-26, His-233 is present in place of Arg-233, which may restrict the depth of the pocket in a similar fashion, rendering the S_1' pocket to an intermediate size.

Based on the findings provided in this study and x-ray crystallographic structures of MMPs, the residue at the position

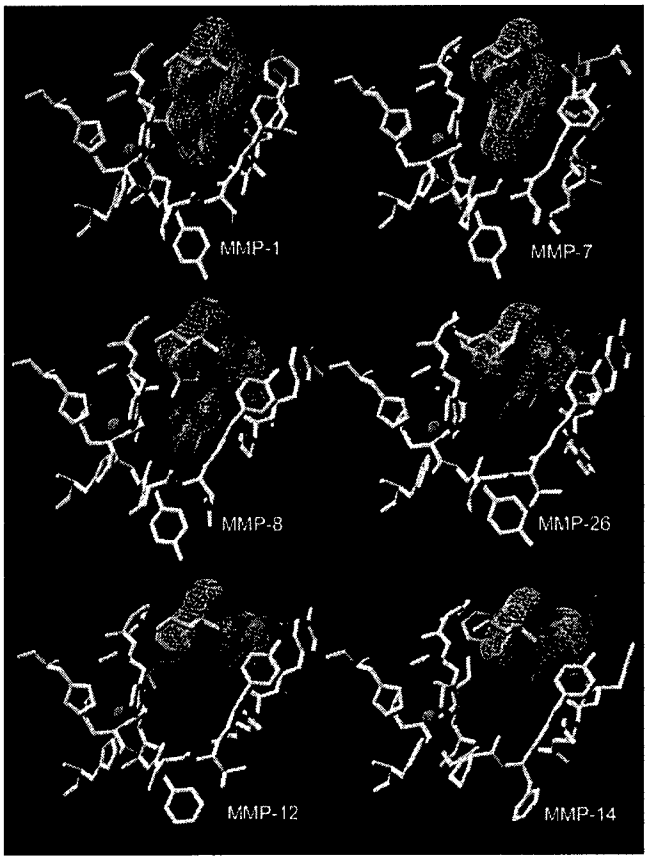

FIG. 7. **The residues forming the S_1' pocket of each enzyme are shown after superimposition of zinc (*magenta sphere*) and histidine N ligands with MacroModel version 7.2.** Inhibitors were removed from the x-ray crystallographic structures with Protein Data Bank accession numbers 1HFC (MMP-1) (44), 1MMQ (MMP-7) (16), 1BZS (MMP-8) (45), 1JK3 (MMP-12) (17), and 1BUV (MMP-14) (21). The MMP-26 structure is a homology model obtained as described under "Experimental Procedures." The key residue 204 that distinguishes a shallow pocket (MMP-1 and -7) is represented by a *yellow* molecular surface. Residue 233 may discriminate between the intermediate (MMP-8 and -26) and deep (MMP-12 and -14) pocket sizes and is represented by a *pink* molecular surface.

equivalent to His-233 of MMP-26 may play a key role in the determination of a deep or intermediate S_1' pocket. The sequence analyses (Fig. 3) showed that the residue at position 233 is hydrophobic in MMPs with deep S_1' pockets and hydrophilic in MMPs with intermediate pockets. The loop containing residue 233 may have a different orientation depending on the hydrophobicity of the side chain. The superimposed x-ray crystallographic structures of MMP-8 (Protein Data Bank number 1BZS) (45) and MMP-3 (Protein Data Bank number 1CIZ) (48) in Fig. 6 reveals this type of structural difference between an intermediate-pocket MMP (MMP-8) and a deep-pocket MMP (MMP-3). These investigations suggest that it is possible to predict the S_1' pocket properties by sequence analyses of the key residues at the Leu-204 and His-233 equivalent positions in other MMPs.

MMPs can be divided into three groups based on the characteristics of their S_1' pockets: shallow-, intermediate-, and deep-pocket MMPs (Fig. 7). Enzyme inhibition kinetic studies using MMPIs in combination with protein sequence analysis and homology modeling reveal that MMP-26 has an intermediate S_1' pocket. Our data may provide important mechanistic and structural information to design MMP-26-specific inhibitors. As the need for innovations and new strategies for MMP inhibition in cancer and inflammation is increasing (49, 50), this study may shed light on the molecular mechanisms by which highly selective and specific inhibitors targeting an individual MMP or subgroups of MMPs may be rationally designed and developed.

Acknowledgments—We thank Sara C. Monroe, Shelbourn Kent, and Katherine E. Berry for excellent assistance with the inhibitor testing, Dr. Mohammad A. Ghaffari for the synthesis of MAG-181 and MAG-182, and Robert Newcomer and Professor Jerzy R. Cioslowski for critical review of the manuscript.

REFERENCES

1. Brinckerhoff, C. E., and Matrisian, L. M. (2002) *Nat. Rev. Mol. Cell. Biol.* **3,** 207–214
2. Egeblad, M., and Werb, Z. (2002) *Nat. Rev. Cancer* **2,** 163–175
3. Overall, C. M. (2002) *Mol. Biotech.* **22,** 51–86
4. Park, H. I., Ni, J., Gerkema, F. E., Liu, D., Belozerov, V. E., and Sang, Q.-X. (2000) *J. Biol. Chem.* **275,** 20540–20544
5. Uría, J. A., and López-Otín, C. (2000) *Cancer Res.* **60,** 4745–4751
6. De Coginac, A. B., Elson, G., Delneste, Y., Magistrelli, G., Jeannin, P., Aubry, J.-P., Berthier, O., Schmitt, D., Bonnefoy, J.-Y., and Gauchat, J.-F. (2000) *Eur. J. Biochem.* **267,** 3323–3329
7. Marchenko, G. N., Ratnikov, B. I., Rozanov, D. V., Godzik, A., Deryugina, E. I., and Strongin, A. Y. (2001) *Biochem. J.* **359,** 705–718
8. Marchenko, G. N., Marchenko, N. D., Leng, J., and Strongin, A. Y. (2002) *Biochem. J.* **363,** 253–262
9. Zhao, Y.-G., Xiao, A.-Z., Newcomer, R. G., Park, H. I., Kang, T., Chung, L. W., Swanson, M. G., Zhau, H. E., Kurhanewicz, J., and Sang, Q.-X. (2003) *J. Biol. Chem.* **278,** 15056–15064
10. Zhao, Y.-G., Xiao, A.-Z., Park, H. I., Newcomer, R. G., Yan, M., Man, Y. G., Heffelfinger, S. C., and Sang, Q.-X. (2003) *Cancer Res.*, in press
11. Park, H. I., Turk, B. E., Gerkema, F. E., Cantley, L. C., and Sang, Q.-X. (2002) *J. Biol. Chem.* **277,** 35168–35175
12. Gooley, P. R., O'Connell, J. F., Marcy, A. I., Cuba, G. C., Salowe, S. P., Bush, B. L., Hermes, J. D., Esser, N. K., Hagmann, W. K., Springer, J. P., and Johnson, B. A. (1994) *Nat. Struct. Biol.* **1,** 111–118
13. Lovejoy, B., Cleasby, A., Hassell, A. M., Longley, K., Luther, M. A., Weigl, D., McGeehan, G., McElroy, A. B. Drewry, D., Lambert, M. H., and Jordon, S. R. (1994) *Science* **263,** 375–377
14. Bode, W., Reinemer, P., Huber, R., Kleine, T., Schnierer, S., and Tschesche, H. (1994) *EMBO J.* **13,** 1263–1269
15. Stams, T., Spurlino, J. C., Smith, D. L., Wahl, R. C., Ho, T. F., Qoronfleh, M. W., Banks, T. M., and Rubin, B. (1994) *Nat. Struct. Biol.* **1,** 119–123
16. Browner, M. F., Smith, W. W., and Castelhano, A. L. (1995) *Biochemistry* **34,** 6602–6610
17. Lang, R., Kocourek, A., Braun, M., Tschesche, H., Huber, R., Bode, W., and Maskos, K. (2001) *J. Mol. Biol.* **312,** 731–742
18. Nar, H., Werle, K., Bauer, M. M., Dollinger, H., and Jung, B. (2001) *J. Mol. Biol.* **312,** 743–751
19. Bode, W., Fernandez-Catalan, C., Tschesche, H., Grams, F., Nagase, H., and Maskos, K. (1999) *Cell. Mol. Life Sci.* **55,** 639–652
20. Nagase, H. (2001) in *Matrix Metalloproteinase Inhibitors in Cancer Therapy* (Clendeninn, N. J., and Appelt, K., eds) pp. 39–66, Humana Press, Totowa, NJ
21. Fernandez-Catalan, C., Bode, W., Huber, R., Turk, D., Calvete, J. J., Lichte, A., Tschesche, H., and Maskos, K. (1998) *EMBO J.* **17,** 5238–5248
22. Morgunova, E., Tuuttila, A., Bergmann, U., and Tryggvason, K. (2002) *Proc. Natl. Acad. Sci. U. S. A.* **99,** 7414–7419
23. Rowsell, S., Hawtin, P., Minshull, C. A., Jepson, H., Brockbank, S. M. V., Barratt, D. G., Slater, A. M., McPheat, W. L., Walterson, D., Henney, A. M., and Pauptit, R. A. (2002) *J. Mol. Biol.* **319,** 173–181
24. Netzel-Arnett, S., Sang, Q.-X., Moore, W. G. I., Narve, M., Birkedal-Hansen, H., and Van Wart, H. E. (1993) *Biochemistry* **32,** 6427–6432
25. Nagase, H., Fields, C. G., and Fields, G. B. (1994) *J. Biol. Chem.* **269,** 20952–20957
26. Mucha, A., Cuniasse, P., Kannan, R., Beau, F., Yiotakis, A., Basset, P., and Dive, V. (1998) *J. Biol. Chem.* **273,** 2763–2768
27. Schwartz, M. A., and Van Wart, H. E. (October 3, 1995) U. S. Patent 5455262
28. Sang, Q.-X., Jia, M. C., Schwartz, M. A., Jaye, M. C., Kleinman, H. K., Ghaffari, M. A., and Luo, Y. L. (2000) *Biochem. Biophys. Res. Commun.* **274,** 780–786
29. Jin, Y., Ghaffari, M. A., and Schwartz, M. A. (2002) *Tetrahedron Lett.* **43,** 7319–7321
30. Sang, Q.-X., Birkedal-Hansen, H., and Van Wart, H. E. (1995) *Biochim. Biophys. Acta* **1251,** 99–108
31. Sang, Q. A., Bodden, M. K., and Windsor, L. J. (1996) *J. Prot. Chem.* **15,** 243–253
32. Hurst, D. R., Schwartz, M. A., Ghaffari, M. A., Jin, Y., Tschesche, H., Fields, G. B., and Sang, Q.-X. (October 8, 2003) *Biochem. J.* 10.1042/BJ20031067
33. Knight, C. G., Willenbrock, F., and Murphy, G. (1992) *FEBS Lett.* **296,** 263–266
34. Morrison, J. F. (1969) *Biochim. Biophys. Acta* **185,** 269–286
35. Copeland, R. A. (2000) *Enzymes: A Practical Introduction to Structure, Mechanism, and Data Analysis*, 2nd Ed., Wiley-VCH, Inc., New York
36. Ellman, G. L., (1959) *Arch. Biochem. Biophys.* **82,** 70–77
37. Riddles, P. W., Blakeley, R. L., and Zerner, B., (1979) *Anal. Biochem.* **94,** 75–81
38. Peitsch, M. C. (1995) *Bio/Technology* **13,** 658–660
39. Peitsch, M. C. (1996) *Biochem. Soc. Trans.* **24,** 274–279

40. Guex, N., and Peitsch, M. C. (1997) *Electrophoresis* **18,** 2714–2723
41. Bohacek, R., de Lombaert, S., McMartin, C., Priestle, J., and Grütter, M. (1996) *J. Am. Chem. Soc.* **118,** 8231–8249
42. Arighi, C. N., Rossi, J. P., and Delfino, J. M. (1998) *Biochemistry* **37,** 16802–16814
43. Chang, G., Guida, W. C., and Still, W. C. (1989) *J. Am. Chem. Soc.* **111,** 4379–4386
44. Spurlino, J. C., Smallwood, A. M., Carlton, D. D., Banks, T. M., Vavra, K. J., Johnson, J. S., Cook, E. R., Falvo, J., Wahl, R. C., Pulvino, T. A., Wendoloski, J. J., and Smith, D. L. (1994) *Proteins* **19,** 98–109
45. Matter, H., Schwab, W., Barber, D., Billen, G., Hasse, B., Neises, B., Schudok, M., Thorwart, W., Schreuder, H., Brachvogel, V., Lönze, P., and Weithmann, K. U. (1999) *J. Med. Chem.* **42,** 1908–1920
46. Galardy, R. E., Cassabonne, M. E., Giese, C., Gilbert, J. H., Lapierre, F., Lopez, H., Schaefer, M. F., Stack, R., Sullivan, M., and Summer, B. (1994) *Ann. N. Y. Acad. Sci.* **732,** 315–323
47. MacPherson, L. J., Bayburt, E. K., Capparelli, M. P., Carroll, B. J., Goldstein, R., Justice, M. R., Zhu, L., Hu, S., Melton, R. A., Fryer, L., Goldberg, R. L., Doughty, J. R., Spirito, S., Blancuzzi, V., Wilson, D., O'Byrne, E. M., Ganu, V., and Parker, D. T. (1997) *J. Med. Chem.* **40,** 2525–2532
48. Pavlovsky, A. G., Williams, M. G., Ye, Q. Z., Ortwine, D. F., Purchase, C. F., 2nd, White, A. D., Dhanaraj, V., Roth, B. D., Johnson, L. L., Hupe, D., Humblet, C., and Blundell, T. L. (1999) *Protein Sci.* **8,** 1455–1462
49. Overall, C. M., and López-Otín, C. (2002) *Nat. Rev. Cancer* **2,** 657–672
50. Coussens, L. M., Fingleton, B., and Matrisian, L. M. (2002) *Science* **295,** 2387–2392

0013-7227/03/$15.00/0
Printed in U.S.A.

Endocrinology 144(5):1656–1663

doi: 10.1210/en.2002-0157

Androgen Stimulates Matrix Metalloproteinase-2 Expression in Human Prostate Cancer

XINBO LIAO, J. BRANTLEY THRASHER, JILL PELLING, JEFFERY HOLZBEIERLEIN, QING-XIANG AMY SANG, AND BENYI LI

Departments of Urology (X.L., J.B.T., J.H., B.L.) and Pathology (J.P.), Kansas Cancer Institute, University of Kansas Medical Center, Kansas City, Kansas 66160; and Department of Chemistry and Biochemistry (Q.-X.A.S.), Florida State University, Tallahassee, Florida 32306

Prostate growth and differentiation is androgen dependent, and increased expression of matrix metalloproteinase 2 (MMP-2) has been found in more aggressive prostate cancers. As part of our efforts to elucidate the mechanisms responsible for prostate cancer progression, we evaluated the MMP-2 expression after androgen stimulation in human prostate cancer LNCaP and LAPC-4 cells, which express a functional androgen receptor. Treatment of the cells with a synthetic androgen R1881 resulted in an increase of pro-MMP-2 expression assessed by Western blot and gelatinolytic zymography in both cell lines. R1881-stimulated pro-MMP-2 expression occurred in a dose-dependent manner, which was completely abrogated in the presence of the nonsteroid androgen antagonist bicalutamide. In accordance with the protein expression, MMP-2 promoter activity was also increased by R1881 in a cell-based luciferase reporter assay. However, R1881 treatment did not significantly affect either the pro-MMP-9 expression or its promoter activity. Although we observed an appearance of active form of MMP-2, its activator MT1-MMP was not changed after R1881 treatment. Pretreatment of the cells with inhibitors of RNA transcription, actinomycin D, or protein translation, cycloheximide, significantly suppressed R1881-induced pro-MMP-2 expression in LNCaP cells, indicating that androgen stimulates pro-MMP-2 gene expression. In addition, phosphatidylinositol 3′-kinase inhibitor, LY294002 or wortmannin, strongly inhibited R1881-induced pro-MMP-2 expression. Finally, R1881-enhanced LNCaP cell migration was clearly suppressed by LY294002 or the MMP-2 inhibitor OA-Hy in an *in vitro* migration assay. In conclusion, our data demonstrated that androgen stimulates pro-MMP-2 expression in LNCaP cells via phosphatidylinositol 3′-kinase-dependent androgen receptor transactivation. (*Endocrinology* 144: 1656–1663, 2003)

PROSTATE CANCER IS the second most frequently diagnosed cancer in men after skin cancer in the United States and is second only to lung and bronchus cancer in the frequency of mortality (1). Since the seminal work of Huggins and Hodges in 1941 (2), it has been widely accepted that prostate growth and differentiation is androgen dependent. As a result of this insight, medical treatment for metastatic prostate cancer has relied heavily on androgen ablation. However, most patients treated by androgen ablation ultimately relapse to more aggressive androgen-refractory prostate cancer with no means to cure (reviewed in Ref. 3).

The matrix metalloproteinase (MMP) family is comprised of secreted and membrane-associated zinc-dependent endopeptidases that can selectively degrade extracellular matrix (ECM) protein and nonmatrix proteins. Currently, up to 25 members of the MMP family have been reported, and the broad range of their substrates conveys a pivotal role for the MMP involvement in normal physiological processes and pathological states including tumor metastasis and angiogenesis (reviewed in Ref. 4). MMP-2, also called gelatinase A, is produced as a latent form (pro-MMP-2), and the activation process is mediated at least partially by MT1-MMP on the cell surface (5). It has been shown that MMP-2 is secreted by the human prostate gland, both *in vivo* and *in vitro*, and higher expression levels of MMP-2 are associated with increasing Gleason score, tumor metastasis, and aggressive behavior of prostate cancer (Refs. 6 and 7 and reviewed in Ref. 8).

To understand the role of the androgen receptors (ARs) in prostate cancer development and progression, it is important first to determine the AR signaling cascades and the genes that are regulated by AR. In view of the evidence for the association of MMP-2 expression and prostate cancer behavior, we evaluated the expression of pro-MMP-2 after androgen treatment in human prostate cancer LNCaP and LAPC-4 cells, which express a functional AR.

Abbreviations: AR, Androgen receptor; ARE, androgen-responsive element; cFBS, charcoal-stripped FBS; CMV, cytomegalovirus; ECM, extracellular matrix; FBS, fetal bovine serum; FGF, fibroblast growth factor; MEK, MAPK and ERK kinase; MMP, matrix metalloproteinase; MMP9-LUC, human MMP-9 gene promoter-luciferase vector; PI3K, phosphatidylinositol 3′-kinase; PMA, phorbol 12-myristate 13-acetate; pro-MMP-2, latent form of MMP-2; PSA, prostate-specific antigen; SEAP, secreted alkaline phosphatase.

Materials and Methods

Cell culture and reagents

The LNCaP cell line was obtained from the American Type Culture Collection (Manassas, VA) and was maintained in a humidified atmosphere of 5% CO_2, RPMI 1640 supplemented with 10% fetal bovine serum (FBS) and antibiotics (Invitrogen, Carlsbad, CA). The LAPC-4 cells were obtained from Dr. Charles L. Sawyers (9) and maintained in Iscoves medium with 15% FBS/1% L-glutamine and antibiotics. The inhibitors of LY294002, rapamycin, PD98059, MMP-2 inhibitor I (OA-Hy), and PP2 were purchased from Calbiochem (San Diego, CA). R1881 and cycloheximide were obtained from ICN (Aurora, OH). Actinomycin D, type-1 rat-tail collagen, and wortmannin were purchased from Sigma (St. Louis, MO). Bicalutamide was a gift from AstraZeneca. Where indicated, the inhibitor was added from a 1000-fold concentrated stock in the solvent, dimethylsulfoxide, or ethanol. Control cultures received

similar amounts of the solvent only. Final concentrations of the solvent did not exceed 0.1%. The antibodies against MMP-2 and MMP-9 were purchased from Chemicon (Temecula, CA). MT1-MMP antibody was described previously (10). The antibodies against AR, prostate-specific antigen (PSA), and actin were obtained from Santa Cruz Biotechnology (Santa Cruz, CA). Charcoal-stripped FBS (cFBS) was obtained from Atlanta Biologicals (Norcross, GA). Phorbol 12-myristate 13-acetate (PMA) and fibroblast growth factor 2 (FGF-2) were obtained from Sigma.

Western blot analysis

For immunoblot analysis, cells were washed in PBS and lysed in a radioimmunoprecipitation assay buffer supplied with protease inhibitors (CytoSignal, Irvine, CA). Equal amounts of protein were separated on an 8% sodium dodecyl sulfate-polyacrylamide gel and blotted onto a polyvinyl difluoride membrane (Bio-Rad Laboratories, Inc., Hercules, CA). Membranes were blocked in a Tris-buffered saline solution with 5% nonfat dry milk and incubated with antibodies overnight at 4 C. Immunoreactive signals were detected by incubation with horseradish peroxidase-conjugated secondary antibodies (Santa Cruz Biotechnology) followed by chemiluminescent detection (SuperSignal West Dura substrate kit, Pierce Chemical Co., Rockford, IL).

Assay of gelatin-degrading MMPs by zymography

Unconcentrated conditioned media from the cell cultures were analyzed for MMP gelatinolytic activities by gelatin zymography as described previously (11). Briefly, conditioned media (mixed with 5× sample buffer) were fractionated by SDS-PAGE on a 10% gel containing 1.0 mg/ml gelatin (Sigma) under nonreducing conditions. After two washes in Tris buffer (50 mM Tris, 200 mM NaCl, 10 mM $CaCl_2$, 1 mM $ZnCl_2$, 1% Triton X-100, pH 7.5), the gel was incubated in the same buffer in the absence of Triton X-100 for 18 h at 37 C. After being stained with Coomassie Brilliant Blue R-250, the gel was destained with 10% (vol/vol) acetic acid, and the nonstaining bands resulting from digestion of the substrate by gelatinase enzymes were then visualized.

Cell migration assay

After serum starvation, the cells were trypsinized and resuspended in RPMI 1640 with 5% cFBS. A Transwell insert with 8-μM pore (Nunc, Naperville, IL) was coated with collagen (50 μg/ml in PBS) for 2 h at 37 C. A total of 1.0×10^5 cells were then seeded in the upper chambers of the Transwells. R1881 was added in both the upper and lower chambers containing RPMI 1640 supplied with 5% cFBS. Where indicated, cells were preincubated with inhibitors (5.0 μM OA-Hy or 10 μM LY294002) for 30 min at room temperature before seeding in the Transwell. Cells were incubated for 48 h, and then the chamber was disassembled. Cells on the upper surface were removed, and cells invaded to the lower surface of the filters were fixed, stained, and counted as described (12).

Luciferase and SEAP reporter assay

A luciferase reporter plasmid controlled by the 1716-bp length of the human MMP-2 promoter (MMP2-LUC) was obtained from Dr. Yi Sun (13, 14). The human MMP-9 gene promoter-luciferase vector (MMP9-LUC) was obtained from Dr. Yasuyuki Sasaguri (15). The reporter vector pCMV-SEAP, expressing secreted alkaline phosphatase (SEAP) under the control of the cytomegalovirus (CMV) promoter, was a kind gift from Dr. David Spencer (16) and was used as an internal reference control. The cells were plated in 6-well tissue culture plates and transfected the following day with 2.0 μg MMP-2 reporter construct and 0.5 μg pCMV-SEAP construct by using the Cytofectene reagent (Bio-Rad Laboratories, Inc.) according to manufacturer's protocol. After 24 h, the cells were serum starved for another 24 h and then treated with R1881 (1.0 nM) or PMA (50 μM) in 2% cFBS. After 24 h, culture supernatants were harvested and assayed for SEAP activity as described previously (17). Cells were lysed with a lysis buffer supplied by a luciferase assay system (catalog no. 4030, Promega Corp., Madison, WI). Protein concentration in the cell lysates was measured by a protein assay kit (Bio-Rad Laboratories, Inc.). An equal amount of protein from each cell lysate was assayed in triplicate for luciferase enzyme activity by using the luciferase assay system (Promega Corp.) and Lumat LB9501 reader (Berthold, Oak Ridge, TN). The luciferase activity of each sample was normalized against the corresponding SEAP activity before the fold induction value relative to control cells was calculated.

Statistical analysis

All experiments were repeated two or three times. Zymographic data and Western blot results are presented from a representative experiment. The mean and SD from two experiments for cell migration and luciferase assay are shown. The number of migrating cells in the absence of either R1881 or inhibitors is assigned a relative value of 100%. The significant differences between groups were analyzed using the SPSS computer software (SPSS, Inc., Chicago, IL).

Results

Androgen stimulates pro-MMP-2 expression

We determined the effect of androgen stimulation on MMP expression/activation in human prostate cancer LNCaP and LAPC-4 cells. The LNCaP cell line is a commonly used *in vitro* model with well-characterized features of androgen responsiveness for prostate cancer research (18). It was originally derived from a lymph node metastatic prostate cancer and secretes PSA. The LAPC-4 cell line is a recently established androgen responsive cell line (9), similar to LNCaP cells, but LAPC-4 cell harbors a wild-type *AR* gene and LNCaP cell has a mutated one. MMP activity is usually analyzed in cell culture-conditioned medium by gelatinolytic zymography (11) because most MMP family members are secreted proteases. Following serum starvation for 24 h, the cells were treated with increasing doses (0.01–10 nM) of the synthetic androgen R1881 in serum-free condition for another 24 h. The conditioned media were analyzed by gelatinolytic zymography without concentrating. Meanwhile, the cells were harvested and the cellular content of MMP-2 protein in whole-cell lysates was determined by Western blot. The conditioned media from the HT-1080 cell culture (RPMI 1640 without serum), which contains high levels of MMP-2 and -9, were used as a positive control (19).

Under serum-free condition and the solvent control, there was no detectable MMP-2 gelatinolytic activity in the conditioned media from the cell culture (Fig. 1, A and E, lanes 1 and 2). On R1881 addition, MMP gelatinolytic activity corresponding to pro-MMP-2 was gradually increased in a dose-dependent manner (lanes 3–6). Furthermore, an additional active form of MMP-2 appeared after higher doses of R1881 in LNCaP cells (1.0–10 nM in lanes 5 and 6) but not in LAPC-4 cells, which may reflect a cell-based specificity. To confirm the MMP-2 induction by R1881 stimulation, MMP-2 protein levels in the whole-cell lysates were determined by Western blot analysis. As shown in Fig. 1B, on R1881 stimulation, the cellular level of pro-MMP-2 protein was increased in a dose-dependent manner. The protein levels of pro-MMP-2 matched well with the gelatinolytic activities secreted into the conditioned media. However, MMP-9 gelatinolytic activity was not detectable under our experimental conditions (Fig. 1, A and E), which is consistent with our previous report (20). The protein level of cellular pro-MMP-9 (Fig. 1C) was unchanged by R1881 treatment. These data indicate that androgen induces pro-MMP-2 but not pro-MMP-9 expression in LNCaP and LAPC-4 cells.

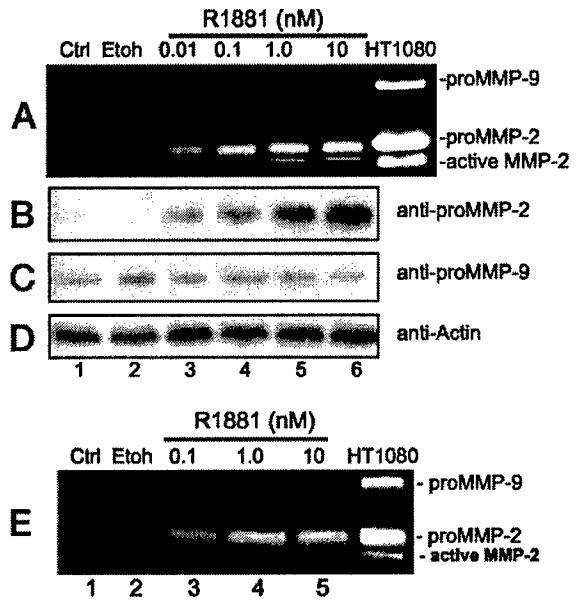

FIG. 1. R1881 stimulates pro-MMP-2 expression. Following serum starvation for 24 h, LNCaP cells were left untreated (lane 1) or treated with solvent ethanol (lane 2, Etoh), increasing dose of R1881 (lane 3–6, 0.01–10 nM) for 24 h in serum-free media. Twenty-four hours later, the MMP gelatinolytic activities secreted into media were examined by zymography (A). Conditioned media from HT1080 cell culture served as positive control. Cells were harvested and protein levels of pro-MMP-2 (B) and pro-MMP-9 (C) were determined by Western blot. Immunoblot for actin served as loading control (D). E, MMP gelatinolytic zymography was also performed using the conditioned media from LAPC-4 cell culture in the same way as used in LNCaP cells. Data represent two independent experiments. Ctrl, Control.

Androgen induction of pro-MMP-2 expression is mediated through AR transactivation

The biological effects of androgens are believed to be mediated through the intracellular AR, which is a ligand-activated transcription factor that regulates gene expression (4), although the nongenomic effect of androgens has been reported recently (Ref. 21 and reviewed in Ref. 22). Androgen action can be abolished by pretreatment of the cells with androgen antagonist bicalutamide (23). To examine whether androgen induction of pro-MMP-2 is mediated through AR transactivation, we pretreated LNCaP cells with a maximally effective dose of bicalutamide (10 μM) for 30 min followed by R1881 (1.0 nM) addition. MMP-2 protein levels in the whole-cell lysates and its gelatinolytic activity in the conditioned media were assessed 24 h later. The well-known AR target gene product PSA served as a positive control. As shown in Fig. 2A, as is the case for PSA, pretreatment with bicalutamide completely abolished androgen-induced pro-MMP-2 expression in LNCaP cells (lane 3 *vs.* lane 2). Paralleling the protein expression, androgen-induced MMP-2 gelatinolytic activity was also suppressed in the presence of bicalutamide (Fig. 2A, *zymography panel*). However, bicalutamide itself when added alone had no effect on MMP-2 expression (data not shown).

To examine whether androgen induction of pro-MMP-2 expression is mediated via AR transactivation at the gene transcription/translation level, an inhibitor for RNA transcription (actinomycin D) and an inhibitor for protein translation (cycloheximide) were used at a level of none-cytotoxic dose (1.0 μg/ml, data not shown). Similar to the effect of bicalutamide on the expression of PSA and pro-MMP-2, these two inhibitors significantly suppressed R1881-stimulated pro-MMP-2 expression (in both Western blot and zymography assays, Fig. 2A, lanes 4 and 5 *vs.* lane 2). However, addition of actinomycin D or cycloheximide did not affect AR protein levels (Fig. 2A, *AR panel,* lanes 4 and 5 *vs.* lane 2), indicating that suppression of R1881-induced pro-MMP-2 expression by the two inhibitors is not due to reduced expression of AR protein. In contrast, AR protein was slightly increased in the presence of R1881 (Fig. 2A, *AR panel,* lane 1 *vs.* lanes 2–5), which is consistent with a previous report (24). These results indicate that androgen induction of MMP-2 is due to AR-mediated gene expression (in other words, AR transactivation).

To further confirm the involvement of AR transactivation in androgen induction of pro-MMP-2, we used a luciferase reporter construct under the control of human MMP-2 promoter (1659 bp of the 5′ region on *MMP-2* gene) to define the stimulating effect of androgen on MMP-2 promoter activity (13). After transfection with the reporter constructs, LNCaP cells were serum starved for 24 h and then stimulated with R1881 (1.0 nM). Luciferase activity in the cell extracts was measured 24 h later. As shown in Fig. 2B, R1881 treatment induced about 3.5-fold increase of the luciferase activity, which was abolished by bicalutamide addition (10 μM), consistent with the results as seen in zymography and Western blot (Fig. 2A). As expected, MMP-9 promoter activity was not affected by R1881 treatment but was strongly induced by a well-known MMP-9 stimulator PMA (25). In addition, PMA suppressed the basal activity of the MMP-2 promoter by almost 50% (Fig. 2B), which is in accordance with a previous report (26). When LAPC-4 cells were used for those luciferase assays, a very similar result was also observed (Fig. 2C). These results clearly suggest that androgen-stimulated pro-MMP-2 expression is mediated through AR transactivation.

MMP-2 is produced in a latent form, which is activated by the membrane type MMP, MT1-MMP, in participation with tissue inhibitor of MMP-2 (5). Because we observed an active form of MMP-2 in gelatinolytic zymography assays when LNCaP cells were treated with higher doses of R1881 (Fig. 1A), we checked the MT1-MMP expression to rule out the possibility that MT1-MMP is activated after R1881 treatment. As expected, MT1-MMP was expressed at a relatively low level in LNCaP cells (Fig. 3), which is consistent with a previous report (27). After R1881 treatment, however, there was no significant alteration to the protein levels of either the pro-form (65 kDa) or the active form (63 kDa) of MT1-MMP (28). These results indicate that MT1-MMP is constitutively expressed in LNCaP cells, and its activity or expression level is not regulated by AR signaling. Appearance of the MMP-2 active form after R1881 treatment at higher doses might be due to increased pro-MMP-2 expression, which in turn leads to subsequent accumulation of the active form in the media.

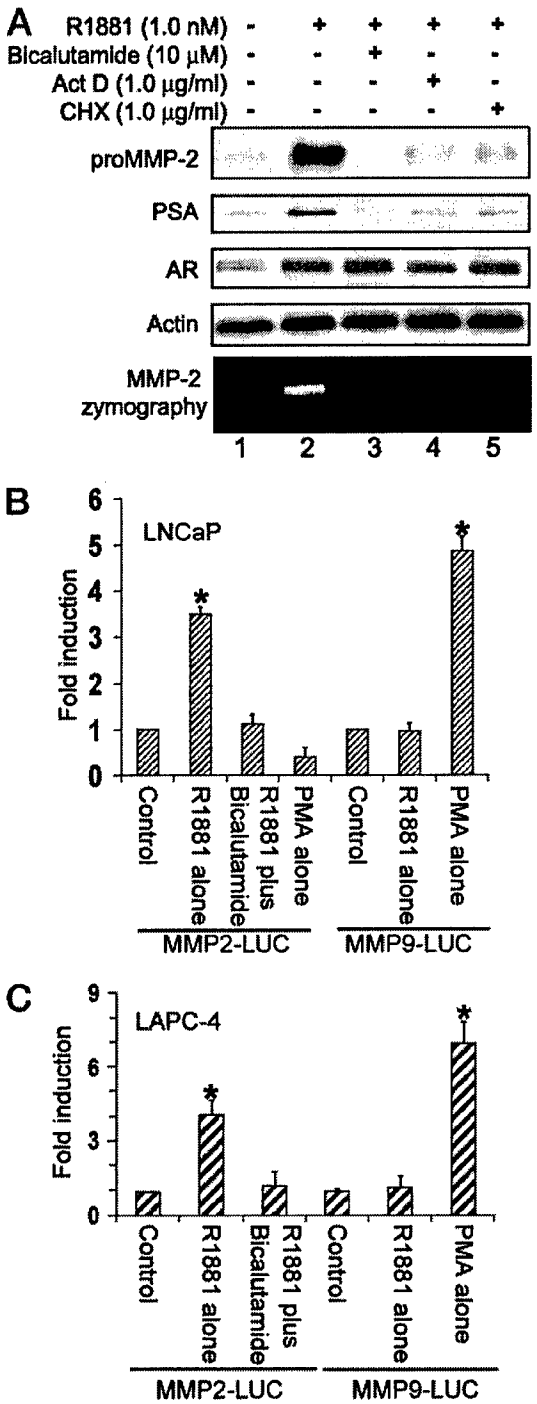

FIG. 2. A, R1881-stimulated pro-MMP-2 expression is mediated through AR transactivation. Following serum starvation for 24 h, LNCaP cells were left untreated (lane 1) or pretreated with bicalutamide (lane 3), actinomycin D (Act D, lane 4), and cycloheximide (CHX, lane 6) for 30 min followed by addition of R1881 for another 24 h in serum-free media. Expression of pro-MMP-2, PSA, AR, and actin (loading control) were determined by Western blot in whole-cell lysates. The MMP gelatinolytic activities secreted into media were examined by zymography. B and C, R1881 induced MMP-2 but not MMP-9 promoter activity. LNCaP (B) or LAPC-4 (C) cells were co-transfected with luciferase reporter constructs MMP2-LUC or MMP9-LUC together with pCMV-SEAP reporter construct overnight by using the Cytofectene reagent (Bio-Rad Laboratories, Inc.) according to the manufacturer's protocol and then serum starved for 24 h. The solvent ethanol (control), R1881 (1.0 nM), or PMA (50 μM) was added once in the culture media containing 2% cFBS for another 24 h. Luciferase or SEAP activity was measured as described in *Materials and Methods*. The luciferase activity was presented as fold induction against control sample after normalized with protein content and SEAP activity. The *asterisk* indicates a significant difference ($P < 0.05$) between R1881 or PMA stimulation *vs.* the solvent control. Data represent three independent experiments.

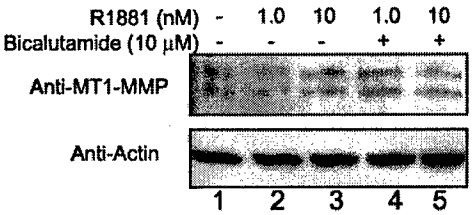

FIG. 3. MT1-MMP remains unchanged after R1881 treatment. Serum-starved LNCaP cells were either left untreated (lane 1) or pretreated with bicalutamide for 30 min (lanes 4 and 5) followed by R1881 addition (lanes 2–5) for another 24 h. MT1-MMP expression was assessed by Western blot in whole-cell lysates. Actin immunoblot served as loading control. Data represent three independent experiments.

AR-mediated pro-MMP-2 expression involves PI3K activity

To gain insights into the signal molecules involved in AR-mediated pro-MMP-2 expression in LNCaP cells, some commonly used specific inhibitors of protein kinase, including PD98059 for MEK-1, LY294002 and wortmannin for phosphatidylinositol 3′-kinase (PI3K), rapamycin for mammalian target of rapamycin, and PP2 for Src kinase, were used to block androgen induction of pro-MMP-2. The concentrations yielding maximum pharmacological effect without cytotoxicity were verified first in a cell-based survival assay (data not shown) and then used in the next experiments. Following serum starvation for 24 h, LNCaP cells were left untreated or pretreated with different kinase inhibitors for 30 min followed by addition of R1881 (1.0 nM) for another 24 h in serum-free media. The MMP gelatinolytic activities secreted into the media were examined by zymography. As shown in Fig. 4A, among the inhibitors used in this study, only the PI3K inhibitor LY294002 completely abolished the androgen induction of MMP-2 in LNCaP cells. To examine whether the inhibitory effect of LY294002 on androgen-induced MMP-2 gelatinolytic activity is in parallel with the protein expression but not caused by inhibition of MMP-2 secretion, protein levels of pro-MMP-2 from equal amounts of whole-cell lysates were determined by Western blot. As shown in Fig. 4B, two commonly used PI3K inhibitors (LY294002 and wortmannin) totally abolished pro-MMP-2 and PSA expression. MEK1 inhibitor PD98059 had no effect on pro-MMP-2 expression, which was consistent with the zymography data. In addition, the inhibitors alone did not cause any change, as shown in the *right panel* of Fig. 4B. These results suggest that PI3K is involved in AR-mediated pro-MMP-2 expression, which is consistent with previous reports that PI3K activity is required for the AR transactivation (29–31).

FGF-2 is an activator for both MEK1 and PI3K kinase cascades (32, 33) and was reported to induce MMP-2 expression in different cell types (34). Therefore, we asked whether

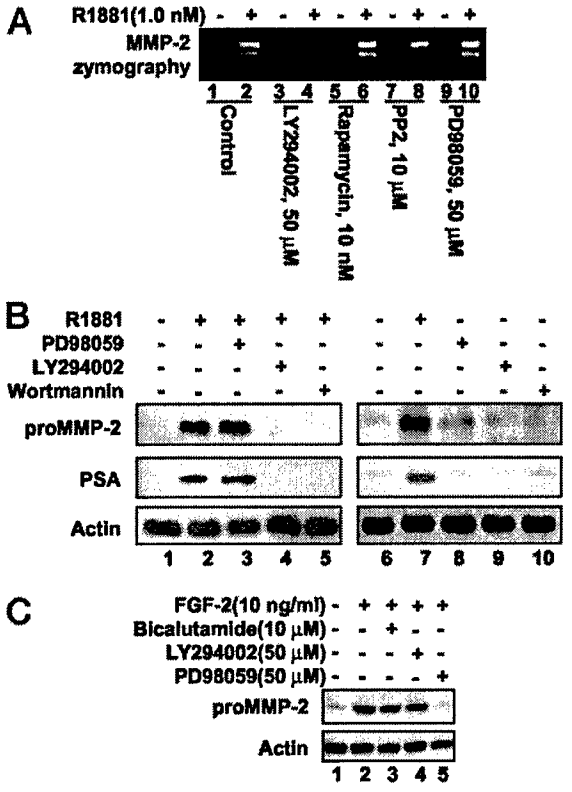

FIG. 4. AR-mediated pro-MMP-2 expression involves PI3K activity. Following serum starvation for 24 h, LNCaP cells were either left untreated (control) or pretreated with different kinase inhibitors as indicated for 30 min followed by R1881 (A and B) or FGF-2 (C) addition for another 24 h in serum-free media. The MMP gelatinolytic activities secreted into media were examined by gelatin zymography (A). Protein levels for pro-MMP-2, PSA, and actin from whole cell lysates were determined by Western blot (B and C). Data represent two separate experiments.

the PI3K signaling pathway is also required for FGF-2 to induce MMP-2 gene expression. To this end, we stimulated serum-starved LNCaP cells with FGF-2 (10 ng/ml) and pro-MMP-2 expression was evaluated 24 h later by Western blot (Fig. 4C) and gelatin zymography (data not shown). As expected, FGF-2 stimulation increased pro-MMP-2 expression dramatically. In contrast to androgen stimulation, pro-MMP-2 induction after FGF-2 stimulation was not suppressed by either the androgen antagonist bicalutamide or PI3K inhibitor LY294002 but by MEK1 inhibitor PD98059 (Fig. 4C). A similar result was also observed when LAPC-4 cells were used (data not shown). These results indicate that the regulatory mechanism for *MMP-2* gene expression is stimulus specific in cells.

Inhibition of MMP or PI3K suppresses LNCaP cell migration in response to R1881

Recently, MMPs have been shown to be correlated with tumor dissemination because of their proteolytic activity on ECM, and tumor cell migration is one of the most important events contributing to tumor dissemination (reviewed in Ref. 35). Because we observed androgen induction of pro-MMP-2 expression in LNCaP cells, we next asked whether MMP-2 inhibition could suppress cell migration in response to R1881 stimulation. Using a collagen-coated Transwell chamber assay, we assessed the ability of LNCaP cells to undergo unstimulated, steroid-depleted serum-stimulated, or R1881-stimulated migration. Without serum stimulation, almost no sign of migration was observed for LNCaP cells (data not shown), which is consistent with a previous report (36). However, addition of charcoal-stripped serum (steroids were depleted) stimulated cell migration. When R1881 (1.0 nM) was added in the culture, cell migration was significantly enhanced by almost 2-fold, compared with that incubated with charcoal-stripped serum alone (Fig. 5). To define the responsibility for MMP-2 in R1881-enhanced cell migration, we evaluated the effect of PI3K inhibitor LY294002 and a potent MMP-2 specific inhibitor OA-Hy (37) on LNCaP cell migration. Indeed, R1881-enhanced LNCaP cell migration was almost completely abolished by pretreatment with either OA-Hy (5.0 μM) or LY294002 (10 μM). In addition, we noticed that LY294002 alone or LY294002 plus R1881 resulted in a slight decrease (not statistical significant) of cell migration, compared with charcoal-stripped serum control, which is consistent with a previous report that PI3K activity is fundamental for serum-stimulated cell migration (38).

Discussion

The present study was undertaken to investigate whether androgen regulates MMP-2 or MMP-9 expression in prostate cancer cells. We found that: 1) androgen stimulated pro-MMP-2 but not MMP-9 expression, and androgen-stimulated pro-MMP-2 expression occurred at the gene transcription level via AR transactivation; 2) AR-mediated pro-MMP-2 expression is dependent on PI3K activity, a known modu-

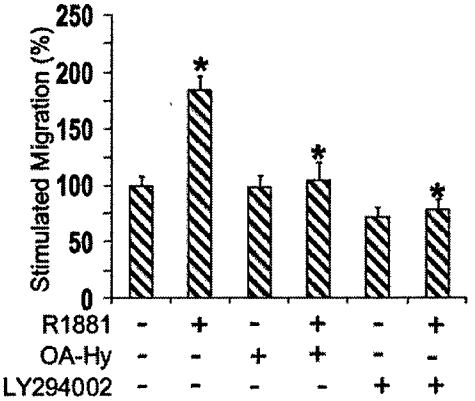

FIG. 5. Inhibition of MMP or PI3K suppresses LNCaP cell migration in response to R1881. After serum starvation, LNCaP cells were resuspended in culture media supplied with 5% cFBS. Then the cells were left untreated (control) or pretreated with OA-Hy (5.0 μM) or LY294002 (10 μM) for 30 min. A total of 1.0×10^5 cells were seeded on collagen-coated (50 μg/ml) Transwell chambers (8 μM pore) containing culture media and 5% cFBS. Cells were incubated in six different conditions: solvent only, R1881 alone, OA-Hy alone, R1881 plus OA-Hy, LY294002 alone, or R1881 plus LY294002. After 48-h incubation, cells on the upper surface were removed, and the filter was stained. The number of migrating cells in the absence of any treatment (solvent only) is assigned a relative value of 100%. The *asterisk* indicates a significant difference ($P < 0.05$) between R1881 stimulation *vs.* solvent only or R1881 alone *vs.* R1881 plus OA-Hy or LY294002. Data represent three independent experiments.

lator of the AR transactivation; and 3) androgen enhanced LNCaP cell migration via MMP-2 induction. These results indicate that androgen regulates MMP-2 expression via PI3K-dependent AR transactivation in prostate cancer cells.

Historically, *MMP-2* has been considered a constitutive gene because of a lack of well-characterized regulatory elements in the *MMP-2* promoter region (reviewed in Ref. 39). However, recent studies of the *MMP-2* promoter sequence analyses have revealed a number of potential *cis*-acting regulatory elements including p53, activator protein-1, Ets-1, CCAAT/enhancer-binding protein, cAMP response element-binding protein, polymavirus enhancer activator 3, surfactant protein 1, and activator protein-2 that could be involved in regulation of MMP-2 expression (13, 14, 40). Several factors, such as TGFβ1 (7), UVB/IL-8 (41), concanavalin A (42), short-term exposure to α- and γ-interferons (43), and transfection of *c-Ha-ras* (44) or Akt1 (45), have been previously reported to induce MMP-2 expression. In contrast, others including retinoic acid (46), PMA (26), long-term exposure to α- and γ-interferons (43), and the calcium influx inhibitor carboxy amidotriazole (47) were shown to suppress MMP-2 expression. We demonstrated for the first time in this study that MMP-2 expression was elevated when prostate cancer LNCaP and LAPC-4 cells were stimulated with androgen, adding androgen as a new member to the list of MMP-2 modulators. Our results are consistent with previous reports that long-term treatment with androgen increased prostate MMP-2 content in rats (48). However, another sex hormone, estrogen, was reported to inhibit MMP-2 expression in human fibroblast-derived cells (49), further suggesting that MMP-2 regulation is cell and stimulus specific.

Androgens such as R1881 produce most cellular responses through their cognate nuclear receptor, AR. On binding to the hormone, the AR forms homodimer. The dimerized protein then interacts with specific DNA sequences directly through an androgen-responsive element (ARE; reviewed in Ref. 50) or indirectly through other transcription factors that bind DNA in the regulatory region of the target gene promoters, such as Ets (51). The result is an alteration in protein synthesis and the generation of a cellular response. In this study, we demonstrated that R1881-stimulated pro-MMP-2 expression was abolished by the androgen antagonist bicalutamide that can block AR-mediated gene transcription (23) and by RNA transcription-specific inhibitor actinomycin D and protein translation inhibitor cycloheximide. Furthermore, in a luciferase reporter assay, human MMP-2 promoter activity was induced by R1881 stimulation that was also abolished by bicalutamide addition. These data all indicate that the expression of *MMP-2* gene is regulated by androgen via an AR transactivation mechanism, although the possibility of an indirect effect of AR on pro-MMP-2 expression could not be fully ruled out. Recently interaction of AR with Ets protein has been reported to negatively modulate MMP-1, 3, and 7 (51), and an Ets-1-binding site was found in the *MMP-2* promoter region (14). However, it might be unlikely that androgen-stimulated pro-MMP-2 expression is also via an interaction between AR and Ets-1 because androgen positively induces pro-MMP-2 expression.

The location, sequence, and number of AREs associated with a given androgen target gene varies, although androgen-responsive regions typically contain multiple nonconsensus AREs (5′-TGTTCT-3′; Ref. 52). By analyzing the published sequence of the *MMP-2* gene promoter (13), we noticed that there are two potential ARE-like motifs located in the promoter of the *MMP-2* gene (−1539-TGT-T*c*CT-1503, and −609-TGT*a*TCT-603) with one nucleotide mismatch (italicized). Further characterization of the *MMP-2* promoter for ARE elements is being carried out currently by our group.

It has been shown that overexpression of the *Akt1* gene induces MMP-2 activity in mouse mammary epithelial cells (45), but reintroduction of the *PTEN* gene reduces *MMP-2* gene expression in human glioma cells (53). In human prostate cancer LNCaP cells, PI3K-Akt activity is elevated because of an inactive mutant of the *PTEN* gene (54). Although the molecular basis in AR signaling is not fully understood, an involvement of PI3K-Akt and PTEN pathways was recently reported (29–31). Consistent with those reports, we also observed that AR-mediated pro-MMP-2 expression is PI3K dependent, further demonstrating that PI3K activity is required for AR transactivation. However, the detailed mechanism for PI3K-Akt's involvement needs further investigation.

Extensive work on the mechanisms of tumor invasion and metastasis has determined the MMP's function as key factors in the process of tumor dissemination. In this regard, the increased expression of various MMPs is strongly associated with tumor invasiveness. Specifically, MMP-2 expression is elevated in metastatic prostate cancers (reviewed in Ref. 8). Previous studies have pointed out that tumor cells achieve increased motility through mechanisms that circumvent the requirement for exogenous motogenic factors (*e.g.* androgen or other serum-derived factors). Among the signal cascades initiated by the factors, the PI3K-dependent pathway is essential in cell migration (38). The LNCaP cell line is the one among those cell lines that require serum stimulation to migrate (36). The failure of LNCaP cells to migrate was not due to their inability to adhere to or spread on ECM but to a requirement of extracellular factors to activate intracellular signals necessary for motility (36). In this study, we also observed androgen-enhanced LNCaP cell migration. Androgen-enhanced cell migration was totally blocked by the MMP-2 specific inhibitor OA-Hy, and the PI3K inhibitor LY294002. These results suggest that androgen-induced MMP-2 played a role in androgen-enhanced cell migration.

In conclusion, we have presented for the first time that pro-MMP-2 expression is induced by androgen-stimulated AR transactivation in human prostate cancer LNCaP and LAPC-4 cells. In addition, AR-mediated pro-MMP-2 expression, like PSA, is dependent on an active PI3K pathway, which is consistent with previous reports (29–31). Moreover, androgen-enhanced LNCaP cell migration is suppressed by the MMP-2 inhibitor OA-Hy or PI3K inhibitor LY294002. These findings suggest that AR-mediated pro-MMP-2 expression may participate in the process of prostate development or prostate cancer invasion/metastasis.

Acknowledgments

We thank AstraZeneca for the generous gift of bicalutamide, Dr. Michael Wolfe (Kansas University Medical Center) for sharing equipment, Dr. Charles L. Sawyers (University of California, Los Angeles) for LAPC-4 cell line, Dr. David M. Spencer (Baylor College of Medicine, Houston, TX) for the pCMV-SEAP plasmid, and Dr. Yasuyuki Sasaguri (University of Occupational and Environmental Health, Kitakyushu, Japan) for the MMP9-LUC reporter. We also thank Mr. Scott Stanley and Mrs. Donna Barnes for excellent secretarial assistance.

Received December 16, 2002. Accepted January 22, 2003.

Address all correspondence and requests for reprints to: Benyi Li, M.D./Ph.D., Kansas University Medical Center Urology, 3901 Rainbow Boulevard, Lied 1042, Kansas City, Kansas 66160. E-mail: bli@kumc.edu.

This work was supported by the William L. Valk Endowment, Mason's Foundation, and Start-Up Fund from the Kansas Cancer Institute (to B.L.), grants from Department of Defense/U.S. Army Prostate Cancer Research Program (DAMD-17-02-1-0238), and NIH Grant CA-78646 (to Q.-X.A.S.).

References

1. **Jemal A, Thomas A, Murray T** 2002 Cancer statistics. CA Cancer J Clin 52:23–47
2. **Huggins C, Hodges CV** 1941 Studies on prostatic cancer: the effects of castration, of estrogen and of androgen injection on serum phosphatases in metastatic carcinoma of the prostate. Cancer Res 1:293–297
3. **Denmeade SR, Lin XS, Isaacs JT** 1996 Role of programmed (apoptotic) cell death during the progression and therapy for prostate cancer. Prostate 28: 251–265
4. **Coussens LM, Fingleton B, Matrisian LM** 2002 Matrix metalloproteinase inhibitors and cancer: trials and tribulations. Science 295:2387–2392
5. **Sato H, Takino T, Okada Y, Cao J, Shinagawa A, Yamamoto E, Seiki M** 1994 A matrix metalloproteinase expressed on the surface of invasive tumour cells. Nature 370:61–65
6. **Upadhyay J, Shekarriz B, Nemeth JA, Dong Z, Cummings GD, Fridman R, Sakr W, Grignon DJ, Cher ML** 1999 Membrane type 1-matrix metalloproteinase (MT1-MMP) and MMP-2 immunolocalization in human prostate: change in cellular localization associated with high-grade prostatic intraepithelial neoplasia. Clin Cancer Res 5:4105–4110
7. **Wilson MJ, Sellers RG, Wiehr C, Melamud O, Pei D, Peehl DM** 2002 Expression of matrix metalloproteinase-2 and -9 and their inhibitors, tissue inhibitor of metalloproteinase-1 and -2, in primary cultures of human prostatic stromal and epithelial cells. J Cell Physiol 191:208–216
8. **Lokeshwar BL** 1999 MMP inhibition in prostate cancer. Ann NY Acad Sci 878:271–289
9. **Klein KA, Reiter RE, Redula J, Moradi H, Zhu XL, Brothman AR, Lamb DJ, Marcelli M, Belldegrun A, Witte ON, Sawyers CL** 1997 Progression of metastatic human prostate cancer to androgen independence in immunodeficient SCID mice. Nat Med 3:402–408
10. **Li H, Bauzon DE, Xu X, Tschesche H, Cao J, Sang QA** 1998 Immunological characterization of cell-surface and soluble forms of membrane type 1 matrix metalloproteinase in human breast cancer cells and in fibroblasts. Mol Carcinog 22:84–94
11. **Heussen C, Dowdle EB** 1980 Electrophoretic analysis of plasminogen activators in polyacrylamide gels containing sodium dodecyl sulfate and copolymerized substrates. Anal Biochem 102:196–202
12. **Nagakawa O, Ogasawara M, Murata J, Fuse H, Saiki I** 2001 Effect of prostatic neuropeptides on migration of prostate cancer cell lines. Int J Urol 8:65–70
13. **Bian J, Sun Y** 1997 Transcriptional activation by p53 of the human type IV collagenase (gelatinase A or matrix metalloproteinase 2) promoter. Mol Cell Biol 17:6330–6338
14. **Qin H, Sun Y, Benveniste EN** 1999 The transcription factors Sp1, Sp3, and AP-2 are required for constitutive matrix metalloproteinase-2 gene expression in astroglioma cells. J Biol Chem 1999 274:29130–29137
15. **Shimajiri S, Arima N, Tanimoto A, Murata Y, Hamada T, Wang KY, Sasaguri Y** 1999 Shortened microsatellite d(CA)21 sequence down-regulates promoter activity of matrix metalloproteinase 9 gene. FEBS Lett 455:70–74
16. **Xie X, Zhao X, Liu Y, Young CYF, Tindall DJ, Slawin KM, Spencer DM** 2001 Robust prostate-specific expression for targeted gene therapy based on the human kallikrein 2 (hK2) promoter. Hum Gene Ther 12:549–561
17. **Spencer DM, Wandless TJ, Schreiber SL, Crabtree GR** 1993 Controlling signal transduction with synthetic ligands. Science 262:1019–1024
18. **Van Steenbrugge GJ, van Uffelen CJ, Bolt J, Schroder FH** 1991 The human prostatic cancer cell line LNCaP and its derived sublines: an *in vitro* model for the study of androgen sensitivity. J Steroid Biochem Mol Biol 40:207–214
19. **Zucker S, Mancuso P, DiMassimo B, Lysik RM, Conner C, Wu CL** 1994 Comparison of techniques for measurement of gelatinases/type IV collagenases: enzyme-linked immunoassays versus substrate degradation assays. Clin Exp Metastasis 12:13–23
20. **Patterson BC, Sang QA** 1997 Angiostatin-converting enzyme activities of human matrilysin (MMP-7) and gelatinase B/type IV collagenase (MMP-9). J Biol Chem 272:28823–28825
21. **Shakil T, Hoque AN, Husain M, Belsham DD** 2002 Differential regulation of gonadotropin-releasing hormone secretion and gene expression by androgen: membrane versus nuclear receptor activation. Mol Endocrinol 16:2592–2602
22. **Falkenstein E, Tillmann HC, Christ M, Feuring M, Wehling M** 2000 Multiple actions of steroid hormones—a focus on rapid, nongenomic effects. Pharmacol Rev 52:513–556
23. **Masiello D, Cheng S, Bubley GJ, Lu ML, Balk SP** 2002 Bicalutamide functions as an androgen receptor antagonist by assembly of a transcriptionally inactive receptor. J Biol Chem 277:26321–26326
24. **Waller AS, Sharrard RM, Berthon P, Maitland NJ** 2000 Androgen receptor localization and turnover in human prostate epithelium treated with the antiandrogen, bicalutamide. J Mol Endocrinol 24:339–351
25. **Hanemaaijer R, Koolwijk P, le Clercq L, de Vree WJ, van Hinsbergh VW** 1993 Regulation of matrix metalloproteinase expression in human vein and microvascular endothelial cells. Effects of tumour necrosis factor α, interleukin 1 and phorbol ester. Biochem J 296:803–809
26. **Brown PD, Levy AT, Margulies IM, Liotta LA, Stetler-Stevenson WG** 1990 Independent expression and cellular processing of Mr 72, 000 type IV collagenase and interstitial collagenase in human tumorigenic cell lines. Cancer Res 50:6184–6191
27. **Nagakawa O, Murakami K, Yamaura T, Fujiuchi Y, Murata J, Fuse H, Saiki I** 2000 Expression of membrane-type 1 matrix metalloproteinase (MT1-MMP) on prostate cancer cell lines. Cancer Lett 155:173–179
28. **Han YP, Tuan TL, Wu H, Hughes M, Garner WL** 2001 TNF-alpha stimulates activation of pro-MMP2 in human skin through NF-κB mediated induction of MT1-MMP. J Cell Sci 114:131–139
29. **Li P, Nicosia SV, Bai W** 2001 Antagonism between PTEN/MMAC1/TEP-1 and androgen receptor in growth and apoptosis of prostatic cancer cells. J Biol Chem 276:20444–20050
30. **Sharma M, Chuang WW, Sun Z** 2002 Phosphatidylinositol 3-kinase/Akt stimulates androgen pathway through GSK3β inhibition and nuclear β-catenin accumulation. J Biol Chem 277:30935–30941
31. **Manin M, Baron S, Goossens K, Beaudoin C, Jean C, Veyssiere G, Verhoeven G, Morel L** 2002 Androgen receptor expression is regulated by PI3-kinase/Akt pathway in normal and tumoral epithelial cells. Biochem J 366:729–736
32. **Raffioni S, Bradshaw RA** 1992 Activation of phosphatidylinositol 3-kinase by epidermal growth factor, basic fibroblast growth factor, and nerve growth factor in PC12 pheochromocytoma cells. Proc Natl Acad Sci USA 89:9121–9125
33. **Graves LM, Northrop JL, Potts BC, Krebs EG, Kimelman D** 1994 Fibroblast growth factor, but not activin, is a potent activator of mitogen-activated protein kinase in *Xenopus* explants. Proc Natl Acad Sci USA 91:1662–1666
34. **Miyake H, Yoshimura K, Hara I, Eto H, Arakawa S, Kamidono S** 1997 Basic fibroblast growth factor regulates matrix metalloproteinases expression and *in vitro* invasiveness in human bladder cancer cell lines. J Urol 157:2351–2355
35. **Stamenkovic I** 2000 Matrix metalloproteinases in tumor invasion and metastasis. Semin Cancer Biol 10:415–433
36. **Slack JK, Adams RB, Rovin JD, Bissonette EA, Stoker CE, Parsons JT** 2001 Alterations in the focal adhesion kinase/Src signal transduction pathway correlate with increased migratory capacity of prostate carcinoma cells. Oncogene 20:1152–1163
37. **Emonard H, Marcq V, Mirand C, Hornebeck W** 1999 Inhibition of gelatinase A by oleic acid. Ann N Y Acad Sci 878:647–649
38. **Jimenez C, Portela RA, Mellado M, Rodriguez-Frade JM, Collard J, Serrano A, Martinez-A C, Avila J, Carrera AC** 2000 Role of the PI3K regulatory subunit in the control of actin organization and cell migration. J Cell Biol 151:249–262
39. **Mauviel A** 1993 Cytokine regulation of metalloproteinase gene expression. J Cell Biochem 53:288–295
40. **Hasan S, Nakajima M** 1999 Retinoic acid synergizes with cyclic AMP to enhance MMP-2 basal promoter activity. Biochem Biophys Res Commun 258: 663–667
41. **Singh RK, Gutman M, Reich R, Bar-Eli M** 1995 Ultraviolet B irradiation promotes tumorigenic and metastatic properties in primary cutaneous melanoma via induction of interleukin 8. Cancer Res 55:3669–3674
42. **Yu M, Sato H, Seiki M, Thompson EW** 1995 Complex regulation of membrane-type matrix metalloproteinase expression and matrix metalloproteinase-2 activation by concanavalin A in MDA-MB-231 human breast cancer cells. Cancer Res 55:3272–3277
43. **Hujanen ES, Vaisanen A, Zheng A, Tryggvason K, Turpeenniemi-Hujanen T** 1994 Modulation of M(r) 72, 000 and M(r) 92, 000 type-IV collagenase (gelatinase A and B) gene expression by interferons α and γ in human elanoma. Int J Cancer 58:582–586
44. **Garbisa S, Pozzatti R, Muschel RJ, Saffiotti U, Ballin M, Goldfarb RH, Khoury G, Liotta LA** 1987 Secretion of type IV collagenolytic protease and

metastatic phenotype: induction by transfection with c-Ha-ras but not c-Ha-ras plus Ad2–E1a. Cancer Res 47:1523–1528
45. **Park BK, Zeng X, Glazer RI** 2001 Akt1 induces extracellular matrix invasion and matrix metalloproteinase-2 activity in mouse mammary epithelial cells. Cancer Res 61:7647–7653
46. **Nakajima M, Lotan D, Baig MM, Carralero RM, Wood WR, Hendrix MJ, Lotan R** 1989 Inhibition by retinoic acid of type IV collagenolysis and invasion through reconstituted basement membrane by metastatic rat mammary adenocarcinoma cells. Cancer Res 49:1698–1706
47. **Kohn EC, Jacobs W, Kim YS, Alessandro R, Stetler-Stevenson WG, Liotta LA** 1994 Calcium influx modulates expression of matrix metalloproteinase-2 (72-kDa type IV collagenase, gelatinase A). J Biol Chem 269:21505–21511
48. **Li SC, Chen GF, Chan PS, Choi HL, Ho SM, Chan FL** 2001 Altered expression of extracellular matrix and proteinases in Noble rat prostate gland after long-term treatment with sex steroids. Prostate 49:58–71
49. **Moalli PA, Klingensmith WL, Meyn LA, Zyczynski HM** 2002 Regulation of matrix metalloproteinase expression by estrogen in fibroblasts that are derived from the pelvic floor. Am J Obstet Gynecol 187:72–79
50. **Gelmann EP** 2002 Molecular biology of the androgen receptor. J Clin Oncol 20:3001–3015
51. **Schneikert J, Peterziel H, Defossez PA, Klocker H, Launoit Y, Cato AC** 1996 Androgen receptor-Ets protein interaction is a novel mechanism for steroid hormone-mediated down-modulation of matrix metalloproteinase expression. J Biol Chem 271:23907–23913
52. **Claessens F, Verrijdt G, Schoenmakers E, Haelens A, Peeters B, Verhoeven G, Rombauts W** 2001 Selective DNA binding by the androgen receptor as a mechanism for hormone-specific gene regulation. J Steroid Biochem Mol Biol 76:23–30
53. **Koul D, Parthasarathy R, Shen R, Davies MA, Jasser SA, Chintala SK, Rao JS, Sun Y, Benvenisite EN, Liu TJ, Yung WK** 2001 Suppression of matrix metalloproteinase-2 gene expression and invasion in human glioma cells by MMAC/PTEN. Oncogene 20:6669–6678
54. **Vlietstra RJ, van Alewijk DC, Hermans KG, van Steenbrugge GJ, Trapman J** 1998 Frequent inactivation of PTEN in prostate cancer cell lines and xenografts. Cancer Res 58:2720–2723

Catalytic- and ecto-domains of membrane type 1-matrix metalloproteinase have similar inhibition profiles but distinct endopeptidase activities

Douglas R. HURST*, Martin A. SCHWARTZ*, Mohammad A. GHAFFARI*, Yonghao JIN*, Harald TSCHESCHE†, Gregg B. FIELDS‡ and Qing-Xiang Amy SANG*[1]

*Department of Chemistry and Biochemistry and Institute of Molecular Biophysics, 203 Dittmer Laboratory of Chemistry Building, Florida State University, Tallahassee, FL 32306, U.S.A., †Department of Biochemistry, University of Bielefeld, 33615 Bielefeld, Germany, and ‡Department of Chemistry and Biochemistry, Florida Atlantic University, Boca Raton, FL 33431, U.S.A.

Membrane type 1-matrix metalloproteinase (MT1-MMP/MMP-14) is a major collagenolytic enzyme that plays a vital role in development and morphogenesis. To elucidate further the structure–function relationship between the human MT1-MMP active site and the influence of the haemopexin domain on catalysis, substrate specificity and inhibition kinetics of the cdMT1-MMP (catalytic domain of MT1-MMP) and the ecto domain ΔTM-MT1-MMP (transmembrane-domain-deleted MT1-MMP) were compared. For substrate **1** [Mca-Pro-Leu-Gly-Leu-Dpa-Ala-Arg-NH_2, where Mca stands for (7-methoxycoumarin-4-yl)acetyl- and Dpa for *N*-3-(2,4-dinitrophenyl)-L-2,3-diaminopropionyl], the activation energy E_a was determined to be 11.2 and 12.2 kcal/mol (1 cal = 4.184 J) for cdMT1-MMP and ΔTM-MT1-MMP respectively, which is consistent with k_{cat}/K_M values of 7.37 and 1.46×10^4 $M^{-1} \cdot s^{-1}$. The k_{cat}/K_M values for a series of similar single-stranded peptide substrates were determined and found to correlate with a slope of 0.17 for the two enzyme forms. A triple-helical peptide substrate was predicted to have a k_{cat}/K_M of 0.87×10^4 $M^{-1} \cdot s^{-1}$ for ΔTM-MT1-MMP based on the value for cdMT1-MMP of 5.12×10^4 $M^{-1} \cdot s^{-1}$; however, the actual value was determined to be 2.5-fold higher, i.e. 2.18×10^4 $M^{-1} \cdot s^{-1}$. These results suggest that cdMT1-MMP is catalytically more efficient towards small peptide substrates than ΔTM-MT1-MMP and the haemopexin domain of MT1-MMP facilitates the hydrolysis of triple-helical substrates. Diastereomeric inhibitor pairs were utilized to probe further binding similarities at the active site. Ratios of K_i values for the inhibitor pairs were found to correlate between the enzyme forms with a slope of 1.03, suggesting that the haemopexin domain does not significantly modify the enzyme active-site structure.

Key words: activation energy, catalytic domain, diastereomeric MMP inhibitors, ecto-domain, membrane type 1-matrix metalloproteinase (MT1-MMP), substrate specificity.

INTRODUCTION

Matrix metalloproteinases (MMPs) are a family of related zinc endopeptidases known to play prominent roles during normal and pathological extracellular matrix remodelling events including cancer progression [1]. The first identified membrane type MMP, MT1-MMP, has been shown to play a key role in tumour cell invasion and metastasis by complex mechanisms, including activation of proMMP-2 and direct hydrolysis of interstitial collagens [2,3]. MT1-MMP is tethered to the cell membrane by a type 1 transmembrane region and is expressed as an active protease on the cell surface upon activation, primarily by proprotein convertases such as furin or furin-like serine proteinases [4]. In addition, consistent with other MMP family members, MT1-MMP has a propeptide, catalytic domain linker region and a haemopexin domain [5].

The haemopexin domain has been supposed to function mainly in protein-substrate recognition [6]. It is necessary for native type I collagen cleavage for reasons that are not completely understood [7,8]. Recently, new roles have been identified for the MT1-MMP haemopexin domain including enzymic regulation and subcellular localization [9,10]. Additionally, the linker region between the catalytic and haemopexin domains has been identified as having the ability to bind the collagen [11]. It is possible that this region is necessary for triple-helical substrate hydrolysis.

Although several groups have reported the cleavage of extracellular matrix constituents by MT1-MMP [12–14], a structural comparison of the active site of the catalytic domain with and without the haemopexin domain has not been accomplished. In the present study, a comparison of the substrate specificity for two truncated forms of MT1-MMP was performed using single-stranded peptide substrates. The haemopexin domain was then found to facilitate the hydrolysis of a triple-helical substrate. To demonstrate that the haemopexin domain does not influence the architecture of the active site, diastereomeric inhibitor pairs were utilized to show identical K_i ratios.

MATERIALS AND METHODS

Materials

Quenched fluorogenic peptide substrates (see Table 1) **1** and **3**–**5** [Mca-Pro-Leu-Gly-Leu-Dpa-Ala-Arg-NH_2, Mca-Pro-Lys-Pro-Leu-Ala-Leu-Dpa-Ala-Arg-NH_2, Mca-Arg-Pro-Lys-Pro-Tyr-Ala-Nva-Trp-Met-Lys-Dpa-NH_2 and Mca-Pro-Leu-Ala-Gln-Ala-Val-Dpa-Arg-Ser-Ser-Arg-NH_2, where Mca stands for (7-methyloxycoumarin-4-yl)acetyl, Dpa stands for *N*-3-(2,4-dinitrophenyl)-L-2,3-diaminopropionyl and Nva for norvaline] were purchased from Bachem and **2** (Mca-Pro-Leu-Ala-Nva-Dpa-Ala-Arg-NH_2) was from Calbiochem (San Diego, CA, U.S.A.). The triple-helical peptide substrate **6** [{(GPP*)$_5$ GPK(Mca)GPQGLRGQK(Dnp)GVR(GPP*)$_5$-NH_2}$_3$, where Dnp stands for 2,4-dinitrophenyl and P* for 4-hydroxy-L-proline] was synthesized as described previously [15]. The mercaptosulphide

Abbreviations used: MMP, matrix metalloproteinase; MT1, membrane type 1; cdMT1-MMP, catalytic domain of MT1-MMP; Dpa, *N*-3-(2,4-dinitrophenyl)-L-2,3-diaminopropionyl; Mca, (7-methoxycoumarin-4-yl)acetyl; Nva, norvaline; RTTI, rat-tail tendon type I collagen; TIMP, tissue inhibitor of metalloproteinase; ΔTM-MT1-MMP, transmembrane-domain-deleted MT1-MMP.

[1] To whom correspondence should be addressed (e-mail qxsang@chem.fsu.edu).

inhibitors were synthesized and characterized as described previously ([16,17]; Y. Jin and M. A. Schwartz, unpublished work). Hydroxamate inhibitors 444237 and 444238 were purchased from Calbiochem. The recombinant human cdMT1-MMP (catalytic domain of MT1-MMP; Ile^{114}–Ile^{318}) was expressed in *Escherichia coli* and was activated by autocatalysis [18] and ΔTM-MT1-MMP (transmembrane-domain-deleted MT1-MMP), the recombinant human ectodomain of MT1-MMP (Tyr^{112}–Glu^{523} consisting of the catalytic domain and the haemopexin domain) was expressed in *Pichia pastoris* and activated by yeast proteinases during maturation [19]. Human TIMP-2 (tissue inhibitor of metalloproteinase-2) was kindly provided by Professor Jack Windsor of Indiana University (Indianapolis, IN, U.S.A.). All standard chemicals were purchased from Fisher with the exception of 5,5′-dithio(bis-2-nitrobenzoate), which was from Sigma.

Enzyme kinetics

Kinetic assays were performed as described previously [20] in 50 mM Hepes buffer (pH 7.5), with 10 mM $CaCl_2$, 0.2 M NaCl and 0.05 % Brij-35 (polyoxyethylene lauryl ether) at 25 °C. The final substrate concentration was 1 μM (1 % DMSO), which is at least 10-fold lower than K_M. Hence k_{cat}/K_M is calculated using the equation:

$$\frac{k_{cat}}{K_M} = \frac{v}{[E][S]}$$

where v is the initial rate and [E] and [S] are the enzyme and substrate concentrations respectively. The activation energy E_a was determined by the Arrhenius equation:

$$\ln v = -\frac{E_a}{RT} + \ln A[ES]$$

where R is the universal/ideal gas constant, T the absolute temperature in Kelvin, A the collision constant/Arrhenius A factor/pre-exponential factor and [ES] the concentration of the enzyme–substrate complex. The initial rates were determined at 283 K and then at increments of 5 K up to 313 K. The fluorescence intensity was corrected for temperature using the standard Mca-Pro-Leu-OH (Bachem). For the inhibition assays, the inhibitors were incubated with enzyme for 15–30 min before adding substrate **1** to ensure equilibrium conditions. The inhibitor dissociation constant K_i was determined as described previously [21] using the Morrison equation [22]:

$$\frac{v_i}{v_o} = \frac{[E]_o + [I]_o - K_i^{app} + \sqrt{([I]_o + K_i^{app} - [E]_o)^2 + 4[E]_o K_i^{app}}}{2[E]_o}$$

where v_i and v_o are the initial rates with and without the inhibitor respectively, $[E]_o$ and $[I]_o$ are the initial enzyme and inhibitor concentrations respectively and K_i^{app} is the apparent K_i that is equal to the true K_i under the conditions of $[S] \ll K_M$ for competitive inhibition according to the equation:

$$K_i^{app} = K_i\left(1 + \frac{[S]}{K_M}\right)$$

The active mercaptosulphide inhibitor concentration was quantified with Ellman's reagent 5,5′-dithiobis-(2-nitrobenzoate) [23,24]. Active cdMT1-MMP and ΔTM-MT1-MMP concentrations were normalized by titration with standardized preparations of recombinant TIMP-2. The titration was performed as described above for determination of K_i with an $[E]/K_i$ ratio > 100 to ensure proper titrating conditions.

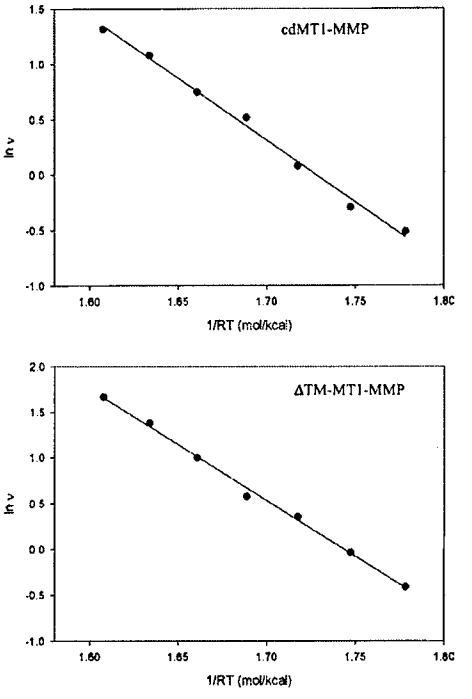

Figure 1 Arrhenius plot

E_a values were determined for the hydrolysis of substrate **1** with (**A**) cdMT1-MMP and (**B**) ΔTM-MT1-MMP as described in the Materials and methods section. Initial rates are expressed in nM/min. Fluorescence intensity was temperature-corrected. The slope of the line $-E_a$ (kcal/mol) was 11.2 and 12.2 for (**A**) and (**B**) respectively.

Collagen hydrolysis and electrophoresis

Samples containing 280 μg/ml purified RTTI (rat-tail tendon type I collagen) [20] were incubated with 80 nM enzyme at 37 °C in 50 mM Hepes (pH 7.5), 10 mM $CaCl_2$, 0.2 M NaCl and 0.05 % Brij-35. The reactions were stopped with 50 mM EDTA, 100 mM dithiothreitol and boiled for 5 min. The samples were analysed by SDS/PAGE (7 % gel) with silver staining. The cdMT1-MMP and ΔTM-MT1-MMP samples were visualized by a Western blot (12 % SDS/polyacrylamide gel) using a previously characterized antibody [3].

RESULTS

Substrate specificity

The catalytic domain alone is predicted to hydrolyse small peptide substrates more efficiently than ΔTM-MT1-MMP if the active sites are identical, possibly due to flexibility, rotational freedom or substrate exosite binding. The activation energy for enzyme hydrolysis of peptides should therefore be lower for cdMT1-MMP when compared with ΔTM-MT1-MMP. The E_a values for substrate **1** (see Table 1) with cdMT1-MMP and ΔTM-MT1-MMP were determined to be 11.2 and 12.2 kcal/mol respectively (Figure 1). Consistently, the k_{cat}/K_M values were 7.37 and 1.46×10^4 $M^{-1} \cdot s^{-1}$ respectively (Table 1). If the peptide binds to a haemopexin exosite region, the effective substrate concentration would be reduced, subsequently lowering the apparent k_{cat}/K_M.

Table 1 Comparison of substrate specificity

Fluorogenic peptide substrates	k_{cat}/K_M ($\times 10^4$ $s^{-1} \cdot M^{-1}$) cdMT1	ΔTM
1 Mca-Pro-Leu-Gly ↓ Leu-Dpa-Ala-Arg-NH_2	7.37	1.46
2 Mca-Pro-Leu-Ala ↓ Nva-Dpa-Ala-Arg-NH_2	2.27	0.25
3 Mca-Pro-Lys-Pro-Leu-Ala ↓ Leu-Dpa-Ala-Arg-NH_2	7.82	1.04
4 Mca-Arg-Pro-Lys-Pro-Tyr-Ala ↓ Nva-Trp-Met-Lys-Dpa-NH_2	1.81	0.15
5 Mca-Pro-Leu-Ala ↓ Gln-Ala-Val-Dpa-Arg-Ser-Ser-Arg-NH_2	0.18	0.02
6 {(GPP*)$_5$GPK(Mca)GPQG ↓ LRGQK(Dnp)GVR(GPP*)$_5$-NH_2}$_3$*	5.12	2.18

* Single-letter amino acid abbreviations are used here. P* stands for 4-hydroxy-L-proline. The arrow indicates the putative cleavage site.

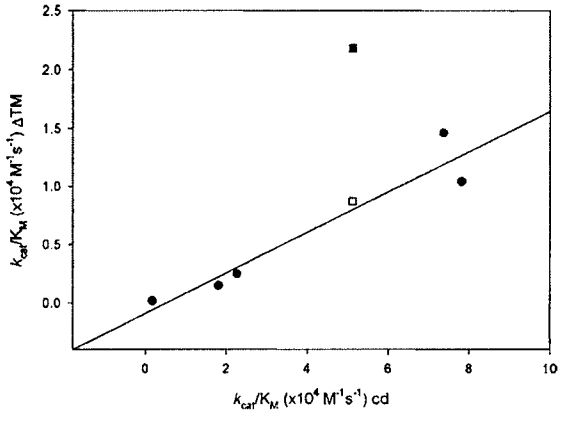

Figure 2 Correlation of specificity constants

The k_{cat}/K_M values from Table 1 for the single-stranded peptides **1**–**5** were plotted (●) and found to have a slope of 0.17. The triple-helical substrate **6** was predicted to have a k_{cat}/K_M value of 0.87×10^4 $M^{-1} \cdot s^{-1}$ for ΔTM-MT1-MMP (□) based on the value of 5.12×10^4 $M^{-1} \cdot s^{-1}$ for cdMT1-MMP. The actual value was determined to be 2.5-fold higher, i.e. 2.18×10^4 $M^{-1} \cdot S^{-1}$ (■).

Since the E_a and k_{cat}/K_M values correlate, exosite binding is probably not a valid reason for differences in hydrolytic efficiency. These results suggest that cdMT1-MMP is slightly more efficient than ΔTM-MT1-MMP for hydrolysing single-stranded peptides as predicted.

This trend was also noted with other similar peptides and a correlation curve was constructed with the k_{cat}/K_M values giving a slope of 0.17 (Table 1 and Figure 2). A prediction of k_{cat}/K_M values for ΔTM-MT1-MMP may then be found by multiplying the k_{cat}/K_M values for cdMT1-MMP by 0.17. The fluorescently labelled triple-helical peptide that was characterized previously [15] was tested with cdMT1-MMP and was found to have a k_{cat}/K_M value of 5.12×10^4 $M^{-1} \cdot s^{-1}$. Assuming this substrate is hydrolysed similarly to the single-stranded peptides, the predicted k_{cat}/K_M value would be 0.87×10^4 $M^{-1} \cdot s^{-1}$ for ΔTM-MT1-MMP (Figure 2, open square); however, the actual value was determined to be 2.18×10^4 $M^{-1} \cdot s^{-1}$, a value 2.5-fold higher (Figure 2, closed square).

Probing the active site

The difference in the predicted and actual values for triple-helical substrate hydrolysis by ΔTM-MT1-MMP may be due to structural differences at the active site. To probe the active-site structure, the inhibition profiles for cdMT1-MMP and ΔTM-MT1-MMP were compared with diastereomeric inhibitor pairs (Figure 3 and Table 2). The correct stereochemistry of these inhibitors is

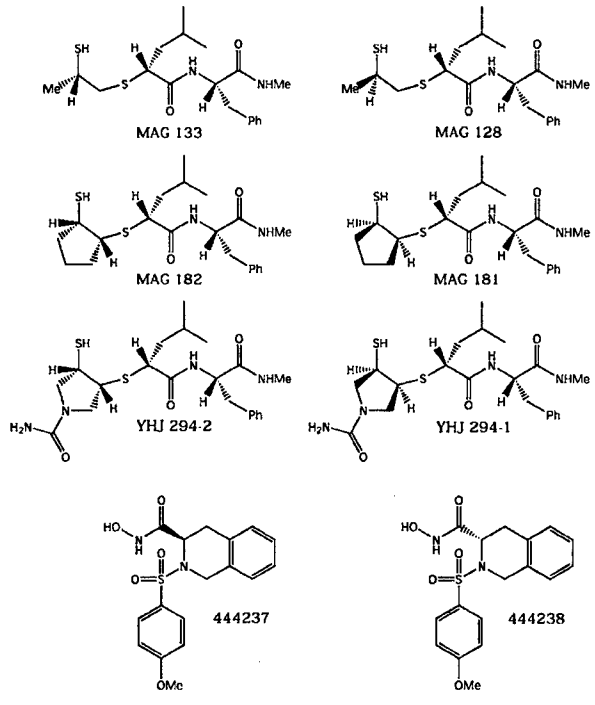

Figure 3 Inhibitor structures

The inhibitors are shown as pairs of diastereomers with the more potent inhibitor on the left. K_i values are shown in Table 2.

Table 2 K_i values of the inhibitor

Inhibitor	cdMT1 K_i (nM)	cdMT1 K_i ratio of the isomer	ΔTM-MT1 K_i (nM)	ΔTM-MT1 K_i ratio of the isomer
MAG 133	19	4	26	6
MAG 128	70		150	
MAG 182	24	11	29	19
MAG 181	259		540	
YHJ 294-2	13	231	24	242
YHJ 294-1	3000		5800	
444237	0.5	90	0.5	110
444238	45		55	

important for potency towards MT1-MMP as noted by the large differences in K_i values between inhibitor pairs. The K_i values were generally lower for cdMT1-MMP when compared with those for ΔTM-MT1-MMP, which is consistent with the peptide studies. Interestingly, the ratios of K_i values for diastereomers correlated with a slope of 1.03 between cdMT1-MMP and ΔTM-MT1-MMP (Figure 4). These results demonstrate that the haemopexin domain has no direct influence on the structure of the active site of the enzyme.

To ensure that ΔTM-MT1-MMP is a fully functional enzyme (i.e. ability to cleave collagen), RTTI was utilized as a substrate. Figure 5(B) shows the ability of this enzyme form to degrade native RTTI at 37 °C (three-quarter and one-quarter fragments not shown). The RTTI was not hydrolysed by cdMT1-MMP under the same conditions (reaction was also followed overnight with the same results; not shown). The same assay was performed with RTTI preparations that were first boiled for 5 min. Both the enzymes rapidly degraded the denatured RTTI (gelatin) samples. These results demonstrate that both enzyme forms maintain hydrolytic characteristics consistent with published reports.

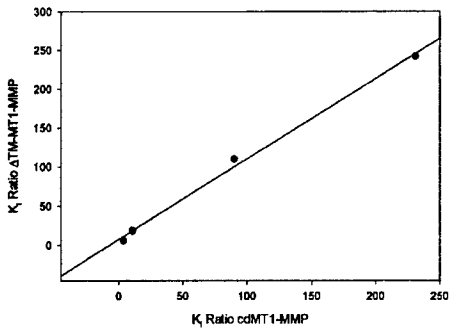

Figure 4 Correlation of diastereomer K_I ratio

The ratios from Table 2 were plotted and found to have a correlation of 1.03 ($r^2 = 0.9961$).

DISCUSSION

The haemopexin domain in MMPs is necessary for the cleavage of native interstitial type I–III collagens by mechanisms that are not completely understood [7,8]. In this study, the substrate specificity and inhibition of cdMT1-MMP was compared with ΔTM-MT1-MMP. The enzyme concentrations were normalized by titration with TIMP-2. Both forms of the enzyme were found to be fully active, as demonstrated by hydrolysis of either native or denatured RTTI, in addition to showing a single band on a Western blot. Although collagenolytic assays are typically performed at 25 °C, no cleavage was detected after incubation for up to 2 days at room temperature (23 °C). This is consistent with an earlier study that showed MT1-MMP does not hydrolyse type I collagen at 25 °C [13], although other groups have demonstrated cleavage [12,14]. The assay temperature was therefore increased to 37 °C to allow more flexibility in the collagen strands that are more readily hydrolysed. ΔTM-MT1-MMP alone is not stable after prolonged incubation at 37 °C; however, in the presence of a substrate (or an inhibitor), the stability is significantly improved (results not shown).

It may be expected that if the active sites were the same, the catalytic domain alone would be a more efficient enzyme to hydrolyse single-stranded peptides due to hindrance by the haemopexin domain. This domain may limit enzyme flexibility, diffusion of peptide into the enzyme-active site or alternatively decrease effective substrate concentration by exosite binding. The activation energies for substrate **1** are consistent with k_{cat}/K_M values which may suggest enzyme flexibility or diffusion as possible reasons for the difference. The k_{cat}/K_M values for five similar single-stranded peptides were correlated between both forms of the enzyme. The k_{cat}/K_M value for triple-helical substrates will correspond to this fit if the enzyme hydrolyses these substrates in a manner similar to the single-stranded substrates. Although the absolute k_{cat}/K_M values were slightly higher for cdMT1-MMP, the values did not correlate with the single-stranded substrates. Therefore the haemopexin domain of MT1-MMP facilitates the hydrolysis of triple-helical peptide substrates, consistent with previous studies, indicating that the haemopexin domain of

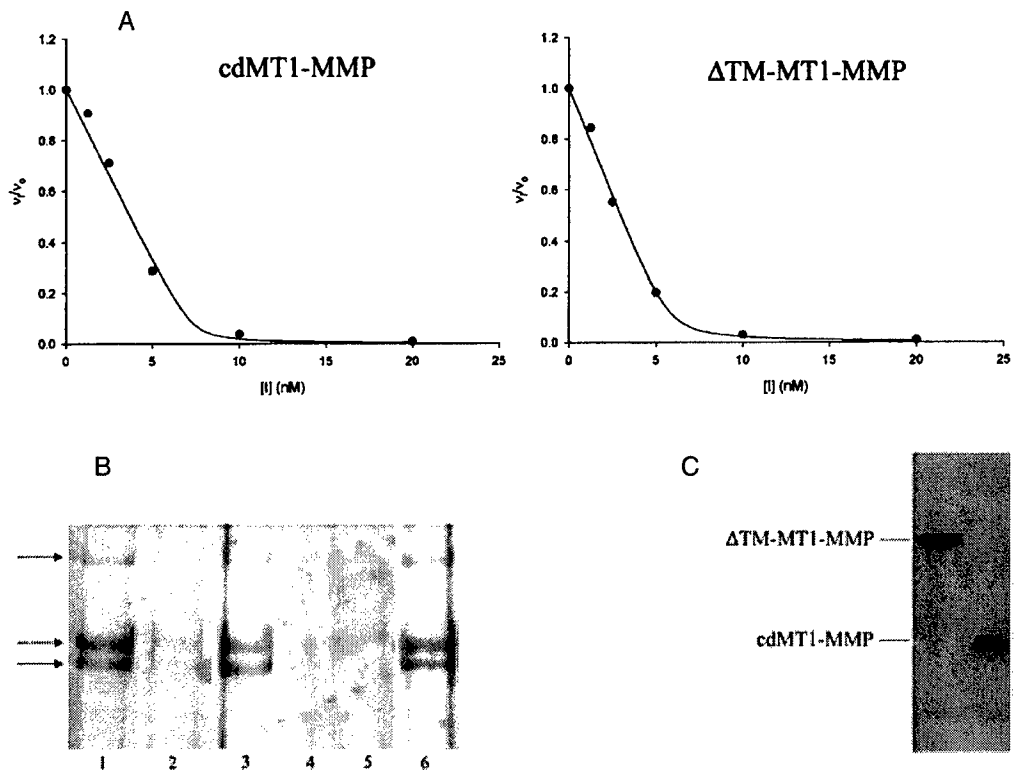

Figure 5 Enzyme titration and collagen cleavage

(A) The concentrations of active cdMT1-MMP and ΔTM-MT1-MMP were normalized by titration with TIMP-2 as described in the Materials and methods section: [E] = [I] at the *x*-intercept. **(B)** Collagen cleavage was verified for ΔTM-MT1-MMP with RTTI. Either ΔTM-MT1-MMP (lanes 2 and 4) or cdMT1-MMP (lanes 3 and 5) at 80 nM was incubated with 280 μg/ml RTTI (lanes 1–3 native; lanes 4–6 denatured by first boiling for 5 min) at 37 °C for 8 h. The reactions were stopped with 50 mM EDTA, 100 mM dithiothreitol and boiling for 5 min. The samples were analysed by SDS/PAGE (7 % gel) with silver staining. Lane 1 is native RTTI only and lane 6 is denatured RTTI only. **(C)** Western blot (SDS/PAGE, 12 % gel) of the purified enzymes shows one band for the ΔTM-MT1-MMP sample.

MT1-MMP modulates activity towards proteinaceous substrates [25].

Diastereomeric inhibitor pairs were utilized to probe the architecture of the enzyme-active site. Structural differences between the enzyme forms would be expected to be shown by different K_i ratios for inhibition by the pairs of stereoisomeric compounds tested. A correlation of 1 between the enzymes demonstrates that no significant differences were found at the active site. Although several groups have published the requirement of the haemopexin domain to hydrolyse native type I–III collagens, no previous report has addressed an active-site comparison for MT1-MMP with and without the haemopexin domain.

The triple-helical peptidase activities of collagenolytic enzymes (MMP-1, MMP-13 and MT1-MMP) exhibit noteworthy differences. MT1-MMP shows triple-helical peptidase activity much greater than either MMP-1 or MMP-13 [15]. The haemopexin domain of MMP-1 appears to have virtually no influence on triple-helical peptidase activity [15,26], unlike MT1-MMP. MMP-13 shows a far greater difference between single-stranded and triple-helical substrate hydrolysis compared with either MMP-1 or MT1-MMP [15,27]. Thus, although a number of MMP family members are classified as 'collagenolytic', their precise mechanisms for binding, distorting and hydrolysing triple-helical structures are almost certainly different in subtle, but as yet undefined, ways.

One important question remaining is how does the haemopexin domain influence the catalytic activity of MT1-MMP? It has been proposed that triple-helical peptidase and collagenase activity are distinguishable, as the catalytic domains of collagenases have the ability to cleave triple-helical peptides but not collagens [26]. The haemopexin domain may therefore be required for proper orientation and distortion of the collagen. Overall and co-workers [11] recently found that it is the linker region between the catalytic and haemopexin domain that is necessary for native type I collagen binding. The linker region may influence triple-helicase activity. Without knowing the three-dimensional structural organization of the linker and haemopexin domain, it is difficult to address specifically how the activities of MMPs are modulated by their structural motifs and domains.

We thank Professor L. Jack Windsor of Indiana University for providing us with purified human TIMP-2 protein and Janelle Lauer-Fields of Florida Atlantic University for synthesizing the triple-helical substrate. We are grateful to Dr Yunge Zhao for isolation of RTTI, and Robert Newcomer, Dr Hyun I. Park and Dr Tiebang Kang for a critical reading of the manuscript and valuable discussions. This work was supported by a predoctoral fellowship award from D. O. D./U.S. Army Breast Cancer Research Program DAMD17-00-1-0243 (to D. R. H.), and grants from D. O. D./U. S. Army Prostate Cancer Research Program DAMD17-02-1-238, National Institutes of Health (NIH) CA78646 (to Q.-X. A. S.), CA77402 and CA98799 (to G. B. F.), a grant from the Molecular Design and Synthesis (MDS) Research Foundation (to M. A. S.), and by the Deutsche Forschungsgemeinschaft (DFG), Bonn (SFB 549, project A05 and DFG grant Ts 8-35/3) to H. T.

REFERENCES

1 McCawley, L. J. and Matrisian, L. M. (2001) Matrix metalloproteinases: they're not just for matrix anymore! Curr. Opin. Cell Biol. **13**, 534–540
2 Sato, H., Takino, T., Okada, Y., Cao, J., Shinagawa, A., Yamamoto, E. and Seiki, M. (1994) A matrix metalloproteinase expressed on the surface of invasive tumour cells. Nature (London) **370**, 61–65
3 Li, H., Bauzon, D. E., Xu, X., Tschesche, H., Cao, J. and Sang, Q.-X. A. (1998) Immunological characterization of cell-surface and soluble forms of membrane type 1 matrix metalloproteinase in human breast cancer cells and in fibroblasts. Mol. Carcinogen. **22**, 84–94
4 Yana, I. and Weiss, S. J. (2000) Regulation of membrane type-1 matrix metalloproteinase activation by proprotein convertases. Mol. Biol. Cell. **11**, 2387–2401
5 Sternlicht, M. D. and Werb, Z. (2001) How matrix metalloproteinases regulate cell behavior. Annu. Rev. Cell Dev. Biol. **17**, 463–516
6 Murphy, G. and Knäuper, V. (1997) Relating matrix metalloproteinase structure to function: why the 'hemopexin' domain? Matrix Biol. **15**, 511–518
7 Overall, C. M. (2002) Molecular determinants of metalloproteinase substrate specificity: matrix metalloproteinase substrate binding domains, modules, and exosites. Mol. Biotech. **22**, 51–86
8 Lauer-Fields, J. L., Juska, D. and Fields, G. B. (2002) Matrix metalloproteinases and collagen catabolism. Biopolymers **66**, 19–32
9 Mori, H., Tomari, T., Koshikawa, N., Kajita, M., Itoh, Y., Sato, H., Tojo, H., Yana, I. and Seiki, M. (2002) CD44 directs membrane-type 1 matrix metalloproteinase to lamellipodia by associating with its hemopexin-like domain. EMBO J. **21**, 3949–3959
10 Lehti, K., Lohi, J., Juntunen, M. M., Pei, D. and Keski-Oja, J. (2002) Oligomerization through hemopexin and cytoplasmic domains regulates the activity and turnover of membrane-type 1 matrix metalloproteinase. J. Biol. Chem. **277**, 8440–8448
11 Tam, E., Wu, Y. I., Butler, G. S., Stack, M. S. and Overall, C. M. (2002) Collagen binding properties of the membrane type-1 matrix metalloproteinase (MT1-MMP) hemopexin C domain. The ectodomain of the 44-kDa autocatalytic product of MT1-MMP inhibits cell invasion by disrupting native type I collagen cleavage. J. Biol. Chem. **277**, 39005–39014
12 Ohuchi, E., Imai, K., Fujii, Y., Sato, H., Seiki, M. and Okada, Y. (1997) Membrane type 1 matrix metalloproteinase digests interstitial collagens and other extracellular matrix macromolecules. J. Biol. Chem. **272**, 2446–2451
13 Pei, D. and Weiss, S. J. (1996) Transmembrane-deletion mutants of the membrane-type matrix metalloproteinase-1 process progelatinase A and express intrinsic matrix-degrading activity. J. Biol. Chem. **271**, 9135–9140
14 d'Ortho, M. P., Will, H., Atkinson, S., Butler, G., Messent, A., Gavrilovic, J., Smith, B., Timpl, R., Zardi, L. and Murphy, G. (1997) Membrane-type matrix metalloproteinases 1 and 2 exhibit broad-spectrum proteolytic capacities comparable to many matrix metalloproteinases. Eur. J. Biochem. **250**, 751–757
15 Lauer-Fields, J. L., Broder, T., Sritharan, T., Chung, L., Nagase, H. and Fields, G. B. (2001) Kinetic analysis of matrix metalloproteinase activity using fluorogenic triple-helical substrates. Biochemistry **40**, 5795–5803
16 Schwartz, M. A. and van Wart, H. E. (1995) Mercaptosulfide metalloproteinase inhibitors. U.S. Patent 5455262
17 Jin, Y., Ghaffari, M. A. and Schwartz, M. A. (2002) A practical synthesis of differentially-protected *cis*-1,2-cyclopentanedithiols and *cis*-3,4-pyrrolidinedithiols. Tetrahedron Lett. **43**, 7319–7321
18 Lichte, A., Kolkenbrock, H. and Tschesche, H. (1996) The recombinant catalytic domain of membrane-type matrix metalloproteinase-1 (MT1-MMP) induces activation of progelatinase A and progelatinase A complexed with TIMP-2. FEBS Lett. **397**, 277–282
19 Roderfeld, M., Büttner, F. H., Bartnik, E. and Tschesche, H. (2000) Expression of human membrane type 1 matrix metalloproteinase in Pichia pastoris. Protein Expr. Purif. **19**, 369–374
20 Park, H. I., Ni, J., Gerkema, F. E., Liu, D., Belozerov, V. E. and Sang, Q.-X. A. (2000) Identification and characterization of human endometase (matrix metalloproteinase-26) from endometrial tumour. J. Biol. Chem. **275**, 20540–20544
21 Park, H. I., Turk, B. E., Gerkema, F. E., Cantley, L. C. and Sang, Q.-X. A. (2002) Peptide substrate specificities and protein cleavage sites of human endometase/matrilysin-2/matrix metalloproteinase-26. J. Biol. Chem. **277**, 35168–35175
22 Morrison, J. F. (1969) Kinetics of the reversible inhibition of enzyme-catalysed reactions by tight-binding inhibitors. Biochim. Biophys. Acta **185**, 269–286
23 Riddles, P. W., Blakeley, R. L. and Zerner, B. (1979) Ellman's reagent: 5,5′-dithiobis(2-nitrobenzoic acid) – a re-examination. Anal. Biochem. **94**, 75–81
24 Sang, Q.-X. A., Jia, M.-C., Schwartz, M. A., Jaye, M. C., Kleinman, H. K., Ghaffari, M. A. and Luo, Y.-L. (2000) New thiol and sulfodiimine metalloproteinase inhibitors and their effect on human microvascular endothelial cell growth. Biochem. Biophys. Res. Commun. **274**, 780–786
25 Itoh, Y., Takamura, A., Ito, N., Maru, Y., Sato, H., Suenaga, N., Aoki, T. and Seiki, M. (2001) Homophilic complex formation of MT1-MMP facilitates proMMP-2 activation on the cell surface and promotes tumour cell invasion. EMBO J. **20**, 4782–4793
26 Lauer-Fields, J. L., Tuzinski, K. A., Shimokawa, K., Nagase, H. and Fields, G. B. (2000) Hydrolysis of triple-helical collagen peptide models by matrix metalloproteinases. J. Biol. Chem. **275**, 13282–13290
27 Knäuper, V., López-Otin, C., Smith, B., Knight, G. and Murphy, G. (1996) Biochemical characterization of human collagenase-3. J. Biol. Chem. **271**, 1544–1550

Received 16 July 2003/2 September 2003; accepted 8 October 2003
Published as BJ Immediate Publication 8 October 2003, DOI 10.1042/BJ20031067

[CANCER RESEARCH 64, 590–598, January 15, 2004]

Endometase/Matrilysin-2 in Human Breast Ductal Carcinoma *in Situ* and Its Inhibition by Tissue Inhibitors of Metalloproteinases-2 and -4: A Putative Role in the Initiation of Breast Cancer Invasion

Yun-Ge Zhao,[1] Ai-Zhen Xiao,[1] Hyun I. Park,[1] Robert G. Newcomer,[1] Mei Yan,[2] Yan-Gao Man,[3] Sue C. Heffelfinger,[2] and Qing-Xiang Amy Sang[1]

[1]Department of Chemistry and Biochemistry and Institute of Molecular Biophysics, Florida State University, Tallahassee, Florida; [2]Department of Pathology and Laboratory of Medicine, University of Cincinnati College of Medicine, Cincinnati, Ohio; and [3]Department of Gynecology and Breast Pathology, The Armed Forces Institute of Pathology, Washington, D.C.

ABSTRACT

Local disruption of the integrity of both the myoepithelial cell layer and the basement membrane is an indispensable prerequisite for the initiation of invasion and the conversion of human breast ductal carcinoma *in situ* (DCIS) to infiltrating ductal carcinoma (IDC). We previously reported that human endometase/matrilysin-2/matrix metalloproteinase (MMP) 26-mediated pro-gelatinase B (MMP-9) activation promoted invasion of human prostate carcinoma cells by dissolving basement membrane proteins (Y. G. Zhao *et al.*, J. Biol. Chem., *278:* 15056–15064, 2003). Here we report that tissue inhibitor of metalloproteinases (TIMP)-2 and TIMP-4 are potent inhibitors of MMP-26, with apparent K_i values of 1.6 and 0.62 nM, respectively. TIMP-2 and TIMP-4 also inhibited the activation of pro-MMP-9 by MMP-26 *in vitro*. The expression levels of MMP-26, MMP-9, TIMP-2, and TIMP-4 proteins in DCIS were significantly higher than those in IDC, atypical intraductal hyperplasia, and normal breast epithelia adjacent to DCIS and IDC by immunohistochemistry and integrated morphometry analysis. Double immunofluorescence labeling and confocal laser scanning microscopy revealed that MMP-26 was colocalized with MMP-9, TIMP-2, and TIMP-4 in DCIS cells. Higher levels of MMP-26 mRNA were also detected in DCIS cells by *in situ* hybridization.

INTRODUCTION

Matrix metalloproteinases (MMPs) are known to be associated with cancer cell invasion, growth, angiogenesis, inflammation, and metastasis (1, 2). MMP-26 is a novel enzyme that was recently cloned and characterized by our group (3) and others (4–6). It has several structural features characteristic of MMPs, including a signal peptide, a propeptide domain, and a catalytic domain with a conserved zinc-binding motif, but it lacks the hemopexin-like domain (3–6). A unique "cysteine switch" sequence in the prodomain, PHCGVPD as opposed to the conserved PRCG*XX*D sequence found in many other MMPs, keeps the enzyme latent.

MMP-26 mRNA is primarily expressed in cancers of epithelial origin, such as endometrial carcinomas (3, 7), prostate carcinomas (7), lung carcinomas (7), and their corresponding cell lines (3–6), and in a small number of normal adult tissues, such as the uterus (3, 5), placenta (4, 5), and kidney (6). Some parallels exist with MMP-7, which is also expressed epithelially and also lacks the hemopexin-like domain. We have also reported that the levels of *MMP-26 gene* and protein expression are higher in a malignant choriocarcinoma cell line (JEG-3) than in normal human cytotrophoblast cells (8). Recently, we found that the levels of MMP-26 protein in human prostate carcinomas from multiple patients were significantly higher than those in prostatitis, benign prostate hyperplasia, and normal prostate tissues (9). MMP-26 is capable of activating pro-MMP-9 by cleavage at the Ala^{93}-Met^{94} site of the pro-enzyme, and this activation facilitates the efficient cleavage of fibronectin (FN), promoting the invasion of highly invasive and metastatic androgen-repressed prostate cancer cells through FN or type IV collagen (9). The activation is prolonged but persistent, which is consistent with the process of tumor cell invasion. These findings indicate that MMP-26-mediated pro-MMP-9 activation may be one biochemical mechanism contributing to human carcinoma cell invasion *in vivo*.

MMP activities are inhibited by endogenous tissue inhibitors of metalloproteinases (TIMPs). Four mammalian TIMPs have been identified: (*a*) TIMP-1 (10); (*b*) TIMP-2 (11); (*c*) TIMP-3 (12); and (*d*) TIMP-4 (13). The hydrolytic activity of MMP-26 against synthetic peptides is blocked by TIMP-1, TIMP-2, and TIMP-4 (5, 6, 8), but the inhibitory potential of TIMP-1 is lower than that of TIMP-2 and TIMP-4 (5). TIMP-1 and TIMP-2 also inhibit the cleavage of denatured type I collagen (gelatin) by MMP-26 (6). TIMPs are expressed in human breast cancer cells (14–16). Here, we continue to explore the possible roles of MMP-26 and the coordination of MMP-26 with MMP-9, TIMP-2, and TIMP-4 in human breast carcinoma invasion.

In the present study, we showed that TIMP-2 and TIMP-4 completely inhibited the activation of pro-MMP-9 by MMP-26. The expressions of MMP-26, MMP-9, TIMP-2, and TIMP-4 proteins in human breast ductal carcinomas *in situ* (DCIS) were significantly higher than those in infiltrating ductal carcinoma (IDC), atypical intraductal hyperplasia (AIDH), and normal breast epithelia around the DCIS and IDC. Furthermore, MMP-26 was colocalized with MMP-9, TIMP-2, and TIMP-4 in human breast DCIS.

MATERIALS AND METHODS

Inhibition Assays of MMP-26 by TIMP-2 and TIMP-4. The quenched fluorescence peptide substrates, *Mca-Pro-Leu-Ala-Nva-Dpa-Ala-Arg-*NH_2 and *Mca-Arg-Pro-Lys-Pro-Val-Glu-Nva-Trp-Arg-Lys(Dnp)-*NH_2 were purchased from Calbiochem. The MMP-26 used in this experiment is recombinant and partially active. Briefly, MMP-26 was expressed in the form of inclusion bodies from transformed *Escherichia coli* cells as described previously (3). The inclusion bodies were isolated and purified using B-PER bacterial protein extraction reagent according to the manufacturer's instructions. The insoluble protein was dissolved in 8 M urea to ~5 mg/ml. The protein solution was diluted to ~100 μg/ml in 8 M urea and 10 mM DTT for 1 h; dialyzed in 4 M urea, 1 mM DTT, and 50 mM HEPES (pH 7.5) for at least 1 h; and then folded by dialysis in 1× HEPES buffer [50 mM HEPES, 0.2 M NaCl, 10 mM $CaCl_2$, and 0.01% Brij-35 (pH 7.5)] with 20 μM $ZnSO_4$ for 16 h. To enhance the activity of MMP-26, the folded enzyme was dialyzed twice for 24 h at 4°C in the folding buffer without Zn^{2+} ions. The total enzyme concentration was measured by UV absorption using ϵ_{280} = 57,130 M^{-1} cm^{-1}, which was

Received 6/30/03; revised 10/29/03; accepted 11/7/03.

Grant support: Department of Defense Congressionally Directed Medical Research Programs Grant DAMD17-02-1-0238, NIH Grant CA78646, American Cancer Society grant, Florida Division Grant F01FSU-1 (to Q-X. A. S.), Florida State University Research Foundation grant (to Q-X. A. S. and Y-G. Z.), and Department of Defense Congressionally Directed Medical Research Programs Grants DAMD17-01-0129 and DAMD17-01-0130 (to Y-G. M.).

The costs of publication of this article were defrayed in part by the payment of page charges. This article must therefore be hereby marked *advertisement* in accordance with 18 U.S.C. Section 1734 solely to indicate this fact.

Requests for reprints: Qing-Xiang Amy Sang, Department of Chemistry and Biochemistry, Florida State University, Chemistry Research Building DLC, Room 203, Tallahassee, Florida 32306-4390. Phone: (850) 644-8683; Fax: (850) 644-8281; E-mail: sang@chem.fsu.edu.

calculated using Genetics Computer Group software. The concentration of active MMP-26 was determined by active site titration with the tight-binding inhibitor GM-6001 as described previously (17). GM-6001 was the most potent inhibitor of MMP-26 tested, with a K_i^{app} of 0.36 nM (17). Because TIMPs are tight-binding and slow-binding inhibitors of MMPs, MMP-26 was incubated for 4 h with human TIMP-2 and TIMP-4 before the measurement of substrate hydrolysis to allow the enzyme and inhibitor to reach their binding equilibrium. Human fibroblast TIMP-2 was provided by Dr. L. Jack Windsor (Indiana University, Indianapolis, IN). Recombinant human TIMP-4 was purchased from R&D Systems (Minneapolis, MN). The concentrations of TIMPs ranged from 0.2 to 60 nM. The assay was initiated by the addition of a substrate stock solution (4 μl) prepared in 1:1 water and DMSO to an enzyme-inhibitor assay buffer (196 μl) for a final concentration of 1 μM. The release of the fluorogenic cleavage product was monitored by measuring fluorescence (excitation and emission wavelengths at 328 and 393 nm, respectively) with a Perkin-Elmer Luminescence Spectrophotometer LS 50B connected to a water bath with a temperature control. All kinetic experiments were conducted in 1× HEPES buffer. Fluorogenic peptide substrate assays were performed following the procedures we reported previously (17). To assess inhibition potency, the apparent inhibition constants (apparent K_i values) were determined by fitting the two trial data sets to the Morrison equation below (18) with nonlinear regression. In this equation, v_i is the initial rate of MMP-26 catalysis in the presence of inhibitor, and v_o is the initial rate without inhibitor. [E] and [I] are the initial enzyme and inhibitor concentrations, respectively, and K_i^{app} is the apparent inhibition constant.

$$\frac{v_i}{v_o} = 1 - \frac{([E] + [I] + K_i^{app}) - \sqrt{([E] + [I] + K_i^{app})^2 - 4[E][I]}}{2[E]}$$

Pro-MMP-9 Activation by MMP-26 and Inhibition of the Activation by TIMP-2 and TIMP-4. Zymography and silver staining were performed as reported previously (3, 7, 19, 20). MMP-26, pro-MMP-9, and active MMP-9 were purified in our laboratory (3, 21). The molar concentration ratios of TIMPs, MMP-26, and pro-MMP-9 were 10:1:4. Two metal chelators/metalloproteinase inhibitors, 1, 10-phenanthroline and EDTA, were used as controls. Briefly, MMP-26 was incubated in the presence or absence of different inhibitors (TIMPs, 1,10-phenanthroline, and EDTA) in 30 μl of 1× HEPES buffer at room temperature (25°C) for 4 h. Pro-MMP-9 was then added and incubated at 37°C for 20 h. For zymography, aliquots of the reaction solution were removed and treated with a nonreducing sample buffer. MMP-9 activity was analyzed by zymography on 9% SDS-polyacrylamide gels containing 1% gelatin (22). For silver staining, aliquots were removed and treated with a reducing sample buffer and boiled for 5 min. After electrophoresis on 9% SDS-polyacrylamide gels, the protein bands were visualized by silver staining (19).

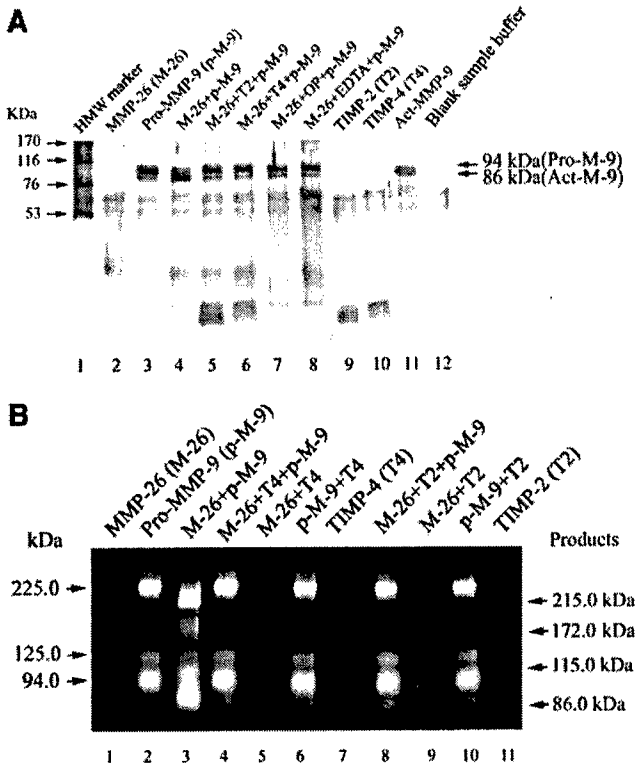

Fig. 2. Tissue inhibitor of metalloproteinases (TIMP)-2 and TIMP-4 inhibit pro-matrix metalloproteinase (MMP)-9 activation by MMP-26. *A*, pro-MMP-9 activation by MMP-26 was inhibited by both TIMP-2 and TIMP-4 (electrophoresis samples were treated under reducing conditions). MMP-26 activates pro-MMP-9, enhancing the 86-kDa band (*Lane 4*). This activation was completely blocked by adding TIMP-2 (*Lane 5*) or TIMP-4 (*Lane 6*). The inhibition by TIMP-2 and TIMP-4 is comparable with that of two broad-spectrum metal chelators/metalloproteinase inhibitors, 1,10-phenanthroline (*OP*) and EDTA (*Lanes 7* and *8*). *B*, zymogram assay of MMP-9 activation by MMP26 and inhibition by TIMP-2 and TIMP-4 (electrophoresis samples under nonreducing conditions). The 225-kDa band is a homodimer of pro-MMP-9, the 125-kDa band is a heterodimer of pro-MMP-9 and neutrophil gelatinase-associated lipocalin, and the 94-kDa band is a monomer of pro-MMP-9. MMP-26 activates pro-MMP-9 to generate new 215-, 172-, 115-, and 86-kDa active fragments (*Lane 3*). This activation was completely blocked by adding TIMP-4 (*Lane 4*) or TIMP-2 (*Lane 8*).

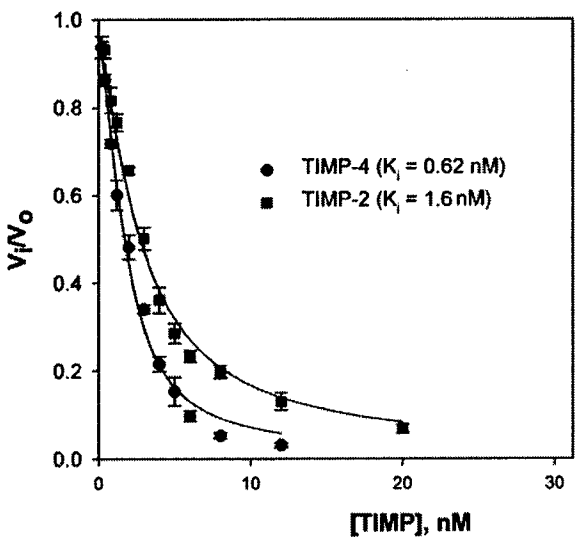

Fig. 1. Inhibition kinetics of matrix metalloproteinase 26 by tissue inhibitor of metalloproteinases (TIMP)-2 and TIMP-4. Matrix metalloproteinase 26 (2 nM) was incubated for 4 h in the presence of TIMP-2 or TIMP-4 at concentrations of 0.2–60 nM. The substrate hydrolysis assay was initiated by the addition of substrate stock solution. The data were fitted to the Morrison equation to calculate the apparent K_i values.

FN Cleavage Assay. MMP-26, pro-MMP-9, MMP-26-activated MMP-9, and TIMPs were prepared as described above. Active MMP-9, purified from human neutrophils (21), was used as a positive control. FN was incubated with MMP-26, pro-MMP-9, active MMP-9, or MMP-26 plus pro-MMP-9 in the presence or absence of TIMP-2 or TIMP-4 in 1× HEPES buffer at 37°C for 18 h. The molar concentration ratio of MMP-26:pro-MMP-9:FN:TIMP was approximately 1:4:10:10. Aliquots were removed and treated with a reducing sample buffer and boiled for 5 min. Samples were then loaded onto 9% polyacrylamide gels in the presence of SDS, electrophoresed, and subjected to silver staining (19).

***In Situ* Hybridization.** The DCIS samples were classified according to our previous reports (23, 24). Briefly, the formalin-fixed, paraffin-embedded samples were sectioned to 5-μm thickness and fixed onto slides. The full-length MMP-26 sense cDNA and antisense cDNA were amplified in pCR 3.1 and purified as described in our previous report (9). The sense and antisense plasmids were linearized with *Xho*I and *Xba*I, respectively. The sense and antisense digoxigenin-labeled RNA probes were generated by *in vitro* transcription with T7 polymerase. *In situ* hybridization was performed as per our previous report (22). Briefly, the paraffin-embedded sections (5 μm) were deparaffinized with xylene and treated with proteinase K solution [50 μg/ml in 0.2 M Tris-HCl (pH 7.5), 2 mM $MgCl_2$] for 15 min at room temperature. After prehybridization, the sections were hybridized to digoxigenin-labeled MMP-26 antisense cRNA probes for 18 h at 45°C and 100% humidity. The

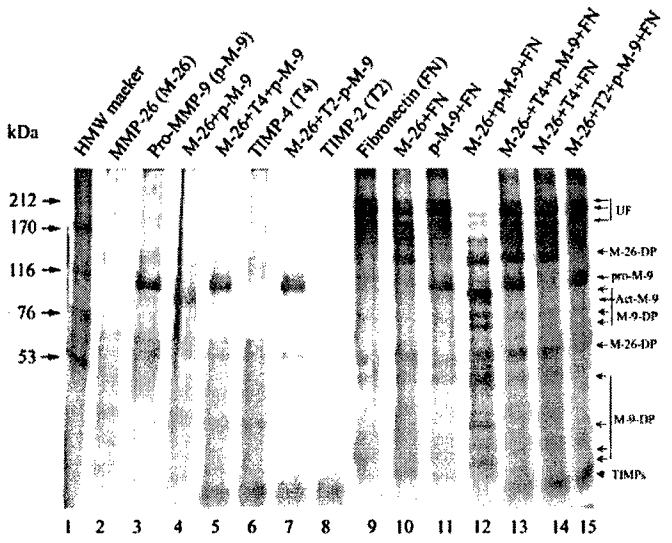

Fig. 3. Cleavage of fibronectin (FN) by matrix metalloproteinase (MMP)-9 and MMP-26. MMP-26 cleaved FN weakly, generating 125- and 58-kDa bands (*Lane 10*), pro-MMP-9 did not cleave FN (*Lane 11*), and MMP-26-activated MMP-9 (*Lane 4*) cleaved FN efficiently (*Lane 12*). Tissue inhibitor of metalloproteinases (TIMP)-4 weakly blocked FN cleavage by MMP-26 (*Lane 14*). Both TIMP-4 and TIMP-2 blocked pro-MMP-9 activation by MMP-26 (*Lanes 5* and *7*), which significantly diminished FN cleavage (*Lanes 13* and *15*). *UF*, uncleaved fibronectin; *M-26-DP*, MMP-26-degraded FN products; *M-9-DP*, MMP-9-degraded FN products; *pro-M-9*, pro-MMP-9; *Act-M-9*, activated MMP-9.

MMP-26 sense RNA probe was used under the same hybridization conditions as the control. After hybridization, the slides were washed with saline sodium citrate buffer and blocked [1% blocking reagents in Tris-buffered saline (pH 7.5)] for 30 min. The slides were then covered with anti-digoxigenin-alkaline phosphatase Fab fragments (1:400) for 2 h. Then the slides were stained with nitroblue tetrazolium/5-bromo-4-chloro-3-indolyl phosphate (Roche Applied Science, Mannheim, Germany). The expression signals were photographed under a microscope.

Immunohistochemistry. The human breast DCIS, IDC, and hyperplasia tissue samples were classified according to our reports (23–26). Immunohistochemistry was performed on consecutive sections according to our previous report (9). Briefly, the formalin-fixed, paraffin-embedded samples were sectioned to 5-μm thickness and fixed onto slides. After dewaxing and rehydrating, the slides were blocked with 3% BSA/Tris-buffered saline for 1 h at room temperature before incubation with affinity-purified, polyclonal rabbit antihuman MMP-26, MMP-9, TIMP-2, and TIMP-4 antibodies (all 25 μg/ml) at room temperature for 90 min. Sections were then incubated with alkaline phosphatase-conjugated secondary antirabbit antibody (1:500; Jackson ImmunoResearch, West Grove, PA) for 1 h at room temperature. The signals were detected with Fast-red (Sigma, St. Louis, MO). Purified preimmune IgGs from the same animal were used as negative controls.

Double Immunofluorescence and Confocal Laser Scanning Microscopy. Double immunofluorescence staining was performed as per our previous description (9). Briefly, the slides were incubated with a rabbit antihuman MMP-26 IgG (25 μg/ml) and a goat antihuman MMP-9 antibody (1:200 dilution; R&D Systems) or a mouse antihuman MMP-26 IgG (25 μg/ml; R&D Systems) and a rabbit antihuman TIMP-4 (25 μg/ml) or a rabbit antihuman TIMP-2 antibody (30 μg/ml) overnight at 4°C. The slides were then incubated with a goat antimouse-IgG IgG for 30 min at room temperature. Secondary Rhodamine Red-X-conjugated donkey antirabbit IgG and FITC-conjugated donkey antigoat IgG (Jackson ImmunoResearch) were subsequently applied at a 1:50 dilution for 30 min at room temperature. Slow Fade mounting medium was added to the slides, and fluorescence was analyzed using a Zeiss LSM510 Laser Scanning Confocal Microscope (Carl Zeiss, Heidelberg, Germany) equipped with a multi-photon laser. Images were processed for reproduction using Photoshop software version 6.0 (Adobe Systems, Mountainview, CA). Purified preimmune IgG and normal goat serum were used as negative controls.

Densitometric and Statistical Analysis. Four to 16 pictures were taken from the glandular epithelia after immunostaining by each of the four antibodies and the two preimmune IgGs in the DCIS, IDC, AIDH, and normal glands around the DCIS and IDC. Quantification of the immunostaining signals was performed using the Metamorph System (version 4.6r8; Universal Imaging Corp., Inc., West Chester, PA) according to our previous description (9). Briefly, an appropriate color threshold was determined (color model, HSI; hue, 230–255; saturation and intensity, full spectrum). The glandular epithelia

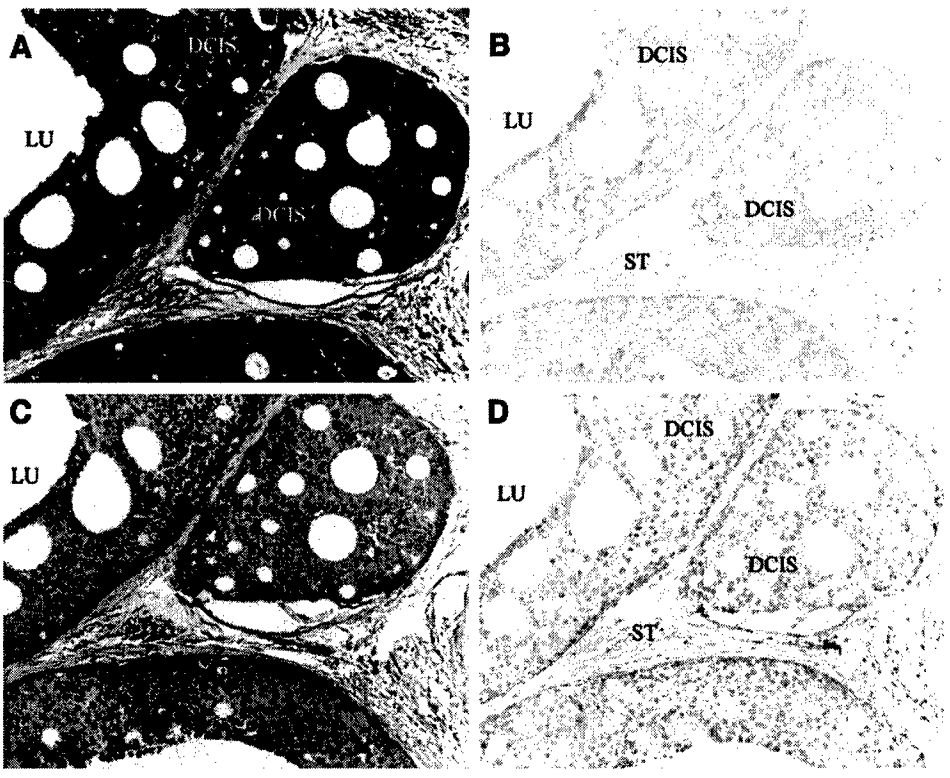

Fig. 4. Matrix metalloproteinase (MMP)-26 mRNA and protein expression in human mammary tissues. *A* and *B* are *in situ* hybridization to detect MMP-26 mRNA expression, and *C* and *D* are immunohistochemical staining to detect MMP-26 protein expression. *A*, MMP-26 antisense probe; *B*, MMP-26 sense probe; *C*, rabbit antihuman MMP-26 metallo domain IgG; *D*, pre-immune IgG. *Blue* indicates MMP-26 mRNA signals, and *red* indicates MMP-26 protein expression. Cells were counterstained lightly with hematoxylin for viewing of negatively stained epithelial and stromal cells in *C* and *D*. *DCIS*, ductal carcinoma *in situ*; *ST*, stroma; *LU*, lumen.

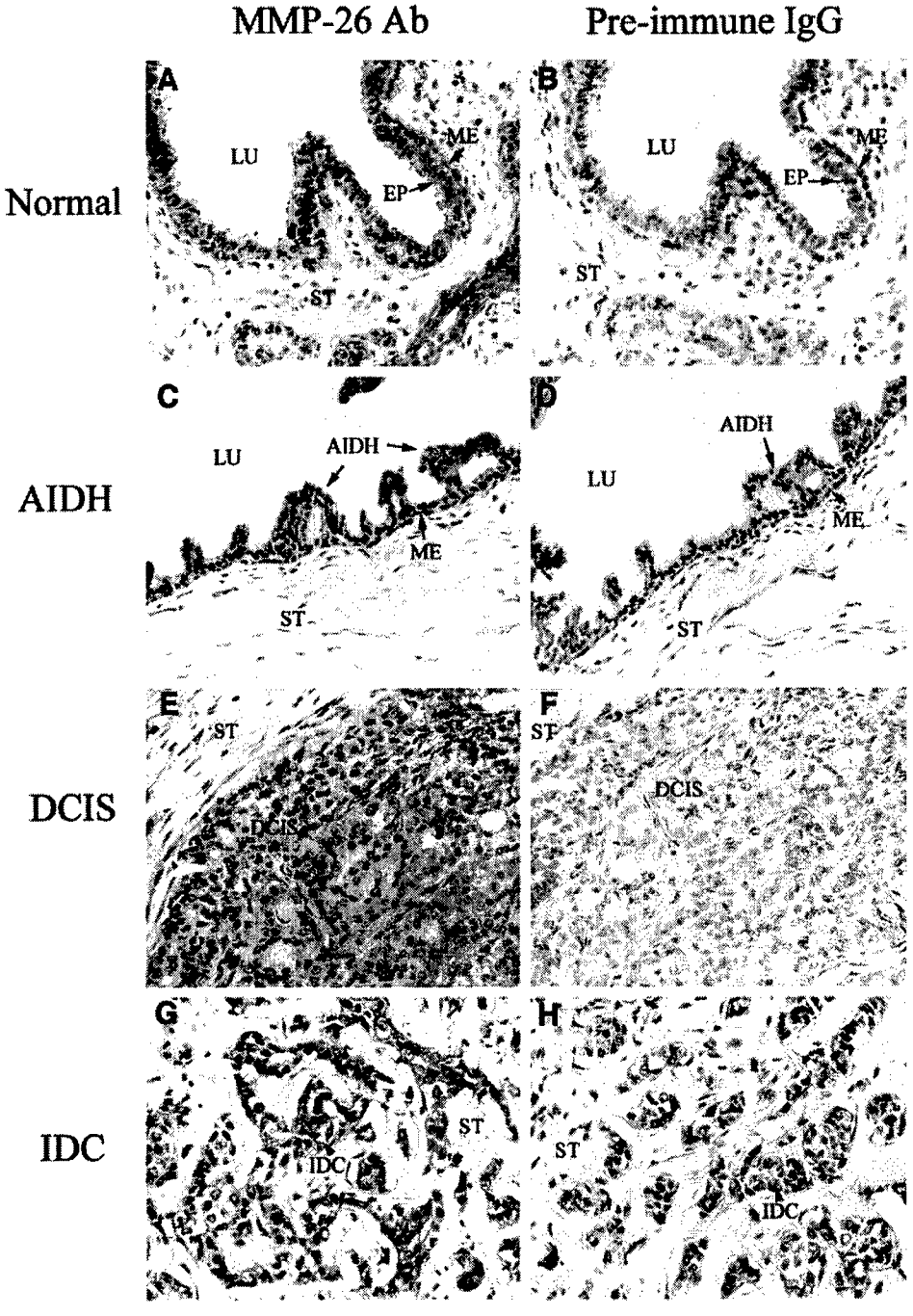

Fig. 5. Expression of matrix metalloproteinase (MMP)-26 protein in human mammary gland. Cells stained *red* indicate MMP-26 protein expression. All sections were counterstained lightly with hematoxylin for viewing negatively stained epithelial and stromal cells. *A, C, E,* and *G* are stained with anti-MMP-26 antibody, and *B, D, F,* and *H* are stained with pre-immune IgG. *A* and *B,* normal breast tissues; *C* and *D,* atypical intraductal hyperplasia (*AIDH*); *E* and *F,* breast ductal carcinoma *in situ* (*DCIS*); *G* and *H,* breast infiltrating ductal carcinoma (*IDC*). All figures are ×200 magnifications. *LU,* lumen; *EP,* epithelial cells; *ST,* stroma; *ME,* myoepithelial cells.

from each image were isolated into closed regions, and the signal areas and intensities of staining in compliance with the chosen parameters were measured by integrated morphometry analysis. The selected epithelial area was obtained by region measurement. The signal intensities were expressed as integrated absorbance (IOD, the sum of the optical densities of all pixels that make up the object). The ratio of the IOD to the selected epithelial area was determined, and the average ratios from each case were then calculated and used for statistical analysis. Statistical analysis of all samples was performed with the least significant difference correction of ANOVA for multiple comparisons. Data represent the mean ± SE, and $P < 0.05$ was considered significant.

RESULTS

Determination of the Apparent Inhibition Constants of TIMP-2 and TIMP-4 against MMP-26. The apparent K_i values of MMP-26 were measured and calculated to be 1.6 and 0.62 nM for TIMP-2 and TIMP-4, respectively (Fig. 1), using the Morrison equation (18). The apparent K_i values show that TIMP-4 is a slightly more potent inhibitor of MMP-26 than TIMP-2.

Activation of Pro-MMP-9 by MMP-26 and Inhibition of the Activation by TIMP-2 and TIMP-4. To explore the inhibition of MMP-26-mediated MMP-9 activation by TIMP-2 and TIMP-4, purified pro-MMP-9 and MMP-26 were incubated with these TIMPs, and the samples were subsequently analyzed by SDS-PAGE. MMP-26 cleaved pro-MMP-9 (94 kDa) to yield an enhanced active form 86-kDa band on a silver-stained gel under reducing conditions as per our recent report (Ref. 9; Fig. 2*A, Lane 4*). Zymography revealed that pro-MMP-9 presented as 225-, 125-, and 94-kDa gelatinolytic bands under nonreducing conditions. The 225-kDa band is a homodimer of pro-MMP-9, the 125-kDa band is a heterodimer of pro-MMP-9 and neutrophil gelatinase-associated lipocalin, and the 94-kDa band is a

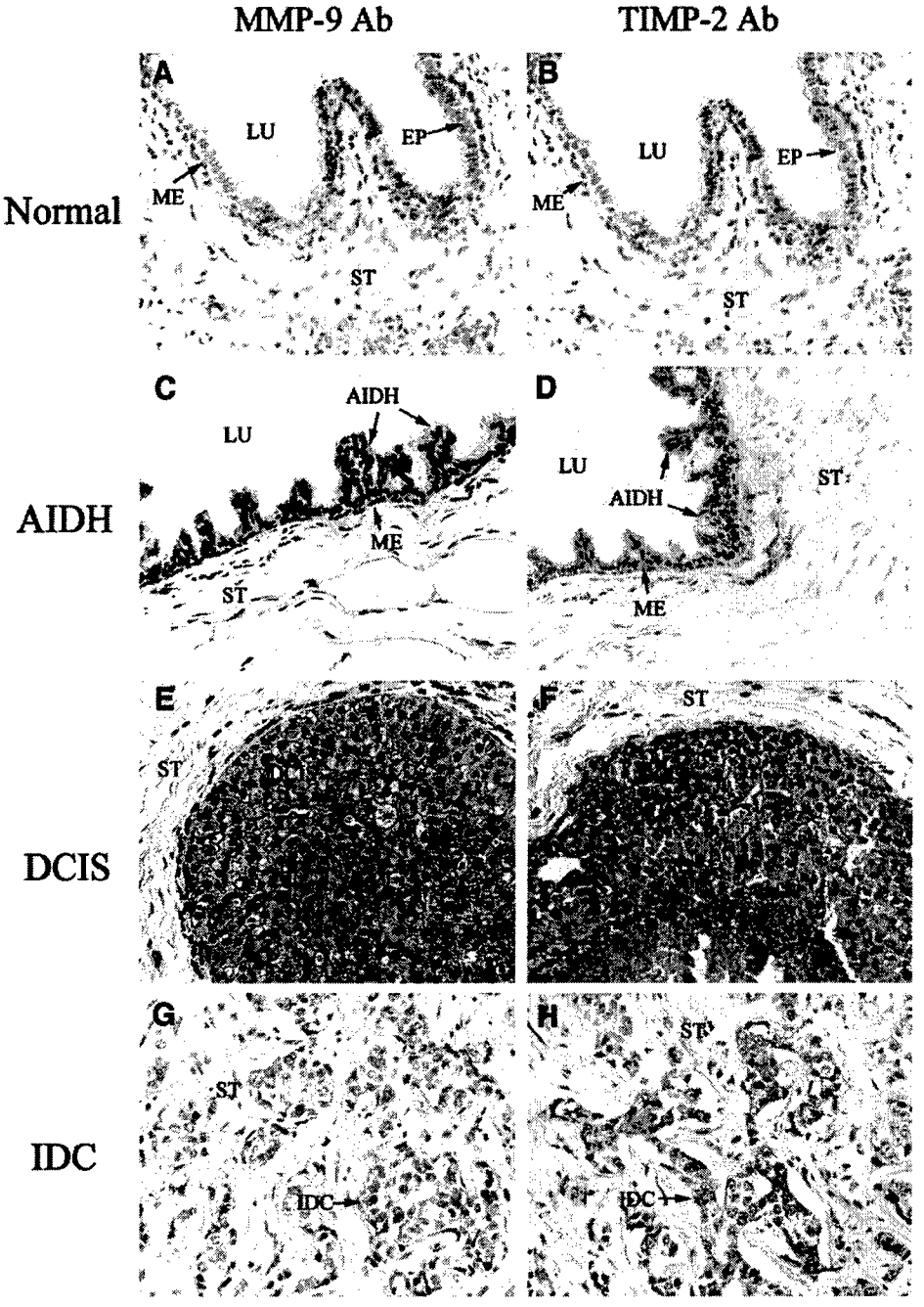

Fig. 6. Expression of matrix metalloproteinase (MMP)-9 and tissue inhibitor of metalloproteinases (TIMP)-2 proteins in human mammary gland. Cells stained *red* indicate MMP-9 or TIMP-2 protein expression. All sections were counterstained lightly with hematoxylin for viewing negatively stained epithelial and stromal cells. *A, C, E,* and *G* are stained with anti-MMP-9 antibody. *B, D, F,* and *H* are stained with TIMP-2 antibody. *A* and *B,* normal breast tissues; *C* and *D,* atypical intraductal hyperplasia (*AIDH*); *E* and *F,* ductal carcinoma *in situ* (*DCIS*); *G* and *H,* infiltrating ductal carcinoma (*IDC*). All figures are ×200 magnifications. *LU,* lumen; *EP,* epithelial cells; *ST,* stroma; *ME,* myoepithelial cells.

monomer of pro-MMP-9 (21, 27, 28). The new active 215-, 172-, 115-, and 86-kDa bands were generated after incubation with MMP-26 (Fig. 2*B, Lane 3*). The 215-, 115-, and 86-kDa bands are the active forms of the 225-, 125-, and 94-kDa forms, respectively. The 172-kDa band is a dimer of the 86-kDa forms. The activation of pro-MMP-9 by MMP-26 was completely inhibited by recombinant TIMP-2 and TIMP-4 (Fig. 2*A, Lanes 5* and *6*; Fig. 2*B, Lanes 4* and *8*). The blocking efficiencies of TIMP-2 and TIMP-4 were comparable with those of two broad-spectrum metal chelators/metalloproteinase inhibitors, 1,10-phenanthroline and EDTA (Fig. 2*A, Lanes 7* and *8*).

To further confirm the inhibition of MMP-26-mediated pro-MMP-9 activation by TIMP-2 and TIMP-4, *in vitro* FN cleavage assays were performed. MMP-26 slowly cleaved FN to generate 125- and 58-kDa bands (Fig. 3, *Lane 10*), whereas pro-MMP-9 did not cleave FN (Fig. 3, *Lane 11*). However, MMP-26-activated MMP-9 cleaved FN completely, generating at least seven new bands (Fig. 3, *Lane 12*). Both TIMP-2 and TIMP-4 completely blocked the activation of pro-MMP-9 by MMP-26, which subsequently resulted in inhibition of FN cleavage (Fig. 3, *Lanes 13* and *15*).

Expression of MMP-26 mRNA in Human Breast Tissues. *In situ* hybridization showed that MMP-26 mRNA was localized in human breast DCIS (Fig. 4*A*). On a serial section of the same tissue, MMP-26 protein was also detected in human breast DCIS (Fig. 4*C*). The MMP-26 sense probe and pre-immune IgG from the same animal as the MMP-26 antibody were used as controls (Fig. 4, *B* and *D*).

Expressions of MMP-26, MMP-9, TIMP-2, and TIMP-4 Proteins in Human Breast Tissues. MMP-26, MMP-9, TIMP-2, and TIMP-4 proteins were detected in human breast epithelia (Figs. 5–7). The expressions of the four proteins were extremely high in human breast DCIS (20 cases) cells (Fig. 5*E*; Fig. 6, *E* and *F*; Fig. 7*E*) but

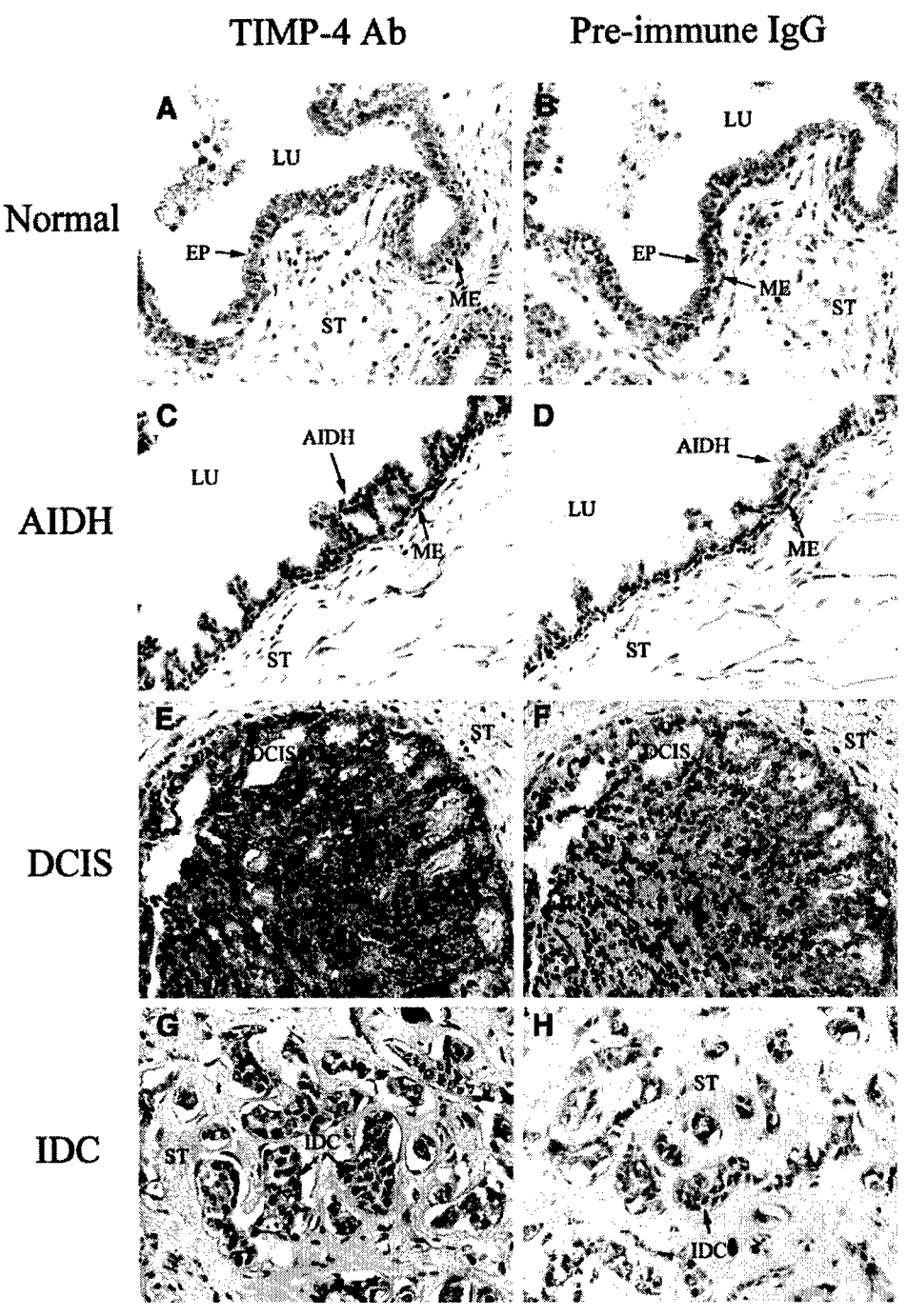

Fig. 7. Expression of tissue inhibitor of metalloproteinases (TIMP)-4 protein in human mammary gland. Cells stained *red* indicate TIMP-4 protein expression. All sections were counterstained lightly with hematoxylin for viewing negatively stained epithelial and stromal cells. *A, C, E,* and *G* are stained with antihuman TIMP-4 antibody. *B, D, F,* and *H* are stained with pre-immune IgG. *A* and *B,* normal breast tissues; *C* and *D,* atypical intraductal hyperplasia (*AIDH*); *E* and *F,* ductal carcinoma *in situ* (*DCIS*); *G* and *H,* infiltrating ductal carcinoma (*IDC*). All figures are ×200 magnifications. *LU,* lumen; *EP,* epithelial cells; *ST,* stroma; *ME,* myoepithelial cells.

very low in the normal glandular epithelial cells (25 cases) around DCIS and IDC (Fig. 5*A*; Fig. 6, *A* and *B*; Fig. 7*A*) and also in AIDH [15 cases (Fig. 5*C*; Fig. 6, *C* and *D*; Fig. 7*C*)]. Their expressions were substantially decreased in IDC [23 cases (Fig. 5*G*; Fig. 6, *G* and *H*; Fig. 7*G*)]. Statistical analysis revealed that the signal intensities of MMP-26, MMP-9, TIMP-2, and TIMP-4 proteins in DCIS were significantly higher than those in IDC, AIDH, and normal epithelia around the DCIS and IDC ($P < 0.05$ or $P < 0.01$; Fig. 8). There was no significant difference for the signals of MMP-26, MMP-9, TIMP-2, and TIMP-4 proteins among the normal epithelia around the DCIS and IDC, or in the AIDH and IDC samples ($P > 0.05$; Fig. 8). Pre-immune IgGs from the same animals as the MMP-26 or TIMP-4 antibodies were used as controls (Fig. 5, *B, D, F,* and *H*; Fig. 7, *B, D, F,* and *H*). There was no significant difference ($P > 0.05$) for the pre-immune IgG signals among the normal, AIDH, DCIS, and IDC samples.

Coexpression of MMP-26 and MMP-9 in Human Breast Carcinoma. To confirm the distributions of MMP-26, MMP-9, TIMP-2, and TIMP-4 within carcinoma cells, double immunofluorescence staining assays were performed in human breast DCIS samples. MMP-26 protein was localized mainly in the cytoplasm of the cancerous cells (Fig. 9*A, red*; Fig. 9*B, green*), which is consistent with our previous report (9). MMP-9 was localized both in the cytoplasm of the cancerous cells and at the cell surface, mainly on the cell membrane (Fig. 9*C, green*). The merged picture shows that MMP-26 and MMP-9 were coexpressed in the cytoplasm of the cancerous cells (Fig. 9*E, yellow*). The high magnification pictures in Fig. 9, *A, C,* and *E*, clearly demonstrate MMP-26 and MMP-9 colocalization (indicated by *ar-*

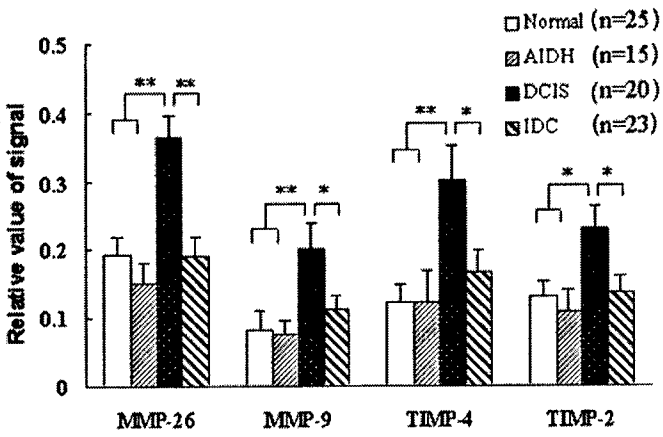

Fig. 8. Densitometric quantification analyses of matrix metalloproteinase 26, matrix metalloproteinase 9, tissue inhibitor of metalloproteinases 2, and tissue inhibitor of metalloproteinases 4 protein expression. The quantification analysis was described in "Materials and Methods." The epithelial regions were isolated, and the staining area and total selected area were obtained by Integrated Morphometry Analysis (IMA) and analyzed by one-way ANOVA with least significant difference (LSD) correction. Each value represents the mean ± SE. *, $P < 0.05$; **, $P < 0.01$. *Normal,* normal breast tissue; *AIDH,* atypical intraductal hyperplasia; *DCIS,* ductal carcinoma *in situ*; *IDC,* infiltrating ductal carcinoma; *n,* the number of cases.

rowheads). TIMP-4 is shown in Fig. 9*D* (*red*). MMP-26 and TIMP-4 were also coexpressed in the cytoplasm of the cancerous cells (Fig. 9*F, yellow*). MMP-26 and TIMP-2 were also colocalized in cancer cells, and minimal signals were detected in control tissues using purified pre-immune rabbit IgG and nonimmune goat sera (data not shown).

DISCUSSION

The epithelial component of the normal and noninvasive human breast is physically separated from the stroma by myoepithelial cells and the basement membrane, which is composed of a group of fibrous proteins, including type IV collagen, FN, laminin, and proteoglycans. The disruption of both the myoepithelial cell layer and the basement membrane is an essential prerequisite for the invasion of DCIS. In this present investigation, we found that the levels of MMP-26 and MMP-9 proteins in human breast DCIS were significantly higher than those in human breast IDC, normal mammary glands, and AIDH. MMP-26 and MMP-9 were colocalized in human breast DCIS cells. MMP-9 is a powerful enzyme associated with human breast cancer development and invasion (29, 30). Scorilas *et al.* (29) and Soini *et al.* (31) demonstrated that *MMP-9 mRNA* and protein were highly expressed in human breast carcinoma cells. MMP-9 protein is also expressed in the breast carcinoma cell lines MCF-7 (32, 33), SKBR-3 (34), MDA-MB-231 (35, 36), and MCF10A (36) and in normal breast epithelial cell lines HMT-3522 and T4-2 (32, 37). Our recent study (9) demonstrated that the level of MMP-26 protein in human prostate carcinomas is also significantly higher than those in prostatitis, benign prostate hyperplasia, and normal prostate tissues. MMP-26 and MMP-9 are not only coexpressed in human prostate carcinomas and in androgen-repressed prostate cancer cells, but they also promoted the invasion of androgen-repressed prostate cancer cells across FN or type IV collagen via MMP-26-mediated pro-MMP-9 activation.

Nguyen *et al.* (38) showed that active MMP-9 accumulates in the cytosol of human endothelial cells, where it is eventually used by invading pseudopodia, and it is possible that endogenous, self-activated MMP-26 serves as an activator for intracellular pro-MMP-9. The active form of MMP-9 may then be stored inside the cell, ready for rapid release when it is required to initiate invasion of human breast DCIS cells. Although DCIS is not invasive cancer, it may have the potential to develop into IDC, given time. The localization of *MMP-26 mRNA* and protein in carcinomas was confirmed by *in situ* hybridization and immunohistochemistry, providing evidence that MMP-26 is an epithelial cell-derived enzyme (3–6).

We demonstrated that the hydrolysis of synthetic peptides by MMP-26 is inhibited by TIMP-2 and TIMP-4, which is consistent with previous reports (5, 6, 8). TIMP-2 and TIMP-4 were also able to completely block MMP-9 activation by MMP-26, as well as the cleavage of FN by MMP-26-activated MMP-9. Therefore, one consequential function of TIMP-2 and TIMP-4 may be their inhibition of MMP-9 activation by MMP-26. TIMP-2 and TIMP-4 possess several distinct cellular functions, but their most widely appreciated biological functions are their roles in the inhibition of cell invasion *in vitro* (39–42) and their *in vivo* contributions to tumorigenesis (43, 44) and growth and metastasis (44–47). The underlying molecular mechanism for the tumor-suppressing activities of the TIMPs is thought to be dependent on their anti-MMP activities.

In our experiments, the expressions of TIMP-2 and TIMP-4 were all increased significantly in human breast DCIS but decreased in IDC, mimicking the expression of MMP-26 and MMP-9 in DCIS and IDC, which indicates that these four proteins are highly coordinated during human breast carcinoma development and progression. It may also suggest that remodeling of the extracellular matrix by MMP-26 and MMP-9 stimulates the expression of TIMP-2 and TIMP-4, implying self-regulation through a negative feedback loop. The consistently high expression of TIMP-2 and TIMP-4 proteins in human breast DCIS is in agreement with reports that the expression of TIMP-2 and TIMP-4 in human breast carcinomas is increased (14, 16,

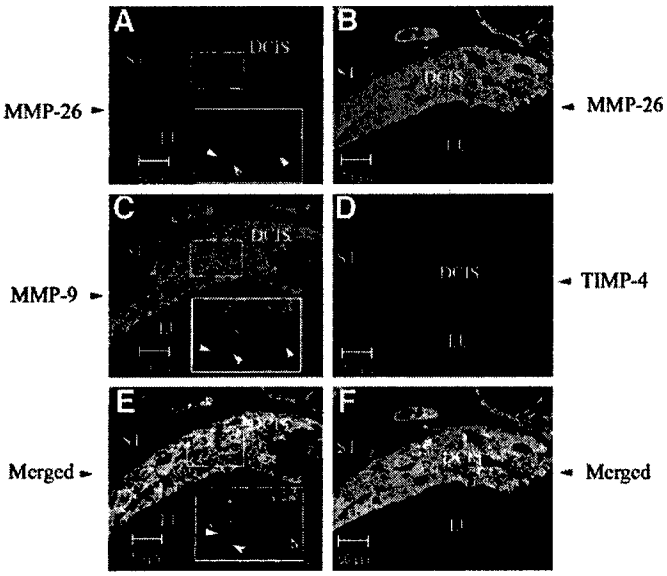

Fig. 9. Coexpression of matrix metalloproteinase (MMP)-26 with MMP-9 or tissue inhibitor of metalloproteinases (TIMP)-4 in human breast ductal carcinoma *in situ* (DCIS). In *A, C,* and *E,* the primary antibodies are rabbit antihuman MMP-26 IgG and goat antihuman MMP-9 IgG, the secondary antibodies are Rhodamine Red-X-conjugated donkey antirabbit IgG and FITC-conjugated donkey antigoat IgG. *A, red* indicates MMP-26 protein staining, which is localized mainly in the cytoplasm of DCIS cells. *C, green* indicates MMP-9 protein staining, which is localized mainly on the cell surface of the cancerous cells. *E,* merged images show a color shift to *orange-yellow,* indicating colocalization between MMP-26 and MMP-9 proteins in DCIS. In *B, D,* and *F,* the primary antibodies are mouse antihuman MMP-26 IgG and rabbit antihuman TIMP-4 IgG. After incubation with primary antibodies, the slides were incubated with goat antimouse-IgG IgG. The secondary antibodies are the same as those described in *A, C,* and *E. B, green* indicates MMP-26 protein staining, which is localized mainly in the cytoplasm of DCIS cells. *D, red* indicates TIMP-4 protein staining. *F,* merged images show a color shift to *orange-yellow,* indicating colocalization between MMP-26 and TIMP-4 proteins in DCIS. *Scale bars,* 50 μm. *ST,* stroma; *LU,* lumen.

39, 48). This may represent a compensatory response to the increased MMP-26- and MMP-9-mediated remodeling stimuli in DCIS in an attempt to reach a new balance between MMP-26/MMP-9 and TIMP-2/TIMP-4 to regulate degradation of the extracellular matrix and to suppress tumor progression by impeding MMP-26, MMP-9, and MMP-26-mediated MMP-9 activation. TIMP-2 and TIMP-4 may play multiple roles in human breast cancer in addition to inhibiting MMPs, including antiapoptotic activity and tumor-stimulating effects when administrated systemically (16). The new paradigms concerning the potential roles of TIMPs in suppressing or promoting tumor progression have been discussed previously (49).

The decreased MMP-26 and MMP-9 expression levels in IDC suggest that these two enzymes may play a role in the very early stages of DCIS invasion, but once the basement membrane has been breached, cancer cells become less dependent on the activities of MMP-26 and MMP-9. Nielsen *et al.* (50) demonstrated that MMP-9 immunostaining or *in situ* hybridization signals were not detected in human breast ductal carcinoma cells but were seen in tumor-infiltrating stromal cells including macrophages, neutrophils, and vascular pericytes. This indicates that MMP-9 may be transiently expressed in cells during the early stages of human breast carcinoma (DCIS), but not in the later stages of breast carcinoma (IDC). The controversy surrounding the expression of MMP-9 found in the literature (29, 31, 50), inclusive of our current findings, might also suggest that these different expression patterns arise from DCIS and IDC representing genetically distinct disease forms, raising the possibility that DCIS does not simply designate a transitory disease state that invariably leads to IDC.

Down-regulation of TIMPs contributed significantly to the tumorigenic and invasive potentials of cancer cells (43, 44). Decreased production of TIMP-2 resulted in increased MMP activity, leading to increased invasiveness by cancer cells (39). Therefore, maintenance of the balance between MMPs and TIMPs appears critical for the suppression of cancer cell invasion and metastasis. Once the balance between MMP-26/MMP-9 and TIMP-2/TIMP-4 in DCIS is destroyed, the inhibition by TIMP-2 and TIMP-4 may be inadequate to block the degradation of extracellular matrix components by MMP-26 and MMP-9 in DCIS, resulting in degradation of basement membrane components and initiation of the invasive processes of DCIS cells. MMP-26, MMP-9, TIMP-2, and TIMP-4 may be spatially and temporally expressed in the very early stages of DCIS invasion, whereas other enzymes/inhibitors are responsible for the late-stage invasion of IDC cells. Further investigations will provide a more complete understanding of the functions of MMP-26, MMP-9, and TIMPs in human breast cancer progression.

ACKNOWLEDGMENTS

We thank Dr. L. Jack Windsor of Indiana University for kindly providing us with TIMP-2 protein and the polyclonal anti-TIMP-2 antibody, Dr. Weiping Jiang of R&D Systems for the monoclonal anti-MMP-26 antibody, Dr. Jianzhou Wang of University of Oklahoma College of Medicine for critical review of the manuscript, and Sara C. Monroe at our laboratory at Florida State University for editorial assistance with manuscript preparation. We are also grateful to Kimberly Riddle and Jon Ekman at the Department of Biological Sciences Imaging Resources at Florida State University for their excellent assistance with confocal microscopy and integrated morphometry analysis.

REFERENCES

1. Sternlicht, M. D., and Werb, Z. How matrix metalloproteinases regulate cell behavior. Annu. Rev. Cell Dev. Biol., *17:* 463–516, 2001.
2. Egeblad, M., and Werb, Z. New functions for the matrix metalloproteinases in cancer progression. Nat. Rev. Cancer, *2:* 163–176, 2002.
3. Park, H. I., Ni, J., Gerkema, F. E., Liu, D., Belozerov, V. E., and Sang, Q. X. Identification and characterization of human endometase (matrix metalloproteinase-26) from endometrial tumor. J. Biol. Chem., *275:* 20540–20544, 2000.
4. de Coignac, A. B., Elson, G., Delneste, Y., Magistrelli, G., Jeannin, P., Aubry, J. P., Berthier, O., Schmitt, D., Bonnefoy, J. Y., and Gauchat, J. F. Cloning of MMP-26. A novel matrilysin-like proteinase. Eur. J. Biochem., *267:* 3323–3329, 2000.
5. Uría, J. A., and López-Otín, C. Matrilysin-2, a new matrix metalloproteinase expressed in human tumors and showing the minimal domain organization required for secretion, latency, and activity. Cancer Res., *60:* 4745–4751, 2000.
6. Marchenko, G. N., Ratnikov, B. I., Rozanov, D. V., Godzik, A., Deryugina, E. I., and Strongin, A. Y. Characterization of matrix metalloproteinase-26, a novel metalloproteinase widely expressed in cancer cells of epithelial origin. Biochem. J., *356:* 705–718, 2001.
7. Marchenko, G. N., Marchenko, N. D., Leng, J., and Strongin, A. Y. Promoter characterization of the novel human matrix metalloproteinase-26 gene: regulation by the T-cell factor-4 implies specific expression of the gene in cancer cells of epithelial origin. Biochem. J., *363:* 253–262, 2002.
8. Zhang, J., Cao, Y. J., Zhao, Y. G., Sang, Q. X., and Duan, E. K. Expression of matrix metalloproteinase-26 and tissue inhibitor of metalloproteinase-4 in human normal cytotrophoblast cells and a choriocarcinoma cell line, JEG-3. Mol. Hum. Reprod., *8:* 659–666, 2002.
9. Zhao, Y. G., Xiao, A. Z., Newcomer, R. G., Park, H. I., Kang, T., Chung, L. W., Swanson, M. G., Zhau, H. E., Kurhanewicz, J., and Sang, Q. X. Activation of pro-gelatinase B by endometase/matrilysin-2 promotes invasion of human prostate cancer cells. J. Biol. Chem., *278:* 15056–15064, 2003.
10. Carmichael, D. F., Sommer, A., Thompson, R. C., Anderson, D. C., Smith, C. G., Welgus, H. G., and Stricklin, G. P. Primary structure and cDNA cloning of human fibroblast collagenase inhibitor. Proc. Natl. Acad. Sci. USA, *83:* 2407–2411, 1986.
11. Stetler-Stevenson, W. G., Brown, P. D., Onisto, M., Levy, A. T., and Liotta, L. A. Tissue inhibitor of metalloproteinases-2 (TIMP-2) mRNA expression in tumor cell lines and human tumor tissues. J. Biol. Chem., *265:* 13933–13938, 1990.
12. Uria, J. A., Ferrando, A. A., Velasco, G., Freije, J. M., and Lopez-Otin, C. Structure and expression in breast tumors of human TIMP-3, a new member of the metalloproteinase inhibitor family. Cancer Res., *54:* 2091–2094, 1994.
13. Greene, J., Wang, M., Liu, Y. E., Raymond, L. A., Rosen, C., and Shi, Y. E. Molecular cloning and characterization of human tissue inhibitor of metalloproteinase 4. J. Biol. Chem., *271:* 30375–30380, 1996.
14. Remacle, A., McCarthy, K., Noel, A., Maguire, T., McDermott, E., O'Higgins, N., Foidart, J. M., and Duffy, M. J. High levels of TIMP-2 correlate with adverse prognosis in breast cancer. Int. J. Cancer, *20:* 118–121, 2000.
15. Hurst, D. R., Li, H., Xu, X., Badisa, V. L., Shi, Y. E., and Sang, Q. X. Development and characterization of a new polyclonal antibody specifically against tissue inhibitor of metalloproteinases 4 in human breast cancer. Biochem. Biophys. Res. Commun., *281:* 166–171, 2001.
16. Jiang, Y., Wang, M., Celiker, M. Y., Liu, Y. E., Sang, Q. X., Goldberg, I. D., and Shi, Y. E. Stimulation of mammary tumorigenesis by systemic tissue inhibitor of matrix metalloproteinase 4 gene delivery. Cancer Res., *61:* 2365–2370, 2001.
17. Park, H. I., Turk, B. E., Gerkema, F. E., Cantley, L. C., and Sang, Q-X. Peptide substrate specificities and protein cleavage sites of human endometase/matrilysin-2/matrix metalloproteinase-26. J. Biol. Chem., *277:* 35168–35175, 2002.
18. Morrison, J. F. Kinetics of the reversible inhibition of enzyme-catalysed reactions by tight-binding inhibitors. Biochim. Biophys. Acta, *185:* 269–286, 1969.
19. Zhao, Y. G., Wei, P., and Sang, Q. X. Inhibitory antibodies against endopeptidase activity of human adamalysin 19. Biochem. Biophys. Res. Commun., *289:* 288–294, 2001.
20. Patterson, B. C., and Sang, Q. A. Angiostatin-converting enzyme activities of human matrilysin (MMP-7) and gelatinase B/type IV collagenase (MMP-9). J. Biol. Chem., *272:* 28823–28825, 1997.
21. Sang, Q. X., Birkedal-Hansen, H., and Van Wart, H. E. Proteolytic and nonproteolytic activation of human neutrophil progelatinase B. Biochim. Biophys. Acta, *1251:* 99–108, 1995.
22. Zhao, Y. G., Xiao, A. Z., Cao, X. M., and Zhu, C. Expression of matrix metalloproteinase-2, -9 and tissue inhibitors of metalloproteinase-1, -2, -3 mRNAs in rat uterus during early pregnancy. Mol. Reprod. Dev., *62:* 149–158, 2002.
23. Heffelfinger, S. C., Yassin, R., Miller, M. A., and Lower, E. Vascularity of proliferative breast disease and carcinoma *in situ* correlates with histological features. Clin. Cancer Res., *2:* 1873–1878, 1996.
24. Heffelfinger, S. C., Yassin, R., Miller, M. A., and Lower, E. E. Cyclin D1, retinoblastoma, p53, and Her2/neu protein expression in preinvasive breast pathologies: correlation with vascularity. Pathobiology, *68:* 129–136, 2000.
25. Moinfar, F., Man, Y. G., Lininger, R. A., Bodian, C., Tavassoli, F. A. Use of keratin 35βE12 as an adjunct in the diagnosis of mammary intraepithelial neoplasia-ductal type-benign and malignant intraductal proliferations. Am. J. Surg. Pathol., *23:* 1048–1058, 1999.
26. Bratthauer, G. L., Moinfar, F., Stamatakos, M. D., Mezzetti, T. P., Shekitka, K. M., Man, Y. G., and Tavassoli, F. A. Combined E-cadherin and high molecular weight cytokeratin immunoprofile differentiates lobular, ductal, and hybrid mammary intraepithelial neoplasias. Hum. Pathol., *33:* 620–627, 2002.
27. Tschesche, H., Zolzer, V., Triebel, S., and Bartsch, S. The human neutrophil lipocalin supports the allosteric activation of matrix metalloproteinases. Eur. J. Biochem., *268:* 1918–1928, 2001.
28. Yan, L., Borregaard, N., Kjeldsen, L., and Moses, M. A. The high molecular weight urinary matrix metalloproteinase (MMP) activity is a complex of gelatinase B/MMP-9 and neutrophil gelatinase-associated lipocalin (NGAL). Modulation of MMP-9 activity by NGAL. J. Biol. Chem., *276:* 37258–37265, 2001.

29. Scorilas, A., Karameris, A., Arnogiannaki, N., Ardavanis, A., Bassilopoulos, P., Trangas, T., and Talieri, M. Overexpression of matrix-metalloproteinase-9 in human breast cancer: a potential favourable indicator in node-negative patients. Br. J. Cancer, *84:* 1488–1496, 2001.
30. Rolli, M., Fransvea, E., Pilch, J., Saven, A., Felding-Habermann, B. Activated integrin $\alpha_v\beta_3$ cooperates with metalloproteinase MMP-9 in regulating migration of metastatic breast cancer cells. Proc. Natl. Acad. Sci. USA, *100:* 9482–9487, 2003.
31. Soini, Y., Hurskainen, T., Hoyhtya, M., Oikarinen, A., Autio-Harmainen, H. 72 KD and 92 KD type IV collagenase, type IV collagen, and laminin mRNAs in breast cancer: a study by *in situ* hybridization. J. Histochem. Cytochem., *42:* 945–951, 1994.
32. Morgan, M. P., Cooke, M. M., Christopherson, P. A., Westfall, P. R., and McCarthy, G. M. Calcium hydroxyapatite promotes mitogenesis and matrix metalloproteinase expression in human breast cancer cell lines. Mol. Carcinog., *32:* 111–117, 2001.
33. Hazan, R. B., Phillips, G. R., Qiao, R. F., Norton, L., and Aaronson, S. A. Exogenous expression of N-cadherin in breast cancer cells induces cell migration, invasion, and metastasis. J. Cell Biol., *148:* 779–790, 2000.
34. Reddy, K. B., Krueger, J. S., Kondapaka, S. B., and Diglio, C. A. Mitogen-activated protein kinase (MAPK) regulates the expression of progelatinase B (MMP-9) in breast epithelial cells. Int. J. Cancer, *82:* 268–273, 1999.
35. Duivenvoorden, W. C., Hirte, H. W., and Singh, G. Transforming growth factor β1 acts as an inducer of matrix metalloproteinase expression and activity in human bone-metastasizing cancer cells. Clin. Exp. Metastasis, *17:* 27–34, 1999.
36. Toth, M., Sado, Y., Ninomiya, Y., and Fridman, R. Biosynthesis of α 2(IV) and α (IV) chains of collagen IV and interactions with matrix metalloproteinase-9. J. Cell. Physiol., *180:* 131–139, 1999.
37. Price, D. J., Avraham, S., Feuerstein, J., Fu, Y., and Avraham, H. K. The invasive phenotype in HMT-3522 cells requires increased EGF receptor signaling through both PI 3-kinase and ERK 1,2 pathways. Cell Commun. Adhes., *9:* 87–102, 2002.
38. Nguyen, M., Arkell, J., and Jackson, C. J. Active and tissue inhibitor of matrix metalloproteinase-free gelatinase B accumulates within human microvascular endothelial vesicles. J. Biol. Chem., *273:* 5400–5404, 1998.
39. Poulsom, R., Hanby, A. M., Pignatelli, M., Jeffery, R. E., Longcroft, J. M., Rogers, L., and Stamp, G. W. Expression of gelatinase A and TIMP-2 mRNAs in desmoplastic fibroblasts in both mammary carcinomas and basal cell carcinomas of the skin. J. Clin. Pathol., *46:* 429–436, 1993.
40. Albini, A., Melchiori, A., Santi, L., Liotta, L. A., Brown, P. D., and Stetler-Stevenson, W. G. Tumor cell invasion inhibited by TIMP-2. J. Natl. Cancer Inst. (Bethesda), *83:* 775–779, 1991.
41. Imren, S., Kohn, D. B., Shimada, H., Blavier, L., and DeClerck, Y. A. Overexpression of tissue inhibitor of metalloproteinases-2 retroviral-mediated gene transfer *in vivo* inhibits tumor growth and invasion. Cancer Res., *56:* 2891–2895, 1996.
42. Liu, Y. E., Wang, M., Greene, J., Su, J., Ullrich, S., Li, H., Sheng, S., Alexander, P., Sang, Q. A., and Shi, Y. E. Preparation and characterization of recombinant tissue inhibitor of metalloproteinase 4 (TIMP-4). J. Biol. Chem., *272:* 20479–20483, 1997.
43. Khokha, R., Waterhouse, P., Yagel, S., Lala, P. K., Overall, C. M., Norton, G., and Denhardt, D. T. Antisense RNA-induced reduction in murine TIMP levels confers oncogenicity on Swiss 3T3 cells. Science (Wash. DC), *243:* 947–950, 1989.
44. Mohanam, S., Wang, S. W., Rayford, A., Yamamoto, M., Sawaya, R., Nakajima, M., Liotta, L. A., Nicolson, G. L., Stetler-Stevenson, W. G., and Rao, J. S. Expression of tissue inhibitors of metalloproteinases: negative regulators of human glioblastoma invasion *in vivo*. Clin. Exp. Metastasis, *13:* 57–62, 1995.
45. DeClerck, Y. A., Perez, N., Shimada, H., Boone, T. C., Langley, K. E., and Taylor, S. M. Inhibition of invasion and metastasis in cells transfected with an inhibitor of metalloproteinases. Cancer Res., *52:* 701–708, 1992.
46. Wang, M., Liu, Y. E., Greene, J., Sheng, S., Fuchs, A., Rosen, E. M., and Shi, Y. E. Inhibition of tumor growth and metastasis of human breast cancer cells transfected with tissue inhibitor of metalloproteinase 4. Oncogene, *14:* 2767–2774, 1997.
47. Celiker, M. Y., Wang, M., Atsidaftos, E., Liu, X., Liu, Y. E., Jiang, Y., Valderrama, E., Goldberg, I. D., and Shi, Y. E. Inhibition of Wilms' tumor growth by intramuscular administration of tissue inhibitor of metalloproteinases-4 plasmid DNA. Oncogene, *20:* 4337–4343, 2001.
48. Ree, A. H., Florenes, V. A., Berg, J. P., Maelandsmo, G. M., Nesland, J. M., and Fodstad, O. High levels of messenger RNAs for tissue inhibitors of metalloproteinases (TIMP-1 and TIMP-2) in primary breast carcinomas are associated with development of distant metastases. Clin. Cancer Res., *3:* 1623–1628, 1997.
49. Jiang, Y., Goldberg, I. D., and Shi, Y. E. Complex roles of tissue inhibitors of metalloproteinases in cancer. Oncogene, *21:* 2245–2252, 2002.
50. Nielsen, B. S., Sehested, M., Kjeldsen, L., Borregaard, N., Rygaard, J., and Dano, K. Expression of matrix metalloprotease-9 in vascular pericytes in human breast cancer. Lab. Investig., *77:* 345–355, 1997.

Available online at www.sciencedirect.com

SCIENCE DIRECT

Experimental Cell Research 298 (2004) 285–295

Experimental Cell Research

www.elsevier.com/locate/yexcr

Evidence for disulfide involvement in the regulation of intramolecular autolytic processing by human adamalysin19/ADAM19☆

Tiebang Kang,[a,b,c] Harald Tschesche,[c] and Qing-Xiang Amy Sang[a,b,*]

[a] *Department of Chemistry and Biochemistry, Florida State University, Tallahassee, FL 32306-4390, USA*
[b] *Institute of Molecular Biophysics, Florida State University, Tallahassee, FL 32306-4390, USA*
[c] *Department of Biochemistry, Faculty of Chemistry, University Bielefeld, Bielefeld 33615, Germany.*

Received 17 February 2004, revised version received 6 April 2004
Available online 19 May 2004

Abstract

Human adamalysin 19 (a disintegrin and metalloproteinase 19, hADAM19) is activated by furin-mediated cleavage of the prodomain followed by an autolytic processing within the cysteine-rich domain at Glu^{586}–Ser^{587}, which occurs intramolecularly, producing an NH_2 terminal fragment (N-fragment) associated with its COOH-terminal fragment (C-fragment), most likely through disulfide bonds. When stable Madin-Darby canine kidney (MDCK) transfectants overexpressing soluble hADAM19 were treated with dithiothreitol (DTT) or with media at pH 6.5, 7.5, or 8.5, the secretion and folding of the enzyme were not affected. Autolytic processing was blocked by DTT and pH 6.5 media, which favor disulfide reduction, but was increased by pH 8.5 media, which promotes disulfide formation. Cys^{605}, Cys^{633}, Cys^{639}, and Cys^{643} of the C-fragment appear to be partially responsible for the covalent association between the C-fragment and the N-fragment. A new autolytic processing site at Lys^{543}–Val^{544} was identified in soluble mutants when these cysteine residues were individually mutated to serine residues. Shed fragments were also detectable in the media from MDCK cells stably expressing the full-length Cys633Ser mutant. Ilomastat/GM6001 inhibited hADAM19 with an IC_{50} of 447 nM, but scarcely affected the shedding process. The cysteine-rich domain likely forms disulfide bonds to regulate the autolytic processing and shedding of hADAM19.

Keywords: A disintegrin and metalloproteinase 19; Meltrin beta; Ectodomain shedding; Proteolytic processing; Enzyme activity regulation; Disulfide bonds; Site-directed mutagenesis; Structure–function analyses; Reducing agent; pH effect

Introduction

Ectodomain shedding, a process by which transmembrane proteins proteolytically release their extracellular domains, plays a critical role in many physiological and pathological conditions [1–3]. Numerous studies have shown that a disintegrin and metalloprotease (ADAMs), also called adamalysin/metalloprotease, disintegrin, cysteine-rich (MDC), such as tumor necrosis factor-alpha converting enzyme (TACE)/ADAM17, ADAM10/Kuzbanian (KUZ), ADAM9, ADAM19/MDC beta, and ADAM12/MDC alpha, are the predominant sheddases responsible for the shedding

Abbreviations: ADAM, a disintegrin and metalloproteinase; ADAMTS, a disintegrin and metalloproteinase with thrombospondin-like motifs; alpha2-M, alpha-2-macroglobulin; APP, amyloid precursor protein; CaM, calmodulin; D-CR, soluble ADAM19 containing the metalloproteinase and disintegrin domains; DMEM, Dulbecco's modified Eagle's medium; DTT, dithiothreitol; ECM, extracellular matrix; FBS, fetal bovine serum; IL-1R-II, interleukin 1 receptor II; MDC, Metalloprotease/Disintegrin/Cysteine-rich; MDCK, Madin-Darby canine kidney; NRG, neuregulin; pAb, polyclonal antibody; PBS, phosphate buffered saline; PKC, protein kinase C; PMA, phorbol-12 myristate 13-acetate; SDS-PAGE, sodium dodecyl sulfate polyacrylamide gel electrophoresis; TACE, tumor necrosis factor alpha convertase; TIMPs, tissue inhibitors of matrix metalloproteinases; TGF-alpha, transforming growth factor-alpha; TGN, *trans*-Golgi networks; TNF-alpha, tumor necrosis factor-alpha; W7, N-(6-aminohexyl)-5-chloro-1-naphthalenesulfonamide.

☆ Supported in part by grants from the National Institutes of Health CA78646, the DOD U.S. Army Medical Research Acquisition Activity DAMD17-02-1-0238, the American Cancer Society, Florida Division F01FSU-1, and the Florida State University Research Foundation (to Q-X. A. S.), as well as the Deutsche Forschungsgemeinschaft, Bonn, by the SFB 549, project A05 and the DFG-grant, Ts 8-35/3 (to H.T.).

* Corresponding author. Department of Chemistry and Biochemistry, Florida State University 203 DLC, Chemistry Research Building, Room 203 Tallahassee, FL 32306-4390. Fax: +1-850-644-8281.
E-mail address: sang@chem.fsu.edu (Q.-X. Amy Sang).
URL: http://www.chem.fsu.edu/editors/sang/sang.htm.

0014-4827/$ - see front matter © 2004 Elsevier Inc. All rights reserved.
doi:10.1016/j.yexcr.2004.04.022

of most molecules identified thus far, such as tumor necrosis factor-alpha (TNF-alpha), transforming growth factor-alpha (TGF-alpha), interleukin 1 receptor II (IL-1R-II), Notch and its ligand Delta, amyloid precursor protein (APP), heparin-binding epidermal growth factor (HB-EGF), mucin MUC1, and neuregulin-beta1(NRG-beta1) [3–5].

The activities of ADAMs are regulated at multiple levels, including transcription, translation, zymogen activation, and inhibition by tissue inhibitors of matrix metalloproteinases (TIMPs) [2–6]. The principle regulatory step is zymogen activation, with the predominant focus on the regulation of prodomain removal [6–18]. Synthesized as zymogens, many ADAMs undergo prodomain cleavage by either furin or furin-like proprotein convertases before they display any proteolytic activities, as in the cases of ADAM1, 9, 12, 15, 17, 19, a disintegrin and metalloproteinase with thrombospondin 1-like motifs (ADAM-TS) 1, 4, 12, [6–16], or by autolysis, as seen in ADAM8 [17] and ADAM28 [18]. However, in some ADAMs, the prodomains are involved in their catalytic activities. For example, deletion of the prodomain destroys the proteolytic activity of ADAM10 [19,20]. In the cases of ADAM12 and 17, the prodomains are not only inhibitors of the catalytic domain, but also appear to act as chaperones, facilitating secretion and folding of the ADAM proteins [12,21]. In addition, many mutations interfere with the folding or processing of ADAMs, resulting in a loss of proteolytic processing. For instance, replacement of the lone cysteine residue in the prodomain of ADAM9 with alanine abolished prodomain removal [12]; both His^{346} and His^{350} substitutions with alanines in the metalloproteinase domain of mouse ADAM19 abrogated the processing of its prodomain [22]; the Leu73Pro mutant of ADAM12 resulted in complete retention of ADAM12 in the endoplasmic reticulum (ER) and inhibition of its processing [14]; the soluble form of ADAM13 has never been converted into its mature form, indicating that the transmembrane domain, cytoplasmic domain, or both, are indispensable for the processing of the prodomain in ADAM13 [23]; and the removal of the disintegrin and cysteine-rich domains of TACE/ADAM17 resulted in secretion of the mature catalytic domain in association with the precursor (pro) domain [21].

Recently, there is increasing evidence that C-terminal truncation plays a critical role in the regulation of the proteolytic activity of ADAMs, as illustrated by ADAM8, 13, 19, and ADAM-TS4 [16,17,23–25]. This truncation produces active enzymes or functional fragments that may then act as sheddases, bind with integrins on the cell surface, or digest components of the extracellular matrix (ECM) [16,17,23–25]. However, the regulation of this processing remains to be uncovered. Smith et al. [26] showed that the cysteine-rich domain affects the proteolytic activity of ADAM13 in vivo, probably by an intramolecular interaction with its metalloproteinase domain, and that this model might be applied to other ADAMs. This prompted us to explore how this intramolecular interaction occurs in ADAMs, as we have previously demonstrated that an autolytic processing of hADAM19 at E^{586}-S^{587} within the cysteine-rich domain takes place in the secretory pathway [24]. Based on the fact that the E^{586}-S^{587} processed active N-fragment containing the metalloproteinase and disintegrin domains and a segment of the cysteine-rich domain is not released from the C-fragment containing the C-terminal segment of the cysteine-rich domain and epidermal growth factor (EGF)-like domain under non-reducing conditions [24], we hypothesized that interfragment disulfide bond(s) may play a crucial role in the processing of hADAM19. This report provides evidence that disulfide bonds most likely formed between cysteine residues in the N-fragment and those in the segment of the cysteine-rich domain of the processed C-fragment may be involved in the regulation of intracellular processing of hADAM19.

Materials and methods

Chemicals, cell lines, cell culture, and immunological reagents

All common laboratory chemicals, proteinase inhibitors, phorbol-12 myristate 13-acetate (PMA), N-(6-aminohexyl)-5-chloro-1-naphthalenesulphonamide (W7), and the anti-clusterin-alpha/beta (H-330) polyclonal antibody and its agarose conjugates were purchased from Sigma (St. Louis, MO). The anti-FLAG-M2 monoclonal antibodies were purchased from Santa Cruz Biotechnology (Santa Cruz, CA). The matrix metalloproteinase inhibitor Ilomastat (GM6001) was purchased from BACHEM (Philadephia, PA). Restriction enzymes were purchased from Promega (Madison, WI) or Invitrogen (Gaithersburg, MD). COS1, Madin Darby canine kidney (MDCK) cells and its derivatives were maintained as described [13,24]. Dulbecco's modified Eagle's medium (DMEM) was purchased from Invitrogen Gibco BRL (Gaithersburg, MD). Fetal bovine serum (FBS), penicillin G, and streptomycin were purchased from Life Technologies (Rockville, MD). Endoglycosidase H (Endo H) and alpha2-macroglobulin (alpha2-M) were purchased from Roche Molecular Biochemicals (Indianapolis, IN). The rabbit polyclonal hADAM19 antibody (anti-disintegrin domain, anti-Dis) was generated by our laboratory as reported [27].

Polymerase chain reaction (PCR) primers, mutagenesis, and expression constructs

All inserts tagged with FLAG at their C-terminus were cloned into pCR3.1uni, including wild type hADAM19 (F46), soluble hADAM19 (D52), D-E346A, D-E586D, D-CR (described in Ref. [24]), and all mutants used in this study. For D586 deleted from S587 to the end of the C-terminal: forward primer, 5′-ACC ATG CCA GGG GGC GCA GGC GCC-3′; reverse primer, 5′-CTC CAG GGG CCG GGC CTC

AGA G-3′. For the soluble C^{605} to S mutants (D-C605S): forward primer, 5′-CAG ATC CAG **TCC** CGG GGC ACC CAC-3′; reverse primer, 5′-GGT GCC CCG **GGA** CTG GAT CTG CC-3′. For the full-length and soluble C^{633} to S mutants (F-C633S and D-C633S): forward primer, 5′-GGA ACC AAG **TCT** GGC TAC AAC C-3′; reverse primer, 5′-GTT GTA GCC **AGA** CTT GGT TCC AG-3′. For the soluble C^{639} to S mutant (D-C639S): forward primer, 5′-C AAC CAT ATT **TCC** TTT GAG GGG CAG-3′; reverse primer, 5′-CCC CTC AAA **GGA** AAT ATG GTT G-3′. For the soluble C^{643} to S mutants (D-C643S): forward primer, 5′-GAG GGG CAG **TCC** AGG AAC ACC TC-3′; reverse primer, 5′-GGT GTT CCT **GGA** CTG CCC CTC AAA G-3′. For the double mutants, including E^{586} to D and C^{633} to S (D-C633S/E586D), E^{586} to D and C^{639} to S (D-C639S/E586D), E^{346} to A and C^{633} to S (F-C633S/E346A and D-C633S/E346A), and E^{346} to A and C^{639} to S (D-C639S/E346A), E^{346} to A and C^{605} to S (D-C605S/E346A), and E^{346} to A and C^{643} to S (D-C643S/E346A), we used D-E586D or D-E346A as the template and the primers for C^{633} to S, C^{639} to S, C^{605} to S, C^{643} to S, or C^{639} to S, respectively. All constructs were confirmed by DNA sequencing.

DNA transfection and generation of stable cell lines

COS1 cells were seeded in 24-well plates for 16–24 h at 80% confluence and transfected or co-transfected with the indicated plasmids using LipofectAMINE2000 according to the instructions provided by Invitrogen (Gaithersburg, MD). After 6–10 h, serum-free DMEM media and the indicated reagents were added and incubated for another 24 h. The conditioned media and cell lysates were then analyzed by Western blotting [13,24]. The same transfection procedure was performed to generate stable MDCK cell lines, and the selection for hADAM19 was begun in the presence of G418 (400 μg/ml) after transfection for 24 h. The conditioned media and/or cell lysates of the clones were subjected to Western blotting to confirm the expression of hADAM19 [13,24]. For co-culture cells, the indicated MDCK stable lines were equally mixed in the same wells overnight, followed by serum-free media for 24 h, and the media were then analyzed by Western blotting.

Western blotting

The experiments were carried out as described previously [13,24]. Briefly, cells were grown to 80% confluence and were treated as indicated. After centrifugation for 15 min at 14,000 × *g* and 4°C to clear any debris, the serum-free media were collected, treated with endoglycosidase H (Endo H) overnight if indicated using the provided protocol and prepared for SDS-PAGE. The cells were lysed with RIPA buffer (50 mM Tris, pH 7.5, 150 mM NaCl, 0.25% sodium deoxycholate, 0.1% NP-40, 1 mM phenyl-methyl-sulfonyl-fluoride, 1 mM of 1, 10-phenasrol, 10 μg/ml aprotinin, 10 μg/ml E64, and 10 μg/ml pepstatin A) for 15 min on ice. The supernatant was collected after centrifugation for 20 min at 14,000 × *g* and 4°C. After electrophoresis, the proteins were transferred onto nitrocellulose membranes, probed with anti-FLAG-M2 or anti-Dis, and developed as before [13,24].

Purification of soluble hADAM19 and co-incubation with purified proteins

D-CR and D-E346A were produced earlier in our laboratory; all proteins were purified on anti-FLAG-M2 affinity columns as described previously [24]. Briefly, cells from stable lines expressing soluble hADAM19, D586, or D-C633S/E586D, were grown to 100% confluence, washed twice with phosphate-buffered saline (PBS), and incubated for 48 h in serum-free media. The conditioned media were collected, centrifuged to clear any debris, and loaded onto an anti-M2 immunoaffinity column (1 ml of resuspended agarose) that had been prewashed with HEPES buffer. The bound materials were extensively washed with HEPES buffer, eluted with FLAG peptides, and collected in 500 μl fractions. The fractions were analyzed by Western blot using anti-hADAM19 antibodies or anti-FLAG-M2, and the protein concentration was quantified by absorbance at 280 nm. The fraction containing the highest concentration of the proteins of interest was characterized by protein N-terminal sequencing as described previously [13,24], and the fractions containing the most wild type or mutant hADAM19 proteins were used for the flourescamine assay or the co-incubation of purified proteins to test substrate cleavage. For the co-incubation of purified proteins, we mixed the purified D-E346A with D-CR or D586 equally at 100 ng/μl overnight, then the processing of D-E346A by D-CR or D586 was detected by Western blotting with anti-FLAG-M2 as above.

Results

Autolytic processing at E^{586}-S^{587} of hADAM19 is an intramolecular interaction

We recently developed a peptide substrate to determine the activity of hADAM19 by a fluorescamine assay, and reported that autolytic processing at E^{586}–S^{587} within the cysteine-rich domain is necessary for the proteolytic activities of hADAM19 against both this peptide substrate and α2-M [24]. To directly prove that the processed N-fragment containing the metalloproteinase and disintegrin domains and a part of the cysteine-rich domain is active, we generated a truncated form of hADAM19, from the N-terminal to E^{586}, tagged with a C-terminal FLAG tag (D586) (see Fig. 3), which was found to have the same activity as D-CR, containing the metalloproteinase and disintegrin domains of hADAM19, against the peptide substrate (24, data not shown). To determine if hADAM19 processing E^{586}-S^{587}

is an intermolecular or intramolecular interaction, we used several independent approaches. As shown in Fig. 1A, the inactive soluble form of hADAM19 (D-E346A) [24] was not processed by either of its active soluble forms, D586 and D-CR, when co-cultured with their stably expressing MDCK cells. Furthermore, both D586 and D-CR failed to process D-E346A when we performed a transient co-transfection using D-E346A with either D586 or D-CR in COS1 cells, as shown in Fig. 1B, or when we incubated the purified proteins together in vitro, using D-E346A with D586 or D-CR (data not shown). These results strongly argue that an intramolecular interaction is responsible for the processing of hADAM19 at E^{586}–S^{587}.

The formation of disulfide bonds affects the processing of hADAM19, but not its folding or its secretion

We have previously surmised that the N-fragment generated by the processing of hADAM19 at E^{586}–S^{587} may be associated with its processed C-fragment via one or more disulfide bonds [24]. To explore this possibility, we ran the conditioned media from MDCK cells stably expressing soluble hADAM19 (D52-5) side by side under either reducing or non-reducing conditions. As shown in Fig. 2A, the mature forms of hADAM19 were detected under both reducing and non-reducing conditions. However, the fragment at 26 kDa, representing the processed C-fragment at E^{586}–S^{587} of hADAM19, was detectable only under reducing conditions (Fig. 2A). Moreover, the processed N-fragments emerged together with the mature forms under non-reducing conditions (Fig. 2A). Therefore, it is highly possible that the processed C-fragment, containing a part of the cysteine-rich domain and EGF-like domain, forms disulfide bonds with the processed N-fragment, including the metalloproteinase and disintegrin domains and a segment of the cysteine-rich domain, in soluble hADAM19.

Given that the formation of disulfide bonds often plays an important role in enzyme folding, secretion, and activity, we incubated cells expressing D52 (D52-5) overnight in serum-free media containing DTT, a membrane permeable thiol reducing agent known to prevent disulfide bond formation in intact cells, including MDCK cells [28–30] and the conditioned media were then treated with endoglycosidase H (Endo H) for 16 h. As shown in Fig. 2B, DTT almost completely blocked the processing of soluble hADAM19, as the fragment at 26 kDa was indiscernable following DTT treatment (Fig. 2B). However, DTT had little or no effect on either the folding or secretion of soluble hADAM19, as the proteins in the media were comparable and resistant to Endo H (Fig. 2B), an enzyme that preferentially hydrolyzes N-glycanses of the high mannose type found predominantly in premature proteins.

To further verify the involvement of disulfide bond formation in the processing of soluble hADAM19, we incubated D52-5 overnight with serum-free media at pH 7.5, 8.5, or 6.5. As shown in Fig. 2C, the processing of soluble hADAM19 is increased at pH 8.5, which is more favorable for the formation of disulfide bonds than normal conditions (pH 7.5) (Fig. 2C) [31]. Conversely, there was little processing of soluble hADAM19 at pH 6.5, which significantly impairs the formation of disulfide bonds [31]. Once again, the protein levels are almost equal among the different treatments.

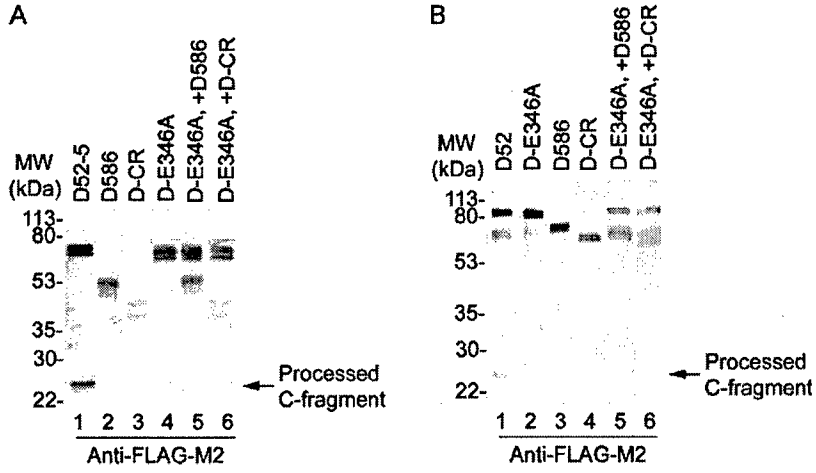

Fig. 1. Processing at E^{586}–S^{587} of hADAM19 occurs intramolecularly. (A) Active forms of hADAM19 fail to cleave its inactive form in the media using a co-culture system. MDCK cells stably expressing soluble inactive hADAM19 (D-E346A) were mixed equally in 24-well plates with MDCK cells transfected with the blank vector (lane 4), D586 (lane 5), or D-CR (lane 6) for 24 h in serum-free media, then the conditioned media were subjected to Western blotting with anti-FLAG-M2. The soluble stable lines, D52-5 (lanes 1), D586 (lane 2), or D-CR (lane 3) alone were used as controls. The processed C-fragments of soluble hADAM19 are indicated. Note that D-E346A is not processed by D586 or D-CR. (B) Active forms of hADAM19 lack the capacity to cleave its inactive form in the media using co-transfection into COS1 cells. COS1 cells were transfected with D52 (lane 1), D-E346A (lane 2), D586 (lane 3), D-CR (lane 4), D586 and D-E346A (lane 5), and D-CR and E346A (lane 6), followed by incubation for 24 h in serum-free media. The conditioned media were analyzed by Western blotting with anti-FLAG-M2. Note that D586 or D-CR is unable to process D-E346A, even they express in the same cell.

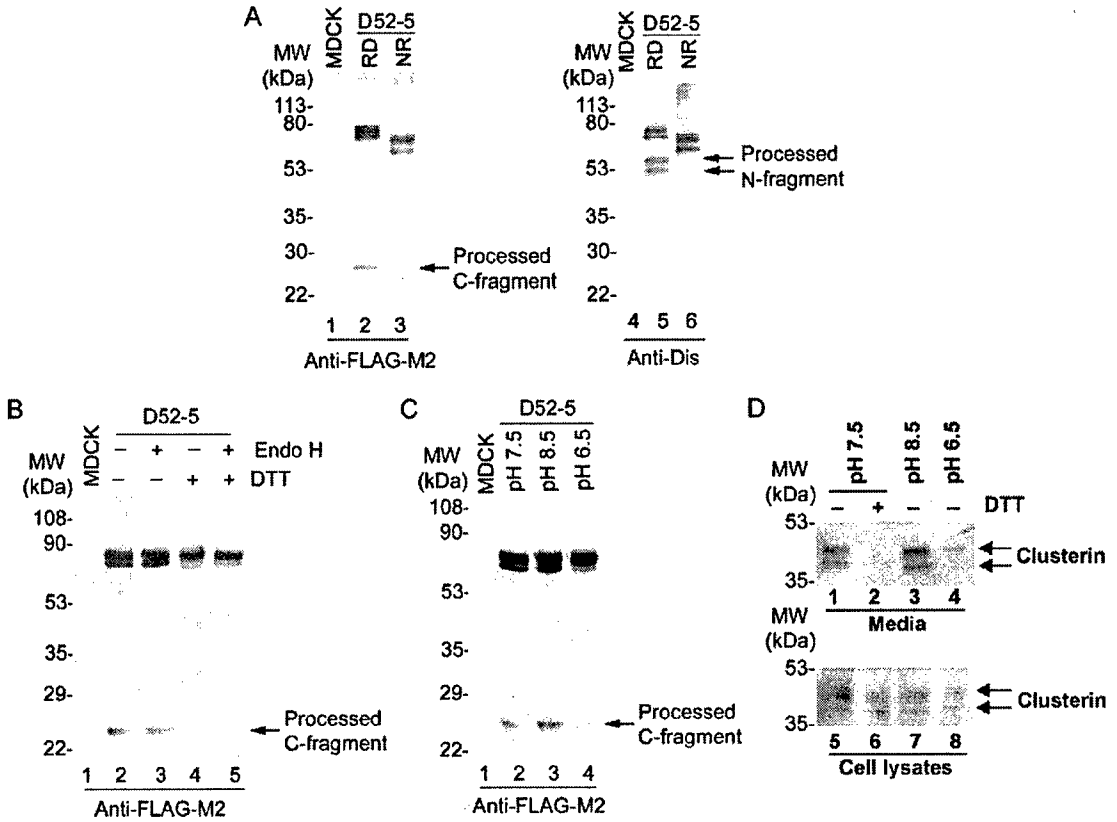

Fig. 2. Potential intramolecular disulfide bonds affect the activity of hADAM19, but not its folding or its secretion. (A) No detection of the processed forms under non-reducing conditions. MDCK cells stably expressing soluble hADAM19, D52-5, were incubated in serum-free media for 24 h, then the conditioned media was subjected to Western blotting by anti-FLAG-M2 (lanes 1–3) or a specific antibody against the disintegrin domain of hADAM19 (anti-Dis) (lanes 4–6) under reducing (lanes 1, 2, 4, 5) or non-reducing conditions (lanes 3, 6). The processed C-fragments or N-fragments of soluble hADAM19 are indicated. The medium from MDCK cells transfected with the blank vector was utilized as a control (lanes 1, 4). (B) The processing, but not the folding or secretion of hADAM19, is affected by DTT treatment. D52-5 were incubated in serum-free media with (lanes 4, 5) or without (lanes 1–3) 5 mM of DTT overnight, then the conditioned media was collected and treated with (lanes 3, 5) or without (lanes 1, 2, 4) 0.015 units of endoglycosidase H (Endo H) overnight before Western blotting by anti-FLAG-M2. The processed C-fragments of soluble hADAM19 are indicated. The media from MDCK cells transfected with the blank vector was utilized as a control (lane 1). (C) The pH of media affects the processing, but not the folding or secretion of hADAM19. D52-5 were incubated in serum-free media at pH 7.5 (lane 2), pH 8.5 (lane 3), or pH 6.5 (lane 4) overnight, then the conditioned media was subjected to Western blotting by anti-FLAG-M2. The processed C-fragments of soluble hADAM19 are indicated. The media from MDCK cells transfected with the blank vector was utilized as a control (lane 1). (D) DTT treatment and medium pH adjustment media affects the secretion of clusterin. D52-5 were incubated in serum-free media at pH 7.5 (lanes 1, 2, 5, 6), pH 8.5 (lanes 3, 7), or pH 6.5 (lanes 4, 8) with (lanes 2, 6) or without 5 mM of DTT for 16 h, then the conditioned media (lanes 1–4) and cell lysates (lanes 5–8) were subjected to Western blotting by anti-clusterin antibodies under reducing condition.

To confirm that DTT treatment or medium pH adjustment alters the rate of disulfide formation during progress through the secretory pathway, we examined clusterin protein levels in the media and cell lysates under these conditions, as clusterin is a highly expressed glycoprotein forming multiple disulfide bonds before its secretion in MDCK cells [32]. As shown in Fig. 2D, clusterin secretion is blocked by DTT treatment, which prevents the formation of intramolecular disulfide bonds by clusterin, consistent with results described previously by others [30]. The secretion of clusterin is dramatically impaired under the condition of pH 6.5, but not of pH 8.5, as medium at pH 6.5 likely impedes the formation of disulfide bonds in intact cells. On the other hand, there is no significant difference in total clusterin levels among the cell lysates under these conditions, as shown in Fig. 2D. Taken together, these data demonstrate that the formation of disulfide bonds is critical for the processing of soluble hADAM19, but are apparently nonessential to its secretion or its folding.

Interfragment disulfide bonds are responsible for the association of the N-fragment with the C-fragment of hADAM19 processed at E^{586}–S^{587}

The proteolytic activity of ADAM13 has recently been shown to be regulated by its cysteine-rich domain through intramolecular interactions with its metalloproteinase domain [26], and the processing of hADAM19 at E^{586}–S^{587} is also an intramolecular event (Fig. 1), after which the processed N-fragments associate with their C-fragments, most likely by disulfide bonds (Fig. 2A). We hypothesized that the disulfide bonds potentially formed between the

cysteine residues of the N-fragment and those within the fraction of the cysteine-rich domain retained by the processed C-fragment may play a critical role in the processing of hADAM19 at E^{586}-S^{587}. To evaluate this, we mutated the cysteine residues at C^{605}, C^{633}, C^{639}, and C^{643} to S within that region of soluble hADAM19 (Fig. 3), then transiently transfected these mutants into COS1 cells. The results shown in Fig. 4 reveal that all mutants produced a new C-fragment of approximately 32 kDa. The normal processing of the 26-kDa fragment at E^{586}–S^{587} remained unchanged in these mutants, although the protein levels in the conditioned media were different. When running these samples under non-reducing conditions, we found that the processed C-fragments at 26 and 32 kDa were not associated with their processed N-fragments, suggesting that the association of the N-fragment with the C-fragment of hADAM19 processed at E^{586}–S^{587} was destroyed by the disruption of one or more disulfide bonds that include C^{605}, C^{633}, C^{639}, or C^{643}.

The new processing at K^{543}–V^{544} is also autolytic, but independent of the processing at E586–S587

Since the processing at E^{586}–S^{587} of soluble hADAM19 is autolytic, we sought to determine if this new processing is also autolytic. Deactivating E^{346} to A mutations were generated in all C to S soluble mutants, then these double

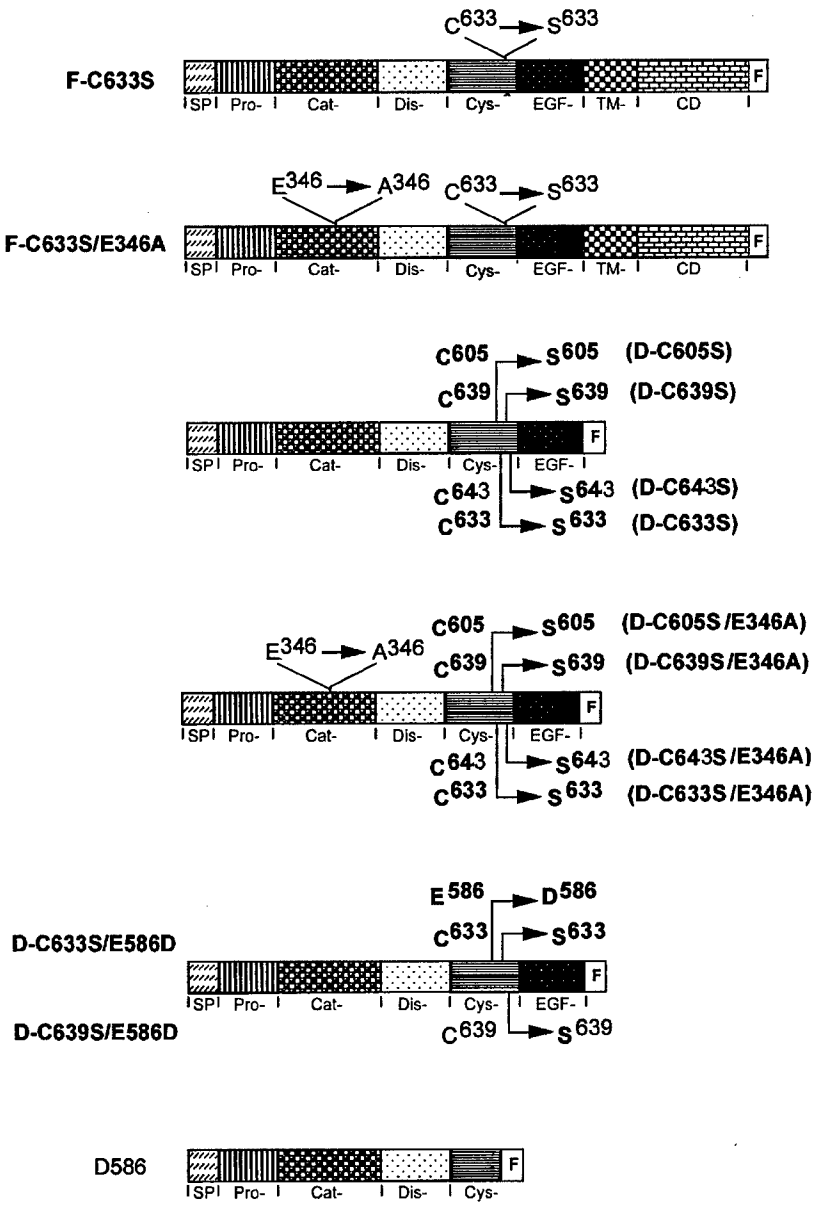

Fig. 3. A schematic illustration of the mutants of hADAM19 inserted in the expression vector pCR3.1. All of the constructs have a C-terminal FLAG tag. SP: Signal peptide; Pro-: Prodomain; Cat-: Catalytic domain; Dis-: Disintegrin domain; Cys-: Cysteine-rich domain; EGF-: EGF-like domain; TM: Transmembrane domain; CD: Cytoplasmic domain; F: FLAG tag.

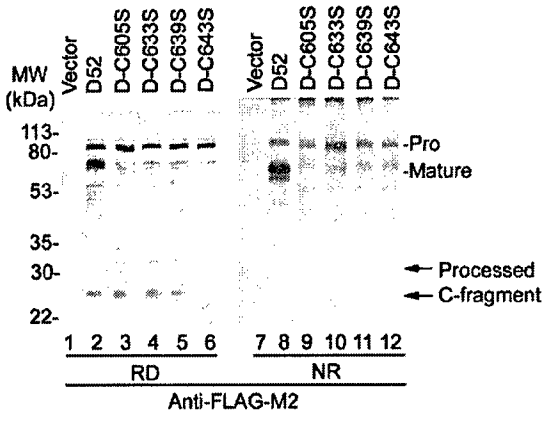

Fig. 4. Any one of the cysteine residues at C^{605}, C^{633}, C^{639}, or C^{643} is indispensable for the association of the processed N-fragment with its C-fragment in soluble hADAM19 in COS1 transfected cells. COS1 cells were transfected with blank vector (lanes 1, 7), D52 (lanes 2, 8), soluble mutants with C^{605} to S (D-C605S, lanes 3, 9), C^{633} to S (D-C633S, lanes 4, 10), C^{639} to S (D-C639S, lanes 5, 11), or C^{643} to S (D-C643S, lanes 6, 12), followed by incubation for 24 h in serum-free media. The conditioned media were analyzed by Western blotting with anti-FLAG-M2 under reducing (lanes 1–6) or non-reducing conditions (lanes 7–12). The pro- and mature forms, and the processed C-fragments of soluble hADAM19 are indicated. Note that any one of these Cys to Ser mutations induces two processing sites.

mutations were transiently transfected into COS1 cells. As shown in Fig. 5A, there is no processing detectable in any of the inactive forms of soluble hADAM19, demonstrating that the new processing induced by mutating these cysteine residues is also autocatalytic. Given that the autolytic processing at E^{586}–S^{587} of soluble hADAM19 is necessary for its proteolytic activity [24], and the new processing is also an autolysis (Fig. 5A), it was intriguing to determine if this new processing was dependent upon the processing at E^{586}-S^{587}. To address this issue, we made two soluble double mutants, C^{633} to S and E^{586} to D (D-C633S/E586D), and C^{639} to S and E^{586} to D (D-C639S/E586D) (Fig. 3) because there is rare processing at E^{586}-S^{587} when E^{586} is mutated to D^{586}, as described in our previous report [24]. We then performed transient transfection with these mutants into COS1 cells. As shown in Fig. 5B, the 32-kDa fragment was detectable in these double mutants, but the 26-kDa fragment, representing the processing at E^{586}-S^{587}, disappeared in these media, suggesting that the new processing is independent of, and not necessarily preceded or followed by, the processing at E^{586}–S^{587}.

To further confirm the results obtained from the COS1 cells, we chose C^{633} to S, C^{633} to S and E^{346} to A, and C^{633} to S and E^{586} to D as representative mutants to generate MDCK stable transfectants, designated D-C633S, D-C633S/E346A, and DC633S/E586D, respectively. As shown in Figs. 6A and B, the fragments at 26 and 32 kDa were clearly detectable by anti-FLAG-M2 in the media from D-C633S (Fig. 6A), but not from D-C633S/E346A (Fig. 6B). In striking contrast, the fragments at 32 kDa presented as the dominant forms in D-C633S/E586D (Fig. 6C). The protein levels in the conditioned media from these stable transfectants were nearly equal (Fig. 6). These results are consistent with those obtained in the COS1 transient transfection as shown in Figs. 4 and 5, confirming that disruption

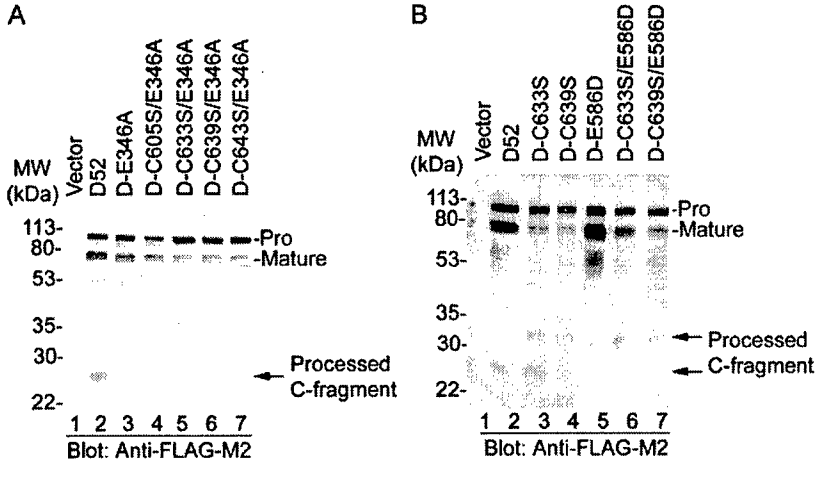

Fig. 5. The new processing induced by mutating the cysteines is autolytic, but independent of the normal processing at E^{586}–S^{587}. (A) The novel processing induced by cysteine residue mutation is autocatalytic. COS1 cells were transfected with blank vector (lane 1), D52 (lane 2), D-E346A (lane 3), soluble mutants with C^{605} to S and E^{346} to A (D-C605S/E346A, lane 4), C^{633} to S and E^{346} to A (D-C633S/E346A, lane 5), C^{639} to S and E^{346} to A (D-C639S/E346A, lane 6), or C^{643} to S and E^{346} to A (D-C643S/E346A, lane 7), followed by incubation for 24 h in serum-free media. The conditioned media were analyzed by Western blotting with anti-FLAG-M2. The pro- and mature forms, and the processed C-fragments of soluble hADAM19 are indicated. There is no processing whatsoever in the media from the COS1 cells transiently transfected with the double mutants. (B) The independence of the new processing in transfected COS1 cells. COS1 cells were transfected with the blank vector (lane 1), soluble hADAM19 (D52, lane 2), C^{633} to S (D-C633S, lane 3), C^{639} to S (D-C639S, lane 4), soluble mutants of hADAM19 with E^{586} to D (D-E586D, lane 5), C^{633} to S and E^{586} to D (D-C633S/E586D, lane 6), or C^{639} to S and E^{586} to D (D-C639S/E586D, lane 7). After incubation for 24 h in serum-free media, the conditioned media were analyzed by Western blotting with anti-FLAG-M2. The pro- and mature forms, and the processed C-fragments of soluble hADAM19 are indicated. Note that D-E586D has no processed forms, but both D-C633S/E586D and D-C639S/E586D execute the novel processing in the absence of normal processing.

of the formation of disulfide bonds by mutating cysteine residues, such as C^{605}, C^{633}, C^{639}, or C^{643}, may not disturb the folding and secretion, but do induce a new processing site in soluble hADAM19. To determine the new peptide bond cleavage site, we chose one representative stable MDCK transfectant, D-C633S/E586D-9, to purify from the media by anti-FLAG-M2 affinity column and electrophoresis. N-terminal sequencing revealed that the starting sequence of the purified 32 kDa protein was VNVAGDT, which is identical to the ^{544}VNVAGDT sequence within the cysteine-rich domain of hADAM19. This suggests that K^{543}–V^{544} is an alternative processing site within the cysteine-rich domain of hADAM19 when the primary site at E^{587}–S^{587} is impaired dramatically or its intramolecular disulfide bonds are destroyed.

Shedding is detectable in the full length of hADAM19 with C^{633} to S^{633}, and this shedding is regulated by protein kinase C (PKC), calmodulin (CaM), and calcium signals

Based upon the results shown in Figs. 2A, 4, 5B, and 6, the shedding ability of the full-length Cys to Ser mutants was further examined by choosing C^{633} to S (F-C633S) as a representative. As shown in Fig. 7A, shed fragments of 44–53 kDa were clearly detected in the media from the MDCK cells stably transfected with F-C633S, but not with the wild type (F46), in which the N-terminal is associated with its C-terminal as described previously [24]. Expression levels were comparable among these stable transfectants (Fig. 7A), consistent with the results obtained earlier with their soluble forms (Figs. 2A, 4, 5B, and 6). The double mutants F-C633S/E346A also failed to shed (data not shown), demonstrating that F-C633S undergoes autolytic shedding. Moreover, we revealed that phorbol-12-myristate 13-acetate (PMA), a PKC activator, apparently enhanced the shedding of full-length hADAM19 with C^{633} to S, and that W7, an inhibitor of CaM, and A23187, a calcium ionophore, inhibited this shedding, consistent with our recent report showing that PKC, CaM, and calcium signal pathways may be involved in the processing of hADAM19 at E^{586}–S^{587} [24]. A potent and broad-spectrum matrix metalloproteinase inhibitor, Ilomastat (GM6001), slightly inhibited the shedding of MDCK cells stably expressing F-C633S (Fig. 7B), although it impedes many shedding processes [3,33]. Interestingly, GM6001 was able to dramatically inhibit the activity of soluble hADAM19 against our peptide substrate, described previously [24], with an IC_{50} value of 447 nM, indicating that GM6001 was largely

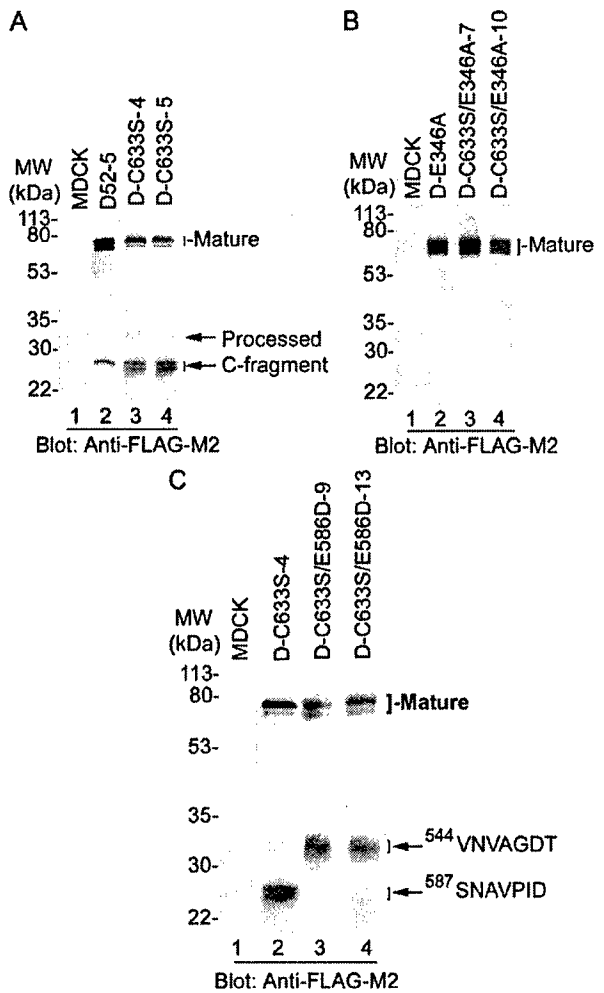

Fig. 6. The new autolytic and independent processing site induced by mutation of cysteines is K^{543}–V^{544}. (A) Soluble C to S mutants of hADAM19 in stable MDCK transfectants have multiple processing fragments. Representative MDCK cells stably expressing D52 (D52-5, lane 2), or D-C633S (D-C633S-4 and D-C633S-5, lanes 3, 4) were seeded in equal amounts into different wells of 24-well plates. After reaching 80% confluence, the cells were incubated in serum-free media for 24 h, and the conditioned media were analyzed by Western blotting using anti-FLAG-M2. The mature forms and the processed C-fragments of soluble hADAM19 are indicated. MDCK cells transfected with the blank vector were used as a control. The stable transfectants of D-C633S seem to exhibit more processing than D52-5. (B) The novel processing in the C^{633} to S mutant is an autolysis in its stable MDCK transfectants. Representative MDCK cells stably expressing soluble inactive hADAM19 (D-E346A, lane 2), C^{633} to S and E^{346} to A (D-C633S/E346A-7 and D-C633S/E346A-10, lanes 3, 4) were seeded in equal amounts and changed to serum-free media when the cells reached 80% confluence. The conditioned media were analyzed by Western blotting using anti-FLAG-M2. MDCK cells transfected with the blank vector were used as a control (lane 1). The complete lack of processing in the media from the MDCK stable lines of the double mutant, C^{633} to S and E^{346} to A, confirms that the new processing is autocatalytic. (C) The novel processing induced by the mutated cysteine residues occurs independently at $K^{543}\downarrow V^{544}$. Representative MDCK cells stably expressing soluble double mutants, C^{633} to S^{633} and E^{586} to D^{586} (D-C633S/E586D-9 and D-C633S/E586D-13, lanes 3, 4), were seeded in equal amounts and changed to serum-free media when the cells reached 80% confluence. The conditioned media were analyzed by Western blotting using anti-FLAG-M2. MDCK cells transfected with the blank vector (lane 1) and D-C633S-4 (lane 2) were used as the controls. The sequences for the processed C-terminal proteins are shown at the right. Note that the $K^{543}\downarrow V^{544}$ processing site is dominant in the media from the MDCK cells stably expressing the soluble double mutants of C633S/E586D, while the $E^{586}\downarrow S^{587}$ site is predominant in D-C633S.

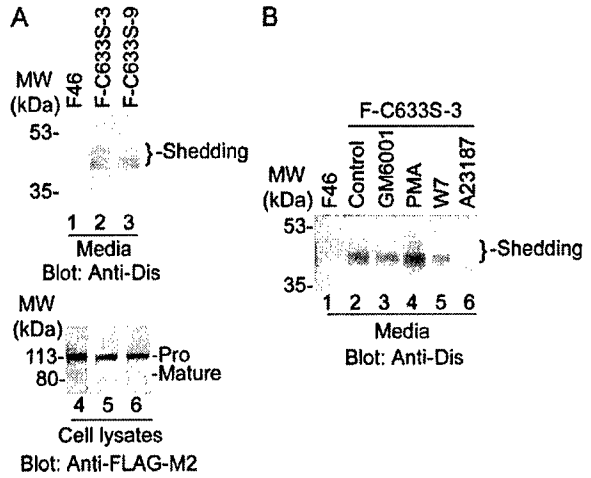

Fig. 7. Shedding of full-length hADAM19 with cysteine to serine mutations. (A) The shedding status of MDCK cells stably expressing full-length mutants of hADAM19. Representative MDCK cells stably expressing wild type hADAM19 (F46, lanes 1, 4), or mutants with C^{633} to S^{633} (F-C633S-3 and F-C633S-9, lanes 2, 5, 3, 6) were seeded at equal amounts into different wells of 24-well plates, then changed to serum-free media when the cells achieved 80% confluence. After 24 h incubation, the conditioned media (lanes 1–3) and the cell lysates (lanes 4–6) were subjected to Western blotting using anti-Dis (lanes 1–3) or anti-FLAG-M2 (lanes 4–6). The pro-, mature, and shed forms of hADAM19 are indicated. F-C633S shed significantly, but not F46. (B) The regulation of shedding in MDCK cells stably expressing F-C633S. MDCK cells stably expressing F-C633S (F-C633S-3) were seeded equally into 24-well plates, and the cells were treated with serum-free media alone (lane 2), or media containing GM6001 (2.5 μM, lane 3), PMA (50 ng/ml, lane 4), W7 (100 μM, lane 5) or A23187 (500 nM, lane 6) for 24 h. The conditioned media were analyzed by Western blotting using anti-Dis. The shed fragments of hADAM19 are indicated. MDCK cells transfected with wild type (F46) were used as a control (lane 1). The shedding of F-C633S was significantly inhibited by A23187 and W7, slightly inhibited by GM6001, and enhanced by PMA.

excluded from the intracellular environment during the shedding process. Our current results also support the concept that the processing of hADAM19 at E^{586}–S^{587} takes place intracellularly [24].

Discussion

In this report, we provide evidence that disulfide bonds, which are most likely intrafragment, play an important role in the processing of hADAM19, and that any one of the cysteine residues within the fraction of the cysteine-rich domain of the C-fragment of hADAM19 processed at E^{586}–S^{587} is indispensable for the association of the processed N-terminal with its C-terminal. This may be the first report that the cysteine-rich domain likely forms disulfide bonds to regulate the autolytic processing/shedding of hADAM19 at E^{586}–S^{587} or K^{543}–V^{544}, thereby modulating the proteolytic activity of this enzyme, as such processing/shedding is an indicator of hADAM19 activity [24]. This report lends in vitro support to the proposed model for the regulation of ADAMs, as was shown in ADAM13 in vivo [26].

Significance of autolytic processing or shedding in hADAM19

Among ADAMs, ADAM8, 13, 19, and ADAM-TS4 have been shown to be processed intracellularly by autolysis [16,17,23–25], producing an active enzyme or a functional fragment responsible for binding with alpha2-M or integrins, mediating cell adhesion, or digesting components of the ECM. Following our previous report [24], we have demonstrated in this report that under certain conditions, hADAM19 processing or shedding occurs at a different site within its cysteine-rich domain, K^{543}–V^{544}, which is before the normal processing site at E^{586}–S^{587}. Conditions leading to this alternative processing include the disruption of disulfide bonds by mutation or reduction. This also produces an active enzyme, as shown in Figs. 4, 5B, and 6, because the processing or shedding of hADAM19 depends on its own proteolytic activity (Figs. 5A and 6B, and Ref. [24]), but the processing at K^{543}–V^{544} occurs independent of the normal processing at E^{586}–S^{587} (Figs. 5B and 6C). Notably, the processing site of E^{586}–S^{587} is the predominant one, even with disruption of the intramolecular disulfide bonds (Figs. 4, 5B, and 6A). However, the site of K^{543}–V^{544} becomes dominant when the intramolecular disulfide bonds are destroyed and its primary site is mutated (Fig. 6B). Given that processing within the cysteine-rich domain is necessary for the proteolytic activities of hADAM19 [24], we speculate that the presence of an alternative processing site within cysteine-rich domain capable of producing fully activated hADAM19 is indicative of its very important roles in both physiological and pathological conditions.

Our results showed that the shorter truncated form D-CR (E^{204}–T^{504}) of hADAM19 had catalytic activity similar to the longer truncated form D586 (E^{204}–E^{586}) against a peptide substrate (data not shown). We presume that the intermediate form (E^{204}–K^{543}) produced by autolytic processing at K^{543}–V^{544} may have comparable proteolytic activity against a peptide substrate and alpha2-M. It is likely that the cleavage of a peptide substrate and alpha-2 macroglobulin by these three truncated forms of hADAM19 is due to an essential interaction between the protease and the substrate. Regarding the mechanism for these two cleavage events, we speculate that they may occur in a similar fashion, as shown by the results obtained by treatment with GM6001, PMA, W7, or A23187 (Fig. 7B and Ref. [24]).

The functions of the cysteine-rich domain in ADAMs

The "cysteine-rich domain" is sometimes referred to together with the disintegrin domain. In these cases, the "cysteine-rich domain" has been shown to be related to cell adhesion, such as in the cases of ADAM8, 12, 13, or to the proteolytic activity of TACE/ADAM17. For example, the recombinant disintegrin/cysteine-rich domain of ADAM8 mediates cell adhesion in cells expressing ADAM8 [17]; the "cysteine-rich domain" of ADAM12 promotes the

adhesion of fibroblasts and myoblasts [34]; the disintegrin and cysteine-rich domains of ADAM13 bind to both fibronectin and to beta1-containing integrin receptors, and the binding can be inhibited by antibodies against the cysteine-rich domain [23]; the "cysteine-rich domain" of TACE/ADAM17 is required for shedding of IL-1R-II while affecting the inhibitor sensitivity of TNF-alpha shedding [35].

Despite knowledge about the combined functions of both the disintegrin and cysteine-rich domains, very little information is available about cysteine-rich-domain-specific functions. Iba et al. [36,37] reported that the cysteine-rich domain of ADAM12 acts as a ligand for the cell-adhesion molecule syndecan. Dr. DeSimone's group [26] recently showed that the cysteine-rich domain of ADAM13 cooperates intramolecularly with the metalloproteinase domain of ADAM13 to regulate its function, providing the first evidence that a downstream extracellular adhesive domain plays an active role in the regulation of ADAM protease function in vivo. In this report, we have demonstrated that disulfide bonds likely play a crucial role in the regulation of hADAM19 processing, but not in its folding or secretion (Figs. 2B, C, 4, 5, and 6), as illustrated by DTT treatment or changes of pH (Figs. 2B and C). DTT is a reducing agent capable of penetrating into cells and preventing the formation of disulfide bonds, as with clusterin, a secreted glycoprotein that forms disulfides intracellularly [32]. As a result of DTT treatment, clusterin is retained in the endoplasmic reticulum and is undetectable in the cultured medium of MDCK cells (Fig. 2D and Ref. [30]). Decreased pH in culture media may also impair the formation of disulfides, interfering with the processing of hADAM19, as shown in Fig. 2C. Moreover, disulfide bonds that include the cysteine residues at C^{605}, C^{633}, C^{639}, and C^{643} within the fraction of the cysteine-rich domain of the C-fragment processed at E^{586}-S^{587} of hADAM19 are necessary for the association of the processed N-fragment with its C-fragment (Fig. 4). A new processing site at K^{543}–V^{544} is exposed when these cysteine residues are mutated individually, suggesting that intrafragment disulfide bonds likely contribute to the normal conformation of hADAM19 and conceal this alternative processing site in hADAM19. This site may become exposed when the conformation of hADAM19 is modified, either by C to S mutations (Figs. 4, 5B, 6A, C, and 7A), reduction with DTT (Fig. 2B), or alteration of pH (Fig. 2C). This may explain why GM6001 slightly inhibits the shedding of F-C633S hADAM19 (Fig. 7A), but has no effect on the processing of soluble hADAM19 [24]. In particular, all mutants with these specific cysteine residues exchanged for serines seem to exhibit increased processing, as the fragment at 26 kDa is more detectable in these mutants (Figs. 4, 5B, and 6). Therefore, we may speculate that the C-fragment, containing part of the cysteine-rich domain after the processing at E^{586}–S^{587}, might have an inhibitory effect on hADAM19 processing through the involvement of interfragment disulfide bonds with the N-fragment containing the metalloproteinase and disintegrin domains and the remainder of the cysteine-rich domain. This proposed model may also be applied to other ADAMs, such as ADAM8, 13, 19, and ADAM-TS4, as they must also be processed at their C-termini by autolysis to be functional after cleavage of their prodomains [16,17,23,25]. Our results may provide the first pieces of in vitro evidence to support the results of the in vivo ADAM13 studies discussed above [26], and show that the processing or shedding of hADAM19 occurs autolytically and intramolecularly within its cysteine-rich domain ([24]; Figs. 1 and 5A).

There are a total 43 cysteine residues available in the metalloproteinase, disintegrin, cysteine-rich, and EGF-like domains of hADAM19. Although we have not conclusively identified the precise disulfide pairs, it is possible that disulfide bonds are formed between the disintegrin domain of hADAM19 and the cysteine-rich domain of the C-fragment because the disintegrin domain of hADAM19 also plays a key role in the proteolytic activity of hADAM19. We have previously shown that our specific antibody against the disintegrin domain inhibited substrate cleavage in vitro [27], and a deletion mutant containing only the metalloproteinase domain of hADAM19 lacked proteolytic activity during alpha2-M and peptide substrate assays in vitro (data not shown). Any one of the four cysteine residues at C^{605}, C^{633}, C^{639}, and C^{643} in the C-fragment cysteine-rich domain is indispensable for the association between the N-fragment and C-fragment processed at E^{586}–S^{587}. We hypothesize three disulfide bonds; one formed between two cysteine residues of the C^{605}, C^{633}, C^{639}, and C^{643} group, and two formed by the remaining two cysteine residues paired with two other cysteine residues, with at least one occurring before the position of E^{586} in the N-fragment. Alternatively, four disulfide bonds may exist, formed between C^{605}, C^{633}, C^{639}, and C^{643} and four other cysteine residues, with at least one before E^{586}. These bonds have a strong coordination with each other, and when one of these disulfide bonds is disrupted, the others will be subsequently disturbed. Therefore, we propose that three or four disulfide bonds, likely linked by the four cysteine residues at C^{605}, C^{633}, C^{639}, and C^{643} with other cysteine residues in the N-fragment, are responsible for the association between the N-fragment and C-fragment processed at E^{586}–$0S^{587}$. In the near future, we would like to determine the identity of these disulfide bonds using multiple approaches including structural biology, analytical chemistry, and biochemical methods.

Acknowledgments

We thank Margaret Seavy at the Bioanalytical Facility of Florida State University for protein N-terminal sequencing. We are also grateful to the members of Professor Sang's laboratory, including Yewseok Suh and Ehsan (Sonny) Achtchi for their excellent technical assistance, Robert G. Newcomer for his editorial assistance, and Drs. Hyun I. Park, Yunge Zhao, and Douglas R. Hurst for their valuable discussions.

References

[1] C.P. Blobel, Remarkable roles of proteolysis on and beyond the cell surface, Curr. Opin. Cell Biol. 12 (2000) 606–612.

[2] J. Schlondorff, C.P. Blobel, Metalloprotease-disintegrins: modular proteins capable of promoting cell–cell interactions and triggering signals by protein-ectodomain shedding, J. Cell Sci. 112 (1999) 3603–3617.

[3] F. Kheradmand, Z. Werb, Shedding light on sheddases: role in growth and development, BioEssay 24 (2002) 8–12.

[4] D.F. Seals, S.A. Courtneidge, The ADAMs family of metalloproteinease: multidomain proteins with multiple functions, Genes Dev. 17 (2003) 7–30.

[5] A. Thathiah, C.P. Blobel, D.D. Carson, Tumor necrosis factor-α converting enzyme/ADAM 17 mediates MUC1 shedding, J. Biol. Chem. 278 (2003) 3386–3394.

[6] K. Brew, D. Dinakarpandian, H. Nagase, Tissue inhibitors of metalloproteinases: evolution, structure and function, Biochim. Biophys. Acta 1477 (2000) 267–283.

[7] S. Cal, J.M. Arguees, P.L. Fernandez, C. Lopez-Otin, Identification, characterization, and intracellular processing of ADAM-TS12, a novel human disintegrin with a complex structural organization involving multiple thrombospondin-1 repeats, J. Biol. Chem. 276 (2001) 17932–17940.

[8] K. Kuno, Y. Terashima, K. Matsushima, ADAMTS-1 is an active metalloproteinase associated with the extracellular matrix, J. Biol. Chem. 274 (1999) 18821–18826.

[9] F. Loechel, B.J. Gilpin, E. Engvall, R. Albrechtsen, U.M. Wewer, Human ADAM 12 (meltrin alpha) is an active metalloprotease, J. Biol. Chem. 273 (1998) 16993–16997.

[10] L. Lum, C.P. Blobel, Evidence for distinct serine protease activities with a potential role in processing the sperm protein fertilin, Dev. Biol. 191 (1997) 131–145.

[11] L. Lum, M.S. Reid, C.P. Blobel, Intracellular maturation of the mouse metalloprotease disintegrin MDC15, J. Biol. Chem. 273 (1998) 26236–26247.

[12] M. Roghani, J.D. Becherer, M.L. Moss, R.E. Atherton, H. Erdjument-Bromage, J. Arribas, R.K. Blackburn, G. Weskamp, P. Tempst, C.P. Blobel, Metalloprotease-disintegrin MDC9: intracellular maturation and catalytic activity, J. Biol. Chem. 274 (1999) 3531–3540.

[13] T. Kang, Y.-G. Zhao, D. Pei, J.F. Sucic, Q.X. Sang, Intracellular activation of human Adamalysin 19/disintegrin and metalloproteinase 19 by furin occurs via one of the two consecutive recognition sites, J. Biol. Chem. 277 (2002) 25583–25591.

[14] Y. Cao, Q. Kang, A. Zolkiewska, Metalloprotease-disintegrin ADAM 12 interacts with alpha-actinin-1, Biochem. J. 357 (2001) 353–361.

[15] J. Schlondorff, J.D. Becherer, C.P. Blobel, Intracellular maturation and localization of the tumour necrosis factor alpha convertase (TACE), Biochem. J. 347 (2000) 131–138.

[16] G. Gao, J. Westling, V.P. Thompson, T.D. Howell, P.E. Gottschall, J.D. Sandy, Activation of the proteolytic activity of ADAMTS4 (aggrecanase-1) by C-terminal truncation, J. Biol. Chem. 277 (2002) 11034–11043.

[17] U. Schlomann, D. Wildeboer, A. Webster, O. Antropova, D. Zeuschner, C.G. Knight, A.J. Docherty, M. Lambert, L. Skelton, H. Jockusch, J.W. Bartsch, The metalloprotease disintegrin ADAM8. Processing by autocatalysis is required for proteolytic activity and cell adhesion, J. Biol. Chem. 277 (2002) 48210–48219.

[18] L. Howard, R.A. Maciewicz, C.P. Blobel, Cloning and characterization of ADAM28: evidence for autocatalytic pro-domain removal and for cell surface localization of mature ADAM28, Biochem. J. 348 (2000) 21–27.

[19] A. Anders, S. Gilbert, W. Garten, R. Postina, F. Fahrenholz, Regulation of the alpha-secretase ADAM10 by its prodomain and proprotein convertases, FASEB J. 15 (2001) 1837–1839.

[20] F. Fahrenholz, S. Gilbert, E. Kojro, S. Lammich, R. Postina, Alpha-secretase activity of the disintegrin metalloprotease ADAM 10. Influences of domain structure, Ann. N. Y. Acad. Sci. 920 (2000) 215–222.

[21] M.E. Milla, M.A. Leesnitzer, M.L. Moss, W.C. Clay, H.L. Carter, A.B. Miller, J. Su, M.H. Lambert, D.H. Willard, D.M. Sheeley, T.A. Kost, W. Burkhart, M. Moyer, R.K. Blackburn, G.L. Pahel, J.L. Mitchell, C.R. Hoffman, J.D. Becherer, Specific sequence elements are required for the expression of functional tumor necrosis factor-alpha-converting enzyme (TACE), J. Biol. Chem. 274 (1999) 30563–30570.

[22] K. Shirakabe, S. Wakatsuki, T. Kurisaki, A. Fujisawa-Sehara, Roles of Meltrin beta/ADAM19 in the processing of neuregulin, J. Biol. Chem. 276 (2001) 9352–9358.

[23] A. Gaultier, H. Cousin, H. Darribere, D. Alfandari, ADAM13 disintegrin and cysteine-rich domains bind to the second heparin-binding domain of fibronectin, J. Biol. Chem. 277 (2002) 23336–23344.

[24] T. Kang, H.I. Park, Y. Suh, Y.-G. Zhao, H. Tschesche, Q.X. Sang, Autolytic processing at Glu(586)-Ser(587) within the cysteine-rich domain of human adamalysin 19/disintegrin-metalloproteinase 19 is necessary for its proteolytic activity, J. Biol. Chem. 277 (2002) 48514–48522.

[25] J. Westling, A.J. Fosang, K. Last, V.P. Thompson, K.N. Tomkinson, T. Hebert, T. McDonagh, L.A. Collins-Racie, E.R. LaVallie, E.A. Morris, J.D. Sandy, ADAMTS4 cleaves at the aggrecanase site (Glu373-Ala374) and secondarily at the matrix metalloproteinase site (Asn341-Phe342) in the aggrecan interglobular domain, J. Biol. Chem. 277 (2002) 16059–16066.

[26] K.M. Smith, A. Gaultier, H. Cousin, D. Alfandari, J.M. White, D.W. DeSimone, The cysteine-rich domain regulates ADAM protease function in vivo, J. Cell Biol. 159 (2002) 893–902.

[27] Y.-G. Zhao, P. Wei, Q.X. Sang, Inhibitory antibodies against endopeptidase activity of human adamalysin 19, Biochem. Biophys. Res. Commun. 289 (2001) 288–294.

[28] E. Chanat, U. Weiss, W.B. Huttner, S.A. Tooze, Reduction of the disulfide bond of chromogranin B (secretogranin I) in the trans-Golgi network causes its missorting to the constitutive secretory pathways, EMBO J. 12 (1993) 2159–2168.

[29] H.F. Lodish, N. Kong, The secretory pathway is normal in dithiothreitol-treated cells, but disulfide-bonded proteins are reduced and reversibly retained in the endoplasmic reticulum, J. Biol. Chem. 268 (1993) 20598–20605.

[30] A. Losch, C. Koch-Brandt, Dithiothreitol treatment of Madin-Darby canine kidney cells reversibly blocks export from the endoplasmic reticulum but does not affect vectorial targeting of secretory proteins, J. Biol. Chem. 270 (1995) 11543–11548.

[31] W.J. Wedemeyer, E. Welker, M. Narayan, H.A. Scheraga, Disulfide bonds and protein folding, Biochemistry 39 (2000) 4207–4216.

[32] B.F. Burkey, H.V. deSilva, J.A. Harmony, Intracellular processing of apolipoprotein J precursor to the mature heterodimer, J. Lipid Res. 32 (1991) 1039–1048.

[33] N. Ilan, A. Mohsenin, L. Cheung, J.A. Madri, PECAM-1 shedding during apoptosis generates a membrane-anchored truncated molecule with unique signalling characteristics, FASEB J. 15 (2001) 362–372.

[34] A. Zolkiewska, Disintegrin-like/cysteine-rich region of ADAM 12 is an active cell adhesion domain, Exp. Cell Res. 252 (1999) 423–431.

[35] P. Reddy, J.L. Slack, R. Davis, D.P. Cerretti, C.J. Kozlosky, R.A. Blanton, D. Shows, J.J. Peschon, R.A. Black, Functional analysis of the domain structure of tumor necrosis factor-alpha converting enzyme, J. Biol. Chem. 275 (2000) 14608–14614.

[36] K. Iba, R. Albrechtsen, B. Gilpin, C. Frohlich, F. Loechel, A. Zolkiewska, K. Ishiguro, T. Kojima, W. Liu, J.K. Langford, R.D. Sanderson, C. Brakebusch, R. Fassler, U.M. Wewer, The cysteine-rich domain of human ADAM 12 supports cell adhesion through syndecans and triggers signaling events that lead to beta1 integrin-dependent cell spreading, J. Cell Biol. 149 (2000) 1143–1156.

[37] K. Iba, R. Albrechtsen, B. Gilpin, F. Loechel, U.M. Wewer, Cysteine-rich domain of human ADAM 12 (meltrin alpha) supports tumor cell adhesion, Am. J. Pathol. 154 (1999) 1489–1501.

Available online at www.sciencedirect.com

SCIENCE DIRECT

Experimental Cell Research 301 (2004) 103–118

Experimental Cell Research

www.elsevier.com/locate/yexcr

Review

The significance of focal myoepithelial cell layer disruptions in human breast tumor invasion: a paradigm shift from the "protease-centered" hypothesis

Yan-Gao Man[a,*], Qing-Xiang Amy Sang[b,*]

[a]*Department of Gynecologic and Breast Pathology, Armed Forces Institute of Pathology and American Registry of Pathology, Washington DC 20306-6000, USA*

[b]*Department of Chemistry and Biochemistry and Institute of Molecular Biophysics, Florida State University, Tallahassee, FL 32306-4390, USA*

Received 30 May 2004, revised version received 8 August 2004
Available online 2 October 2004

Abstract

Human breast epithelium and the stroma are separated by a layer of myoepithelial (ME) cells and basement membrane, whose disruption is a prerequisite for tumor invasion. The dissolution of the basement membrane is traditionally attributed primarily to an over-production of proteolytic enzymes by the tumor or the surrounding stromal cells. The results from matrix metalloproteinase inhibitor clinical trials, however, suggest that this "protease-centered" hypothesis is inadequate to completely reflect the molecular mechanisms of tumor invasion. The causes and signs of ME cell layer disruption are currently under-explored. Our studies revealed that a subset of pre- and micro-invasive tumors contained focal disruptions in the ME cell layers. These disruptions were associated with immunohistochemical and genetic alterations in the overlying tumor cells, including the loss of estrogen receptor expression, a higher frequency of loss of heterozygosity, and a higher expression of cell cycle, angiogenesis, and invasion-related genes. Focal ME layer disruptions were also associated with a higher rate of epithelial proliferation and leukocyte infiltration. We propose the novel hypothesis that a localized death of ME cells and immunoreactions that accompany an external environmental insult or internal genetic alterations are triggering factors for ME layer disruptions, basement membrane degradation, and subsequent tumor progression and invasion.

Keywords: Human breast tumor microinvasion; Ductal carcinoma in situ; Focal myoepithelial layer disruption; Basement membrane degradation; Leukocyte infiltration; Epithelial–stromal interactions; Cell proliferation; Loss of heterozygosity (LOH); "Protease-centered" hypothesis; Matrix metalloproteinase inhibitors (MMPIs)

Contents

Introduction 104
The normal distribution, morphology, and functions of myoepithelial cells 105
Production of tumor suppressor proteins 105
Paracrine down-regulation of matrix metalloproteinase (MMP) expression 105
Turnover of extracellular matrix (ECM) 105
Regulation of normal development 106
Establishment and stabilization of the polarity of the bilayer epithelial structure 106
Steroid hormone metabolism 106

* Corresponding authors. Yan-Gao Man is to be contacted at fax: +1 202 782 3939. Qing-Xiang Amy Sang, fax: +1 850 644 8281.
E-mail addresses: man@afip.osd.mil (Y.-G. Man), sang@chem.fsu.edu (Q.-X.A. Sang).

0014-4827/$ - see front matter © 2004 Elsevier Inc. All rights reserved.
doi:10.1016/j.yexcr.2004.08.037

Exclusively or preferentially expressed bio-molecules in myoepithelial cells . . . 107
Structure-specific proteins (related to microfilaments and intermediate filaments) . . . 107
Smooth muscle actin (SMA) . . . 107
Smooth muscle myosin heavy chain (SMMHC) . . . 107
Calponin . . . 107
H-caldesmon (HCD) . . . 107
P-cadherin . . . 107
Cytokeratins (CK) 5, 7, 14, and 17 . . . 107
Non-structural molecules . . . 107
Maspin . . . 107
Wilms' tumor 1 (WT-1) . . . 107
p63 and p73 . . . 107
14-3-3Sigma . . . 108
Neuropilin-1 (NRP-1) . . . 108
CD 10 . . . 108
S100 . . . 108
Other important molecules . . . 108
Common myoepithelial markers used in distinguishing in situ from invasive tumors . . . 108
Major myoepithelial cell lesions . . . 108
Myoepitheliosis . . . 108
Adenomyoepithelioma . . . 109
Myoepithelial carcinoma . . . 109
Impacts of ME cell alterations on adjacent epithelial cells . . . 109
Focal ME layer disruptions and loss of ER expression in overlying epithelial cells are correlated events . . . 110
Cells in ducts with and without focal ME disruptions have different proliferation rates . . . 110
Loss of heterozygosity (LOH) in estrogen receptor (ER)-negative cells . . . 110
Breast epithelial cell clusters at the site of ME layer disruptions have increased expression of genes related to proliferation, apoptosis, invasion, and metastasis . . . 110
Leukocyte infiltration is increased at focal ME disruptions . . . 111
Ductal tumors with and without ME disruptions have different rates of leukocyte infiltration . . . 112
ME cells surrounded by or adjacent to leukocytes show distinct morphologic alterations . . . 112
The vast majority of proliferating clusters of epithelial cells is located at or near focally disrupted ME layers . . . 112
Our hypothesized mechanism for ME cell layer disruption and tumor invasion . . . 112
Implications of our hypothesis . . . 114
Conclusions . . . 115
Acknowledgments . . . 115
References . . . 115

Introduction

The epithelium of normal human breasts and in situ breast tumors is physically separated from the stroma by both the myoepithelial (ME) cell layer and the basement membrane, whose degradation is an absolute prerequisite for tumor invasion and metastasis. Basement membrane degradation and tumor invasion have been attributed primarily, if not solely, to the over-production of proteolytic enzymes by the tumor or the surrounding stromal cells [1]. This hypothesis alone, though compelling, appears inadequate to completely reflect the intrinsic mechanisms of these events for three main reasons: first, the ME cell layer is a normal structural constituent that should not be a target of the host's own enzymes; second, neither the natural turnover nor the dynamic alterations of ME cells during tumor invasion have been elucidated; and third, although results from in vitro tests and animal models have clearly demonstrated that protease inhibitors could effectively inhibit or prevent tumor invasion or metastasis, results from protease inhibitor-based human oncology clinical trials have not been successful [2,3].

This review attempts to elucidate the biological and clinical profiles of ME cells based on previously published reports and our own recent studies, and to assess the potential significance of ME cells in tumor progression and invasion. In addition, this article presents several unique findings from our recent studies correlating the structural integrity of ME cell layers with the genetic and immunohistochemical profiles in adjacent tumor cells. These unconventional findings and other supportive data have led to the novel hypothesis that ME cell layer disruption and basement membrane degradation, and subsequent tumor invasion, are triggered by a localized ME cell death and the resultant leukocyte infiltration and immunoreactions that accompany an external environmental insult or internal genetic alterations. The rationale and postulated steps for our hypothesis are summarized and discussed.

The normal distribution, morphology, and functions of myoepithelial cells

The normal human breast consists of two major compartments, the epithelium and the stroma. The epithelium contains two cell types, ME cells and luminal cells, which form both the secretory lobules and branching ducts. ME cells are positioned between the luminal cells and basement membrane, attaching to luminal cells by desmosomes and the basement membrane by hemidesmosomes [4–6]. The basement membrane is composed laminin, type IV collagen, entactin, heparan sulfate proteoglycans, glycosaminoglycans, and other components, forming a continuous lining surrounding the ME cells [7,8]. ME cells are joined by intercellular junctions and adhesion molecules, forming a continuous layer that encircles the entire duct system, and a discontinuous layer or a basket-like structure that covers a vast majority of the cells at terminal duct-lobular units and lobules. The ME layer and the basement membrane are normal structures, separating the epithelium from the stroma (Fig. 1).

In clear-cut normal breast tissues, ME and epithelial cells are approximately equal in number, and ME cells are generally of a cuboid or spindle shape, with pale cytoplasm and nuclei. The number and morphology of ME cells, however, can vary substantially at different stages of tumor progression. In hyperplastic and in situ lesions, ME cell layers are often substantially attenuated, and the cells stretched out, with little or no distinct cytoplasm (Fig. 2), morphologically resembling the smooth muscle cells of small blood vessels and fibroblasts. In invasive lesions and a rare benign lesion, microglandular adenosis, ME cells are either not appreciable or are occasionally found in residual normal tissues trapped in these lesions. ME cells contain a large number of microfilaments, a unique structural component of smooth muscle cells, and intermediate filaments, a unique structural component of epithelial cells [9].

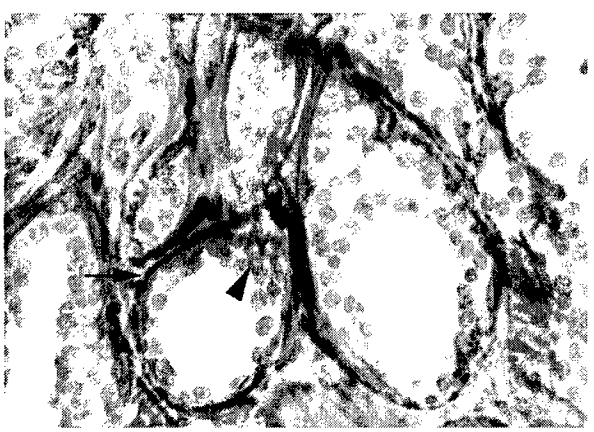

Fig. 1. The architectural relationship of the basement membrane, myoepithelial (ME) cells, and epithelial cells of ducts in a normal human mammary gland. A paraffin section double-immunostained for ME cells and basement membrane with anti-smooth muscle actin (red) and collagen IV (brown) antibodies, respectively. The arrow identifies the basement membrane (brown), the arrowhead designates a ME cell (red), and blue nuclei stained by hematoxylin are those of the luminal epithelial cells (400×).

This architecture confers upon the ME cells and basement membrane two essential biological and clinical functions. First, as normal epithelial components are devoid of blood vessels and lymphatic ducts, and are therefore totally dependent upon the stroma for their nutritional, metabolic, and survival needs, the ME cells and basement membrane serve as natural structural barriers that directly mediate communications between these two compartments. Second, the cells of in situ tumors must first pass through the ME cell layer, then the basement membrane, to physically reach the stroma. Thus, the degradation of both the ME cell layer and the basement membrane is an absolute prerequisite for tumor invasion (Fig. 3).

In addition to these passive functions, recent studies have revealed that ME cells might also possess the following active functions.

Production of tumor suppressor proteins

A number of tumor suppressor proteins, including maspin, Wilms' tumor 1, p63, p73, and 14-3-3Sigma have been detected exclusively or preferentially in ME cells [10–15]. In vitro and in vivo studies have demonstrated that these proteins have significant inhibitory functions against tumor growth and invasion [10,12–15].

Paracrine down-regulation of matrix metalloproteinase (MMP) expression

ME cells may modulate breast tumor invasion by controlling the expression of MMPs in both the tumor and the surrounding fibroblasts. To explore this possibility, a recent study quantitatively compared MMP expression levels in breast cancer cell lines and fibroblasts co-cultured with and without ME cells purified from normal breast tissues [16]. Results revealed that both cancer cells and fibroblasts co-cultured with ME cells had significantly lower expression of MMP-2, MMP-9 and MT1-MMP when compared to those cultured without ME cells, and this reduction of MMP expression was accompanied by reduced invasion [16].

Turnover of extracellular matrix (ECM)

While many ECM-degrading enzymes found in breast tissues are manufactured by the stromal cells, several such enzymes, including a recently described angiogenesis-related matrix metalloproteinase, MMP-19, are reported to be produced by normal ME cells [17], and are expected to participate in the turnover of ECM [17,18].

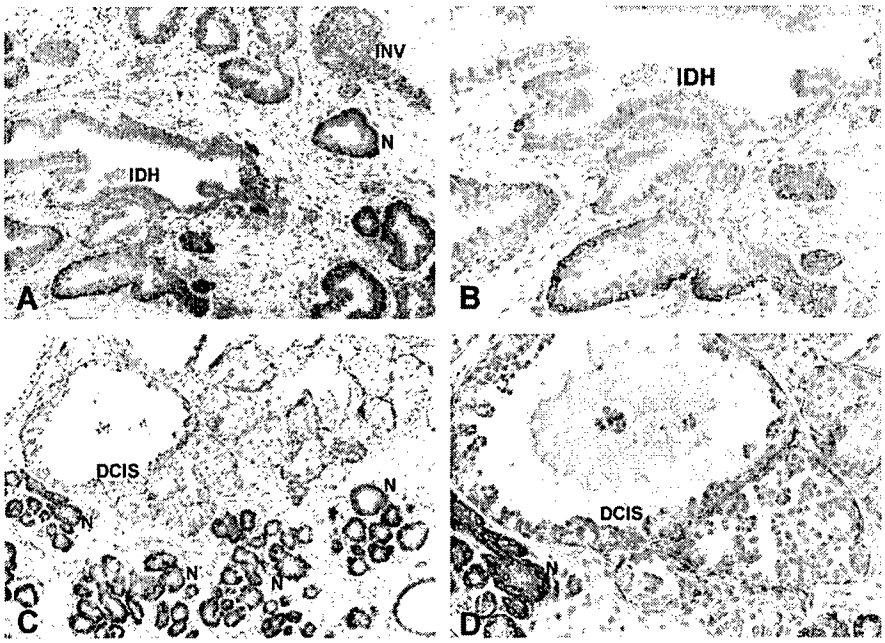

Fig. 2. The morphology of human breast tissues containing normal and hyperplastic epithelial cells, ductal carcinoma in situ, and invasive carcinoma. Two paraffin sections were immunostained for smooth muscle actin (red). The ratio of ME cells to epithelial cells is approximately 1:1 in the normal ducts (N). The ME cell layer is generally intact and distinct in the normal ducts, but attenuated in intraductal hyperplasia (IDH) and ductal carcinoma in situ (DCIS), and absent in the invasive lesion (INV). 2B and 2D (200×) are higher magnifications of 2A and 2C (100×), respectively.

Regulation of normal development

During normal development, a number of growth factors and their corresponding receptors, including the epidermal growth factor, basic fibroblast growth factor and its receptor, Tcf transcription factors, and transforming growth factors, are differentially expressed in the luminal and ME cells [19–22]. A perturbation in the expression of these and other related molecules in ME cells led to abnormal breast morphogenesis and development [20,21].

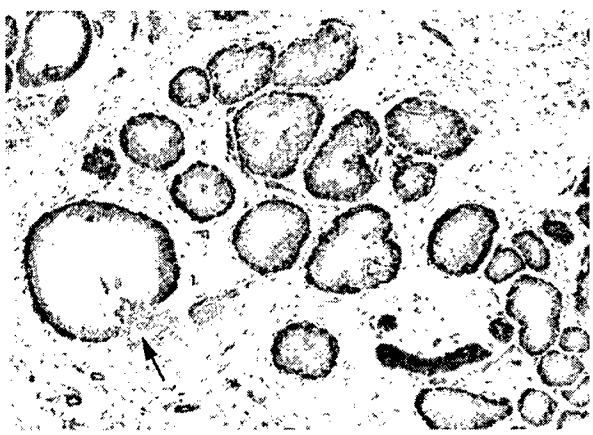

Fig. 3. Disruption of the ME cell layer and degradation of the basement membrane are prerequisites for invasion. A paraffin section was immunostained for both smooth muscle actin and collagen IV using the same chromogen (red). The ME cell layer and basement membrane in one duct is focally disrupted and the epithelial cells are in direct contact with the stroma (an arrow; 100×).

Establishment and stabilization of the polarity of the bilayer epithelial structure

In tissue cultures, luminal cells alone could form acinus-like structures with a reversed polarity [18]. The addition of ME cells from normal breast tissues could establish and stabilize a correct polarity, whereas ME cells from breast tumors failed to correct the reversed polarity, suggesting that normal ME cells play important roles in the establishment and stabilization of bilayer epithelial structures [18].

Steroid hormone metabolism

A recent study assessed the mRNA expression and enzymatic activity of steroid sulfatase (STS) in normal human breast ME and human adenocarcinoma (MCF-7) cells, and the effects of 17-beta estradiol on the activity of STS [23]. The study revealed that sulfatase activity was about 120 times greater in the ME cells than in the MCF-7 cells, and that exposure to 17-beta estradiol was associated with a 70% reduction of sulfatase activity in the MCF-7 cells, but a 9% increase in ME cells, suggesting a potential role for ME cells in the conversion of hormone precursors into active steroid hormones [23].

Exclusively or preferentially expressed bio-molecules in myoepithelial cells

Currently, there are more than a dozen commercially available antibodies that can be used for immunohistochemistry in formalin-fixed, paraffin-embedded sections to detect the molecules reported to be exclusively or preferentially present in ME cells. Based on their compositions, subcellular localizations, and potential functions, these molecules can be roughly classified into two groups.

Structure-specific proteins (related to microfilaments and intermediate filaments)

Smooth muscle actin (SMA)

SMA forms microfilamentous contractile polypeptides, and presents in cells with myogenous features such as smooth muscle cells, myoepithelial cells, myofibroblasts, and vascular pericytes. Each smooth muscle cell contains thick (myosin) and thin (actin) filaments that slide against each other to produce contraction of the cells. Smooth muscle cells are found in the walls of many hollow organs of the body, and their contraction reduces the size of these structures. In human breast tissues, SMA immunostaining is present in the cytoplasm of about 95% of the ME cells in normal ducts and lobules, as well as in non-invasive breast lesions [24,25]. Invasive lesions, and a very rare benign lesion, microglandular adenosis, are devoid of SMA immunoreactivity due to the lack of ME cells surrounding these lesions. A diagnosis of invasive malignancy may be confirmed when both type IV collagen and SMA are negative, and ruled out when both markers are positive. In some instances, false-positive SMA staining may represent the smooth muscle cells of small blood vessels or myofibroblast cells of the stroma that are often adjacent to the invasive components.

Smooth muscle myosin heavy chain (SMMHC)

SMMHC, a cytoplasmic structural protein, is a major component of the contractile apparatus of smooth muscle cells, and is specific for the early development of smooth muscle. It is also a myoepithelium-associated protein, presenting heavily in the ME cells of normal and benign breast tissues, and has been reported to be a very useful marker in differentiation between noninvasive and invasive breast lesions [26,27].

Calponin

Calponin, a calmodulin, binds tropomyosin and F-actin, and is thought to be involved in the regulation of smooth muscle contraction. The expression of calponin is largely restricted to smooth muscle cells, but has also been demonstrated in human breast ME cells. It is a useful marker in the differentiation between ME cells and spindle cells of the stroma, and also between non-invasive and invasive lesions [27,28]. However, calponin staining in ME cells may occasionally be discontinuous or absent in in situ ductal lesions [29].

H-caldesmon (HCD)

HCD is a cytoskeleton-associated actin-binding protein. In human breast tissues, HCD is predominantly expressed in ME cells, but a high level of HCD expression is also often seen in the smooth muscle cells of small blood vessels [30,31].

P-cadherin

P-cadherin, like E-cadherin, is a Ca^{2+}-dependent cell adhesion molecule with a fundamental role in the maintenance of the integrity of multicellular structures and the phenotype of epithelial cells [32]. In breast tissues, p-cadherin is preferentially expressed in the ME cells of normal ducts, lobules, and sclerotic lesions [33]. However, p-cadherin is also occasionally seen in hyperplastic tissues and in some tumor cells of in situ carcinomas [34].

Cytokeratins (CK) 5, 7, 14, and 17

Cytokeratins 5, 7, 14, and 17 are a group of cellular structural proteins found in epithelial cells and cells with epithelioid features [35]. In human breast tissues, these molecules are predominantly present in the myoepithelial cell layer [36,37]. CK-17 is also related to early skin development and wound repair [38].

Non-structural molecules

Maspin

Maspin, or mammary-specific serpin, is a tumor suppressor protein belonging to the serine proteinase inhibitor family [39,40]. It is present in both breast and prostate glands. In the breast, maspin is predominantly a soluble cytoplasmic protein that is consistently detectable in normal human ME cells and ME-derived tumors [39,41]. The expression of maspin decreases with increasing malignancy of breast tumors [39–41]. Both in vitro and in vivo studies have shown that maspin exhibits significant inhibition of tumor growth and invasion [39,40].

Wilms' tumor 1 (WT-1)

WT-1 is as a transcription factor regulating gene expression in a fashion similar to that of p53 [42]. The expression of WT-1 in the breast appears to correlate with the behavior and progression of breast tumors [43]. Our previous study showed that WT-1 expression was consistently detectable in ME cells, and that the level of WT-1 expression was inversely correlated with breast tumor progression [44].

p63 and p73

p63 is a nuclear protein that shares significant amino acid identity with the p53 protein in the transactivation domain, the DNA-binding domain, and the oligomerization domain [12,13]. The expression of p63 in the breast is exclusive to

the nuclei of ME cells, and neither stromal fibroblasts nor vascular smooth muscle cells show p63 immunostaining [45]. p63 is believed to be critical for maintenance of the progenitor cell populations that are necessary to sustain epithelial development and morphogenesis [12,13]. p73 is also a homologue of p53, and is believed to have a function and distribution similar to that of p63 [14].

14-3-3Sigma

This recently introduced ME cell marker is a candidate tumor suppressor gene transactivated by p53 in response to DNA damage [15]. It is consistently present in benign and pre-invasive breast lesions, and is preferentially expressed by myoepithelial cells. It might also serve as a novel prognostic factor for breast cancer patients [15].

Neuropilin-1 (NRP-1)

NRP-1 is a recently identified specific receptor for the vascular endothelial growth factor [46,47]. ME cells in both hyperplastic and neoplastic lesions displayed a higher level of NRP-1 expression than those in normal breast tissues. NRP-1 expression is also detectable in vascular smooth muscle and endothelial cells [46,47].

CD 10

CD10 is a 100-kDa cell surface metalloendopeptidase, also called neprilysin, which inactivates a variety of biologically active peptides. This protein was initially classified as a common acute lymphoblastic leukemia antigen. Subsequent studies have shown that CD10 was consistently positive in the ME cells of all normal breast tissues, whereas the number of ME-positive cells and the intensity of the immunostaining were substantially reduced in distended ducts and ductal adenomas [48–50].

S100

The S100 gene family comprises more than 20 members whose protein sequences encompass at least one EF-hand Ca^{2+}-binding motif. The expression of individual family members appears to be tissue-specific [51]. S100 proteins are consistently present in human breast ME cells, but are often expressed in luminal epithelial cells, thus, they are not specific markers for myoepithelial cells [52–54]. Molecular analysis of breast tumors has revealed that several S100s, including S100A2, S100A4, and S100A7, exhibit altered expression levels during breast tumorigenesis and progression [51]. S100A4 is considered a tumor promoter gene [55]. Elevated levels of S100A4 are associated with poor survival rates in breast cancer patients and induce metastasis in rodent models, as well as increased cell motility and invasion in vitro [56]. S100A9 expression in human invasive breast adenocarcinoma is closely associated with poor tumor differentiation [57]. Further studies are needed to better understand the important roles of S100s in human breast cancer.

Other important molecules

A number of growth factors, growth factor receptors, and other biologically important molecules have also been reported to be present in ME cells, but their clinical significance has yet to be determined [20–22,35].

Common myoepithelial markers used in distinguishing in situ from invasive tumors

Immunohistochemically, some of the above-mentioned ME cell markers have been routinely used in the clinic for the detection of ME cells in the differentiation between in situ and invasive tumors. Among these, SMA is the most frequently employed, and is considered to be very reliable. We and others, however, have repeatedly noticed that about 4–6% of morphologically distinct ME cells in hematoxylin and eosin (H&E) stained sections fail to show SMA immunostaining [24,25]. In an attempt to further characterize these SMA-negative cells, one of our recent studies assessed H&E- and SMA-immunostained sections from 175 breast cancer patients, and identified three cases harboring ducts that displayed morphologically distinct ME cell layers in H&E sections while showing no SMA immunostaining in $\geq$ 1/3 or the entire ME cell layer [11]. Eight additional consecutive sections from each of these cases were stained for SMA with a black chromogen, and the same ducts with SMA-negative ME cells in each of the eight sections were photographed. Then, each section was re-stained with a red chromogen for one of eight additional markers that are supposed to be exclusively or preferentially expressed in ME cells. The same duct with SMA-negative cells in each of the eight sections was then re-examined for the expression of the other markers. Results showed that SMA-negative ME cells in two cases also failed to display immunoreactivity for any of the other markers, including calponin, CD10, smooth muscle myosin-heavy chain (SMMHC), maspin, Wilms' tumor-1, and cytokeratins 5, 14, and 17 (CK5, 14, and 17). SMA-negative ME cells in one case, however, showed distinct immunoreactivities for maspin, as well as CK5, 14, and 17 [11].

Major myoepithelial cell lesions

Compared to epithelial lesions, ME cell lesions are very rare, which frustrates a detailed biological and clinical profiling of this entity. Morphologically, ME cell lesions can be classified into three primary categories [58,59].

Myoepitheliosis

This lesion is characterized by a mild proliferation of ME cells within and around ducts. The proliferating cells are of spindle or cuboid shape, often distending or occluding the involved ducts. These ME cells can be easily distinguished from the adjacent ductal epithelial cells by immunohisto-

chemical staining because antibodies against microfilament- and intermediate filament-related molecules will recognize ME cells, while antibodies against epithelial-specific antigen (ESA) will uniformly identify the epithelial cells.

Adenomyoepithelioma

This lesion is characterized by extensive proliferation of ME cells. Morphologically, these proliferating cells can be divided into spindle cells, tubular cells, and lobular variants. The common feature of this abnormality is the formation of solid masses that distend or occlude the ductal structures. Similar to myoepitheliosis, these hyperplastic lesions can be easily differentiated from epithelial cells by immunohistochemical staining with antibodies against microfilament- and intermediate filament-related molecules or epithelial-specific antigen (ESA).

Myoepithelial carcinoma

These lesions are rare, accounting for less than 1% of breast malignancies. Based on published reports, the most commonly seen type of this lesion is the spindle cell type. This type of lesion is not typically clinically aggressive, although examples of metastases from pure ME carcinomas have been reported [60–62]. Breast carcinomas composed in part or entirely of myoepithelial cells have been diagnosed in well-defined categories: benign tumors, tumors with low malignant potential, and malignant tumors, including adenomyoepithelioma, low-grade adenosquamous carcinoma, adenoid cystic carcinoma, and malignant myoepithelioma [58,59,63]. Pure myoepithelial carcinoma of the breast is rare, and little is known about its natural history or long-term outcome following treatment. A recent report showed that it adopts an aggressive clinical course, with an outcome comparable to poorly differentiated adenocarcinoma of the breast [64]. Comparative genomic hybridization analysis of myoepithelial carcinomas of the human breast compared to ductal carcinomas revealed that the mean number of genetic alterations was 2.1 for myoepithelioma and 8.6 for ductal carcinoma [65]. The relatively few genetic alterations found in otherwise aggressive neoplasms indicate that myoepithelial tumors may be useful models for the delineation of genes important in breast tumorigenesis.

Impacts of ME cell alterations on adjacent epithelial cells

While attempting to identify the early signs of ME layer disruptions and precursors of invasive breast lesions, we have recently carried out a number of studies focusing on the correlation between structural integrity in the ME cell layers and the immunohistochemical and genetic profiles in adjacent epithelial cells. Our studies have revealed, for the first time, several lines of evidence suggesting that the structural integrity of ME cells directly impacts the biological phenotypes of epithelial cells, tumor progression, and invasion processes.

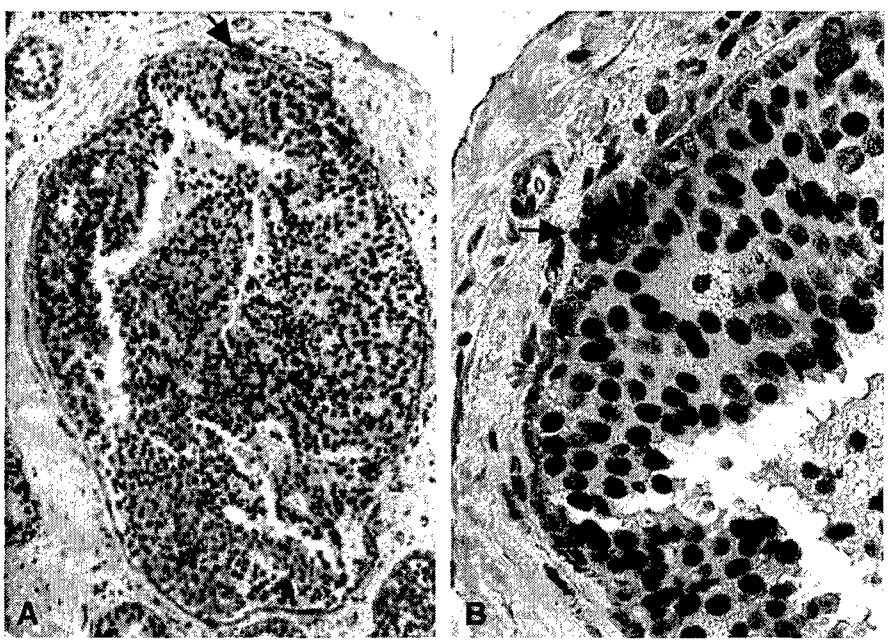

Fig. 4. Focal disruptions in ME cell layers and loss of ER expression in overlying tumor cells. A paraffin section was double-immunostained for ER (black or brown) and SMA (red). Arrows identify focal ME disruptions and overlying ER-negative cell clusters. (A) 100× magnification; (B) 400× magnification. (Adapted from Fig. 2, Ref. No. 44, copyright of Dr. Yan-Gao Man).

Focal ME layer disruptions and loss of ER expression in overlying epithelial cells are correlated events

In 5698 duct cross-sections from 220 patients with estrogen receptor (ER) positive, in situ breast tumors, we detected a total of 405 (7.1%) focal ME cell layer disruptions, defined as the absence of ME cells resulting in a gap equal to or greater than the combined size of 3 ME cells [44]. Of these, 350 (86.4%) were overlaid by clusters of epithelial cells with no or substantially reduced ER expression, in sharp contrast to adjacent epithelial cells within the same duct, which showed strong ER immunoreactivity and overlaid a non-disrupted ME cell layer (Fig. 4) [44].

Cells in ducts with and without focal ME disruptions have different proliferation rates

Compared to those in morphologically comparable ducts without focal ME layer disruptions, cells in ducts with focally disrupted ME layers with or without ER-negative clusters had a significantly higher ($P < 0.01$) proliferation rate, 19.05% with disruptions versus 4.0% without disruptions (Man et al., unpublished data [66]), as determined by immunohistochemical staining for Ki-67 (Fig. 5). From 200 patient cases, positive cells were counted under a microscope, and the proliferation rate was statistically analyzed in morphologically similar ducts (defined as the same histological type and grade, with similar size, shape, and architecture) with and without focal ME disruptions from 20 randomly selected cases (one section for each case) using Student's t test. A cell was considered Ki-67-positive if a distinct nuclear staining was seen, based on the instructions provided by the manufacturers (Vector and Dako). The expression of the human Ki-67 protein is strictly associated with cell proliferation. Ki-67 is present during all active phases of the cell cycle, including G(1), S, G(2), and mitosis, but is absent from resting cells, in G(0), making it an excellent marker for cell proliferation [67].

Loss of heterozygosity (LOH) in estrogen receptor (ER)-negative cells

ER-negative cells had a substantially higher frequency and different pattern of loss of heterozygosity (LOH) at multiple chromosomal loci when compared to ER-positive cells, including those harboring tumor suppressor genes fragile histidine triad and Wilms' tumor 1 [11,44] (Fig. 6).

Breast epithelial cell clusters at the site of ME layer disruptions have increased expression of genes related to proliferation, apoptosis, invasion, and metastasis

ER-negative and adjacent ER-positive cells within the same duct were microdissected for RNA extraction and amplification from consecutive sections of 30 frozen DCIS tissues with focally disrupted ME cell layers. Amplified RNA molecules were converted to biotin-labeled cDNA molecules and interrogated with "Cancer PathwayFinder"

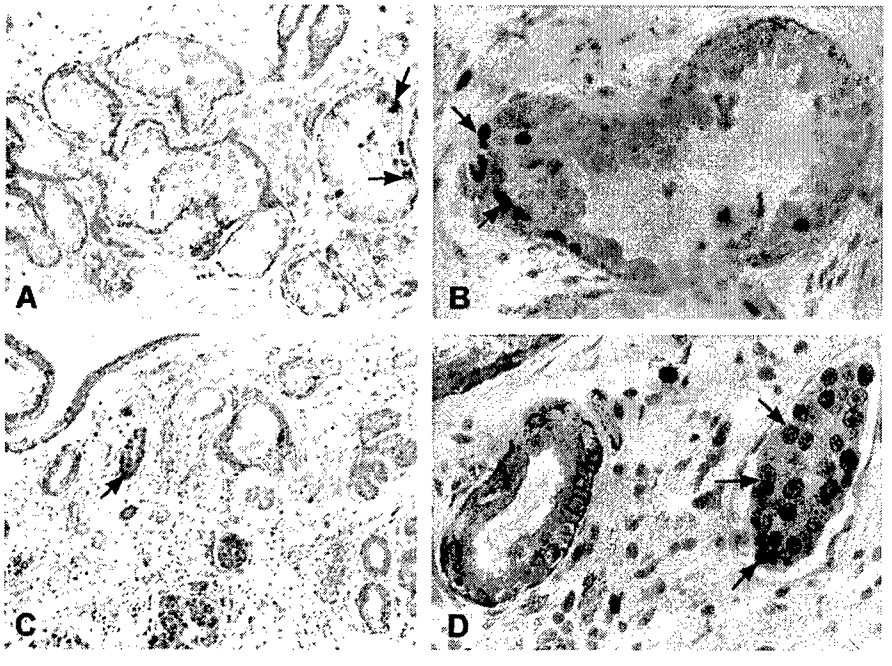

Fig. 5. Cells in ducts with and without focal ME cell layer disruptions show a different proliferation rate and localization of clusters of proliferating cells. Three paraffin sections were double-immunostained for Ki-67 (brown to black) and SMA (red). Note that more Ki-67-positive cells are seen in the ducts with a focally disrupted ME cell layer (arrows) compared to adjacent ducts without focal ME cell layer disruptions. Many Ki-67-positive cells are located near focal ME layer disruptions (A and B), or in the ducts without distinct SMA staining (C and D) (arrows). A (200×) and B (400×) are from two different slides, while C (100×) and D (400×) are from the same slide.

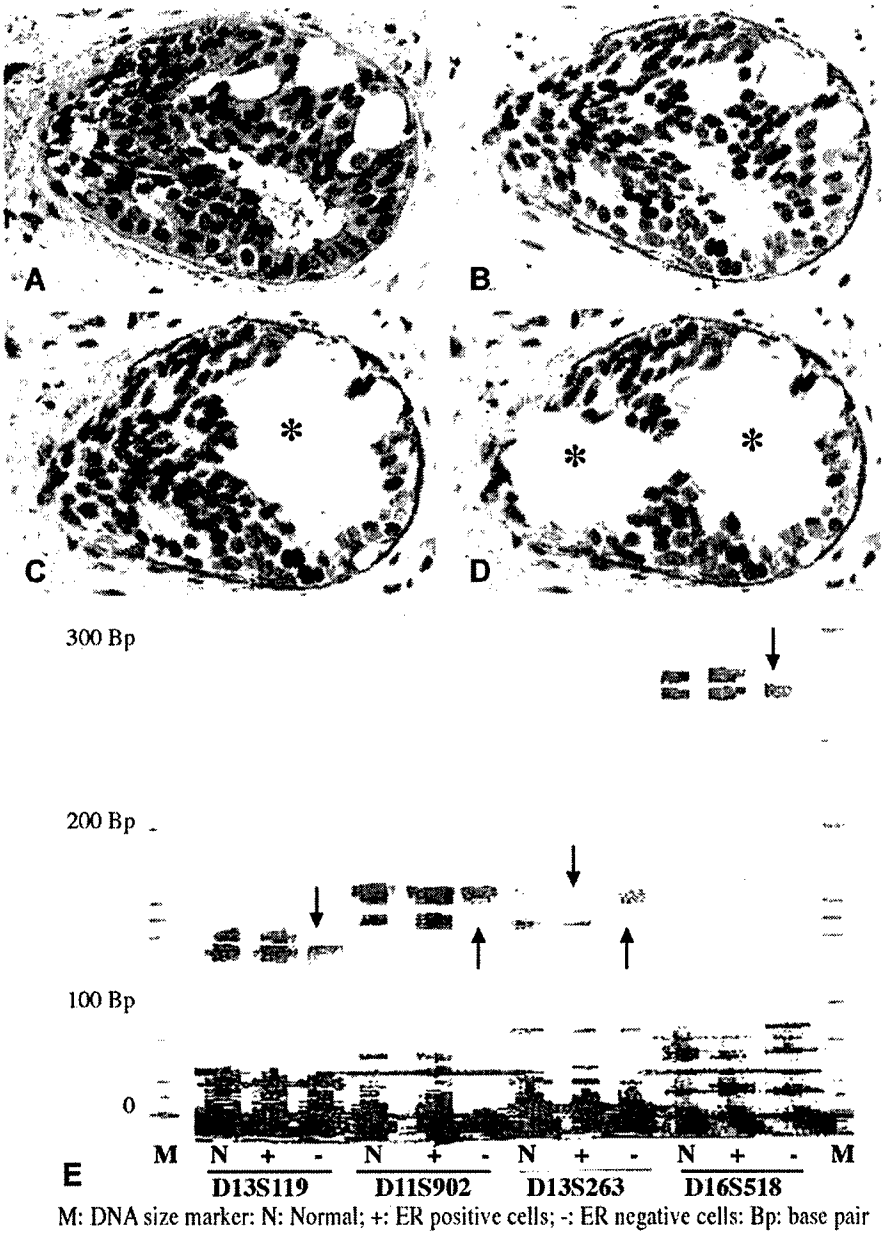

Fig. 6. Comparison of the loss of heterozygosity (LOH) pattern in ER-negative and ER-positive cells within the same duct. (A) H&E staining of a duct with atypical intraductal hyperplasia. (B) The adjacent section of A, immunostained for ER (brown) and SMA (red). (C) Microdissection of ER-positive cells. (D) Microdissection of ER-negative cells. (E) LOH at four selected DNA markers. Asterisks indicate the ER-positive and negative cells removed for LOH assessment; arrows identify LOH. (Adapted from Fig. 7, Ref. No. 44, copyright of Dr. Yan-Gao Man).

arrays. Epithelial cell clusters overlying focally disrupted ME layers had higher levels of mRNA expression in genes related to proliferation, apoptosis, invasion, and metastasis when compared to their adjacent counterparts within the same duct [68] (Fig. 7 and Table 1). Among the 11 up-regulated genes in ER-negative cell clusters overlying focally disrupted ME cell layers, 8 directly or indirectly promote proliferation and tumor progression, while 3 promote apoptosis. The intrinsic mechanism for a simultaneous elevation of both proliferation and apoptosis-related genes in the same cell cluster after a focal ME disruption is unknown and counterintuitive, but this may represent a defensive response resulting from leukocyte infiltration and immunoreactions.

Leukocyte infiltration is increased at focal ME disruptions

As macrophages and other leukocytes contain digestive enzymes capable of degrading the basement membrane and injuring host cells, our recent studies assessed the possible roles of these cells in ME cell layer disruptions and tumor invasion. A total of 23 DCIS samples containing ducts with

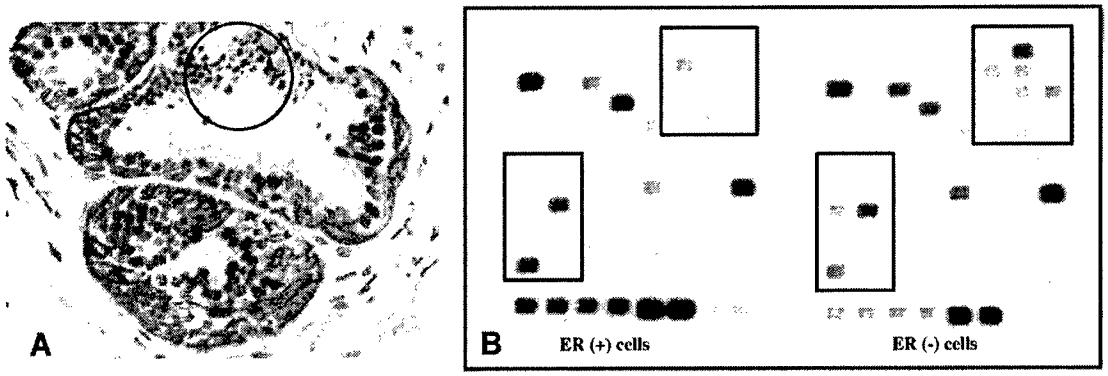

Fig. 7. Comparison of the frequency and level of mRNA expression in ER (−) and adjacent ER (+) cells within the same duct. Frozen sections from 30 selected cases were double-immunostained for ER (brown) and SMA (red). The ER-negative cells overlying focally disrupted ME cell layers and their adjacent ER-positive counterparts within the same duct were microdissected for RNA extraction, amplification, and analyses using a focused cDNA microarray containing 96 tumor progression and invasion related genes. Chemiluminescent array images were captured and digitized using the FluorChem 8800 Imaging System. The integrated density values in paired samples with distinct signals in both ER-negative and ER-positive cells were measured and compared. Of 15 differentially expressed genes, 11 were higher in ER (−), 2 were higher in ER (+), and 2 were equal in these two cell types ($P < 0.01$). (A) The microdissected ER (−) and ER (+) cells. (B) cDNA microarray images of ER (−) and ER (+) cells in a selected case.

focally disrupted ME cell layers were selected from 94 cases identified in our previous studies. Two consecutive sections from each case were double immunostained, one with leukocyte common antigen (LCA) plus smooth muscle actin (SMA), the other with Ki-67 plus SMA. Ducts lined by ≥50 epithelial (EP) cells and distinct ME cell layers were similarly examined. To the best of our knowledge, our studies have revealed several interesting phenomena that have not been reported previously:

Ductal tumors with and without ME disruptions have different rates of leukocyte infiltration

A total of 191 duct cross-sections were found to contain focal ME cell layer disruptions; of which, 186 (97.4%) were with and 5 (2.6%) were without leukocyte infiltration. Of 207 morphologically similar sections without ME disruptions, 46 (22.2%) were with and 161 (77.8%) were without leukocyte infiltration (Man et al., unpublished data [69]) (Fig. 8 and Table 2).

Table 1
Comparison of the frequency and level of mRNA expression in ER (+) and ER (−) cells

Gene group	Gene name	Higher in ER (−)	Higher in ER (+)	Equal in both	Case number
Adhesion	CD44	13	4	1	18
	CDH1	13	4	3	20
	MUC18L	5	5	2	12
Angiogenesis	EGFR	5	6	1	12
	IFNA1	10	5	2	17
	TNF	5	9	6	20
Apoptosis	BAX	9	4	0	13
	CASP9	9	5	5	19
	CFLAR	10	5	1	16
Cell cycle	CDC25A	9	1	7	17
	CDKN2A	10	4	2	16
	RAD53	9	1	2	12
Inv and metastasis	NME4	10	4	6	20
	TIMP1	6	6	3	15
Signal transduct	NFKB1	11	6	3	20
Total		134 (54.3%)	69 (27.9%)	44 (17.8%)	247
P	<0.01				

ME cells surrounded by or adjacent to leukocytes show distinct morphologic alterations

When compared to their counterparts farther away from the leukocytes, ME cells surrounded by or adjacent to leukocytes, where focal disruptions of the ME cell layer are observed, often show distinct morphologic alterations, including the loss of SMA immunostaining (Fig. 8 and Man et al., unpublished results]. The ME cells surrounding focally disrupted ME layers, in contrast to the epithelial cells, generally display a substantially lower proliferation rate when compared to those in non-disrupted layers (Man et al., unpublished results).

The vast majority of proliferating clusters of epithelial cells is located at or near focally disrupted ME layers

Ki-67-positive cells in ducts with focally disrupted ME cell layers were generally subjacent to disruptions, and over 30 clusters of proliferating cells were seen directly overlying or near focally disrupted ME cell layers (Fig. 5). In contrast, Ki-67-positive cells in ducts without ME disruptions were scattered randomly over the entire epithelial compartment [69].

Our hypothesized mechanism for ME cell layer disruption and tumor invasion

The mechanisms for focal ME layer disruptions and the formation of ER-negative cell clusters are unknown, but these are likely the result of localized ME cell death, leukocyte infiltration, and the resultant responses, based

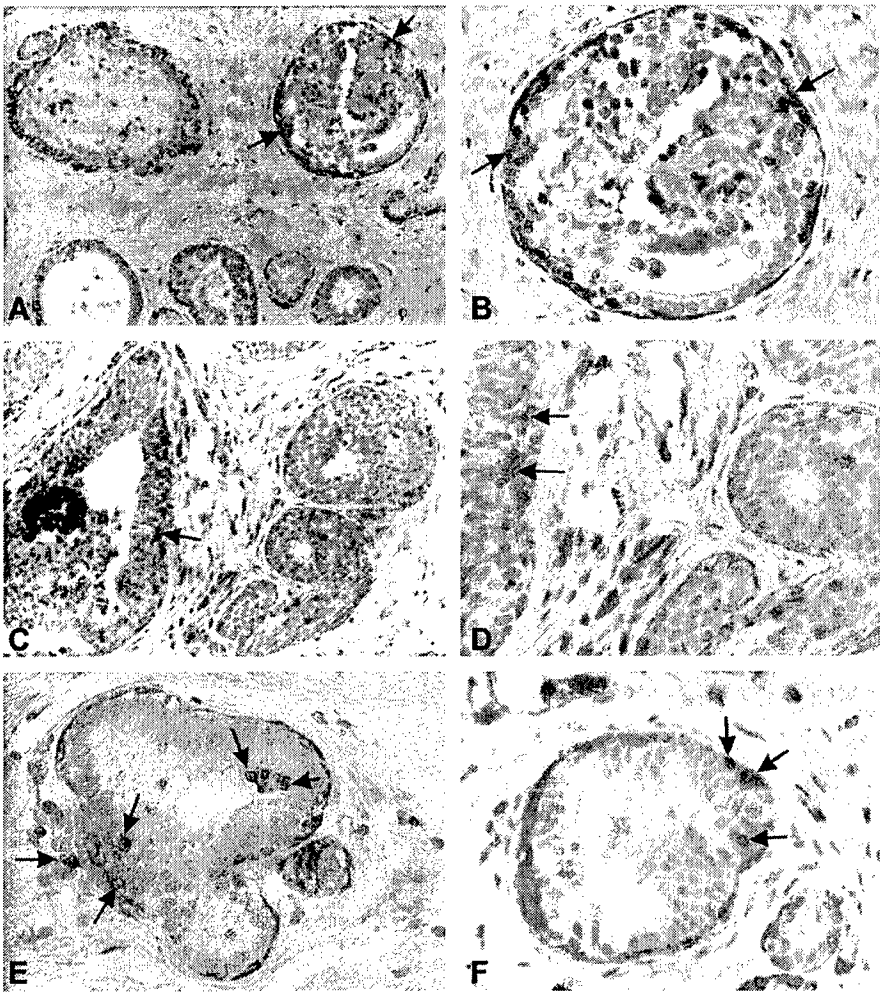

Fig. 8. The correlation between focal ME cell layer disruption and leukocyte infiltration. Four sections were double-immunostained for SMA (red) and leukocyte common antigen (brown). Many leukocytes (arrows) are located at or near the focal ME cell layer disruptions, suggesting a correlation between focal ME cell layer disruptions and leukocyte infiltration. Epithelial cells adjacent to leukocytes often show noticeable changes in size and nuclear shape compared to cells farther away from the leukocytes. A (200×) and B (400×) are from the same slide, C (200×) and D (400×) are from the same slide, and E (400×) and F (400×) are from two different slides. Human lymph nodes and blood smears were used as positive controls for leukocytes and normal mouse serum was used as a negative control for the monoclonal antibody directed against the leukocyte common antigen (data not shown).

upon the following observations. First, no morphologically distinct ME cells are detectable at the disruptions in multiple consecutive sections in all cases, indicating a physical absence of ME cells. Second, our previous studies have shown that the frequency of focal ME cell layer disruptions is independent of the size, length, and architecture of the ducts and acini [44], suggesting that it is unlikely the disruption is induced by mechanical forces, such as elevated pressure in the lumen or an increased cell number. Third, our previous studies have shown that 97.4% of the ducts with focal ME disruptions showed leukocyte infiltration, significantly increased when compared to 22.2% ($P < 0.01$) in morphologically similar ducts without focal ME cell layer disruptions [66,68]. Fourth, ME cells surrounded by or adjacent to leukocytes often showed distinct morphological alterations. Fifth, the ME cells near the focally disrupted layers, in contrast to the epithelial cells, seem to have a substantially lower proliferation rate compared to those with intact ME layers (Man et al. unpublished data [68]).

Table 2
Frequencies of white blood cell infiltration in mammary ducts with and without focal myoepithelial cell layer disruptions

	Section number	With WBC	Without WBC	*P*
Disrupted	191	186 (97.4%)	5 (2.6%)	<0.01
Non-disrupted	207	46 (22.2%)	161 (77.8%)	

Our speculation is further supported by several lines of evidence. More and more data have shown that a variety of external and internal insults could specifically affect the physical and functional status of ME cells. A wide variety of proteolytic enzymes produced by tumor or stromal cells could substantially change the physical integrity of the base-

ment membrane, which might subsequently affect the functions of ME cells [1,70]. A number of chemical compounds or biological reagents could also target ME cells. For example, exposure to lambda carrageenan, an anionic polymer, could result in filament disassembly and loss of the ME cells, while exposure to oxytocin could substantially enhance the rate of ME cell proliferation and differentiation [71,72].

The human immunosurveillance system could specifically or non-specifically target the ME cells. It has been well documented that leukocyte infiltration into tumor tissues is a common event, and that the number of leukocytes within tumor tissues is linearly increased with tumor progression [73,74]. This increase of leukocytes is particularly evident during the progression of DCIS to infiltrating ductal carcinoma, in which up to a four-fold increase of lymphoid infiltration has been reported. The extent of increased macrophage presence in tumor tissues has been found to correlate with a worse prognosis and a significantly higher mortality rate [73,74]. Furthermore, patients with lymphocyte infiltration at the tumor edge were found to have a noticeably poorer short-term prognosis compared to those with lymphocyte infiltration in other locations [75]. More importantly, leukocytes are capable of freely crossing both the basement membrane and ME cell layer, and leukocytes contain a number of digestive enzymes that can effectively degrade the basement membrane and alter host cells [76–79].

Based on these findings, we propose that a localized ME cell death and the resultant immunoreactions are the triggering factors for disruptions in ME cell layers, the formation of ER-negative cell clusters, and subsequent stromal and vascular invasion. These ER-negative cell clusters are most likely to be of epithelial origin, derived from mutated primitive stem cells or de-differentiated proliferating cells. We hypothesize that the major steps leading to the initiation and progression of tumor invasion are as follows:

(1) The ME cells constitute a self-renewing population, which normally undergoes proliferation to replace aged or injured ME cells.
(2) An external or internal insult, such as a localized trauma, inflammatory reactions of the stroma, or exposure to lambda-carrageenan, directly disrupts the structural integrity of the ME cell layers or impairs the normal replacement process, resulting in a cluster of damaged or dying ME cells.
(3) The damaged or dying ME cells lose their capacity to manufacture tumor-suppressor proteins, with subsequent loss of the paracrine regulation of adjacent tumor cells.
(4) The residual products of dying ME cells attract macrophages and other leukocytes, which migrate to the injured site and interact with altered ME cells.
(5) Macrophages and other leukocytes release digestive enzymes, leading to the physical destruction of altered ME cells and the local basement membrane, resulting in a focal disruption or gap that allows direct communication between the tumor and stromal cells.
(6) The focal disruption or gap results in a focally increased permeability for the supply of metabolism- and growth-related molecules to overlying and adjacent tumor cells.
(7) This altered micro-environment leads to variable consequences in overlying tumor and adjacent ME cells, depending on the nature of these cells: First, if the overlying and adjacent cells are fully differentiated, no substantial alteration may be detectable; second, if these cells are partially differentiated, a limited or mild increase in cell proliferation might be seen, which may lead to a localized stromal invasion; third, if they are primitive stem cells, extensive cell proliferation might be observed, which may lead to the formation of new structures with normal morphology and functions; and fourth, if they are mutated stem cells, a series of events that differ markedly from both primitive stem cell-mediated and differentiated progenitor-mediated proliferation may take place, possibly leading to the inauguration of cancer cell clones. Previous studies have shown that a mutated stem cell is the common cellular origin of teratocarcinomas and epithelial cancers [80,81].
(8) The newly formed cell clusters undergo differentiation, releasing invasion-associated molecules, which triggers angiogenesis, tissue remodeling, and increased production of growth factors in the stroma, providing a favorable environment for tumor cell growth [3,82–86].
(9) The interactions between tumor and stromal cells lead to further destruction of ME layers and degradation of the basement membrane, accompanied by deeper and wider migration and invasion of the newly formed cell clusters.
(10) In addition to in situ ductal carcinoma, the above processes could potentially occur in normal breast tissues and hyperplastic lesions, which may lead to direct invasion. These processes may also be triggering factors for the progression of tumor stages.

Implications of our hypothesis

At present time, it is unknown what factors initiate the localized ME cell death. It remains to be investigated whether myoepithelial cell death is triggered by the primary lesion during carcinoma development, inflammatory changes of the stroma, or other factors. This question would be resolved through the study of developing disruptions as opposed to existing disruptions, but as yet, the formation of these disruptions cannot be predicted. Thus, it is very difficult to solve this problem, and this review article

concentrates on the elucidation of the significance of ME cell layer disruptions in tumor progression and invasion rather than the causes of ME cell death. We submit that localized ME cell death and subsequent immunoreactions are the direct cause for ME cell layer degradations based upon five observations arising from our current studies and other reports.

(1) Our previous studies have shown that the form, size, or frequency of ME cell layer disruptions seemed to be independent of the size, length, architecture, and overall ER negativity of the ducts, and also of the histological grade of the lesions [44,84–86]. This observation indicates that it is less likely that the developing tumor cells initiated the ME cell death, as a fraction of ducts with focal ME disruptions maintain an appearance that is otherwise morphologically normal.
(2) Ducts with focal ME cell layer disruptions have a significantly higher leukocyte infiltration, and most leukocytes are located at or near the disruptions [69]. Similar correlated events of basal cell layer disruptions and leukocyte infiltration have been observed in human prostate tumors [87]. It appears that the leukocyte infiltration is in response to ME cell death, with inflammatory responses following ME cell death rather than preceding it.
(3) Proteolytic enzyme inhibitor-based human clinical trials have been disappointing, indicating that blocking basement membrane-degrading proteases alone is not sufficient to inhibit tumor invasion and metastasis [2,3]. These reports also suggest that additional factors are involved in the processes of tumor invasion and metastasis.
(4) Both mammary epithelial and ME cells belong to self-renewing populations, with a life span of about 300 days. Aged and damaged cells are constantly replaced by normal cellular replacement and regeneration processes. If the rate of ME renewal is slower than the rate of death due to genetic alternations or microenvironmental factors at a highly localized site, focal ME cell layer disruptions may occur.
(5) As described earlier in this review article, previous studies have documented that a number of chemicals and the host's own leukocytes could specifically and non-specifically impact the physical integrity and functions of ME cells. These observations suggest that microenvironmental factors may induce ME cell death and ME cell layer disruptions. Therefore, ME cell death and ME cell layer disruptions are highly intricate processes that may be caused by multiple factors, and they may represent the earliest signs of tumor invasion and progression.

Although our hypothesis is intriguing, it is not known to what extent it reflects the intrinsic mechanism of ME cell disruptions and the formation of ER-negative tumor cell clusters for two main reasons: first, our data are limited, as observations are extracted from a small sample size, which may not reflect the real status of the general population; and second, the underlying mechanisms and detailed processes for each of our hypothesized steps have not been elucidated. However, given the facts that; first, the disruption of the ME cell layer is an absolute prerequisite for tumor invasion; second, cells overlying focally disrupted ME cells are morphologically, immunohistochemically, and genetically distinct from their adjacent counterparts within the same duct; and third, focal ME cell layer disruptions and leukocyte infiltration appear to be correlated events, our hypothesis might have important scientific and clinical implications.

In the scientific research field, our hypothesis may open a new window for the exploration of the mechanism of ME cell layer disruptions and tumor invasion. Our hypothesis might also be useful in the reconciliation of conflicting reports regarding the immunohistochemical and genetic profiles of breast lesions, as our findings clearly indicate that those conflicts are likely the result of the presence or absence of ME cell layer disruptions, and the differences in the molecular nature and growth pattern of the cells overlying or adjacent to these disruptions. In the clinical field, our hypothesis might be beneficial for the early detection and treatment of breast tumors. As genetic alterations determine the scope and extent of, and frequently precede, biochemical and morphologic changes, microdissection of these ER-negative cell clusters and their adjacent ER-positive counterparts for genetic and biochemical comparisons could potentially lead to the identification of specific molecules associated with the early events of ME cell layer disruption, tumor invasion, and metastasis.

The development of antibodies or chemical reagents to target these ER-negative cells and potential markers for tumor invasion and progression might provide a more effective and less toxic means to block tumor invasion at the earliest stages. Furthermore, microdissection of these ER-negative cell clusters in frozen tissues for tissue culture may lead to the establishment of useful cell lines for the benefit of cancer and stem cell researchers. More importantly, as our studies suggest that leukocytes and other immunosurveillance-related cells might be direct triggering factors for breast tumor progression and invasion, and that invasion could potentially occur from normal or hyperplastic lesions, the development of new strategies and approaches to attack these problems may have direct impact on the diagnosis, treatment, and prognosis of breast cancer patients [88].

Conclusions

The ME cell layer and the basement membrane are positioned between the mammary epithelium and the stroma, normally permitting the exchange of only small

molecules between these two cellular compartments. Due to this structural characteristic, the disruption of both the ME cell layer and the basement membrane is absolutely required for the progression of ductal carcinoma in situ to invasive status. In addition to this passive function as a structural barrier, ME cells have been found to possess several active functions, including the production of tumor suppressors, paracrine down-regulation of MMP expression, and participation in steroid hormone metabolism.

ME cells exclusively or preferentially express a number of proteins, and are subject to a variety of pathological alterations. Focal disruptions in ME cell layers are associated with the emergence of unusual cell clusters overlying these disruptions exhibiting several unique features, including the loss of estrogen receptor expression, a significantly higher proliferation rate, a significantly higher and different pattern of LOH, and a significantly higher frequency and level of mRNA expression for cell cycle, apoptosis, and invasion-related genes when compared to their adjacent counterparts in the same duct. Focal ME layer disruptions are also correlated with significantly higher leukocyte infiltration, and a higher rate of epithelial cell proliferation at or near the disruptions. Based on these and other findings, we have proposed the novel hypothesis that focal ME cell layer disruptions, leukocyte infiltration, and the emergence of ER-negative cell clusters might be correlated events, representing an early sign of ME disruption and the formation of a biologically more aggressive cell clone(s) inaugurating the processes of invasion. This novel hypothesis appears to be useful in the reconciliation of conflicting reports regarding the heterogeneous genetic and immunohistochemical profiles of breast lesions, and it may lead to the development of more effective and specific approaches for breast cancer detection, treatment, and prevention.

Acknowledgments

Supported in part by Congressionally Directed Medical Research Program/DOD grants DAMD17-01-1-0129 and DAMD17-01-1-0130 to YGM, and DAMD17-02-1-0238 and NIH grant CA78646 to QXAS. The authors appreciate Robert G. Newcomer at Professor Sang's laboratory for his excellent editorial assistance.

References

[1] R.H. Goldfarb, L.A. Liotta, Proteolytic enzymes in cancer invasion and metastasis, Semin. Thromb. Hemostasis 12 (1986) 294–307.
[2] L.M. Coussens, B. Fingleton, L.M. Matrisian, Matrix metalloproteinase inhibitors and cancer: trials and tribulations, Science 295 (2002) 2387–2392.
[3] L.M. Matrisian, G.W. Sledge Jr., S. Mohla, Extracellular proteolysis and cancer: meeting summary and future directions, Cancer Res. 63 (2003) 6105–6109.
[4] A. Tsubura, N. Shikata, T. Inui, S. Morii, T. Hatano, T. Oikawa, Immunohistochemical localization of myoepithelial cells and basement membrane in normal, benign and malignant human breast lesions, Virchows Arch. 413 (1988) 133–139.
[5] M.J. Slade, R.C. Coope, J.J. Gomm, R.C. Coombes, The human mammary gland basement membrane is integral to the polarity of luminal epithelial cells, Exp. Cell Res. 247 (1999) 267–278.
[6] F. Jolicoeur, T.A. Seemayer, G. Gabbiani, A. Robidoux, L. Gaboury, L.L. Oligny, W. Schurch, Multifocal, nascent, and invasive myoepithelial carcinoma(malignant myoepithelioma) of the breast: an immunohistochemical and ultrastructural study, Int. J. Surg. Pathol. 10 (2002) 281–291.
[7] A. Nerlich, Morphology of basement membrane and associated matrix proteins in normal and pathological tissues, Veroff. Pathol. 145 (1995) 1–139.
[8] N. Miosge, The ultrastructural composition of basement membrane in vivo, Histol. Histopathol. 16 (2001) 1239–1248.
[9] T.M. Murad, E. von Haam, Ultrastructure of myoepithelial cells in human mammary gland tumor, Cancer 21 (1986) 1137–1149.
[10] M.D. Sternlicht, S.H. Barsky, The myoepithelial defense: a host defense against cancer, Med. Hypotheses 48 (1997) 37–46.
[11] R. Zhang, Y.-G. Man, R.S. Vang, J.S. Saenger, R. Barner, D. Wheeler, C.Y. Liang, T.N. Vinh, G.L. Bratthauer, A subset of morphologically distinct mammary myoepithelial cells lacks corresponding immunophenotypic markers, Breast Cancer Res. 5 (2003) R151–R156.
[12] A. Yang, R. Schweitzer, D. Sun, M. Kaghad, N. Walker, R.T. Bronson, C. Tabin, A. Sharpe, D. Caput, C. Crum, F. McKeon, p63 is essential from regenerative proliferation in limb, craniofacial and epithelial development, Nature 398 (1999) 714–718.
[13] A.A. Milis, B. Zheng, X.J. Wang, H. Vogel, D.R. Roop, A. Bradley, p63 is a p53 homologue required for limb and epidermal morphogenesis, Nature 398 (1999) 708–713.
[14] T. Yamamoto, K. Oda, K. Miyazaki, Y. Ichiyotani, Y. Takenouchi, T. Kamei, N. Shirafuji, Y. Nimura, M. Hamaguchi, S. Matsuda, p73 is highly expressed in myoepithelial cells and in carcinomas with metaplasia, Int. J. Oncol. 19 (2001) 271–276.
[15] P.T. Simpson, T. Gale, J.S. Reis-Filho, C. Jones, S. Parry, D. Steele, A. Cossu, M. Bodroni, G. Palmieri, S.R. Lakhani, Distribution and significance of 14-3-3sigma, a novel myoepithelial marker, in normal, benign, and malignant breast tissue, J. Pathol. 202 (2004) 274–285.
[16] J.L. Jones, J.A. Shaw, J.H. Pringle, R.A. Walker, Primary breast myoepithelial cells exert an invasion-suppressor effect on breast cancer cells via paracrine down-regulation of MMP expression in fibroblasts and tumor cells, J. Pathol. 201 (2003) 562–572.
[17] V. Djonov, K. Hogger, R. Sedlacek, J. Laissure, A. Draeger, MMP-19: cellular localization of a novel metalloproteinase within normal breast tissue and mammary gland tumors, J. Pathol. 195 (2001) 147–155.
[18] T. Gudjonson, L. Ronnov-Jessen, R. Villadsen, F. Rank, M.J. Bissell, O.W. Peterson, Normal and tumor-derived myoepithelial cells differ in their ability to interact with luminal breast epithelial cells for polarity and basement membrane deposition, J. Cell Sci. 115 (2002) 39–50.
[19] P. Moller, G. Mechtersheimer, M. Kaufmann, G. Moldenhauer, F. Momburg, T. Mattfeldt, H.F. Otto, Expression of epidermal growth factor receptor in benign and malignant primary tumours of the breast, Virchows Arch. A: Pathol. Anat. Histopathol. 414 (1989) 157–164.
[20] M.A. Deugnier, M.M. Farado, P. Rousselle, J.P. Thiery, M.A. Glukhova, Cell–extracellular matrix interactions and EGF are important regulators of the basal mammary epithelial cell phenotype, J. Cell Sci. 112 (1999) 1035–1044.
[21] J.J. Gomm, P.J. Browne, R.C. Coope, G.S. Bansal, C. Yiangou, C.L. Johnston, R. Mason, R.C. Coombes, A paracrine role for myoepithelial cell-derived FGF2 in the normal human breast, Exp. Cell Res. 234 (1997) 165–173.
[22] J. Roose, G. Huls, M. van Beest, P. Moerer, K. van der Horn, R. Goldschmeding, T. Logtenberg, H. Clevers, Synergy between tumor

suppressor APC and the beta-catenin-Tcf4 target Tcf1, Science 285 (1999) 1923–1926.
[23] J.K. Tobacman, M. Hinkhouse, Z. Khalkhali-Ellis, Steroid sulfatase activity and expression in mammary myoepithelial cells, J. Steroid Biochem. Mol. Biol. 81 (2002) 65–68.
[24] S. Bose, C.M. Derosa, L. Ozzello, Immunostaining of type IV collagen and smooth muscle actin as a aid in the diagnosis of breast lesions, Breast J. 5 (1999) 194–201.
[25] M.G. Joshi, A.K. Lee, C.A. Pedersen, M.G. Schnitt Camus, K.S. Hughes, The role of immunohistochemical markers in the differential diagnosis of proliferative and neoplastic lesions of the breast, Mod. Pathol. 9 (1996) 57–62.
[26] H. Yoshida, Immunohistochemical studies on expression of human vascular smooth muscle myosin heavy chain isoforms in normal mammary glands, benign mammary disorders and mammary carcinomas, Pathol. Int. 48 (1998) 433–439.
[27] D.J. Dabbs, A.M. Gown, Distribution of calponin and smooth muscle myosin heavy chain in fine-needle aspiration biopsies of the breast, Diagn. Cytopathol. 20 (1999) 203–207.
[28] S. Damiani, M. Ludvikova, G. Tomasic, S. Bianchi, A.M. Gown, V. Eusebi, Myoepithelial cells and basal lamina in poorly differentiated in situ duct carcinoma of the breast. An immunocytochemical study, Virchows Arch. 434 (1999) 227–234.
[29] I. Ohyabu, T. Takasaki, S. Akiba, S. Nomura, N. Enokizono, Y. Sagara, J. Hiroi, R. Nagai, H. Yoshida, Immunohistochemical studies on expression of human vascular smooth muscle myosin heavy chain isoforms in normal mammary glands, benign mammary disorders and mammary carcinomas, Pathol. Int. 48 (1998) 433–439.
[30] M.M. Miettinen, M. Sarlomo-Rikala, A.J. Kovatich, J. Lasota, Calponin and h-caldesmon in soft tissue tumors: consistent with h-caldesmon immunoreactivity in gastrointestinal stromal tumors indicates traits of smooth muscle differentiation, Mod. Pathol. 12 (1999) 756–762.
[31] A. Batistatou, D. Stefanou, E. Arkoumani, N.J. Agnantis, The usefulness of p63 as a marker of breast myoepithelial cells, In Vivo 17 (2003) 573–576.
[32] Y. Shimoyama, T. Yoshida, M. Terada, Molecular cloning of a human Ca-dependent cell–cell adhesion molecule homologous to mouse placental cadherin: its low expression in human placental tissues, J. Cell Biol. 109 (1989) 1787–1794.
[33] D.F. Jarrard, R. Paul, A. van Bokhoven, S.H. Nguven, G.S. Bova, M.J. Wheelock, K.R. Johnson, J. Schalken, M. Bussemakers, W.B. Isaacs, P-cadherin is a basal cell-specific epithelial marker that is not expressed in prostate cancer, Clin. Cancer Res. 3 (1997) 2121–2128.
[34] A.P. Soler, K.A. Knudsen, H. Salaxar, A.C. Han, A.A. Keshgegian, P-cadherin expression in breast carcinoma indicates poor survival, Cancer 86 (1999) 1263–1272.
[35] R. Moll, W.W. Franke, D.L. Schiller, B. Geiger, R. Krepler, The catalog of human cytokeratins: patterns of expression in normal epithelia, tumors and cultured cells, Cell 31 (1982) 11–24.
[36] R.H. Wetzels, R. Holland, U.J. Van Haelst, E.B. Lane, I.M. Leigh, F.C. Ramaekers, Detection of basement membrane components and basal cell keratin 14 in noninvasive and invasive carcinomas of the breast, Am. J. Pathol. 34 (1989) 571–579.
[37] R.H. Wetzels, H.J. Kuijpers, E.B. Lane, I.M. Leigh, S.M. Troyanovsky, R. Holland, U.J. Van Haelst, F.C. Ramaekers, Basal cell-specific and hyperproliferation-related keratins in human breast cancer, Am. J. Pathol. 138 (1991) 751–763.
[38] K.M. McGowan, P.A. Coulumbe, Onset of keratin 17 expression coincides with the definition of major epithelial lineages during skin development, J. Cell. Biol. 143 (1998) 469–486.
[39] N. Maass, T. Hojo, M. Zhang, R. Sager, W. Jonat, K. Nagasaki, Maspin—A novel protease inhibitor with tumor suppressing activity in breast cancer, Acta Oncol. 39 (2000) 931–934.
[40] M. Zhang, O. Volpert, Y.H. Shi, N. Bouck, Maspin is an angiogenesis inhibitor, Nat. Med. 6 (2000) 196–199.
[41] J.S. Reis-Filho, F. Milanezi, P. Silva, F.C. Schmitt, Maspin expression in myoepithelial tumors of the breast, Pathol. Res. Pract. 197 (2001) 817–821.
[42] V. Scharnhorst, A.J. van der Eb, A.G. Jochemsen, WT1 proteins: functions in growth and differentiation, Gene 273 (2001) 141–161.
[43] A. Fabre, A.H. McCabb, D. O'Shea, D. Broderick, G. Keating, B. Tobin, T. Gorey, P.A. Dervan, Loss of heterozygosity of the Wilms' tumor suppressor gene (WT-1) in in-situ and invasive breast carcinoma, Hum. Pathol. 30 (1999) 661–665.
[44] Y.-G. Man, L. Tai, R. Barner, R. Vang, J.S. Saenger, K.M. Shekitka, G.L. Bratthauer, D.T. Wheeler, C.L. Liang, T.N. Vinh, B.L. Strauss, Cell clusters overlying focally disrupted mammary myoepithelial cell layers and adjacent cells within the same duct display different immunohistochemical and genetic features: implications for tumor progression and invasion, Breast Cancer Res. 5 (2003) R231–R241.
[45] M. Barbareschi, L. Pecciarini, M.G. Cangi, E. Macri, A. Rizzo, G. Viale, C.W. Doglioni, p63, a p53 homologue, is a selective nuclear marker of myoepithelial cells of the human Breast, Am. J. Surg. Pathol. 25 (2001) 1954–1960.
[46] J.M. Stepheson, S. Banerjee, N.K. Saxena, R. Cherian, S.K. Banerjee, Neuropilin-1 is differentially expressed in myoepithelial cells and vascular smooth muscle cells in preneoplastic and neoplastic human breast: a possible marker for the progression of breast cancer, Int. J. Cancer 101 (2002) 409–414.
[47] M. Fakhari, D. Pullirsch, D. Abraham, K. Paya, R. Hofbauer, P. Holzfeind, M. Hofmann, S. Aharinejad, Selective upregulation of vascular endothelial growth factor receptors neuropilin-1 and -2 in human neuroblastoma, Cancer 94 (2002) 258–263.
[48] S. Moritani, R. Kushima, H. Sugihara, M. Bamba, T. Kobayashi, T. Hattori, Availability of CD10 immunohistochemistry as a marker of breast myoepithelial cells on paraffin sections, Mod. Pathol. 15 (2002) 397–405.
[49] K. Iwaya, H. Ogawa, M. Izumi, M. Kuroda, K. Mukai, Stromal expression of CD10 in invasive breast carcinoma: a new predictor of clinical outcome, Virchows Arch. 440 (2002) 589–593.
[50] H. Yaziji, A.M. Gown, N. Sneige, Detection of stromal invasion in breast cancer: the myoepithelial markers, Adv. Anat. Pathol. 7 (2002) 100–109.
[51] E.D. Emberley, L.C. Murphy, P.H. Watson, S100A7 and the progression of breast cancer, Breast Cancer Res. 6 (2004) 153–159.
[52] C.E. Gillett, L.G. Bobrow, R.R. Millis, S100 protein in human mammary tissue-immunoreactivity in breast carcinoma, including Paget's disease of the nipple, and value as a marker of myoepithelial cells, J. Pathol. 160 (1990) 19–24.
[53] S. Dwarakanath, A.K. Lee, R.A. Delellis, M.L. Silverman, L. Frasca, H.J. Wolfe, S-100 Protein positivity in breast carcinomas: a potential pitfall in diagnostic immunohistochemistry, Hum. Pathol. 18 (1987) 1144–1148.
[54] S. Lunde, J.M. Nesland, R. Holm, J.V. Johannessen, Breast carcinomas with protein S-100 immunoreactivity. An immunocytochemical and ultrastructural study, Pathol. Res. Pract. 182 (1987) 627–631.
[55] S.R. Grey, S.S. Dlay, B.E. Leone, F. Cajone, G.V. Sherbet, Prediction of nodal spread of breast cancer by using artificial neural network-based analyses of S100A4, nm23 and steroid receptor expression, Clin. Exp. Metastasis 20 (2003) 507–514.
[56] S.R. Jenkinson, R. Barraclough, C.R. West, P.S. Rudland, S100A4 regulates cell motility and invasion in an in vitro model for breast cancer metastasis, Br. J. Cancer 90 (2004) 253–262.
[57] K. Arai, T. Teratani, R. Kuruto-Niwa, T. Yamada, R. Nozawa, S100A9 expression in invasive ductal carcinoma of the breast: S100A9 expression in adenocarcinoma is closely associated with poor tumor differentiation, Eur. J. Cancer 40 (2004) 1179–1187.
[58] M.P. Foschini, V. Eusebi, Carcinomas of the breast showing myoepithelial cell differentiation. A review of the literature, Virchows Arch. 432 (1998) 303–310.
[59] J.D. Coyne, P.A. Dervan, L. Barr, High-grade carcinomas of the breast showing patterns of mixed ductal and myoepithelial differentiation

(including myoepithelial cell-rich carcinoma of the breast), Histopathology 44 (2004) 580–584.
[60] F.A. Tavassoli, Myoepithelial lesions of the breast: myoepitheliosis, adenomyoepithelioma, and myoepithelial carcinoma, Am. J. Surg. Pathol. 15 (1991) 554–568.
[61] W. Schurch, C. Potvin, T.A. Seemayer, Malignant myoepithelium (myoepithelial carcinoma) of the breast: an ultrastructural and immunohistochemical study, Ultrastruct. Pathol. 8 (1985) 1–11.
[62] P.S. Thorner, H.J. Kahn, R. Baumal, K. Lee, W. Moffatt, Malignant myoepithelioma of the breast: an immunohistochemical study by light and electron microscope, Cancer 57 (1986) 745–750.
[63] M. Tamai, Intraductal growth of malignant mammary myoepithelioma, Am. J. Surg. Pathol. 16 (1992) 1116–1125.
[64] K.A. Behranwala, N. Nasiri, R. A'Hern, G.P. Gui, Clinical presentation and long-term outcome of pure myoepithelial carcinoma of the breast, Eur. J. Surg. Oncol. 30 (2004) 357–361.
[65] C. Jones, M.P. Foschini, R. Chaggar, Y.J. Lu, D. Wells, J.M. Shipley, V. Eusebi, S.R. Lakhani, Comparative genomic hybridization analysis of myoepithelial carcinoma of the breast, Lab. Invest. 80 (2000) 831–836.
[66] Y.-G. Man, R. Zhang, R. Mattu, T. Shen, Q.-X. Sang, A subset of mammary epithelial cells overlying focally disrupted myoepithelial cell layers shows an unusual immunostaining pattern for proliferation-related proteins (abstract), Breast Cancer Res. Treat. 82 (2003) S163–S164 (Suppl.).
[67] T. Scholzen, J. Gerdes, The Ki-67 protein: from the known and the unknown, J. Cell. Physiol. 182 (2000) 311–322.
[68] Y.G. Man, Y. Zhang, T. Shen, X. Zeng, J. Tauler, J.L. Mulshine, B.L. Strauss, cDNA expression profiling reveals elevated gene expression in cell clusters overlying focally disrupted myoepithelial cell layers: implications for breast tumor invasion, Breast Cancer Res. Treat. (2004) (in press).
[69] M. Yousefi, R. Mattu, C. Gao, Y.-G. Man, Mammary ducts with and without focal myoepithelial cell layer disruptions show a different frequency of white blood cell infiltration and growth pattern: implications for tumor progression and invasion, AIMM (2004) (in press).
[70] P. Mignatti, E. Robbins, D.B. Rifkin, Tumor invasion through the human amniotic membrane: requirement for a proteinase cascade, Cell 47 (1986) 487–498.
[71] J.K. Tobacman, Filament disassembly and loss of mammary myoepithelial cells after exposure to lambda-carrageenan, Cancer Res. 57 (1997) 2823–2826.
[72] A. Sapino, L. Macri, L. Tonda, G. Bussolati, Oxytocin enhances myoepithelial cell differentiation and proliferation in the mouse mammary gland, Endocrinology 133 (1993) 838–842.
[73] H. Ben-Hur, O. Cohen, D. Schneider, P. Gurevich, R. Halperin, U. Bala, M. Mozes, I. Zusman, The role of lymphocytes and macrophages in human breast tumorigenesis: an immunohistochemical and morphometric study, Anticancer Res. 22 (2002) 1231–1238.
[74] J.H. Harmey, E. Dimitriadis, E. Kay, H.P. Redmond, D. Bouchier-Hayes, Regulation of macrophage production of vascular endothelial growth factor (VEGF) by hypoxia and transforming growth factor beta-1, Ann. Surg. Oncol. 5 (1998) 271–278.
[75] F. Hartveil, Breast cancer: poor short-term prognosis in cases with moderate lymphocyte infiltration at the tumor edge: a preliminary report, Oncol. Rep. 5 (1998) 423–426.
[76] X.D. Zhang, G.D. Schiller, P.G. Gill, B.J. Coventry, Lymphoid cell infiltration during cancer growth: a syngeneic rat model, Immunol. Cell Biol. 76 (1998) 550–555.
[77] R. Steadman, M.H. Irwin, P.L. St. John, W.D. Blackburn, L.W. Heck, D.R. Abrahamson, Laminin cleavage by activated human neutrophils yields proteolytic fragments with selective migratory properties, J. Leukocyte Biol. 53 (1993) 354–365.
[78] L.W. Heck, W.D. Blackburn, M.H. Irwin, D.R. Abrahamson, Degradation of basement membrane laminin by human neutrophil elastases and cathepsin G, Am. J. Pathol. 136 (1990) 1267–1274.
[79] S. Nzula, J.J. Going, D. Stott, The role of B lymphocytes in breast cancer: a review and current status, Cancer Therapy 1 (2003) 81–91.
[80] S. Sell, G.B. Pierce, Maturation arrest of stem cell differentiation is a common pathway for the cellular origin of teratocarcinomas and epithelial cancers, Lab. Invest. 70 (1994) 6–22.
[81] J.E. Trosko, C.C. Chang, Role of stem cells and gap junctional intercellular communications in human carcinogenesis, Radiation Res. 155 (2001) 175–180.
[82] L.A. Rudolph-Owen, L.M. Matrisian, Matrix metalloproteinases in remodeling of the normal and neoplastic mammary glands, J. Mammary Gland Biol. Neoplasia 3 (1998) 177–189.
[83] F. Moinfar, Y.-G. Man, L. Arnould, G.L. Bratthauer, M. Ratschek, F.A. Tavassol, Concurrent and independent genetic alterations in the stromal and epithelial cells of mammary carcinoma: Implications for tumorigenesis, Cancer Res. 60 (2000) 2562–2566.
[84] Y.-G. Man, J.S. Saenger, R.S. Vang, R. Barner, D. Wheeler, A. Martinez, J.L. Mulshine, Identification of invasive precursor cells in normal and hyperplastic breast tissue (abstract), Proc. Am. Assoc. Cancer Res. 44 (2003) 68.
[85] Y.-G. Man, R.S. Vang, J.S. Saenger, B.L. Strauss, R. Barner, D.T. Wheeler, C.Y. Liang, G.L. Bratthauer, C. Mannion, Development and progression of mammary ductal tumors appear to be mediated by surrounding myoepithelial cells (abstract), Mod. Pathol. 16 (2003) 39A–40A.
[86] Y.-G. Man, R. Mattu, R. Zhang, M. Yousefi, Q.-X. Sang, T. Shen, A subset of normal and hyperplastic appearing mammary ductal cells display invasive features (abstract), Breast Cancer Res. Treat. 82 (2003) S141 (suppl.).
[87] Y.-G. Man, T. Shen, Y.-G. Zhao, Q.-X. Sang, Focal prostate basal cell layer disruptions and leukocyte infiltration are correlated events: a potential mechanism for basal cell layer disruptions and tumor invasion, Cancer Detection and Prevention, (Accept pending revision).
[88] B.S. Herbert, Advances in breast cancer therapy and chemoprevention: current strategies and new approaches, Cancer Ther. 1 (2003) 363–371.

ELSEVIER

Cancer Detection and Prevention xxx (2005) xxx–xxx

Cancer Detection and Prevention

www.elsevier.com/locate/cdp

Focal prostate basal cell layer disruptions and leukocyte infiltration are correlated events: A potential mechanism for basal cell layer disruptions and tumor invasion☆

Yan-Gao Man MD, PhD[a,*], Ting Shen MD, PhD[b], Yunge Zhao MD, PhD[c], Qing-Xiang Amy Sang PhD[c]

[a] *Department of Gynecologic and Breast Pathology, Armed Forces Institute of Pathology and American Registry of Pathology, 6825 16th Street NW, Washington, DC 20306-6000, USA*

[b] *Department of Pathology, Quest Diagnostics Inc., Teterboro, NJ, USA*

[c] *Department of Chemistry and Biochemistry, Florida University, Tallahassee, FL, USA*

Abstract

To assess the potential correlation between basal cell layer disruptions and leukocyte infiltration, consecutive sections of normal ($n = 5$) and tumor ($n = 50$) prostate tissues were double immunostained for cytokeratin 34βE12 (CK 34βE12) plus leukocyte common antigen, Ki-67, or proliferating cell nuclear antigen (PCNA). Of 2047 acini and ducts examined, 201 contained focal basal cell layer disruptions. Of those, 183 (91%) showed leukocyte infiltration, compared to 67 (33.3%) in 201 morphologically comparable structures with an intact basal cell layer ($P < 0.01$). Basal cell layers adjacent to or surrounded by leukocytes were often attenuated or fragmented, and leukocytes were generally located at or near disruptions. Disrupted basal cell layers showed a markedly reduced proliferation rate, compared to their non-disrupted counterparts. Cells overlying focal basal cell layer disruptions often displayed distinct changes in the size, nuclear shape, density, and polarity, compared to those away from disruptions. A vast majority of proliferating tumor cells were located at or near basal cell layer disruptions. These findings suggest that focal basal cell layer disruptions and leukocyte infiltration are correlated events, representing a potential trigger factor for prostate tumor invasion.

Keywords: Tumor progression and invasion; Focal basal cell layer disruption; Leukocyte infiltration; Epithelial–stromal interactions; Cell growth pattern

1. Introduction

The epithelium of normal and pre-invasive human prostate tissues is physically separated from the stroma by both the basement membrane and basal cells, which rest on the basement membrane and form a continuous layer that surrounds the epithelium [1–5]. This architectural feature confers the basal cell layer and basement membrane two important biological and clinical functions. First, as the epithelium is normally devoid of lymphatic and blood vessels and totally depends on the stroma for its metabolism and survival needed materials, the basement membrane and basal cell layer function as gatekeepers, directly mediating the communication between these two compartments. Second, due to the physical interposition of the basal cell layer and basement membrane, tumor cells have to first pass through the basal cell layer, followed by the basement membrane, to physically reach the stroma. In other words, a physical or functional disruption of both the basal cell layer and basement membrane is a pre-requisite for tumor progression from an in situ to invasive status.

A generally accepted hypothesis for the cause of basement membrane disruptions and subsequent tumor invasion has been attributed primarily, if not solely, to the over-production of proteolytic enzymes by tumor and/or stromal cells [6]. A wide variety of enzymes, including glycanases and proteases, have been found to promote

☆ The opinions and assertions contained herein represent the personal views of the authors and are not to be construed as official or as representing the views of the Department of the Army or the Department of Defense.

* Corresponding author. Tel.: +1 202 782 1612; fax: +1 202 782 3939.
E-mail address: man@afip.osd.mil (Y.-G. Man).

0361-090X/$30.00 © 2005 Published by Elsevier Ltd. on behalf of International Society for Preventive Oncology.
doi:10.1016/j.cdp.2005.01.004

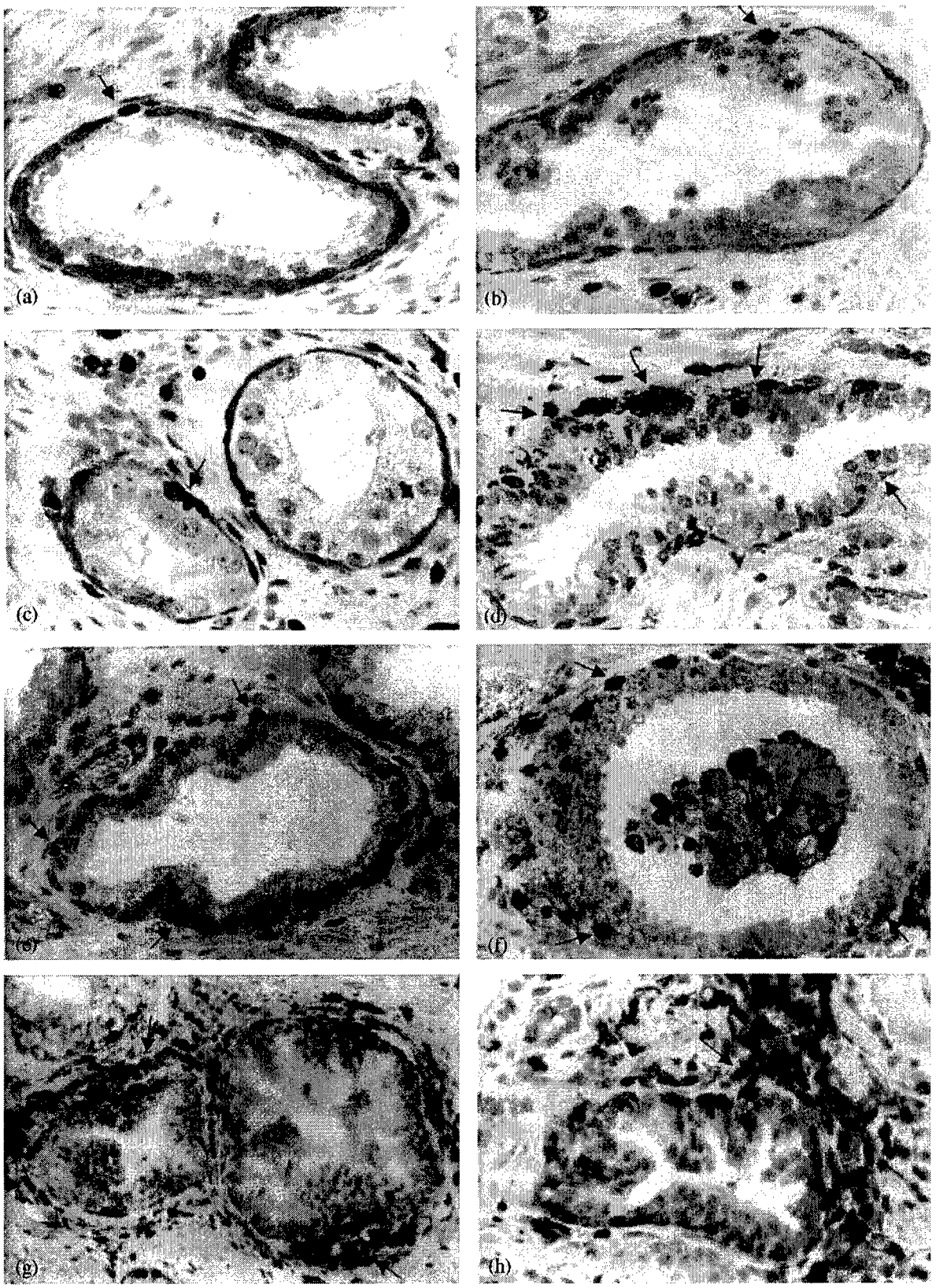

Fig. 1. Focal basal cell layer disruptions in non-invasive prostate tumors sections were double immunostained for CK 34βE12 (red) and LCA (brown). Arrows identify focal disruptions and leukocytes: (a, c, e, and g) 150×; (b, d, f, and h) are a higher magnification 300× of (a, c, e, and g), respectively.

basement membrane degradations and tumor invasion, while the corresponding inhibitors to these enzymes specifically suppress or block these processes in both test tubes and animal models [7–10]. This hypothesis, however, might not reflect the intrinsic mechanism of basal cell degradations and tumor invasion for two reasons: (1) neither the normal cellular kinetics nor the dynamic alterations of basal cells during tumor invasion have been well elucidated; and (2) results from proteinase inhibitor-based human clinical trials have been disappointing [11,12].

While attempting to identify the intrinsic mechanism and early signs of tumor invasion, we have carried out a number of studies on mammary ductal carcinoma in situ (DCIS), focusing on the correlation between the structural integrity of the myoepithelial (ME) cell layer and the biologic presentations of the overlying tumor cells. In focally disrupter ME cell layers, 97.4% of the ducts showed leukocyte infiltration at or near the disruption at a higher cell proliferation rate than ducts without focal ME cell layer disruption. A majority of the proliferating cells were located at or near ME cell layer disruptions [13–15].

Because the prostate basal cell layer is apparently structurally and functionally comparable to the ME cell layer [1–4], this study attempted to assess: (1) whether focal basal cell layer disruptions and leukocyte infiltration are detectable in prostate tumors; (2) whether epithelial cells in ducts and acini with and without focal basal layer disruptions have a different rate and clusters of multiple proliferating cells; and (3) whether a focal basal cell layer disruption and leukocyte infiltration are triggered by localized basal cell death or degenerations.

2. Materials and methods

Consecutive sections at 4–5 μm thickness were made from formalin-fixed, paraffin-embedded human prostate tissues, and placed on positively charged microscope slides. Sections were stained with hematoxylin and eosin (H&E) for morphological classification based on published criteria [17]. Sections from 5 normal and 50 prostate tumors with co-existing normal, hyperplastic, prostatic intraepithelial neoplastic (PIN), and invasive components were selected for immunohistochemical assessment as previously described [18,19]. Briefly, two adjacent sections from each case were incubated at 70 °C for 30 min, deparaffinized with three changes of xylene, and washed in descending concentrations of ethanol and tap water. Deparaffinized sections were incubated at about 70 °C overnight in 1X antigen retrieval solution (BioMedcare, Foster City, CA, USA), washed in warm tap water, and incubated with H_2O_2 blocking solution and normal serum. Then, one section was sequentially immunostained with antibodies to leukocyte common antigen (LCA, clones PD7/26 and 2B11, which reacts with both nucleated cells of the haematopoietic origin and lymphocytes) plus cytokeratin (CK) 34βE12, and the other with antibodies to Ki-67 plus CK 34βE12 (Dako Corporation, Carpinteria, CA, USA).

Each immunostained section was examined with attention to the cross section profiles of ducts and acini with ≥40 epithelial cells and morphologically distinct basal cell layers on H&E and immunostained sections. A focal basal cell layer disruption was defined as the absence of basal cells in at least three adjacent sections, resulting in a gap equal to or greater than the combined size of at least three basal cells, or multiple such gaps in a given duct or acinus. Leukocyte infiltration was defined as the appearance of a single or a group of LCA positive cells within the epithelial compartment or at a direct physical contact with the basal cells.

As the disruptions were generally small and not readily appreciable, the physical status of the basal cell layers and leukocyte infiltration in a given acinus or duct were first photographed with 35 mm slide films by an investigator. Then, developed slide films were reviewed under a slide projector by at least two investigators. The interpretation of the physical status of each structure was based on the uniform conclusion of all reviewers. The disagreement was settled by either excluding the section or repeating the immunostaining on a new slide.

The rate and distribution of proliferating cells in ducts with and without focal basal cell layer disruptions were similarly evaluated as above with focusing on the clusters of multiple proliferating cells (at least four Ki-67 positive tumor cells) located within a given site.

To assess the possibility that a focal basal cell layer disruption and leukocyte infiltration are triggered by a localized basal cell death or degeneration, sections from each case were double immunostained for CK 34βE12 and proliferating cell nuclear antigen (PCNA), whose expression in prostate appeared to be preferentially present in basal

Table 1
Frequencies of leukocyte infiltration in acini and ducts with and without focal basal cell layer disruptions

Cell type	No. examined	No. of disruptions	No. of infiltration	*P*-value
Normal	85	3 (3.5%)	2 (66.6%)	
Normal in tumor	500	43 (8.6%)	38 (88.4%)	
Hyperplasia in tum	800	82 (10.3%)	76 (92.7%)	
PIN in tumor	747	76 (10.2%)	69 (90.7%)	
Normal and hyperplasi and PIN[a]	201	0	67 (33.3%)	<0.01

[a] A total of 201 morphologically comparable normal appearing ($n = 43$), hyperplastic (HP, $n = 82$), and neoplastic (prostatic intraepithelial neoplasia, PIN, $n = 76$) acini and ducts without focal basal cell layer disruptions were used for comparison.

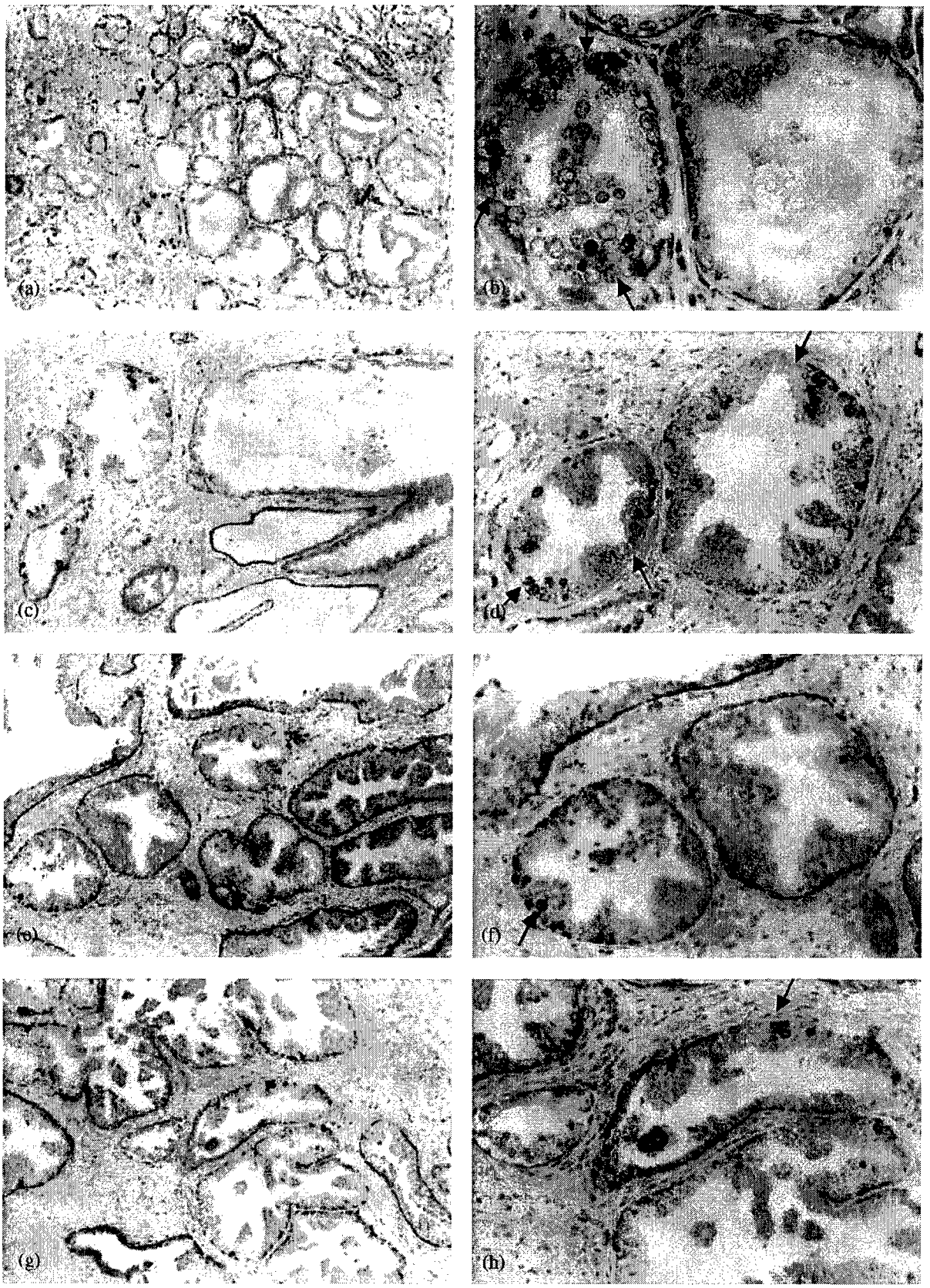

Fig. 2. Cell proliferation status in ducts with and without focal basal cell layer disruptions sections were double immunostained for CK 34βE12 (red) and Ki-67 (brown). Arrows identify focal basal cell layer disruptions and associated proliferating cells: (a) 150×; (b) is a higher magnification of (a) 300×; (c and e) 100×; (d and f) are a higher magnification of (c and e) 200×, respectively.

cells, based on our own experience. The proliferation status of basal cells in ducts and acini with and without focal disruptions, and near and away from the disruptions, were semi-quantitatively compared.

3. Results

Distinct focal basal cell layer disruptions and leukocyte infiltration were detected in both normal and tumor tissues. The size of the disruptions varied substantially, from a few cells (Fig. 1a and b) to over 80% of the entire basal cell layer (Fig. 1e and f). The rate and size of basal cell layer disruptions appeared to be independent of the size, length, and architecture of the ducts and acini, and also of the histologic type and grade of the lesions, but appeared to correlate with the extent and location of leukocyte infiltration.

Leukocyte infiltration occurred in four main forms: (1) a single or few leukocytes inter-positioning at or near the center of a single small disruption (Fig. 1a and b); (2) leukocytes lined along a basal cell layer with a large (Fig. 1c–f) or multiple disruptions; (3) sheet-, or belt-like leukocyte aggregates partially surrounding a duct or acinus (Fig. 1g and h); and (4) leukocytes scattered among epithelial cells of a duct or acinus without distinct basal cell layer disruption (not shown). A majority of the infiltrates are cytotoxic lymphocytes and natural killer (NK) cells, based on our most recent studies [20–22].

Of a total of 85 acini and ducts examined in five normal controls, 3 (3.5%) contained focal basal cell layer disruptions in one case. Two of the three focal disruptions were associated with leukocyte infiltration. Of 50 cases with co-existing normal ($n = 500$), hyperplastic ($n = 800$), and PIN ($n = 747$) ducts and acini examined, the frequencies of focal basal cell layer disruptions were 8.6, 10.3, and 10.2%, respectively, and the frequencies of leukocyte infiltration were 88.4, 92.7, and 90.7%, respectively (Table 1). Overall, of a total of 2047 acini and ducts examined, 201 focal disruptions were identified. Of the 201 disruptions, 183 (91%) showed leukocyte infiltration, compared to 67 (33.3%) in 201 morphologically comparable (the same histological type and grade and similar architecture and size) acini and ducts without basal cell layer disruptions (Table 1).

A vast majority of the proliferating (Ki-67 positive) cells were located at or near the disruptions (Fig. 2). In addition, 22 clusters of multiple proliferating duct and acinar cells were seen directly overlying or near focally disrupted basal cell layers, but only four such clusters were seen in 201 morphologically comparable acini and ducts without basal cell layer disruptions (Table 2).

Table 2
Frequencies of clusters of multiple proliferating cells in acini and ducts with and without focal basal cell layer disruptions

Acinar and duct type	No. examined	No. of cluster (%)	*P*-value
With disruptions	201	22 (10.9%)	
Without disruptions	201	4 (2.0%)	<0.01

Basal cell layers adjacent to or surrounded by leukocytes and lymphocytes were often attenuated or fragmented, with substantial reduction of CK 34βE12 immunostaining, compared to those away from leukocytes (Fig. 3). Tumor cells immediately overlying focal basal cell layer disruptions were often morphologically distinct from their adjacent counterparts within the same duct or acinus in cell size, density, nuclear shape, and polarity (Fig. 3a, b, and e). Some of them appeared to invade the stroma (Fig. 3 b and e).

The frequency of PCNA expression in basal cells among cases and among different foci of the same case varied substantially. Of 50 ducts and acini with focally disrupted basal cell layers examined, 38 (76%) showed markedly reduced PCNA expression in the remaining basal cells, compared to 50 morphologically similar counterparts with intact basal cell layers. A vast majority of the basal cells immediately below focal disruptions had a markedly reduced PCNA expression, compared to their adjacent counterparts within the same duct, but away from disruptions (Fig. 4).

4. Discussion

The frequency and pattern of focal basal cell disruptions and leukocyte infiltration that were detected in prostate tumors in our current study are very similar to those of our previous studies in human breast tumors [13–16]. It appeared that focal basal or ME cell layer disruptions and leukocyte infiltration seem to be correlated events, which substantially impact the behavior and functions of overlying tumor cells, representing a potential trigger factor for tumor invasion.

A focal basal or ME cell layer disruption is likely caused by localized basal or ME cell death or degenerations and leukocyte infiltration, for several reasons. Leukocyte infiltration into tumor tissues is a common event, and that the number of infiltrated leukocytes appears to be linearly increased with tumor progression [23–25]. Furthermore, leukocytes contain a number of digestive enzymes that could specifically or non-specifically degrade both altered host cells and the basement membrane [26,27].

A localized basal cell death or degenerations and leukocyte infiltration could trigger tumor invasion through the following mechanisms:

1. Basal cells belong to a self-renewal population, and normally undergo proliferation and differentiation to replace aged or injured basal cells [28,29].
2. An external or internal insult, such as a localized trauma, chronic inflammation, or the exposure to lambda-

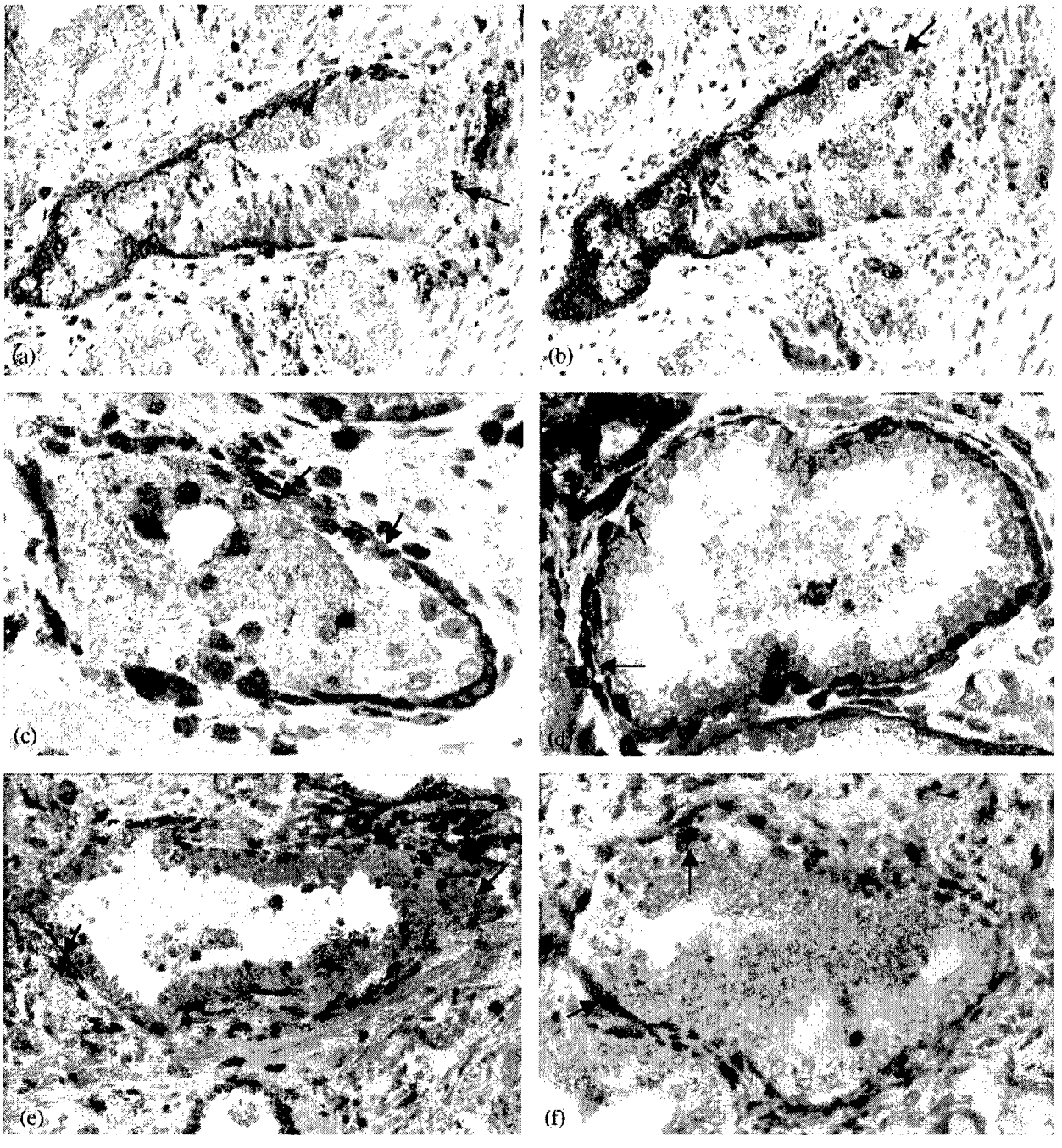

Fig. 3. Morphological and immunohistochemical alterations in cells adjacent to leukocytes sections were double immunostained for CK 34βE12 (red) and LCA or Ki-67 (brown). Arrows identify leukocytes or morphologically and immunohistochemically altered basal or tumor cells: (a) CK 34βE12 plus LCA; (b) a sequential section of (a), 34βE12 plus Ki-67; (c–f) 34βE12 plus LCA 200×.

carrageenan [30], directly disrupts the structural integrity of the basal cell layer or impairs the normal replacement process, resulting in a single or in a cluster of degenerated basal cells.

3. The degraded products of degenerated basal cells attract leukocytes, which migrate to the injured site and interact with altered basal cells.
4. Leukocytes release their digestive enzymes, leading to the physical destruction of altered basal cells and the adjacent basement membrane, as well as the formation of a foal disruption or gap that allows the direct contact between tumor and stromal cells.
5. The focal disruption in the basal cell layer and basement membrane results in an increased permeability of metabolism- and growth-related molecules to overlying and adjacent cells.
6. The altered micro-environment leads to variable consequences in overlying tumor and adjacent basal cells,

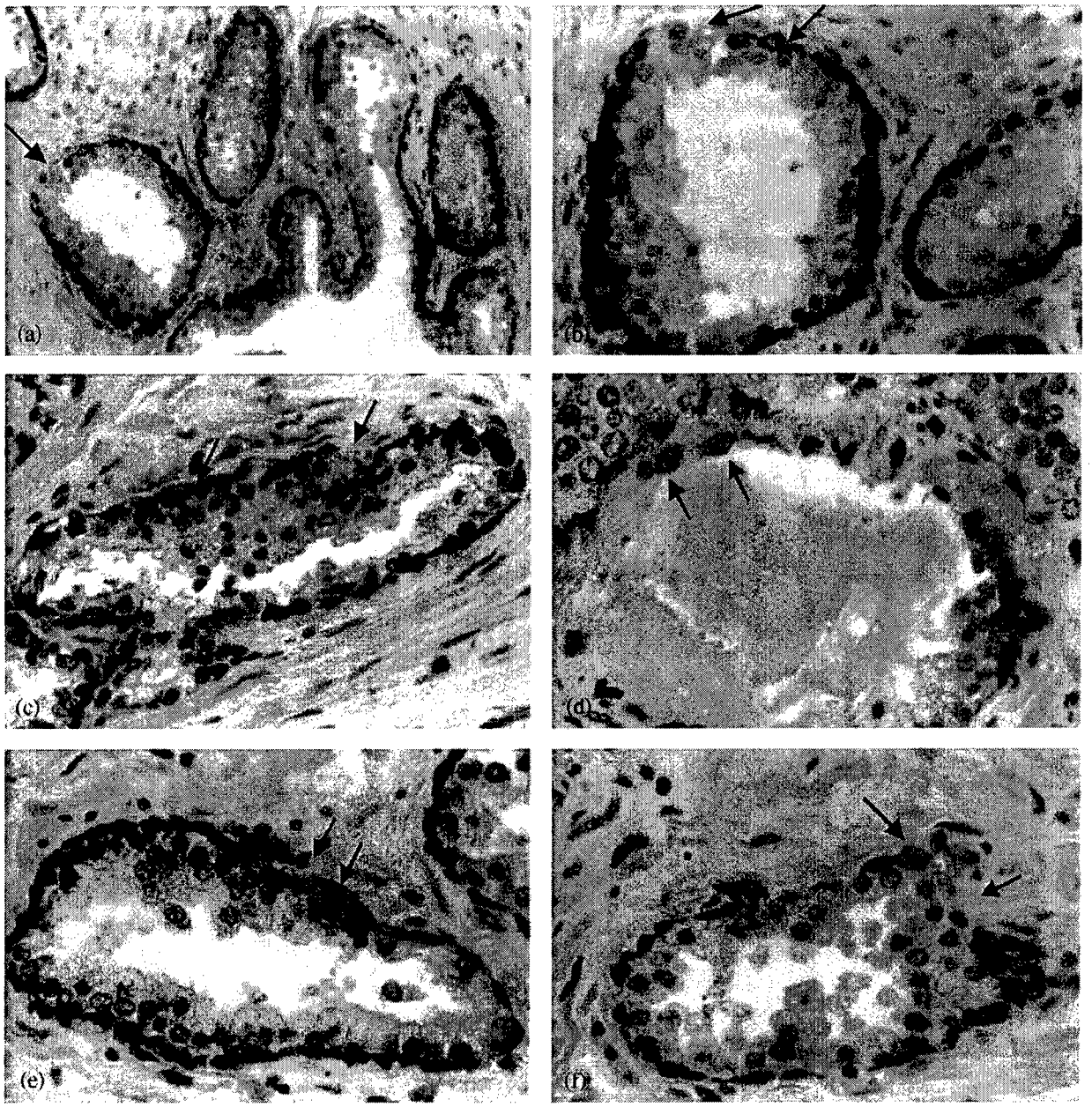

Fig. 4. The expression of PCNA in basal cells near and away from focal disruptions sections were double immunostained for CK 34βE12 (red) and PCNA (black). Arrows identify cells without PCNA expression. Note that most cells near the disruption are PCNA negative, while most cells away the disruption are PCNA positive: (a and c) 100×; (b and d) a higher magnification 200× of (a and c), respectively.

depending on the nature of these cells. If the overlying tumor cells are fully differentiated, no substantial alteration might be detectable. In contrast, if they are uncommitted stem or progenitor cells, an extensive cell proliferation can be expected, which leads to the formation of a biologically more aggressive cell cluster that invades the stroma.

7. The cell cluster undergoes cytodifferentiation and release stage-restricted and invasion-associated molecules, triggering angiogenesis, tissue remodeling, and increasing production of growth factors in the stroma, providing a favorable environment for tumor cell growth [31–34].
8. The interactions between tumor and stromal cells lead to further degradation of the basal cell layer and basement membrane, and a further expansion and stromal invasion of the newly formed cell cluster [31–34].

Knowledge is lacking as to whether or to what extent our hypothesis reflects the intrinsic mechanism of basal cell disruptions and tumor invasion, for the following reasons: (1) our data are extracted from a small sample size, which

may not reflect the real status in a larger number of cases; (2) the underlying mechanism for each of hypothesized steps have not been elucidated; and (3) the specific subtype of leukocytes associated with focal basal cell layer disruptions has not been determined. However, given the facts that the disruption of the basal cell layers is a prerequisite for tumor invasion and that results from proteinase inhibitor-based human clinical trials disfavor the traditional proteolytic enzyme theory [11,12], our hypothesis might open a new window to explore the intrinsic mechanism of tumor invasion. Currently, several studies on a larger number of cases are in progress to explore the issues that were not addressed in this study. Our recent studies have revealed that basal cells near a focal disruption have a significantly lower rate of p63 expression than their counterparts away from the disruption, and that cytotoxic lymphocytes and NK cells are preferentially associated with focal basal cell layer disruptions [20–22].

Acknowledgments

Supported in part by DOD grants DAMD17-01-1-0129 and DAMD17-01-1-0130 to Y.-G.M. and DOD grant DAMA17-02-1-0238, NIH grant CA78646, American Cancer Society grant F01FSU-1 to Q.-X.A.S. The authors are grateful to Doug Landry and James A. Nola of the AFIP Exhibition Section for their technical assistance in preparation of the figures.

References

[1] Mostofi FK, Price EB Jr. Tumors of the male genital system. Atlas of tumor pathology, 2nd series, Fascicle 8. Washington, DC: Armed Forces Institute of Pathology; 1973.

[2] Goldstein NS, Underhiel J, Roszka N, Neill JS. Cytokeratn 34 beta E-12 immunoreactivity in benign prostate acini. Quantitation, pattern assessment, and electron microscopic study. Am J Clin Pathol 1999;112:69–74.

[3] Bonkhoff H, Wernert N, Dhom G, Remberger K. Basement membranes in fetal, adult normal, hyperplastic and neoplastic human prostate. Virchows Arch A Pathol Anat Histopathol 1991;418:375–81.

[4] El-Alfy M, Pelletier G, Hermo LS, Labrie F. Unique features of the basal cells of human prostate epithelium. Microsc Res Tech 2000;51:436–46.

[5] Barsky SH, Siegal GP, Jannotta F, Liotta LA. Loss of basement membrane components by invasive tumors but not by the benign counterparts. Lab Invest 1983;49:140–7.

[6] Goldfarb RH, Liotta LA. Proteolytic enzymes in cancer invasion and metastasis. Semin Thromb Hemost 1986;12:294–307.

[7] Kosir MA, Wang W, Zukowski KL, Tromp G. Degradation of basement membrane by prostate tumor heparanase. J Surg Res 1999;81:42–7.

[8] Dawson LA, Maitland NJ, Turner AJ, Usmani BA. Stromal–epithelial interactions influence prostate cancer cell invasion by altering the balance of metallopeptidase expression. Br J Cancer 2004;90:1577–82.

[9] Udayakumar TS, Chen ML, Bair EL, et al. Membrane type-1-matrix metalloproteinase expressed by prostate carcinoma cells cleaves human laminin-5 beta3 chain and induces cell migration. Cancer Res 2003;63:2292–9.

[10] Hashimoto K, Kihira Y, Matuo Y, Usui T. Expression of matrix metalloproteinase-7 and tissue inhibitor of metalloproteinase-1 in human prostate. J Urol 1998;160:1872–6.

[11] Coussens LM, Fingleton B, Matrisian LM. Matrix metalloproteinase inhibitors and cancer: trial and tribulations. Science 2002;295(5564):2387–92.

[12] Matrisian LM, Sledge Jr GW, Mohla S. Exacellular proteolysis and cancer: meeting summary and future directions. Cancer Res 2003;63:6105–9.

[13] Yousefi M, Mattu R, Gao C, Man YG. Mammary ducts with and without focal myoepithelial cell layer disruptions show a different frequency of white blood cell infiltration and growth pattern: implications for tumor progression and invasion. Appl Immunohistochem Mol Morphol, in press.

[14] Man YG, Tai L, Barner R, Vang R, et al. Cell clusters overlying focally disrupted mammary myoepithelial cell layers and adjacent cells within the same duct display different immunohistochemical and genetic features: implications for tumor progression and invasion. Breast Cancer Res 2003;5:R231–41.

[15] Man YG, Zhang Y, Zeng X, et al. cDNA expression profiling reveals elevated gene expression in cell clusters overlying focally disrupted myoepithelial cell layers: implications for breast tumor invasion. Breast Cancer Res Treat, in press.

[16] Man YG, Sang QXA. The Significance of focal myoepithelial cell layer disruptions in human breast tumor invasion: a paradigm shift from the "protease-centered" hypothesis. Exp Cell Res 2004;301:103–18.

[17] Young RH, Srigley JR, Amin MB, et al. Tumors of the prostate gland, semenal vesicles, male urehtra, and penis. Atlas of tumor pathology, 3rd series, Fascicle 28. Washington, DC: Armed Forces Institute of Pathology; 2000.

[18] Man YG, Tavassoli FA. A simple epitope retrieval method without the use of microwave oven or enzyme digestion. Appl Immunohistochem Mol Morphol 1996;4:139–41.

[19] Man YG, Ball WD, Culp AJ, Hand AR, Moreira JE. Persistence of a perinatal cellular phenotype in the ducts of adult glands. J Histochem Cytochem 1995;43:1203–15.

[20] Man YG, Vinh T, Zhao C, Walker A, Barner R. Potential roles of T-lymphocytes and natural killer cells in human mammary myoepithelial cell layer disruptions and tumor invasion. Mod Pathol [abstract], in press.

[21] Wang LP, Mannion C, Man YG. Reduction of tumor suppressors and elevation of cytotoxic cells in myoepithelial cell layers of inflammatory breast carcinoma: implication for tumor aggressiveness. Mod Pathol [abstract], in press.

[22] Zhao C, Mannion C, Man YG. Potential roles of T-lymphocytes and natural killer cells in prostate basal cell layer disruptions and tumor invasion. Mod Pathol [abstract], in press.

[23] McClinton S, Miller ID, Eremin O. An immunohistochemical characterization of the inflammatory cell infiltrate in benign and malignant prostatic disease. Br J Cancer 1990;61:400–3.

[24] Steiner G, Gessl A, Kramer G, et al. Phenotype and function of peripheral and prostatic lymphocytes in patients with benign prostatic hyperplasia. J Urol 1994;151:480–4.

[25] Leiber C, Deckart A, Wetterauer U. Comparison of the activation status of tumor infiltrating and peripheral lymphocytes of patients with adenocarcinomas and benign hyperplasia of the prostate. Prostate 2000;45:1–7.

[26] Steadman R, Irwin MH, St John PL, et al. Laminin cleavage by activated human neutrophils yields proteolytic fragments with selective migratory properties. J Leukoc Biol 1993;53:354–65.

[27] Heck LW, Blackburn WD, Irwin MH, Abrahamson DR. Degradation of basement membrane laminin by human neutrophil elastases and cathepsin G. Am J Pathol 1990;136:1267–74.

[28] Bonkhoff H, Remberger K. Differentiation pathways and histogenetic aspects of normal and abnormal prostatic growth: a stem cell model. Prostate 1996;28:98–106.
[29] Foster CS, Ke Y. Stem cells in prostatic epithelia. Int J Exp Pathol 1997;78:311–29.
[30] Tobacman JK. Filament disassembly and loss of mammary myoepithelial cells after exposure to lambda-carrageenan. Cancer Res 1997;57:2823–6.
[31] Bonkhoff H. Analytic molecular pathology of epithelial–stromal interactions in the normal and neoplastic prostate. Anal Quant Cytol Histol 1998;20:437–42.
[32] Moinfar F, Man YG, Arnould L, et al. Concurrent and independent genetic alterations in the stromal and epithelial cells of mammary carcinoma: implications for tumorigenesis. Cancer Res 2000;60: 2562–6.
[33] Bubendorf L, Sauter G, Moch H, et al. Ki67 labeling index: an independent predictor of progression in prostate cancer treated by radical prostatectomy. J Pathol 1996;178:437–41.
[34] Man YG, Ball WD, Marchetti L, Hand AR. Contributions of intercalated duct cells to normal parenchyma of submandibular glands of adult rats. Anat Rec 2001;263:202–14.